SIMULATION AND OPTIMAL CONTROL OF HYBRID GROUND SOURCE HEAT PUMP SYSTEMS

By

XIAOWEI XU

Bachelor of Thermal Engineering
Tsinghua University
Beijing, China
2000

Master of Mechanical Engineering
Tsinghua University
Beijing, China
2003

Submitted to the Faculty of the
Graduate College of the
Oklahoma State University
in partial fulfillment of
the requirements for
the Degree of
DOCTOR OF PHILOSOPHY
December, 2007

SIMULATION AND OPTIMAL CONTROL OF

HYBRID GROUND SOURCE HEAT

PUMP SYSTEMS

Dissertation Approved:

Jeffrey D. Spitler

Dissertation Adviser

Daniel E. Fisher

Lorenzo Cremaschi

James Bose

A. Gordon Emslie

Dean of the Graduate College

ACKNOWLEDGEMENTS

First and the most, I would like to express sincere gratitude to my advisor Dr. Jeffrey D. Spitler for his constructive guidance, constant support, patience, and support for me during the past four years. His scientific attitude, sharp thinking, broad knowledge benefited me so much and will be never forgotten. I have learned a lot from him even how to tie flies for fishing. From Dr. Spilter, I learned how to do research, but more important I learned how to have a happy life.

I would like to extend my appreciation and respect to Dr. Daniel Fisher who served as co-advisor of this research project. His many years of building system simulation experience was quite valuable in helping me to achieve the project goals.

I would also like to thank my other committee members, Dr. Jim Bose and Dr. Lorenzo Cremaschi. Their committed service, support, ideas and suggestions are deeply appreciated and thankfully acknowledged.

I would like to thank all my colleagues at the Building and Environmental Thermal Systems Research Group in Oklahoma State University. I want to thank Xiaobing Liu, Zheng Deng, Haider Khan, Kenneth Tang, Ray Young, Shawn Hern, Jason Gentry, James Cullin, and Sankar S. P. for all the help with the research. Without their outstanding work, this project would not have been done. I would also like to thank

Bereket Nigusse, Edwin Lee, Stephen Szczepanski, Calvin Iu, Sam Hobson, Michael Largent, Jiangpeng Yang, and Nan Wang for the fun time we spent all together. Your friendship will be the most precious treasure in my life.

I would like to thank all of my family for their continues love and support over my life. I would especially like to thank my parents, Guorong Xu and Yongying Yu, for raising me. Words will never be able to express how much I own to you. I would like to tell my grandfather and grandmother I am always doing the right thing to make you two proud of me. I would also like to thank my wife's parents. They treated me like their own son and I thank them for bringing me such a good wife.

Finally, and most important I would like to thank my most loving wife Huafeng. With your love, I will never walk alone. This is for you.

TABLE OF CONTENTS

LIST OF TABLES

LIST OF FIGURES

1 INTRODUCTION

Ground-source heat pump (GSHP) systems offer an attractive alternative for residential and commercial heating and cooling applications because of their higher energy efficiency compared with conventional systems. However, the higher first cost of GSHP systems has been a significant constraint for wider application of the technology, especially in commercial and institutional applications. The first cost of a GSHP system in residential applications is almost double that of standard central equipment. Compared to rooftop unitary systems in commercial applications, the first cost of a GSHP system is 20% to 40% higher (Kavanaugh and Rafferty 1997). Many commercial and institutional buildings have high internal heat gains and are generally cooling-dominated, therefore rejecting more heat to the ground than they extract on an annual basis. Less typical, some commercial and institutional buildings are heating-dominated, and extract more heat from the ground than they reject to the ground on an annual basis. Depending on the imbalance, the ground temperature surrounding the heat exchanger can rise or fall over the system operation period. This will negatively impact the system performance. This may be mitigated by increasing the ground-loop heat exchanger (GLHE) size, further increasing the system first cost.

One option to reduce the size of the GLHE, and therefore the first cost of the system, is to reduce the imbalance in the ground thermal loads by incorporating a supplemental heat source or sink into the system. GSHP systems that incorporate a supplemental heat source or sink have been referred to as 'hybrid GSHP systems' (HGSHP systems). Supplemental heat rejection can be accomplished with a cooling tower, fluid cooler, pond, or pavement heating system. Supplemental heat sources could be solar thermal collectors, boilers, greenhouses and so on.

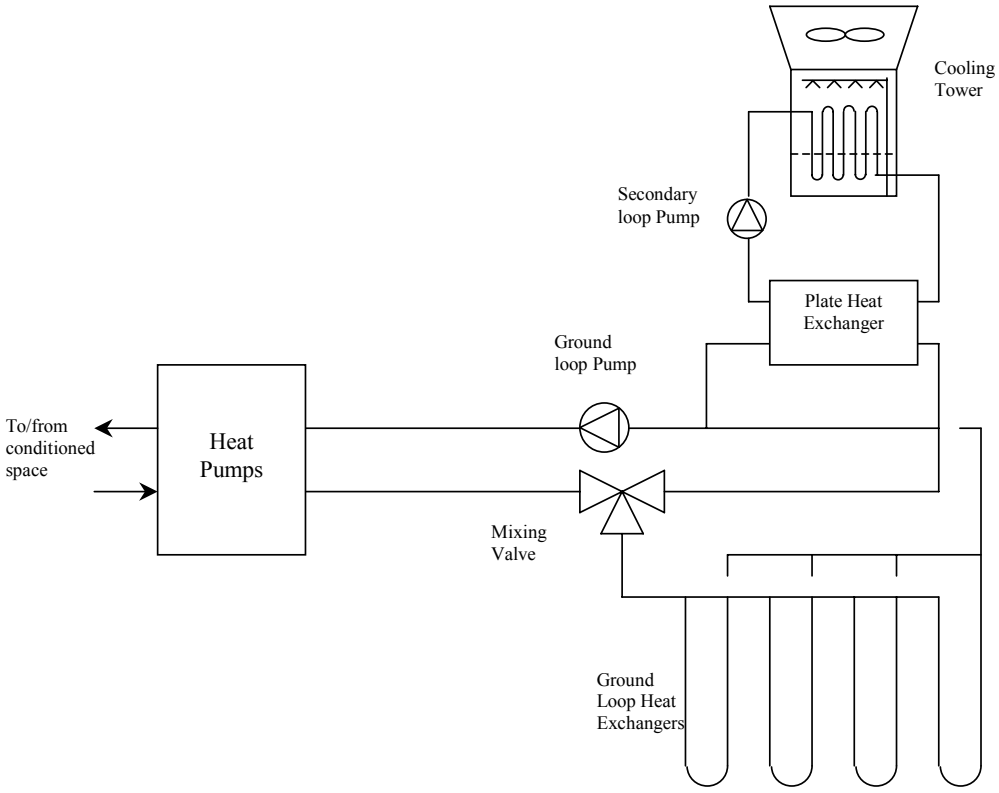

Figure 1.1 A schematic of a typical hybrid GSHP system using a closed-circuit cooling tower as a supplemental heat rejecter

In the hybrid ground source heat pump system, the most common configuration of the system usually uses a cooling tower or fluid cooler as the supplemental heat rejecter,

as shown in Figure 1.1. For this system, the tower is typically isolated from the ground loop heat exchanger with a plate frame heat exchanger. The ground loop heat exchanger and the plate frame heat exchanger are placed in parallel in the system and a mixing valve is used to control the fluid flow through these two components.

1.1 Design of HGSHP Systems

Kavanaugh and Rafferty (1997) developed a design procedure to size the GLHE and the supplemental heat source or sink. For the cooling dominated building, the ground loop heat exchanger of the hybrid ground source heat pump system is then sized to meet the heating loads of the system, balanced by a reduced portion of the cooling loads. The required ground loop is then much smaller compared to the ground loop that would meet all of the heating and cooling loads. For the heating dominated building, the ground loop of the hybrid ground source heat pump system is then sized to meet the cooling loads of the system, balanced by a reduced portion of the heating loads.

One paper (Singh and Foster 1998) described a cooling dominated elementary school with 85,000ft^2 of conditioned area in Atlantic City, New Jersey. The estimated installation cost of a hybrid ground source heat pump system was $1,139,100 compared to the $1,204,100 for the 100% geothermal heat pump system. The $65,000 savings was achieved by replacing 90 boreholes (400 ft deep) with 66 boreholes (400 ft deep) and a 117 ton closed circuit cooler. The predicted annual maintenance expense of the hybrid ground source heat pump system was $3,896 more than that of the 100% geothermal heat pump system. The annual cost of the energy consumption for the hybrid GSHP system was $1,618 less than the cost of the GSHP system. The overall life-cycle cost analysis

of two systems showed that the hybrid GSHP system has a shorter payback time than the GSHP system because the savings of the drilling costs and system energy consumption costs more than offset the increased maintenance costs and for the cooling tower.

1.2 Modeling of HGSHP Systems

In order to evaluate design procedures, control strategies and energy consumption, the ability to model the HGSHP system is needed. In this study, the system will be modeled and simulated using the HVACSIM+ (Clark 1985) modeling environment. Various system component models including heat pumps, pumps, GLHE and open-circuit cooling towers have been developed or modified for use in HVACSIM+ (Khan et al. 2003; Khan 2004; Liu and Spitler 2004).

The ability to predict the short-term behavior of ground loop heat exchangers is critical to the design and energy analysis of both the GSHP and HGSHP systems. Thermal load profiles vary significantly from building to building – GLHE designs can be dominated by long-term heat build-up or short-term peak loads. In some extreme cases, where the GLHE design is dominated by short-term peak loads, temperatures in the GLHE can rise rapidly; say 5-10ºC in one to two hours. For such short-term peak loads, the thermal mass of the fluid can significantly dampen the temperature response of the ground loop. The over prediction of the temperature rise (or fall) in turn can cause an over prediction of the required GLHE length. Furthermore, the temperature response can be damped by the fluid in the rest of the system, in addition to the fluid in the borehole. The temperature response also has a secondary impact on the predicted energy consumption of the system, as the COP of the heat pump varies with entering fluid

temperature. Therefore, it is desirable to be able to model the effect of fluid thermal mass on the short-term behavior of the GLHE accurately.

In GSHP systems, antifreeze mixtures are often used as a heat transfer fluid. Generally, the flow rate in the GLHE is designed so as to ensure turbulent flow in the tube to guarantee a low convective heat transfer resistance. However, for some antifreeze types, the large increase in viscosity as the temperature decreases may result in transition to laminar flow, or require an otherwise unnecessarily high system flow rate. For example, at 20ºC, the viscosity of 20% weight concentration propylene glycol is 0.0022 Pa·s and the density is 1021 kg/m^3. At –5ºC, the viscosity increases to 0.0057 Pa·s and the density increases to 1026 kg/m^3. Thus, with the same volumetric flow rate, the Reynolds number at –5ºC is only about 39% of the value at 20ºC. If this results in transition from turbulent to laminar flow, the convective resistance will increase significantly. In order to evaluate the trade-offs between high system flow rates and occasional excursions into the laminar regime, it is desirable to include the effects of varying convective resistance in the GLHE model.

While it is desirable to model both the variable convective resistance and the thermal mass in the borehole, the previous published GLHE models (Carslaw and Jaeger 1947; Eskilson 1987; Deerman and Kavanaugh 1991; Yavuzturk and Spitler 1999) did not simultaneously account for these two phenomena. Therefore, a more accurate GLHE model is highly desired for the HGSHP system simulation.

1.3 Control of HGSHP Systems

Control of the supplemental heat rejecter is an important issue for the hybrid ground source heat pump system. A wide range of control strategies and setpoints are possible, and it is expected that they will have a significant effect on the system performance. Figure 1.2 shows the relationship between the COP of a heat pump (ClimateMaster GS060) and the entering fluid temperature (EFT) of the heat pump. In cooling mode, the heat pump has better performance as the EFT decreases. In heating mode, performance of the heat pump improves with higher EFT. Operating the supplemental heat rejecter at the cooling mode will help to lower the EFT of the heat pump, giving a higher efficiency. A common method of HGSHP system control runs the supplemental heat rejecter only when the heat pump EFT exceeds 90°F. However, there may be many hours when the supplemental heat rejecter could reduce EFT to 70°F. If this is done, heat pump COP can increase from 3.4 to 4.5, reducing electricity consumption by 24%, while minimally increasing cooling tower power costs. Running at lower loop temperature could also have a penalty for heating. Despite these complications, there is significant potential for energy savings by carefully controlling the supplemental heat rejecter.

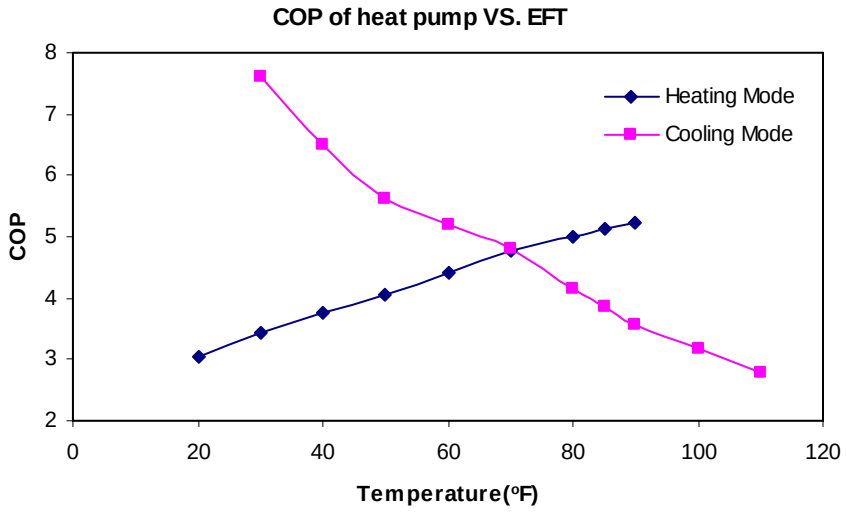

Figure 1.2 COP of a heat pump (ClimateMaster GS060) with the entering fluid temperature of the heat pump

For a hybrid ground source heat pump system, a set point temperature control strategy is often used to operate the cooling tower (Kavanaugh and Rafferty 1997; Yavuzturk and Spitler 2000; Ramamoorthy et al. 2001). The cooling tower is activated when the entering fluid temperature (EFT) of the heat pump or the exiting fluid temperature (ExFT) exceeds an upper limit temperature. However, for different locations and systems, the value of the upper limit temperature could vary over a wide range, that is "anywhere between 75°F and 95°F" (ASHRAE 1995) (p. 8.2).

Another control strategy might be called a temperature difference control strategy (Yavuzturk and Spitler 2000). When the temperature difference between the entering or exiting fluid temperature of the heat pump and the ambient wet-bulb temperature (open circuit cooling tower) or the ambient dry-bulb temperature (closed circuit fluid cooler) exceeds a set value, the supplemental heat rejecter is activated. Yavuzturk and Spitler

looked at temperature difference setpoints of 3.6°F (2°C) and 14.4°F (8°C) but did not attempt to optimize the design and control. It should be noted that the temperature difference control strategy depends on the measurement of the ambient wet-bulb temperature. The wet bulb temperature has a typical uncertainty of ± 0.5ºC even in an experiment (Gentry et al. 2006). Simulations in which the wet bulb temperature is assumed to be measured perfectly do not reflect reality. This suggests that, in practice, caution is warranted in using a control based on wet bulb temperature.

A third type of control strategy, which might be called a "preset schedule control" was evaluated by Yavuzturk and Spitler (2000). To avoid a long-term temperature rise, the supplemental heat rejecters were set to run for six hours during the night to store "cool" in the ground. Also, a set point temperature control strategy works with the "preset schedule control" to avoid potentially high loop temperatures. Yavazturk and Spitler used three different preset schedules to run the supplemental heat rejecter: 12:00 a.m. to 6:00 a.m. year-round, 12:00 a.m. to 6:00 a.m. during the months of January through March, and 12:00 a.m. to 6:00 a.m. during the months of June through August. Yavuzturk and Spitler did not apply time-of-day utility rates to calculate the electricity cost and did not attempt to optimize the schedule.

All of the control strategies face the challenge of how to choose a proper setpoint value or preset schedule to optimally control the system to get the minimum system operating cost. A lot of issues will effect the choice of the setpoint value or the preset schedule such as building location, building type, HGSHP system design, HGSHP system component characteristics, etc. Since optimization of the HGSHP system control strategy

has not been investigated, the current available control strategies might be far from optimal. Therefore, more sophisticated control strategies which are able to optimally control the HGSHP system are highly desirable. With these control strategies, the setpoint choice should be less dependent on the building type, HGSHP system design, etc and should be easier to be determined.

1.4 Optimal Control of HGSHP Systems

In a hybrid ground source heat pump system, there are multiple degrees of freedom in controlling the supplemental heat rejecter. As a result, the HGSHP system would have a different performance and the energy consumption. In the Paragon Center in Allentown, Pennsylvania (Gilbreath 1996), the HGSHP system performance for different system designs and control strategies was investigated with a spreadsheet analysis. Comparison of results showed that the estimated energy usage of one of the HGSHP system scenarios would vary about 3% with different control strategies. In an office building in Tulsa, Oklahoma, Yavuzturk and Spitler (2000) showed variations of 4-6% in HGSHP system operating cost with different control strategy setpoints and similar cooling tower sizes. For a wider range of cases, with different control strategies, setpoints, and cooling tower sizes, operating costs varied by up to 15%.

As mentioned above, previously published works have not tried to optimize the control strategies. Yet, there is clearly potential for energy savings by adjusting the control of HGSHP systems. Therefore, investigation of optimal control strategies is highly desirable.

1.5 Objectives

The objectives of this research are discussed in detail after the background and literature review. But, in short, the objective is to develop optimal control strategies and set points for hybrid ground source heat pump systems. When we talk about the optimal control, it means we try to find the best control of the system to get the minimum system operation cost. Firstly, the HGSHP system will be modeled and simulated using the HVACSIM+. In this part, because the previous ground loop heat exchanger models did not account for variable convective resistance and thermal mass in the borehole simultaneously, a revised GLHE model will be developed. Also, some additional components of the HGSHP system will be modeled and cast as HVACSIM+ component models. Secondly, because only a few control strategies for HGSHP system have been investigated, a wide range of the control strategies will be developed. Optimization will be applied in an attempt to develop generally applicable optimal control strategies.

2 BACKGROUND AND LITERATURE REVIEW

In this chapter, a review of component models of hybrid ground source heat pump systems will be presented. Secondly, literature about the design of hybrid GSHP systems and control approaches for hybrid GSHP systems will be summarized.

2.1 HGSHP System Component Models

In this section, the literature review focuses on modeling of the ground loop heat exchanger, heat pumps, cooling towers and fluid coolers.

2.1.1 Ground Loop Heat Exchanger Model

The ground loop heat exchanger can be buried either horizontally in trenches or vertically in boreholes. The choice of whether the system is horizontal or vertical depends on available land, local soil type, and excavation costs. In many cases, a vertical ground loop heat exchanger system is used where the available land area is limited. The vertical ground loop heat exchanger configuration options include single and double U-tubes, small and large-diameter spirals, standing column wells, and “spider” heat exchangers (IGSHPA 1997). In practice, spirals and “spider” configuration of heat exchangers are not used commercially due to the installation difficulty. The standing column well had limited geographical range (Deng et al. 2005; O'Neill et al. 2006). Therefore, the focus of this work is vertical ground heat exchangers with single and double U-tube.

A typical configuration is shown in Figure 2.1, though most HGSHP system would have more boreholes. The working fluid (usually water or antifreeze solution) circulates through the ground loop heat exchanger, rejects heat to the ground in cooling mode or extracts heat from the ground in heating mode.

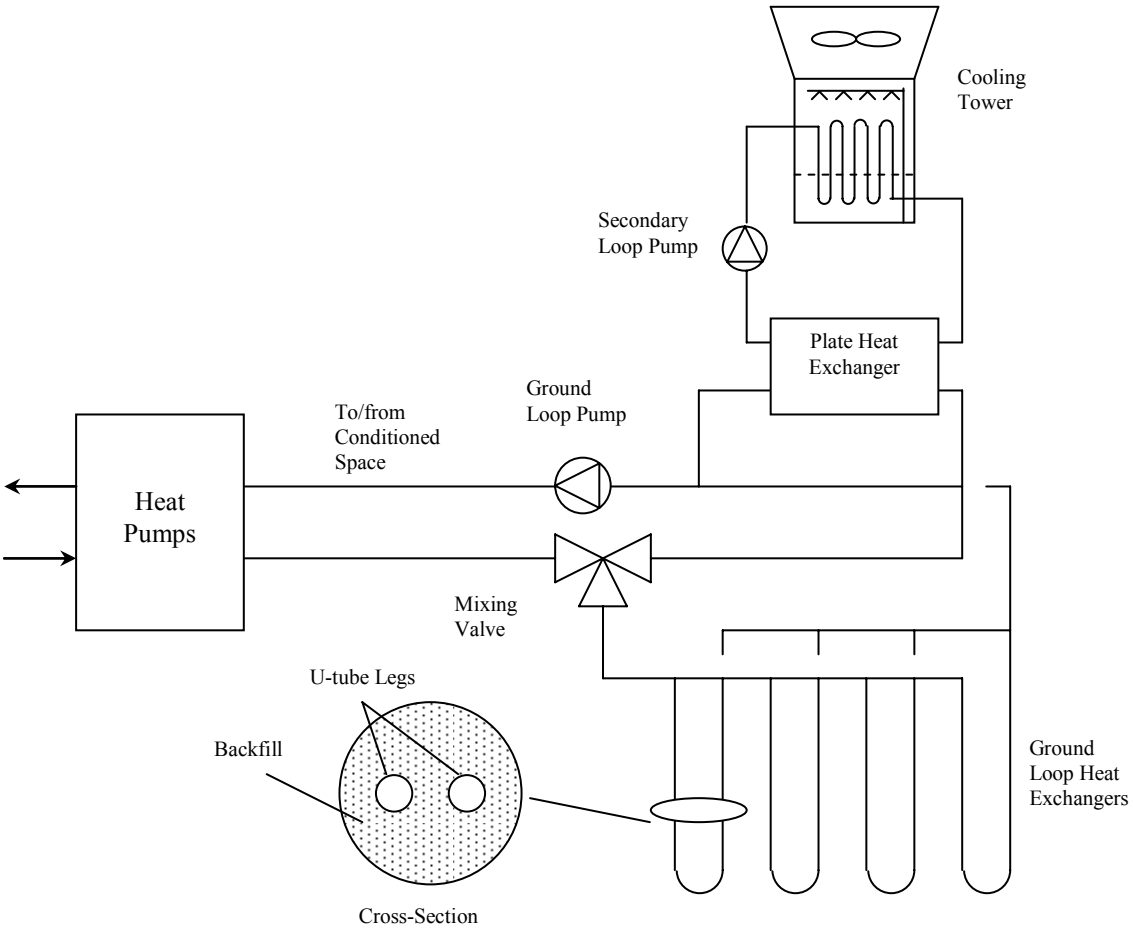

Figure 2.1 A schematic of a typical hybrid GSHP system using a closed-circuit cooling tower as a supplemental heat rejecter

Vertical single U-tube boreholes typically range from 50 to 120 meters (164 to 394 ft) deep and are typically around 10 to 15 cm (4 to 6 inches) in diameter. All but the smallest systems use multiple boreholes. It is not uncommon for large systems to have

more than 100 boreholes. In order to decrease the thermal interaction between the boreholes, each borehole is typically placed at least 4.5 m (15ft) from all other boreholes. After the U-tube installation, the borehole will be backfilled with grout, as shown in Figure 2.1. The backfill is used to prevent pollution transfer via water movement and to provide good thermal contact between the U-tube and the soil. The fluid temperature varies through the U-tube and the pipe wall temperatures of each U-tube pipe are different, therefore there is thermal short-circuiting between the pipe legs of the U-tube.

Both the dimensional scale and thermal capacitance of the borehole are much smaller relative to those of the infinite ground outside of the borehole. The thermal energy change of the borehole over a year is a very small portion of the total heat flow (Rottmayer et al. 1997). However, the short-term response is important for design considerations that limit the minimum and maximum entering fluid temperature to the borehole. Also the existence of a backfill leads to a nonhomogeneous medium around the U-tubes. Therefore, the heat transfer process of the ground loop heat exchanger is usually analyzed in two separated regions: outside and inside the borehole. To simulate the detailed thermal transfer process of the vertical ground loop heat exchanger, there are three domains of interest.

1. Outside the borehole — conduction. The thermal transfer process outside a single borehole may be treated as a line or cylinder source in a finite or semi-infinite medium heat conduction transfer problem. The end effects may or may not be accounted for. Approaches include: infinite line source model (Ingersoll and Plass 1948), finite line source model (Eskilson 1987; Zeng et al. 2002),

infinite cylindrical source model (Kavanaugh 1985; Deerman and Kavanaugh 1991; Dobson et al. 1995; Bernier 2001; Young 2004), numerical models (Eskilson 1987; Hellstrom 1991; Muraya 1994; Rottmayer et al. 1997; Yavuzturk et al. 1999; Rees 2000) and response factor models (Eskilson 1987; Yavuzturk and Spitler 1999; Young 2004).

The thermal interaction between the boreholes in long time scale is significant (Yavuzturk 1999) and must be accounted for (Eskilson and Claesson 1988; Sutton et al. 2002).

In area where groundwater movement in cracks and permeable zones is significant, the groundwater impact on the heat transfer may have a significant effect (Eskilson 1987; Rees 2000) and must be accounted for (Deng 2004).

2. Inside the borehole — conduction and convection. The heat transfer inside the borehole includes heat conduction between the U-tube inner pipe wall and borehole wall, heat conduction between the different U-tube legs, and heat convection between the working fluid and the U-tube inner pipe wall. The heat conduction depends on tube geometry in the borehole, pipe thermal properties, and grout thermal properties. To a lesser degree, it may also depend on the ground thermal properties. The heat convection depends on working fluid properties, fluid flow rate, and fluid temperatures.

   The heat transfer process inside the borehole can be simplified as a one-dimensional, two-dimensional, or quasi-three-dimensional problem depending

on the assumptions made. If the fluid temperature variation along the borehole depth is not considered and the axial heat conduction in the borehole is assumed to be negligible because the borehole depth is far greater than its diameter, then the heat transfer process inside the borehole can be regarded as a two-dimensional heat transfer problem (Muraya 1994; Rottmayer et al. 1997; Yavuzturk et al. 1999; Rees 2000). The two-dimensional heat transfer model can be further simplified as a one-dimensional model with the "equivalent U-tube diameter" (Deerman and Kavanaugh 1991; Gu and O'Neal 1998). In the axial direction, the axial heat conduction of grout, pipe and fluid are assumed to be negligible compared to the axial heat transfer amount carried by the fluid flow. Thus, only heat diffusion carried by the fluid flow is considered. The heat transfer process inside the borehole can be also treated as a quasi-three-dimensional model (Dobson et al. 1995; Rottmayer et al. 1997; Zeng et al. 2002), which allows the fluid temperature to vary with the borehole depth.

As mentioned above, the annual thermal energy change of the borehole is very small compared to the amount outside the borehole. Thus it is a common practice that the heat transfer in the borehole is approximated as a quasi-steady-state phenomenon in annual simulations and the thermal capacitance of grout and fluid is neglected. However, for dynamic simulation of the ground loop heat exchanger down to hourly and sub-hourly time steps, the thermal capacitance of the grout and fluid would have a significant impact on the short term response of the borehole system (Young 2004; Xu and Spitler 2006). This, in turn, impacts the design of GLHE. In some extreme cases, where the GLHE

design is dominated by short-term peak loads, temperatures in the GLHE can rise rapidly; say 5-10ºC in one to two hours. For such short-term peak loads, the thermal mass of the fluid can significantly dampen the temperature response of the ground loop.

Another facet of the heat transfer process inside the borehole is the short-circuiting between the U-tube legs. In cooling mode, the warmer fluid flows into the U-tube, rejects heat to the ground and a relatively cold fluid flows back to the heat pump. Near the top of the borehole, the two fluid streams may have a significant temperature difference, on the order of 5°C. The existence of heat conduction between the U-tube different legs reduces the borehole heat rejection/extraction of the ground loop heat exchanger. Therefore, some models have included the effects of short-circuiting in the heat transfer process inside the borehole (Kavanaugh 1985; Deerman and Kavanaugh 1991; Dobson et al. 1995; Muraya et al. 1996; Zeng et al. 2002).

3. Building and heat pumps — time-varying boundary conditions. A constant heat transfer rate or fluid temperature is often used as the boundary condition in the development of the ground loop heat exchanger model. In practical systems, the heat transfer rate of the ground loop heat exchanger varies continuously due to the heating/cooling system load variations. To apply the models to a variable heat transfer rate, the temperature change is calculated by superposition of the contributions of different heat pulses with different time intervals (Ingersoll and Plass 1948). However, for a long time period simulation, the computational

time for superposition of the "historical" temperature would be tremendous. Therefore, several algorithms have been developed to aggregate the loads to reduce the computational time (Deerman and Kavanaugh 1991; Yavuzturk and Spitler 1999; Bernier 2001; Bernier et al. 2004).

A literature review yields several approaches for design and dimensioning of the vertical ground loop heat exchangers. Most of the approaches fall into one of three categories: analytical models, numerical models, and response factor models. A summary of the ground loop heat exchanger models published in the literature is shown in Table 2.1.

In Table 2.1, each GLHE model is summarized in terms of the three domains of interest: conduction outside borehole, heat transfer inside borehole, treatment of time-varying boundary conditions. Also Table 2.1 indicates whether or not the model is validated against experimental measurements. The following details are summarized.

1. Conduction outside borehole

    a. Whether the model may be characterized as analytical, numerical or response factor based.

    b. The model performs one-dimensional, two-dimensional, or three-dimensional simulation.

    c. Does the model account for interference between the boreholes?

    d. Can the model account for the impact of groundwater movement?

2. Heat transfer inside borehole

    a. Is this treated with an analytical or numerical model?

    b. The model performs one-dimensional, two-dimensional, or three-dimensional simulation.

    c. The model performs steady-state or dynamic simulation (Is the thermal capacity of fluid, pipe wall, and grout accounted for?).

    d. Can the model account for grout or other backfill with different thermal properties? (If soil is selected, this means the model cannot account for different thermal properties of the grout or backfill.)

    e. What GLHE configurations does the model support (e.g., single U-tube, double U-tube)?

    f. Does the model account for short-circuiting between the U-tube legs?

3. Does the model include a load aggregation algorithm?

4. Is the model experimentally validated?

For additional information or qualification not included above, footnotes are provided and listed after the Table 2.1.

In the following section, a selective literature review of these GLHE models will be included. Due to the large amount of literature, the literature review mainly focuses on

those models which are aimed at GSHP/HGSHP system simulation, though some background is provided on analytical models.

Table 2.1 Literature Review Summary for Ground Loop Heat Exchanger Models

Citation	Model	Conduction Outside Borehole							Heat Transfer Inside Borehole												Load Aggregation Algorithm	Experimental Validation
		Analytical	Numerical	Response Factor	1-D	2-D	Interference	Ground Water	Analytical	Numerical	1-D	2-D	Steady-State	Dynamic	Borehole Filling			Single U-tube	Double U-tube	Short-Circuiting		
															Soil	Grout	Water					
Ingersoll and Plass (1948)	LSM	√			√				√		√		√		√							
Eskilson (1987)	FLSM	√				√	√	√	√		√		√			√		√				
Zeng et al. (2002; 2003)	FLSM	√				√	√		√			√ 1	√			√		√				
Kavanaugh et al.(1985; 1997); Deerman and Kavanaugh (1991)	CSM	√			√		√		√		√		√			√		√	√	√	√	√
Gu and O'Neal (1998; 1998)	CSM	√			√				√		√		√			√		√				√
Fujii et al. (2004)	CSM	√			√																	
Bernier et al. (2001; 2004)	CSM	√			√		√		√		√		√			√		√			√	
Dobson et al. (1995)	CSM	√			√		√			√		√		√	√			√		√		√
Young (2004)	STSM	√			√		√		√			√		√		√		√			√	
Eskilson et al. (1987; 1988)	LSTM		√	√	√		√	√	√		√		√			√		√	√			
Mei and Baxter (1986)	FDM																					
Muraya et al. (1994; 1996)	FEM		√			√				√		√		√		√		√		√		
Rottmayer et al. (1997)	FDM		√			√	√			√		√ 1		√ 2		√		√		√		
Rees (2000)	FVM		√			√		√		√				√		√		√	√			
Yavuzturk and Spitler (1999; 2001)	STSM		√	√		√	√			√		√		√		√		√			√	√
Hellstrom (1991); Shonder et al, (1999)	DST		√			√	√			√	√			√		√		√	√	√		
Sutton et al. (2002)	CSM		√			√	√			√	√			√		√		√	√	√		
Lei (1993)	FDM		√							√		√		√	√			√		√		√
Shonder and Beck (1999)	FDM		√		√					√	√			√		√		√				
Kohl et al. (1995; 2002); Signorelli et al. (2005)	FEM		√			√ 3	√	√		√		√ 3		√		√		√	√	√		√
Al-Khoury et al. (2005)	FEM		√			√ 4		√		√		√ 4		√		√		√				
Bi et al. (2002)	FDM		√			√				√		√		√	√				√ 5			√

1: A quasi-three dimensional model. The fluid temperature changes over the borehole depth.
2: The thermal capacity of grout and pipe wall is neglected, but thermal capacity of fluid is accounted for.
3: For co-axial tube borehole, the model performs 3-D simulation by 2-D geometry.
4: The model performs 3-D simulation.
5: The ground heat exchanger configuration is vertical double spiral coil.

2.1.1.1 Modeling of Vertical Ground Loop Heat Exchangers - Analytical

Analytical solutions, e. g. line source model (LSM), finite line source model (FLSM), and infinite cylindrical source model (ICSM) have been used for modeling and dimensioning vertical ground loop heat exchangers. They are described below.

Kelvin's Line Source Theory

The earliest approach to calculate the heat transfer of the heat exchanger in the ground is Kelvin's line source model (Ingersoll and Plass 1948). This model is based on approximating the borehole as an infinite long line source of heat, or sink in an infinite medium (i.e., soil) and assuming end effects are negligible. The soil acts as a heat rejection (extraction) medium, which has an assumed uniform and constant initial temperature. The temperature at any point in the medium is calculated by:

$$T - T_{ff} = \frac{Q'}{2\pi k_s} \int_X^\infty \frac{e^{-\beta^2}}{\beta} d\beta = \frac{Q'}{2\pi k_s} I(X) \qquad (2\text{-}1)$$

Where

$$X = \frac{r}{2\sqrt{\alpha t}} \qquad (2\text{-}2)$$

T = Temperature of ground at any selected distance, r from the line source (°C [°F]). When the distance r equals to the pipe radius, the temperature represents the pipe wall temperature.

T_{ff} = Far-field undisturbed ground temperature (°C [°F]).

Q' = Heat transfer rate of the source (W/m [Btu/ft-hr]),

r = Distance from center line of the borehole (m [ft]),

k_s = Thermal conductivity of the ground (W/m-K [Btu/hr-ft-°F]),

α = Thermal diffusivity of the ground, defined as $\alpha = \frac{k_s}{\rho c}$, ($m^2$/s [$ft^2$/hr]),

ρ = Density of the ground (kg/m^3 [lbm/ft^3]),

c = Specific heat of the ground (kJ/kg-K [Btu/lbm-F]),

t = Time since the start of operation (s [hr]),

β = Integration variable, defined as $\beta = \frac{r}{2\sqrt{\alpha(t-t')}}$

Ingersoll and Plass estimated that the line source model is exact for a true line source and it can be applied to small pipes (2" diameter or less) with negligible error after a few hours of operation. For large pipes (e.g. 4" to 8") and for periods less than a few days, the line source model would have an error in temperature calculation, which can be estimated.

Ingersoll and Plass provided several examples of using the line source model for calculating the pipe wall and the soil temperature for a single tube in homogeneous medium. However, the real U-tube configuration is different from Ingersoll and Plass's examples. The use of a U-tube and grout with different thermal conductivity from the

surrounding soil further complicated the analysis. In order to practically use this model, further assumptions and additions are needed. One possible approach (Spitler 2003) involves using the LSM to compute the temperature at the borehole wall due to a line source at the center of the borehole, and then a borehole resistance is used to compute the difference between the borehole wall temperature and the average fluid temperature. Thus the thermal mass of the fluid and ground are, at best, approximated as if the borehole were filled with soil. Borehole-to-borehole thermal interference may be modeled by superposition (Ingersoll and Plass 1948).

Finite Line-Source Model

A finite line source analytical model has been developed for a single borehole ground loop heat exchanger (Eskilson 1987; Eskilson and Claesson 1988; Zeng et al. 2002; Zeng et al. 2003; Diao et al. 2004). The heat conduction outside the borehole is treated as a finite line source in a semi-infinite medium, which has a constant initial and boundary temperature for field and upper surface. In the finite line source model, end effects are not negligible and the real borehole wall temperature varies along the borehole depth, especially near the end of borehole region.

The analytical solution of the finite line source model was derived by Eskilson (1987) and Zeng et al. (2002) respectively. The temperature is obtained by integrating contributions of imaginary point source distributed along the borehole (Eskilson 1987).

$$T_q(r,z,t) = -\frac{q_l}{4\pi k_s}\int_D^{D+H}\{\frac{1}{r_+}erfc(\frac{r_+}{\sqrt{4\alpha t}}) - \frac{1}{r_-}erfc(\frac{r_-}{\sqrt{4\alpha t}})\}ds \qquad (2\text{-}3)$$

$$r_+ = \sqrt{r^2 + (z-s)^2} \qquad r_- = \sqrt{r^2 + (z+s)^2}$$

Where

D = Depth of thermally insulated upper part of the borehole (m [ft]).

H = Depth of borehole (m [ft]).

z = The depth of selected point around the finite line source (m [ft]).

s = Integrating parameter.

Zeng et al. (2002) gave a similar equation to Eskilson, except for setting the D value as zero.

The borehole wall temperature T_b varies along the borehole depth, especially near the end; therefore, it is more reasonable to use the integral mean temperature of the borehole wall to represent the heat transfer between the borehole and the ground (Eskilson 1987). The borehole wall temperature for a single borehole can be calculated by:

$$T_b = \frac{q_l}{2\pi k_s} \cdot g(t/t_s, r_b/H) \tag{2-4}$$

$$g(t/t_s, r_b/H) \approx \begin{cases} \ln(\frac{H}{2r_b}) + \frac{1}{2}\ln(\frac{t}{t_s}) & ,5r_b^2/\alpha < t < t_s \\ \ln(\frac{H}{2r_b}) & , \quad t > t_s \quad t_s = \frac{H^2}{9\alpha} \end{cases} \tag{2-5}$$

Eskilson states that the lower time limit $t > 5r_b^2 / \alpha$ is necessary for the use of a line sink at $r = 0$ instead of $r = r_b$. For a typical borehole of 10cm (4") diameter and saturated clay, the time would correspond to about 1~2 days. Therefore, the finite line source model may be used to model the heat transfer of the ground loop heat exchanger for long time steps.

Since the finite-line source model has the lower time limited $t > 5r_b^2 / \alpha$, the thermal capacity of the borehole is negligible at this time scale. A one-dimensional steady-state analytical model is used by Eskilson (1987) to represent the heat transfer process inside the borehole and the thermal resistance is calculated using the Multipole method (Bennet et al. 1987), which is able to model the complicated configurations inside the borehole.

As a follow-up study, Zeng et al. (Zeng et al. 2003; Diao et al. 2004) developed a quasi-three-dimensional model to calculate the heat transfer inside the borehole. In their model, the fluid temperature and pipe wall temperature vary in the axial direction. The quasi-three-dimensional model inside the borehole is able to estimate the impact of the short-circuiting among U-tube legs, and to evaluate the system performance of the different fluid circuit arrangements in the double U-tube. The solution of this problem was derived by Laplace transformation (Zeng et al. 2003). Zeng and Diao (2003) represent the fluid temperature profiles of five different fluid circuit arrangements for the double U-tubes. They show that the double U-tube in parallel circuit demonstrates a better performance than the double U-tube in series circuit.

Infinite Cylindrical Heat Source Model

A literature search revealed a number of publications on the cylindrical source model of the vertical ground loop heat exchanger. The infinite cylindrical heat source model, first presented by Carslaw and Jaeger (1947) and Ingersoll et al. (1954), and later refined by Kavanaugh at al. (Kavanaugh 1985; Deerman and Kavanaugh 1991; Kavanaugh 1995) to model the heat transfer process of the vertical ground loop heat exchanger. Subsequent work on the cylindrical model includes: Gu and O'Neal's (1998; 1998) analytical solution of the cylindrical source model and the "equivalent U-tube diameter", Fugii et al.'s (2004) approximation of cylindrical source function calculation, Dobson et al.'s (1995) short-circuiting calculation between U-tube legs and on-off cycle model of GLHE, and Bernier's (2001) whole ground-coupled heat pump system simulation based on the most refined cylindrical source model.

The cylindrical source model assumes the single borehole as a single infinite isolated pipe surrounded by an infinite solid with constant properties. With a constant heat flux at the pipe wall, the temperature of point under consideration at or near the pipe is calculated as follows:

$$T_b = \frac{q'}{k_s H} G(Fo, p) + T_{ff} \qquad (2\text{-}6)$$

Where

q' = Heat transfer rate applied to the ground per unit of borehole depth (W/m [Btu/ft-hr]), a positive value implies heating.

k_s = Thermal conductivity of the soil, (W/m-K [Btu/hr-ft-F]),

$G(Fo, p)$ = Referred as the cylindrical source function (Ingersoll et al. 1954),

p = Ratio of the radius where the temperature is calculated over the outside of pipe (r_o). When the ratio is equal to 1, the temperature represents the outer pipe wall temperature.

Fo = The Fourier number, defined as: $Fo = \alpha_s t / r^2$. And α_s is the soil diffusivity (m^2/s [ft^2/hr]).

The cylindrical source model only works directly for the single borehole. Kavanaugh and Rafferty (1997) developed a procedure to adjust the initial undisturbed ground temperature T_{ff} to estimate the interference between adjacent boreholes.

The heat transfer inside the borehole is represented by solving a one-dimensional (Deerman and Kavanaugh 1991; Bernier 2001) or quasi-two-dimensional (Dobson et al. 1995) steady-state heat transfer process in a cylindrical pipe. Deerman and Kavanaugh used the "equivalent U-tube diameter" (Bose 1984; Mei and Baxter 1986) to evaluate the equivalent thermal resistance between the fluid and the borehole wall. Bernier (2001) used the "shape factors" (Remund 1999) of the borehole to calculate the thermal resistance of the borehole.

Applying the most refined cylindrical source model of GLHE, a heat pump model that interpolates the manufacturer's catalog data, and a curve fit model of variable speed

drive circulation pump, Bernier (2001) developed an annual simulation of the ground-coupled heat pump system based on an hourly time step. The simulated temperatures and system energy consumption are compared against the DST model (Hellstrom et al. 1996; Shonder et al. 2000) results and the agreement of the temperatures from these two models is quite good.

Carslaw and Jaeger (1959) presented two forms of the cylindrical source solution. The first form (Carslaw and Jaeger, 1959, Section 11.5, p. 334-339) assumes either a fixed temperature or fixed flux at the boundary $r = a$, and does not consider heat transfer within the cylinder. This form was used by Deerman and Kavanaugh (1991); Dobsen et al. (1995); Bernier (2001) and Fujii et al. (2004). In all of these works, the heat transfer from the fluid to the borehole wall is approximated as a quasi-steady-state phenomenon and the thermal capacitance of grout and fluid is neglected. Therefore, like the line source model, the cylindrical source model has limited accuracy for dynamic simulation at short time steps.

The second form of the cylindrical source solution given by Carslaw and Jaeger (1959) assumes that the infinite region with uniform properties is bounded internally by a single infinite circular cylinder of a perfect conductor with thermal capacitance (Carslaw and Jaeger, 1959, Section 11.7, p. 341-345). Carslaw and Jaeger (1959) gave, as an example, a model of a buried electrical cable (BEC).

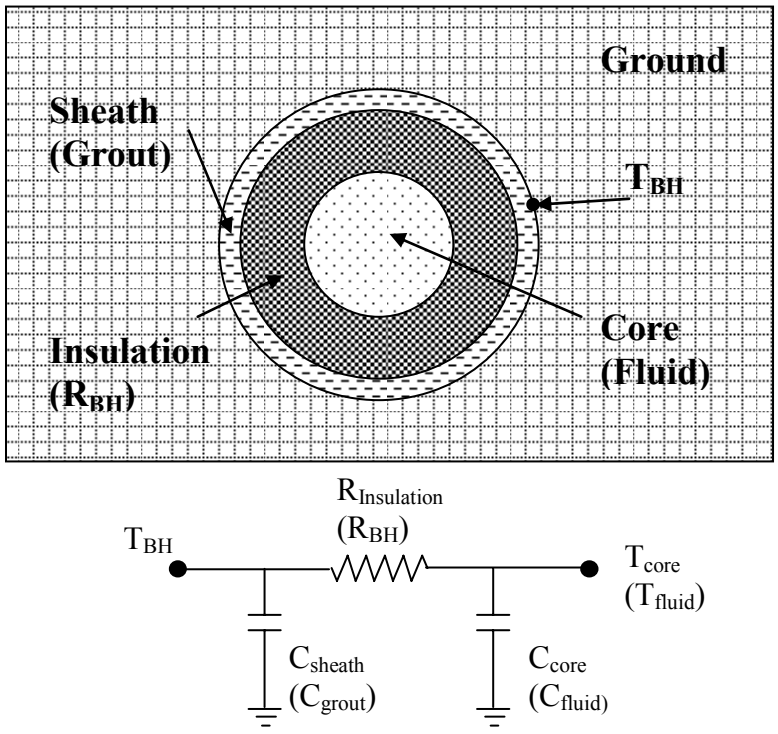

Figure 2.2 Diagram of a buried electrical cable model (and Borehole Fluid Thermal Mass Model)

The diagram of the buried electrical cable is shown in Figure 2.2, where there is a core surrounded by insulation which is surrounded by a sheath. The core and sheath have finite thermal capacitance, but infinite conductivity. The insulation has a finite thermal conductivity but no thermal capacitance. Young (2004) applied this BEC model to the borehole system, with each input of the BEC model having an analogous input with respect to the borehole. These are shown parenthetically in Figure 2.2. The solution is then given for core temperature T_{core} due to a constant heat input to the core.

In the ground loop heat exchanger, fluid in the U-tube helps to damp the response to peak loads. Furthermore, fluid outside the U-tube, but circulating through the system has the same effect – it damps the response to peak loads. Therefore, Young introduced a

fluid factor to offer the capability of accounting for fluid thermal mass, both inside the U-tube and in the rest of the system. Thus, the model was called the borehole fluid thermal mass (BFTM) model (Young 2004). The fluid factor is defined as the ratio of the fluid thermal mass in the system to the fluid thermal mass in the U-tube and a typical value for an actual system is two.

The analytical solution of the core temperature can be calculated (Carslaw and Jaeger 1959):

$$T_{core} = \frac{q_l}{k_s} G(h, \alpha_1, \alpha_2, \tau) + T_{ff} \tag{2-7}$$

Where

$$h = 2\pi R_b k_s,\ \alpha_1 = 2\pi r_b^2 \rho c / S_1, \alpha_2 = 2\pi r_b^2 \rho c / S_2 \quad \tau = \alpha t / r_b^2$$

Where (In the following, "BEC" refers to the Carslaw and Jaeger presentation of the buried electrical cable model. "BFTM" refers to Young's adaptation as the borehole fluid thermal mass model.)

k_s = Thermal conductivity of soil (W/m-ºC [Btu/hr-ft-ºF]);

R_b = BEC: thermal resistance of insulation; BFTM: borehole thermal resistance, (m-ºC/ W [hr-ft-ºF/ Btu]);

r_b = BEC: cable radius; BFTM: borehole radius, (m [ft]);

ρ = Density of soil (kg/m^3 [lbm/ft^3]);

c = Special heat of the soil (J/kg-K [Btu/lbm-ºF]);

S_1 = BEC: volumetric thermal capacity of core; BFTM: volumetric thermal capacity of fluid, (J/m-K [Btu/ft-ºF]);

S_2 = BEC: volumetric thermal capacity of sheath; BFTM: volumetric thermal capacity of grout, (J/m-K [Btu/ft-ºF]);

α = Thermal diffusivity of the soil (m^2/s [ft^2/s]).

Since the geometry of the borehole with a single U-tube is not the same as the buried electrical cable, Young developed a procedure for matching the BEC parameters to the U-tube geometry. To maintain the identical thermal mass of fluid and grout, the cross sectional areas of the fluid and grout were maintained from the actual U-tube to the BEC representation. This is done by choosing an equivalent diameter of the core as $\sqrt{2}$ of the original diameter of inner U-tube.

In the BEC model, the sheath (grout) and core (fluid) are assumed to be thermal masses without resistance and might be called "lumped capacitances" located at the outside and inside of the "lumped thermal resistance" of borehole, as shown in Figure 2.2. In the borehole, the thermal capacity of grout and fluid is distributed continuously in the borehole domain, as well as the thermal resistance of borehole. In practice, the continuous distribution of thermal capacitance might be adequately approximated with enough lumps, as in a finite volume model.

However, Young (2004) found that two lumps, with one lump being the fluid and the other being the grout, did not give sufficient accuracy. Since the distribution of the two lumps in somewhat arbitrary, Young introduced a grout allocation factor (GAF) that adjusted the distribution of the grout thermal mass between the two lumps. The GAF

value is defined as a fraction of the thermal capacity of the grout to be moved from the outside of the borehole thermal resistance to the inside of the borehole thermal resistance. The new equivalent thermal capacitance of grout and fluid was used in modeling the borehole thermal heat transfer process. A detailed finite volume model, GEMS2D (Rees 2000), was used to validate the accuracy of the BFTM model and to determine the suitable GAF values for different configurations of borehole. It was found that the best GAF value was related to borehole diameter, shank spacing, borehole diameter and fluid factor. Young attempted to find a functional relationship between GAF and these parameters, but was unsuccessful. Instead, he tabulated values of GAF for various combinations of these parameters.

Nevertheless, since the BFTM model accounts for the thermal capacity of grout and fluid, it is expected to give better accuracy of the GLHE temperature response at short time steps than the first form of the cylindrical source solution. However, Young compared the BFTM model to the line source model. He showed that, for very short duration peak loads of 1 to 2 hours, the difference in peak temperature predictions could be 1.3ºC (2.3ºF) between the BFTM model and the line source model.

Young used the BFTM model to calculate the short time response of the borehole; this was integrated with another model to find the long-term response. More details of the response factor model will be introduced in the section 2.1.1.3. Applying the BFTM model in the GLHE design procedure, Young also showed that the sizing of the ground heat exchangers could be highly sensitive to the peak temperature prediction, especially for buildings dominated by short-term peak loads. Furthermore, the temperature response

also has a secondary impact on the predicted energy consumption of the system, as the COP of the heat pump varies with entering fluid temperature. Therefore, it is desirable to be able to model the short-term behavior accurately.

2.1.1.2 Modeling of Vertical Ground Loop Heat Exchangers - Numerical

Direct numerical solutions have been used to model ground heat exchangers. Various methods have been used to solve the physical field problem, e.g. finite difference (Lei 1993; Rottmayer et al. 1997), finite element (Muraya et al. 1996; Kohl et al. 2002; Signorelli et al. 2005), finite volume model (Rees 2000). But, due to computational time requirements, these numerical models are not useful for incorporation into a building simulation program with hourly or sub-hourly time steps. In the following section, only a brief selective literature review of these numerical models will be given.

Finite Difference Method

Finite Difference Models (FDM) have been used for modeling ground heat exchangers. In FDM, the borehole/U-tube geometry is not conveniently represented in either a rectangular or a radial-angular grid. Different treatments of geometry of borehole/U-tube (Rottmayer et al. 1997; Yavuzturk et al. 1999; Rees 2000) have been used in FDM and the following discussion will focus on these treatments.

Lei (1993) developed a two-dimensional finite difference model on a radial-axial coordinate system for vertical ground heat exchanger. The Hopkins' (1983) thermal short-circuiting model was used. The model assumed that, in the vertical direction, the heat transfer in the pipe and ground was negligible and there was only heat transfer

caused by the fluid flow in the U-tube. In the horizontal cross section, it was assumed that there was only heat flow in the radial direction for all regions except in the pipe the small area between the two adjacent pipes. The U-tube interval surface area was divided into two parts: surface area that exchanges heat with an infinite ground and surface area that exchanges heat with the adjacent tube section. The former surface temperatures and areas were used as boundary conditions to calculate the heat conduction between the tube wall and the infinite ground. The latter surface temperatures were used to calculate the short-circuiting between U-tube legs. These two surface temperatures were obtained by solving the heat balance equation of each tube interval, including the heat transfer rate brought by the fluid flow. In Lei's model, the proportion of two parts of U-tube interval surface is important and depends on the geometric relation between two pipes. Lei chose six different proportion values to run the simulation and compared against experimental data. However, Lei mentioned how to divide the U-tube interval surface into two parts was not determined and needed to be investigated.

Rottmayer et al. (1997) developed a quasi-three-dimensional finite difference method for vertical single U-tube ground heat exchanger. Like Lei's assumption, Rottmayer et al. assume that the only axial heat transfer is via the fluid.

In Rottmayer et al's model, a cylindrical finite-difference grid is used for the horizontal cross section. The U-tube in the finite-difference mesh is not circular but is approximated by matching the perimeter of the modeled non-circular tube to the actual circular tube perimeter, as shown in Figure 2.3. The borehole resistance with noncircular mesh differs from the circular tube and an empirically determined geometric factor is

used to modify the thermal resistance of noncircular mesh to get a better agreement of simulated results between the noncircular mesh and the circular tube.

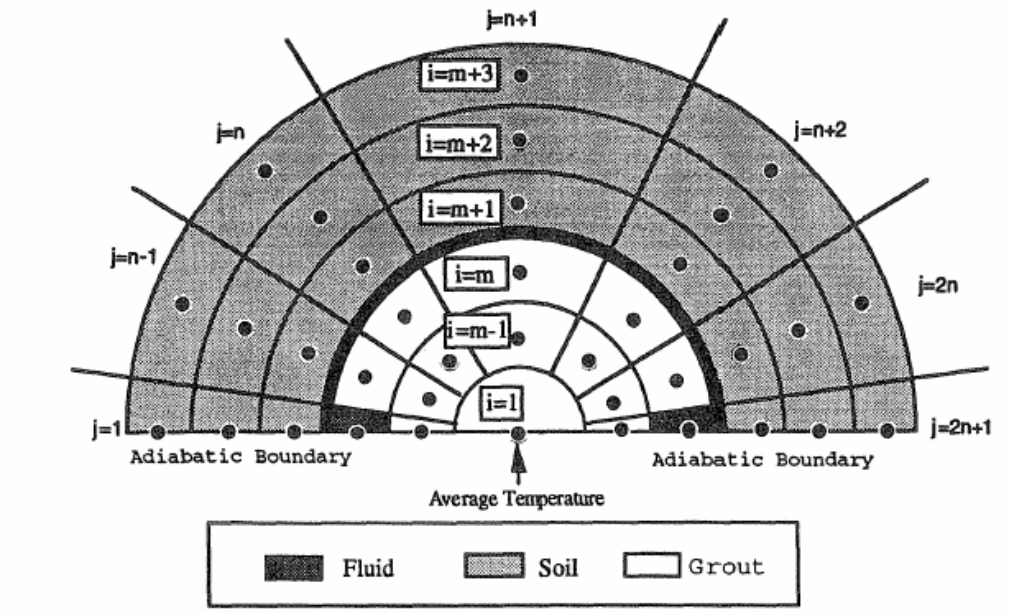

Figure 2.3 Cylindrical finite-difference grid used to calculate the heat transfer at one depth (Rottmayer et al. 1997)

In this model, the thermal mass of the tube wall and grout is neglected and the authors claim this approximation is acceptable in annual simulations. However, as the authors indicated, neglecting the pipe wall and grout capacitances might affect the short time temperature response.

Compared to Lei's model, Rottmayer et al's model presents the geometry of the borehole more accurately. But it is expected that the computational time is expensive to solve this quasi-three-dimensional numerical problem.

Yavuzturk and Spitler (1999) developed a transient two-dimensional model for vertical ground heat exchangers. Neglecting the heat transfer in the vertical direction, the

heat transfer of the ground heat exchanger was simplified as a two-dimensional (radial-angular) heat transfer problem. Similar to Rottmayer et al's work, a cylindrical finite-difference grid was used for the horizontal cross section and treatment must be adopted for modeling the non-circular tube. Yavuzturk and Spitler developed an algebraic algorithm to automatically generate numerical grids in polar coordinates for the ground heat exchanger geometry, as shown as Figure 2.4. The "pie sector" in the figure has an equivalent inner perimeter with the tube inside perimeter and has an identical wall thickness with the pipe thickness.

A constant heat flux is used as the boundary condition for the "pie-sector" approximation. In order to get near-identical result to the real geometry of the circular U-tube, an equivalent heat flux is calculated by matching the inside perimeter of the circular pipe to the inside perimeter of the pie sector and by establishing identical heat flux and resistance conditions near the pipe wall. An equivalent conductivity of pipe wall is determined which gives the same resistance as the actual convection coefficient at the inside of the U-tube and conduction though the pipe wall.

Rottmayer et al's model and Yavuzturk and Spitler's model are three-dimensional or two-dimensional numerical models and both require expensive computational time and not suitable for direct incorporation into a building simulation program with hourly or shorter time steps. However, Yavuzturk and Spitler's model accounts for the thermal mass of grout, tube wall and fluid, and is capable of modeling the short term response of ground loop heat exchanger. Yavuzturk and Spitler's model is used to generate response

factors, which are suitable for annual HGSHP system simulation. More details will be introduced in Section 2.1.1.3.

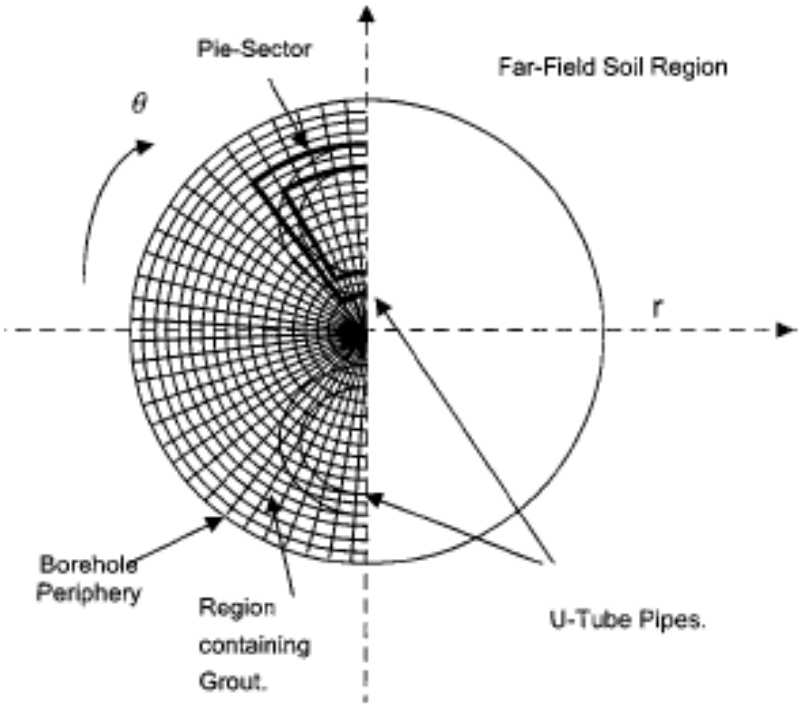

Figure 2.4 Simplified representation of the borehole region on the numerical model domain using the pie-sector approximation for the U-tube pipes. (Yavuzturk and Spitler, 1999)

Noting that the temperature distribution in the soil at a large distance from the U-tube is similar to that which is caused by single pipe, Shonder and Beck (1999) developed a one-dimensional radial finite difference model for single borehole. In this one-dimensional model, the U-tube was simplified as one tube in the borehole and an effective pipe radius was used to represent the U-tube geometry. A film was added at the outer surface of the pipe to account for the thermal capacity of the pipes and fluid. The purpose of this model was prediction of ground thermal conductivity from in-situ thermal conductivity test. Accordingly, parameters such as thermal conductivity of the thermal

film, volumetric heat capacity of the thermal film, the thickness of the thermal film and the effective pipe radius are treated as unknown and then estimated from the experimental data. While this one-dimensional model was originally developed to predict the thermal properties of the grout and soil, it might be useful for GLHE simulation if methodology for determining the parameters without experimental measurements was developed. Since this one-dimensional model requires much less computational time than the detailed numerical models, it could be suitable for incorporation into a building simulation program.

Finite Element Model

Muraya et al. (1996) developed a two-dimensional finite element model (FEM), which they used to perform a parametric study of the ground loop heat exchanger. Kohl et al. (2002) developed a three-dimensional finite element program – FRACTure (Kohl and Hopkirk 1995) for the co-axial tube borehole (Kohl et al. 2002). This program was also used for the double U-tube borehole (Signorelli et al. 2005).

One of advantages of the finite element model is that its grid scheme is able to closely represent the actual borehole with little geometrical approximation. Therefore, the finite element model can easily evaluate the impact of (1) irregular geometry because of the U-tube two legs; (2) unsymmetric loading of the two legs; (3) nonhomogeneous media caused by backfill which is used to enhance the heat transfer of the U-tube. However, due to the expensive computational time reason, these finite elemental models are not directly useful for the building system simulation.

Finite Volume Method

The heat transfer of ground loop heat exchanger can be solved by using the finite volume model (FVM). A General Elliptical Multi-block Solver (GEMS2D), a finite volume program, was developed by Building and Environment Thermal Systems Research Group at Oklahoma State University (Rees 2000) and is used to simulate the heat transfer of the ground heat exchanger (2004) and standing column well (Deng 2004).

GEMS2D is developed with both orthogonal Cartesian grids and boundary fitted grids. The boundary fitted grids enable the method to be applied to complex geometries such as U-tube in a ground loop heat exchanger. A two dimensional boundary fitted grid representing a cross section through a ground loop heat exchanger is shown in Figure 2.5. Unsymmetric loading of the two legs can be modeled. Based on Young's work (2004), GEMS2D can closely match the thermal resistances calculated by the Multipole resistance method (Bennet et al. 1987). Without the sort of simplifications required for the FDM, GEMS2D is able to solve complicated two-dimensional grids. Also the thermal mass of the borehole and fluid are accounted for in the model and GEMS2D is capable of dealing with both steady-state and transient problems. Therefore, GEMS2D was used as a reference model for the other numerical models (Deng 2004; Young 2004). However, like other detailed numerical models, the computational time of GEMS2D limits its application for the HGSHP system simulation.

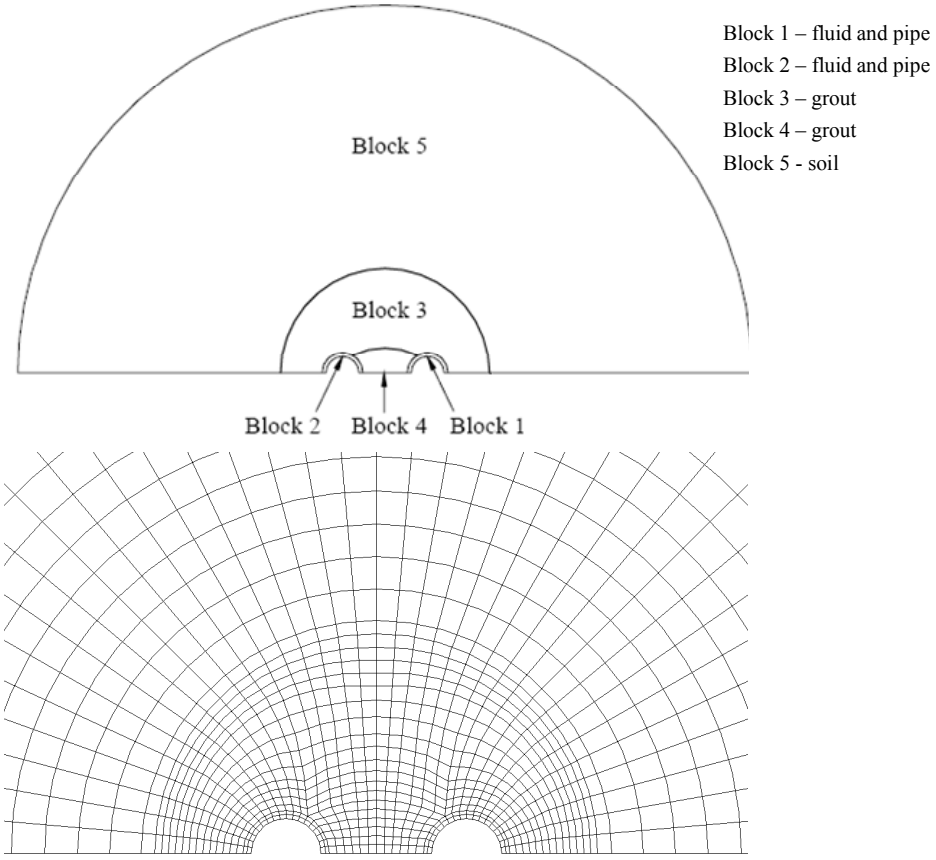

Figure 2.5 Grid for a cross section of a borehole (Young 2004)

2.1.1.3 Modeling of Vertical Ground Loop Heat Exchangers – Response Factors

A third approach, which allows for computationally efficient simulation, involves the development of response functions, used in a response factor (g-function) model, which allows the ground heat exchangers to be modeled with a time series. Eskilson (1987) developed g-functions for long time steps, and later a short time step response factor method was developed by Yavuzturk and Spitler (1999). Using the response factor model, the simulation of the ground loop heat exchanger is computationally efficient and

the annual simulation of HGSHP systems with hourly or shorter time steps becomes practical. The following section introduces the response factor models.

Long Time Step (LTS) Response Factor Model

Eskilson (1987) developed an approach to determine the temperature distribution around a borehole based on a hybrid model combining analytical and numerical solution techniques. First, a two-dimensional numerical calculation is made using transient finite-difference equations on a radial-axial coordinate system for a single borehole in homogeneous ground with constant initial and boundary conditions. The thermal capacitance of the individual borehole elements such as the pipe wall and the grout are neglected. The temperature fields from a single borehole with a step heat input are superimposed in space to obtain the response from the whole borehole field.

Secondly, the temperature response of the borehole field is converted to a set of non-dimensional temperature response factors, called g-functions. The g-function allows the calculation of the temperature change at the borehole wall in response to a step heat input for a time step. Once the response of the borehole field to a single step heat pulse is represented with a g-function, the response to any arbitrary heat rejection/extraction function can be determined by devolving the heat rejection/extraction into a series of step functions, and superimposing the response to each step function, as shown in the following example that is based on the nomenclature presented in Figure 2.6.

Multiple borehole systems are used to support the large heat pump systems. The thermal process in the ground field with a number of thermal interacting boreholes is

quite complex. Instead of using three-dimensional numerical method to solve the problem, Eskilson uses the superposition method to simply the three-dimensional heat transfer process with the complex geometry to cylindrically symmetric ones.

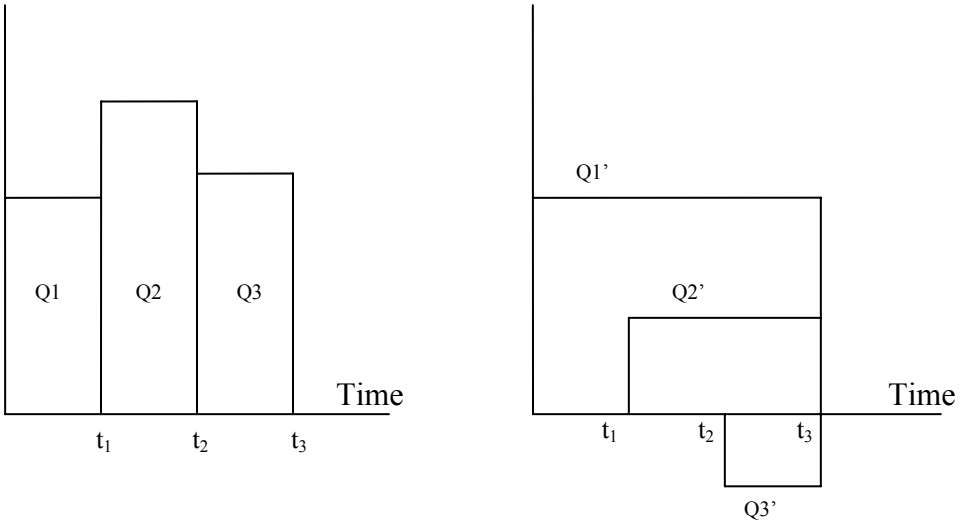

Figure 2.6 Superposition of Piece-Wise Linear Step Heat Inputs in Time

In this case, the irregular heat pulse as shown in the left of the Figure 2.5 can be discretized into several continuous heat pulses with different durations. For example, the basic heat pulse of level $Q_1'=Q_1$ applied for the entire duration from 0 to t_3. The subsequent pulses are superimposed as $Q_2'=Q_2-Q_1$ effective for time from t_1 to t_3 and $Q_3'=Q_3-Q_2$ effective for the time from t_2 to t_3. Thus, the borehole wall temperature at time t_3 can be determined by adding the responses of the three step functions. Mathematically, the superposition gives the borehole wall temperature at the end of the n^{th} time period as:

$$T_b = T_{ff} + \sum_{i=1}^{n} \frac{(q_i - q_{i-1})}{2\pi k} g\left(\frac{t_n - t_{n-1}}{t_s}, \frac{r_b}{H}\right) \qquad 2\text{-}8$$

Where:

t = Time, (s)

t_s = Time scale, defined as $t_s = H^2 / 9\alpha$, (-)

H = Borehole depth, (m)

k = Ground thermal conductivity, (W/m-K)

T_b = Average borehole temperature, (ºC)

T_{ff} = Undisturbed ground temperature, (ºC)

q = Heat rejection pulse, (W/m)

r_b = Borehole radius, (m)

i = The index to denote the end of a time step (the end of the 1st hour or 2nd month etc.)

Figure 2.7 shows the temperature response factor curves (g-functions) plotted versus non-dimensional time for various multiple borehole configurations and a single borehole. The g-functions in Figure 2.7 correspond to borehole configurations with a fixed ratio of 0.1 between the borehole spacing and the borehole depth. The thermal interaction between the boreholes is stronger as the number of boreholes in the field is increased and as the time of operation increases.

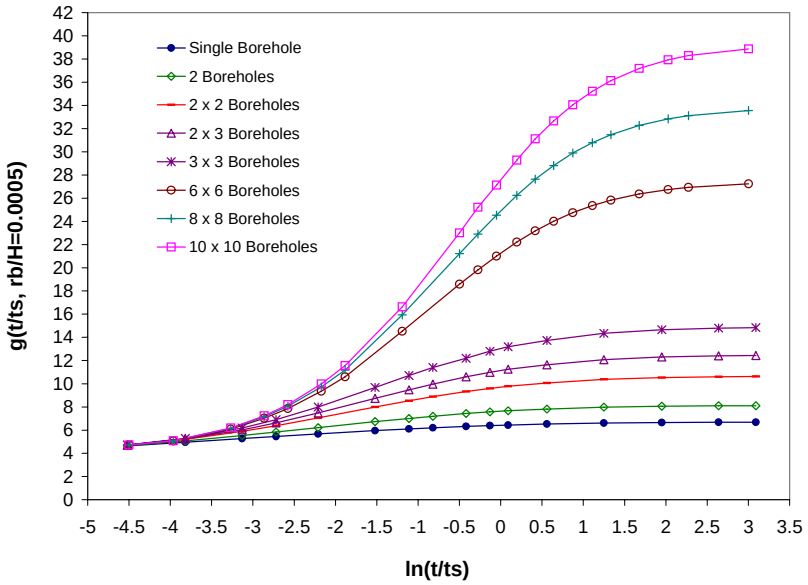

Figure 2.7 Temperature response factors (g-functions) for various multiple borehole configurations compared to the temperature response curve for a single borehole (Yavuzturk 1999)

The detailed numerical model used in developing the g-functions approximates the borehole as a line source of finite length, so that the borehole end effects can be considered. The approximation of the borehole as a finite-length line source has the resultant problem that it is only valid for times estimated by Eskilson to be greater than $5r_b^2/\alpha$. However, much of the data developed by Eskilson does not cover periods of less than a month. (For a heavy, saturated soil and a 76 m deep borehole, the g-function for the single borehole presented in Figure 2.7 is only applicable for times in excess of 60 days.) When applied for a short-time system simulation, Eskilson's method cannot accurately model a system with transient operation. Eskilson's method may then be referred to as the long time-step g-function method.

Short Time Step (STS) Response Factor Model

Yavuzturk et al. (Yavuzturk and Spitler 1999; Yavuzturk et al. 1999) extended Eskilson's long time-step model to short time steps by developing short time-step g-functions with a two-dimensional (radial-angular) finite volume method, which utilized an automated gridding procedure and a "pie-sector" representation of the U-tubes. The two-dimensional numerical method was discussed previously in Section 2.1.1.2. Because the short time-step g-function represented the response of the entire ground heat exchanger including the fluid, it necessarily utilized a fixed convective resistance.

The short time-step g function values can be obtained from the borehole temperature and they line up very well with Eskilson's long time-step g functions. For typical rations of borehole radius to borehole depth, the short time-step g function data respond to the time step between 2.5 minutes and 200 minutes. For practical purpose, the short time-step response factor model is used for the time shorter than 200 hours and the long time-step response factor model is applicable for the time longer than 200 hours (Yavuzturk 1999).

Using the short time-step g function model, Yavuzturk and Spitler (1999) developed a TRNSYS component model for GLHE and presented an annual hourly simulation of the GSHP system. Later, Yavuzturk and Spitler (2001) validated the short time-step model of the vertical GLHE against the actual operational data from an elementary school building.

Following the same general approach, but with a simpler model of the borehole, Young's BFTM model (2004) was also used to generate the short time step response factors of GLHE. Integrated with Eskilson's long time-step response factor model, a

response factor model of the GLHE was built into GLHEPRO (Spitler 2006), which is a tool for designing ground loop heat exchangers for use with ground source heat pump systems.

Response factor models of GLHE can simulate the heat transfer of ground loop heat exchanger in any time scale. These models are computationally efficient, and therefore suitable to run an annual simulation of GSHP system with hourly or sub-hourly time steps in a relatively short time.

2.1.1.4 Modeling of Vertical Ground Loop Heat Exchangers – Load Aggregation Algorithm

In analytical and response factor models of ground loop heat exchangers, the current borehole wall temperature is calculated by superimposing the response from different "historical" heat pulses with different durations, as shown in Figure 2.6. For a long time period simulations, the computational time for superposition of the "historical" temperatures would be considerable expensive. However these temperature changes are negligible when happened time of the "historical" heat flux is long enough. Therefore, some load aggregation algorithms have been developed to deal with the "historical" heat flux and try to save the computational time and they are introduced in this section.

Deerman and Kavanaugh's Work

Deerman and Kavanaugh (1991) described two simplified methods to truncate the cumulative effect of the prior heat flux on the temperature of current time. Method 1 includes one prior day's heat flux effect on the temperature change of the current time.

Method 2 sets the number of prior days based on the magnitude of the current daily run time fraction of heat pumps. The rule of method 2 is descried as follows: (1) when the current run fraction of heat pumps is greater than 35%, then no prior days will be considered, and (2) when the current run fraction of heat pumps is 10%, 15 prior days "historical" heat flux would be used. Based on the comparison against the measurement data, Deerman and Kavanaugh suggested that method 1 should be used for both hourly and daily simulations.

Yavuzturk and Spitler's Work

Yavuzturk and Spitler (1999) developed a loads aggregation algorithm for ground loop heat exchangers. The loads on the ground loop heat exchanger were divided into the "lumped" and immediate thermal history. The loads that occur more than a certain time ago (for example, 192hours) were be "lumped" together into large blocks and an average heat flux was used for calculating the temperature response. For any give time-step after the first load-aggregated time block, the average borehole wall temperature is computed by superimposing the temperature changes from the "lumped" block loads and then the temperature changes from the short time-step loads. By using this load aggregation algorithm (192 hours recent history and lumped periods of 730 hours), for a 20-year hourly time step simulation, the computational time was reduced to less than 1% of non-aggregated scheme (Yavuzturk 1999).

Bernier et al. Work

Bernier (2001; 2004) developed a load aggregation scheme for ground loop heat exchanger. Bernier (2001) split the historical heat flux into two time periods at the time t_m. The borehole wall temperature varying caused by the heat flux before the time t_m is calculated by an average heat transfer rate over the time interval from 0 to t_m. The temperature varying after the time t_m to the current time t_n is calculated by the individual heat transfer rate of each period.

Bernier made a comparison of the computational time, the heat pump and pump energy consumption by using different $t_n - t_m$ values as 24, 168, 672 and 1344 hours. The computational time in case of 24 hours was 2.2% of the time for the case of 1344 hours. The maximum fluid temperature leaving the heat pump of the 24-hour case was 5°C (9°F) lower than the temperature of the 1344-hour case. The annual energy consumption of the heat pump(s) and circulation pump(s) in case of 24 hours was 3.3% lower than the annual energy consumption for the case of 1344 hours.

As the follow-up study, Bernier et al. (2004)) developed a multiple load aggregation algorithm (MLAA) for the GSHP system. As with the previous work, the loads were divided into main intervals under the "past" and "immediate" thermal history. The new feature is that the "past" thermal history has four time intervals, defined as daily, weekly, monthly and yearly time intervals. Period X_m, X_w, X_d and X_h of 360, 168, 48, and 12 hours are recommended for the ground loop heat exchanger simulation. Applying MLAA, the one-year and ten-year simulations of GSHP system were compared against the DST method results (Hellstrom 1991) and had a very good agreement. It took three

minutes to run annual hourly simulation of GSHP system with the MLAA on a Pentium 166 MHz PC equipped with 32MB RAM and using Windows 98.

2.1.2 Heat Pump Model

In HGSHP systems, air-to-water or water-to-water heat pumps are used. The approaches for modeling heat pump generally fall into extremes which are detailed deterministic models and equation-fitting models.

Detailed deterministic heat pump models are based on applying thermodynamic laws and fundamental heat and mass transfer relations for individual components, namely compressor, expansion device, condenser and evaporator (Parise 1986; Bennet et al. 1987; Cecchini and Marchal 1991; Stefanuk et al. 1992; Iu et al. 2003). Parameters are introduced to describe the detailed physical geometry and operation of each component. The model is able to reproduce the behavior of the actual units. Detailed deterministic heat pump models require many details for each component to get the parameters, which are usually not available from heat pump manufacturers' catalogs, such as compressor speed, displacement volume, clearance ratio (Parise 1986), saturation pressures in both evaporator and condenser, superheating and subcooling (Cecchini and Marchal 1991). Therefore, detailed deterministic heat pump models are usually suitable for heat pump designers but not for engineers designing heat pump system and who only have heat pump manufacturer catalog data available.

Equation-fitting heat pump models treat the system as a black box and fit the system performance to one or a few equations (Lash 1992; Tang 2005). The equation

coefficients are estimated from the catalog data using somewhat procedures. The equation-fitting approach does not require internally measured data, thus the equation-fitting models are suitable for users that only have access to manufacturers' catalog data. As mentioned above, the parameters are estimated from the catalog data and the models usually have a good prediction of heat pump performance. In actual practical systems, the fluid temperatures and flow rates occasionally go beyond the catalog data. Therefore, the equation-fit model may not be able to predict heat pump performance well when the fluid temperatures and/or flow rates are too high or too low.

Jin and Spitler (2002; 2003) developed a parameter estimation-based heat pump model. This model is developed from the detailed deterministic approach, but it only requires input data that are readily available from manufacturers' catalog. The parameters were estimated from catalog data using a multi-variable optimization procedure. This new heat pump model has a better capacity of modeling heat pump than the equation-fitting model and allows some extrapolation beyond the catalog data.

In this HGSHP system study, Tang's (2005) equation-fit heat pump model and Jin and Spitler's (2002) parameter estimation heat pump model equation-fit model are used for modeling a single heat pump. However, in the study of a multiple heat pumps system, an equation-fit multiple heat pump model is used to simplify the system simulation without modeling each single heat pump.

In the study of buildings with many heat pumps, it is difficult to model each heat pump independently. As an alternative, a new "gang-of-heat-pumps" model will be developed.

2.1.3 Cooling Tower/Fluid Cooler Model

In an HGSHP system, cooling towers or fluid cooler are typically used as the supplemental heat rejecter. There are two-basic types of cooling tower: open-circuit cooling tower and closed-circuit cooling towers. The open cooling tower exposes water to be cooled directly to the atmosphere and is also called a direct-contact cooling tower. In the closed-circuit cooling tower, the fluid to be cooled flows in the internal circuit and never contacts the atmosphere and the tower is also called an indirect-contact cooling tower.

Using open-circuit cooling tower as the heat rejecter for HGSHP systems has disadvantage of turning low-maintenance GSHP system into high-maintenance HGSHP system. Also, due to concerns about legionnaires' disease, many building owners are reluctant to use open-circuit cooling tower. A closed-circuit cooling tower/fluid cooler can be used as a supplemental heat rejecter. The closed-circuit cooling tower/fluid cooler requires low maintenance and water treatment, and can be operated during the winter without labor-intensive anti-icing measures.

2.1.3.1 Modeling of Cooling Tower/Fluid Cooler

A number of cooling tower models has be developed for both open cooling towers (Bernier 1994; Soylemez 1999; Benton et al. 2002; Lebrun and Silva 2002; Khan et al. 2004; Kloppers and Kroger 2005) and closed-circuit cooling tower/fluid coolers (Zalewski and Gryglaszewski 1997; Hasan and Siren 2002; Lebrun et al. 2004; Stabat and Marchio 2004; DOE 2007).

The fundamental heat transfer theory of the open cooling tower was developed by Merkel (1925). In Merkel's model, three critical assumptions used to simplify the calculation are the Lewis factor is equal to 1, the air exiting the tower is saturated vapor and the water loss due to evaporation can be neglected.

Based on the same assumptions of Merkel's model, Webb et al. (Webb 1984; Webb and Villacres 1984) introduced the effectiveness-NTU (number of transfer units) (ε-NTU) design method for counterflow or crossflow cooling towers. The ε-NTU method usually only requires dry-bulb, wet-bulb, and water inlet temperature as input data to predict the performance of cooling tower. It is suitable for users that have limited data available.

Various methods have been used to practically size and predict cooling tower (Soylemez 1999) based on NTU method, e.g. variable UA model for indirect-contact cooling tower model (Stabat and Marchio 2004), variable UA model for both direct and indirect contact cooling tower model (Lebrun and Silva 2002; Lebrun et al. 2004), the fouling model for the open cooling tower (Khan et al. 2004).

Beyond the ε-NTU method, more detailed models have been developed for cooling tower (Bernier 1994; Zalewski and Gryglaszewski 1997; Hasan and Siren 2002; Kloppers and Kroger 2005). These models divide the cooling tower into small elements along the height of cooling tower and heat and mass transfer are considered for each elemental volume. The arrangement of tubes may or may not be considered (Hasan and Siren 2002). These detailed models can predict how cooling tower performance is

affected by fill height, water retention time, and air and water mass flow rates. However, these models need data which are usually not available from manufacturer catalogs.

In this study of HGSHP system, an ε-NTU method will be used for modeling both open and closed-circuit cooling towers. Also a fluid cooler model will be developed.

2.1.3.2 Control of Cooling Tower/Fluid Cooler

Most of the time, cooling towers and fluid coolers are not running at their full capacity. Accordingly, some form of capacity control is required to optimally control a cooling tower to maintain desired fluid temperatures and to give the best performance. EPRI (1993) and ASHRAE (2000) have presented several scenarios for control the cooling tower: a bypass valve, modulating dampers, fan cycling, a two-speed fan, variable frequency drives (VFD), and multiple cells.

When a cooling tower is to be used in subfreezing climates, treatment is required to prevent the cooling tower from freezing. For an open cooling tower, capacity control is used to maintain the temperature of the water leaving the tower well above freezing. For closed-circuit cooling towers, a common protection is to use an antifreeze solution. Or supplemental heat may be provided to the heat exchanger. ASHRAE Standard 90.1 also suggests, in a closed-circuit tower, a minimal flow of water around the tower shall be provided for freeze protection. However, this minimal flow protection might also be applied in open cooling tower, especially in where the atmosphere temperature is only occasionally below zero.

In this study of HGSHP system, a single speed fan cooling tower/fluid cooler will be used as the supplemental heat rejecter.

2.2 HGSHP Systems and Control Approaches

In this section, hybrid GSHP system configurations will be discussed. Secondly, design procedures for HGSHP system will be reviewed. Then, performance of several real and hypothetical hybrid GSHP systems will be presented. In addition, currently recommended controls of HGSHP systems will be summarized.

2.2.1 HGSHP System Configuration

The design of an HGSHP system has many degrees of freedom and there are many possible configurations of HGSHP systems. For example, the supplemental heat rejecter can be in series or in parallel with the ground heat exchanger. Flow to individual heat pumps might be controlled with two-way valves or primary-secondary pumping. The supplemental heat rejecter might be an open cooling tower, a closed-circuit cooling tower or a dry fluid cooler.

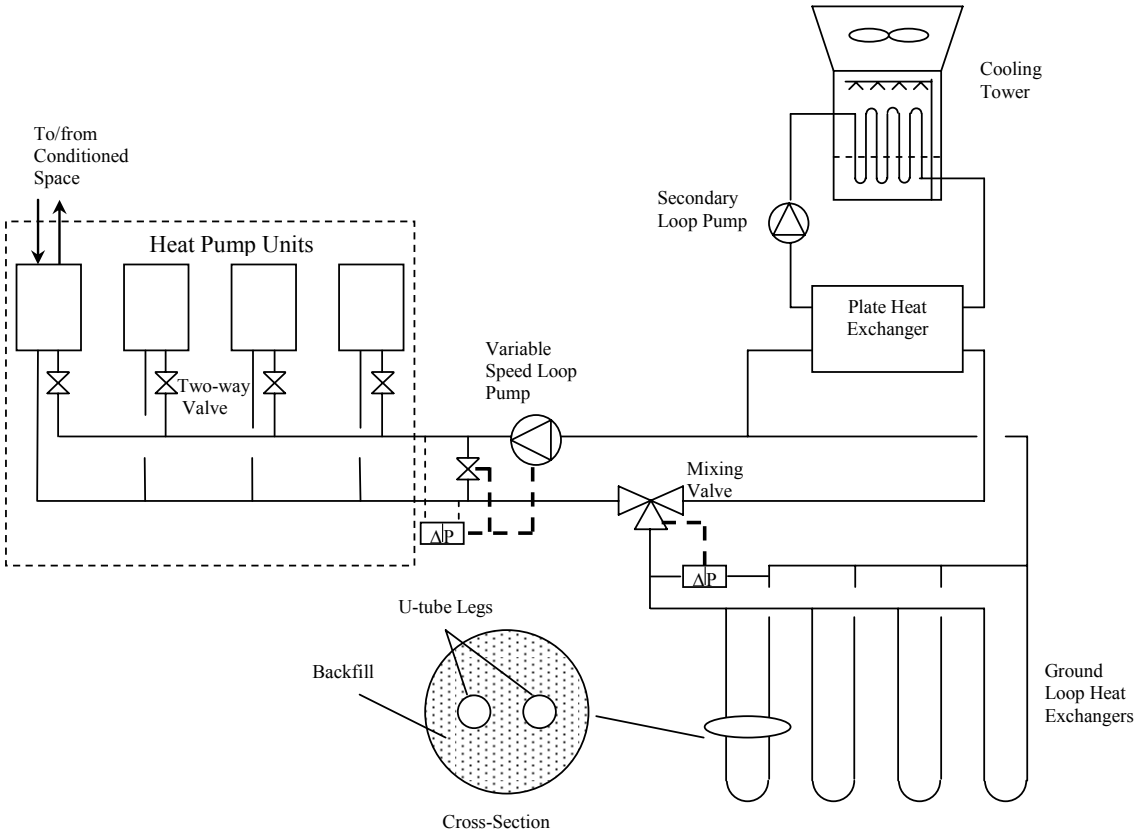

Figure 2.8 A schematic of a typical hybrid GSHP system using a closed-circuit cooling tower as a supplemental heat rejecter

A common configuration of the system uses a cooling tower or fluid cooler as the supplemental heat rejecter, as shown in Figure 2.9. For this configuration, the tower is typically isolated from the ground loop heat exchanger with a plate frame heat exchanger. The ground loop heat exchanger and the plate frame heat exchanger are placed in parallel in the system and a mixing valve is used to control the fluid flow through these two components. This "parallel-connected" system layout is suitable for an HGSHP system with large flow rate and a relatively small number of boreholes. In this case, all of the system flow cannot feasibly pass through the GLHE without requiring excessive pumping power. No recommendation for distribution of the flow between the GLHE and

the plate heat exchanger are given in the literature. However, distribution must be made and this will be investigated in this study.

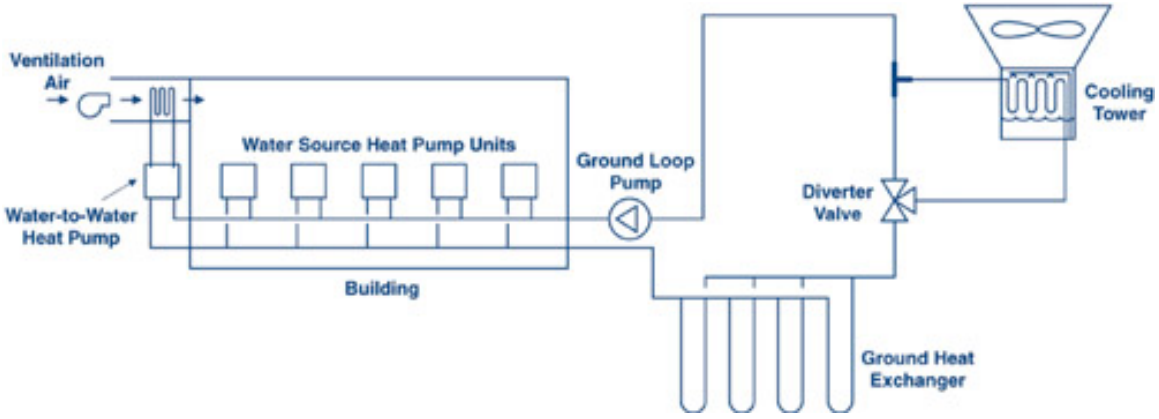

Figure 2.9 A schematic of a typical hybrid GSHP system using a closed-circuit cooling tower as a supplemental heat rejecter (DOE 2006)

Another configuration of the HGSHP is shown as in Figure 2.9. For this system, the tower (presumably a closed-circuit tower) is piped in series with the ground heat exchanger. This "serially-connected" system layout is suitable for the system with a relatively small cooling tower and large number of boreholes. In this case, the entire system flow can pass through the boreholes and the pressure drop will still be acceptable. A diverter valve is used to control the flow rate through the cooling tower.

2.2.2 HGSHP System Design Method

Designing an HGSHP system requires sizing of both GLHE and supplemental heat source or sink. In the following section, the literature related to sizing these two components will be reviewed.

2.2.2.1 Sizing GLHE of GSHP System

Several procedures are available for sizing the vertical ground loop heat exchanger of GSHP system, such as IGSHPA (Bose 1984), Kavanaugh et al. (Kavanaugh and Rafferty 1997; Kavanaugh 1998). Also some commercial software is available for vertical ground heat exchanger design, such as GLHEPRO (Spitler 2006), GCHPCalc (GeoKISS 2006), GS2000^{TM} (CRI 2006), Ground Loop Design (GaiaGeothermal 2006), GLD (GBTI 2006). Shonder et al. (1999; 2000) compared six vertical ground heat exchanger design methods for residential and commercial applications. However, the only published procedures for sizing HGSHP are given by Kavanaugh and Rafferty (1997) and Kavanaugh (1998). These are discussed in the following section.

2.2.2.2 Sizing GLHE and Supplemental Heat Source or Sink of HGSHP System

Kavanaugh and Rafferty (1997) gave a design procedure for sizing the GLHE and supplemental heat source or sink of the HGSHP system and later Kavanaugh (1998) revised this design procedure.

Firstly, Kavanaugh and Rafferty developed a procedure (they referred to this as the "Long Way" procedure) to calculate the required length for the 100% geothermal ground source heat pump system. The required borehole length for cooling is:

$$L_c = \frac{q_a R_{ga} + (q_{lc} - 3.41\overline{W}_c)(R_b + PLR_m R_{gm} + R_{gd} F_{sc})}{t_g - \frac{t_{wi} + t_{wo}}{2} - t_p} \qquad (2\text{-}9)$$

The required borehole length for heating is:

$$L_h = \frac{q_a R_{ga} + (q_{lh} - 3.41\overline{W}_h)(R_b + PLR_m R_{gm} + R_{gd} F_{sc})}{t_g - \frac{t_{wi} + t_{wo}}{2} - t_p} \qquad (2\text{-}10)$$

Where:

F_{sc} = short-circuit heat loss factor, (-)

L_C = required borehole length for cooling, (ft)

L_h = required borehole length for heating, (ft)

PLF_m = part-load factor during design month, (-)

q_a = net annual average heat transfer to the ground, (Btu/h)

q_{lc} = building design cooling block load, (Btu/h)

q_{hc} = building design heating block load, (Btu/h)

R_{ga} = effective thermal resistance of the ground, annual pulse, (h-ft-ºF/Btu)

R_{gd} = effective thermal resistance of the ground, daily pulse, (h-ft-ºF/Btu)

R_{gm} = effective thermal resistance of the ground, monthly pulse, (h-ft-ººF/Btu)

R_b = thermal resistance of borehole, (h-ft-ºF/Btu)

t_g = undisturbed ground temperature, (ºF)

t_p = temperature penalty for interference of adjacent borehole, (ºF)

t_{wi} = liquid temperature at heat pump inlet, (ºF)

t_{wo} = liquid temperature at heat pump outlet, (ºF)

$\overline{W_c}$ = power input at design cooling load, (W)

$\overline{W_h}$ = power input at design heating load, (W)

In the above formulas, heat transfer rates, building loads, and temperature penalties are positive for heating and negative for cooling.

In the design manual, Kavanaugh and Rafferty (1997) describe detailed procedures to determine each term in Equations 2-10 and 2-11, including U-tube thermal resistance R_b, soil properties and ground thermal resistance (R_{ga}, R_{gd} and R_{gm}), heat rates for the system (PLF_m, q_a, q_{lc}, q_{lc}, $\overline{W_c}$ and $\overline{W_h}$), and GCHP system temperature (t_g, t_{wi}, t_{wo} and t_p).

After getting two borehole lengths for heating and cooling of the system, a larger one will be chosen as the borehole length of the 100% geothermal ground source heat pump system.

In the "Long Way" design procedure, zone-by-zone design day loads and annual equivalent heating and cooling hours are required and the heat rates for the system is calculated with a spreadsheet procedure. To simplify the calculation procedure, a "Shorter Method" was described in the design manual (Kavanaugh and Rafferty 1997). The simplified method includes:

1. Using the building block load rather than zone-by-zone loads.

2. Using estimates of average equivalent full-load operating hours rather than individual zone hours.

3. Using average values of equivalent EER and COP rather than using individual unit values.

4. Using the tabulated values to estimate the temperature penalty t_p due to long-term heat change in the ground loop.

Then Equation (2-10 and (2-10 are simplified to

$$L_c = \frac{q_a R_{ga} + (C_{fc} \times q_{lc})(R_b + PLR_m R_{gm} + R_{gd} F_{sc})}{t_g - \frac{t_{wi} + t_{wo}}{2} - t_p} \qquad (2\text{-}11)$$

$$L_h = \frac{q_a R_{ga} + (C_{fh} \times q_{lh})(R_b + PLR_m R_{gm} + R_{gd} F_{sc})}{t_g - \frac{t_{wi} + t_{wo}}{2} - t_p} \qquad (2\text{-}12)$$

Where:

C_{fc}, C_{fh} = Correction factors account for the amount of heat rejected or absorbed by the heat pumps. The values depend on the respective EER and COP of the units and are provided in the design manual.

And the net annual average heat transfer to the ground, q_a is calculated by

$$q_a = \frac{C_{fc} \times q_{lc} \times EFLH_c + C_{fh} \times q_{lh} \times EFLH_h}{8760 \quad Hours} \qquad (2\text{-}13)$$

Where:

$EFLH_c$, $EFLH_H$ = Annual equivalent full-load cooling and heating hours, hours.

For the cooling or heating constrained GSHP system, a supplemental heat source or sink is incorporated to eliminate the imbalance of the ground thermal load (More discussion about the cooling/heating constrained is presented in Section 6.3.1). Kavanaugh and Rafferty (1997) gave a design procedure for sizing the borehole and supplemental heat source or sink of a HGSHP system, later revised by Kavanaugh (1998). After calculating the required borehole lengths for the cooling demand and heating demanding respectively, the supplemental heat source or sink is sized from the difference between the two required borehole lengths. For a cooling constrained GSHP system, the required borehole length for cooling is greater than the required heating length. Therefore, when designing an HGSHP system, the borehole length of the hybrid ground source heat pump system is sized to meet the heating loads of the system, and it will handle some portion of the system cooling loads as well. The additional system cooling loads are handled by the supplemental heat rejection component(s). Similarly, for a heating constrained GSHP system, the required borehole length for cooling is less than the required heating length. For the HGSHP system design, the borehole length of the hybrid ground source heat pump system is sized to meet the system cooling loads, and it will handle some portion of the system heating loads as well. The additional system heating loads are handled by the supplemental heat source(s).

After getting the capacity, the cooling tower is specified by the nominal water flow rate, which is defined as the flow rate of water cooled from 95ºF to 85ºF with a 78ºF

wet bulb temperature. However, in an actual HGSHP system, the peak inlet water temperature of cooling tower might be higher than 95ºF (110ºF) and the local peak wet bulb temperature is often lower than 78ºF. As a result, the cooling tower/fluid cooler would provide more cooling capacity than the nominal capacity expected in the HGSHP system. Therefore, Kavanaugh's design procedure will tend to oversize the cooling tower/fluid cooler.

Later, Kavanaugh (1998) recommended a new procedure based on the "Shorter Method". The new recommended procedure is:

1. Use Equation (2-11 and (2-12 to get the required borehole lengths for heating and cooling respectively. And the total flow rate of the system is also calculated. The optimal flow rate of the system is usually between 2.5 to 3.0 gpm/ton (Kavanaugh and Rafferty 1997).

2. Choose a minimum design heat pump entering water temperature (EWT) to calculate the required borehole length for heating. In warm climates, a value of 45ºF (7ºC) for EWT is recommend to avoid the use of antifreeze solution of the system. This calculation will reduce the borehole length to a smaller but acceptable value.

3. Size the cooler using the Equation (2-14 based on the assumption that fluid has a 10ºF temperature change through both the heat pump condenser and cooling tower. In that case, the capacity of heat pump and cooler can be specified by giving the fluid flow rate of the each component.

$$gpm_{cooler} = gpm_{system} \times \frac{L_c - L_h}{L_c} \quad (2\text{-}14)$$

Where:

gpm_{cooler} = Heat rejection capacity of cooler in gallons per minute (gpm) based on a 10ºF range. To convert this to Mbtu/h, multiple gpm by 5, and to convert to kW, multiply gpm by 1.465.

4. Recalculate the net annual average heat being rejected into the ground q_a based on the current capacity of the fluid cooler. For typical buildings (occupancy 40 to 100 hours per week with internal loads less than 50% if the total at design cooling conditions), new equivalent full-load hours in cooling ($EFLCH_C$) are estimated from:

$$EFLH_{c,new} = EFLH_{c,old} \times (1 - \frac{gpm_{Cooler}}{2 \times gpm_{sys}})$$

5. Repeat Step 2, Step 3 and Step 4 until the calculation of the size of the fluid cooler is converged.

6. The required operating hours of the fluid cooler $Hours_{Cooler}$ is calculated by:

$$Hours_{Cooler} = \frac{C_{fc} \times q_{lc}(Btu/h) \times EFLH_c - C_{fh} \times q_{lh}(Btu/h) \times EFLH_h}{500 \times gpm_{cooler} \times Range(^oF)} \quad (2\text{-}15)$$

or

$$Hours_{Cooler} = \frac{C_{fc} \times q_{lc}(watts) \times EFLH_c - C_{fh} \times q_{lh}(watts) \times EFLH_h}{Specific \quad Heat \times Mass \quad Flow \quad Rate \times Range(^oC)} \qquad (2\text{-}16)$$

Using the revised GSHSP system design procedure, Kavanaugh (1998) presented an example of HGSHP design procedures in three locations: Mobile, Ala., Louisville, Ky,; and Minneapolis, Minn. The results showed that the HGSHP system is more economic in moderate climates where the required borehole length for cooling is much greater than the required borehole length for heating. In that case, the savings of the drilling costs more than offsets the increased maintenance costs and for the cooler.

The procedures described above are intended for design of a new HGSHP system. In some existing GSHP systems, an improperly-sized GLHE can not meet the cooling/heating loads of the system. In this case, a supplemental heat source or sink is added into the system to help meet loads of the system. This might be referred to as a "retrofit design". Because Kavanaugh's design procedure simultaneously sizes the GLHE and supplemental heat rejecter, it cannot be used for sizing heat source when the GLHE size is fixed. At this point, Kavanaugh's design procedure cannot be used for sizing heat source or sink for a "retrofit" HGSHP system. Therefore, a suitable design procedure is desired. Also as mentioned above, Kavanaugh's design procedure will tend to oversize the cooling tower/fluid cooler and an improved procedure should be investigated.

2.2.3 HGSHP System Performance

The design of an HGSHP system depends on various factors, such as investment budget, building layout, available layout of borehole field, geological conditions, etc. The

design and performance of several real and hypothetical HGSHP systems have been published. In this section, published work on HGSHP system design and operation is summarized.

2.2.3.1 K-12 School Building, Southeastern Wyoming

Chiasson et al. (2004) examined energy-saving opportunities in a retrofit of an HVAC system for a typical kindergarten through twelfth grade (K-12) school in Southeastern Wyoming using an HGSHP system with a supplemental solar thermal collector array and ventilation air heat recovery.

The building is a 4,925m^2, single-story school building and is divided into six main zones. In each zone, an air handling units (AHU) is used to distribute air to each room. Two different configurations of hypothetical GSHP system were designed for the school building. Decentralized GSHP systems, were used for each classroom, which has its own ground loop. A central HGSHP system with ground loop and solar collector array is used to handle all the non-classroom building loads and all outdoor air loads, as shown in Figure 2.11. A constant flow pumping system was simulated in the solar collector loop. A variable flow pumping system was used in the primary building loop.

The solar collector was activated when two conditions were met: (1) solar radiation was greater than zero; and (2) the exiting fluid temperature from the solar collector was greater than its entering fluid temperature. The flow rate in the primary building loop was scaled to the peak flow rate according to the ratio of the current hourly load to the peak building load.

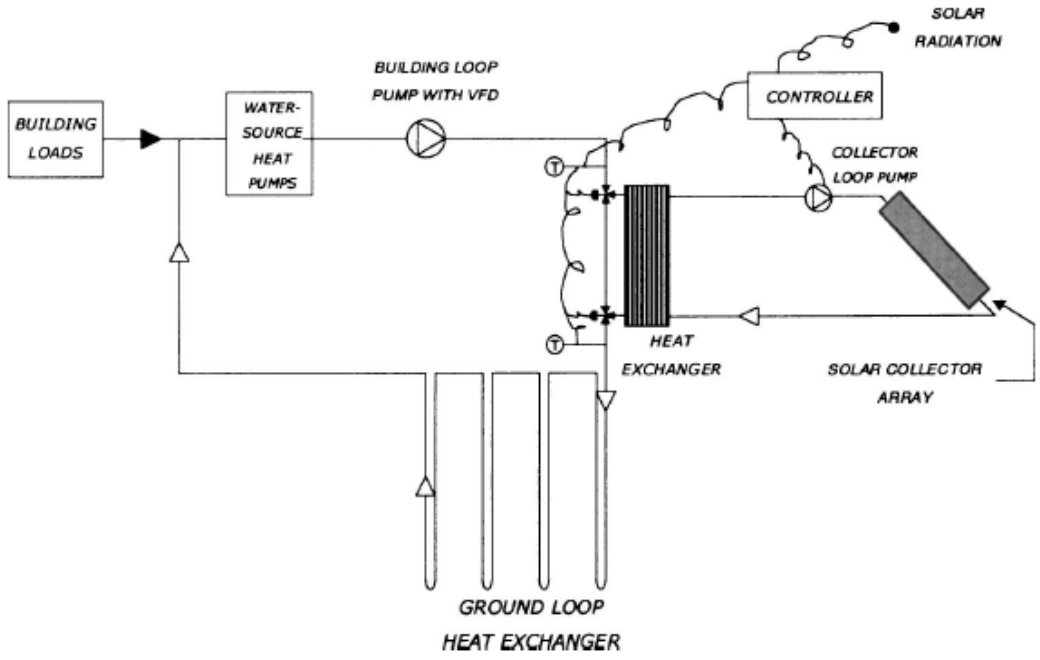

Figure 2.10 Schematic diagram of the geothermal heat pump/solar collector system (Chiasson et al. 2004)

Chiasson and Yavuzturk simulated the hypothetical HGSHP system and compared against the simulated existing AHU system. First, the results show that the use of the solar collector array yields a savings in the central GLHE size of 34%. Secondly, the results showed that new GSHP/HGSHP system would save about 74% operating energy annually and a large portion of saving is from eliminating AHU fan power. Consider the first cost of the retrofit system, the proposed GSHP/HSGHP system yields a simple payback period of about 9.5 years.

Chiasson and Yavazturk (2003) also presented a study of this same school building, located in six U.S. cities using typical meteorological year (TMY) weather data. Both fixed solar collector array and an azimuth-tracking solar collector array were investigated for the HGSHP system. The authors carried out an economic analysis based on different ground thermal conductivities, borehole drill costs. Increasing the thermal

conductivity of the ground would result in a decrease in the reduction of GLHE length per unit collector area. The HGSHP system with solar collectors was economically viable at drilling costs exceeding a range of $6/ft to $10/ft.

2.2.3.2 Building 1562, Fort Polk, LA

Phetteplace and Sullivan (1998) investigated a hybrid GSHP system with a closed-circuit cooling tower. A 24,000ft^2 (2,230m^2) administration building, at Ft. Polk, La., was renovated in 1994. The new system includes 14 water-to-air heat pumps with a total cooling capacity of approximately 120 tons (422kW). The system includes 79 closed-loop vertical geothermal wells and a 78 ton (274kW) closed-circuit cooling tower. The cooling tower and the geothermal well are placed in series. Because the total flow rate in the system was about 300gpm (18.9L/s) and greater than the nominal flow rate of the cooling tower (100gpm, 6.3 L/s), a bypass across the cooling tower was designed.

The cooling tower was controlled by the water loop temperature. The cooling tower and sump pump were activated when the loop temperature leaving the heat pumps reached 97ºF (36ºC). The cooling tower and sump pump were off when loop temperature was lower than approximately 95ºF (35ºC).

The information of all the components was measured to inspect the performance of the HGSHP system. The measurement results showed, for 22 months of operation, the ground loops rejected about 2,304 Mbtu (765 MWh) of heat, while they supplied 53.2 Mbtu (15.6 MWh) of heat. The cooling tower rejected a total of 2,375 Mbtu (696 MWh) during the whole period.

Over the 22 months period, the total energy consumption for the HGSHP system was 726 MWh. The energy consumption of the heat pump is about 77% of the total, the circulation pump is about 19%, the closed-circuit cooling tower is 3%, and the tower sump pump is 1%. Since a constant flow circulation pump was designed for the system, a large pumping energy consumption was observed. Phetteplace and Sullivan predicted the total energy consumption of the system if a variable speed pumping system was incorporated. As a result, the total energy consumption of the system would be reduced by 8.5% and the circulating pump energy would be reduced by 45%.

Phetteplace and Sullivan observed a maximal loop temperature (105.6 ºF) of the system. At this temperature, the efficient of the heat pump would be lower than desired. The reason was that a 97ºF (36ºC) set point was used to control the cooling tower, however, a set point value of 85ºF (29.4ºC) was originally recommended by the designer. Phetteplace and Sullivan noticed that the average run time for the cooling tower over the 22 months was approximately 30%. To prevent the loop temperature from continuously rising over the operation periods, a lower set point temperature was recommend by Phetteplace and Sullivan to increase the run time of the cooling tower to reject more heat to the ground. According to their analysis, if the EWT were lowered from its average value of 94.6ºF (34.8ºC) to an average value of 85ºF (29.4ºC), the cooling EER would increase by 9%. Thus, the energy consumption of heat pumps would drop by 9% and the total system energy consumption would drop by 7%. Even if the cooling tower energy consumption was doubled, the increase in energy consumption would be offset by the increased cooling performance of the heat pumps.

2.2.3.3 Paragon Center - Allentown, PA

The Paragon Center is a 7432 m^2 (80,000ft^2), 4-story office building in Allentown, Pennsylvania (Singh and Foster 1998). The original system design for the building was a 100% geothermal closed loop heat pump system, with 55 boreholes, 52 m (152ft) deep. However, subsequent drilling in the intended ground loop location was not able to go below 33.5 m (115ft) because of the high water flow in a limestone strata. Either drilling a 52m deep borehole or increasing the number of boreholes at the 33.5m borehole depth would increase the installation costs and exceed the project budget.

Instead of a 100% geothermal heat pump system, the system design was modified to use a hybrid ground source heat pump system with a closed circuit cooler. A total of 88 boreholes, 38m (125ft) deep was used for 281 kW (80tons) of cooling capacity of the system and a closed circuit cooler was selected to remove the remaining 422 kW (120tons) of cooling capacity. Using the hybrid GSHP system, the first cost of the projected was able to be controlled within the construction budget.

Singh and Foster did not mention the control strategy of the hybrid system. They noted that after using the heat recovery, variable speed drives on the pump and monitoring control, over more than two full years of operation, the project annual operating cost was less than \$0.0929/m^2 (\$1.00/ft^2) at an average electric cost of \$0.08/kWh, including demand charges.

2.2.3.4 Elementary School Building, West Atlantic City, NJ

An elementary school, in the Atlantic City, New Jersey area, has total 7898m^2 (85,000ft^2) conditional space (Singh and Foster 1998). (More details were given in Section 1.1) The total cooling requirement including the outside air is 967kW (275tons). Using heat recovery equipment, the cooling requirement for the loop would be reduced to 879 kW (250 tons). The original design was a 100% closed loop geothermal heat pump system with 90 boreholes, 122m (400ft) deep.

The available area was not sufficient for the 90 borehole arrangement. Therefore, a hybrid GSHP system with a closed circuit cooler was designed to reduce the number of boreholes to fit within the available area. The revised system design incorporated 66 boreholes, 122 m (400ft) deep to cover all the heat extraction of the system and to provide 468 kW (133 tons) of cooling capacity. The additional 411 kW (117 tons) cooling capacity was provided by the closed circuit cooler.

2.2.4 HGSHP System Optimal Design and Control

The following section describes previous research work. The word "optimal" should be taken broadly; some of this work compared different control strategies and recommended the best strategies; other work attempted to optimize set points.

2.2.4.1 Yavuzturk and Spitler (2000) Investigation of Control Strategy

Yavuzturk and Spitler (2000) presented a study of various control strategies of a HGSHP system with a cooling tower as the supplemental heat rejecter. A 1,320 m^2

(14,205ft^2) office building was chosen as the example building for the comparative study. The example building was analyzed considering two different climate regions, Houston, TX, for its hot and humid climate and Tulsa, OK, for its moderate climate. Both of the buildings in two locations were cooling dominated but the building in Tulsa, OK also had a significant heating load.

The hybrid ground-source heat pump system was constructed in the TRNSYS modeling environment (Klein 1996). The open-circuit cooling tower was isolated with a plate frame heat exchanger. The plate frame heat exchanger and the ground loop heat exchanger were in series and a two-position valve was used to divert flow to the plate heat exchanger.

Yavuzturk and Spitler used an iterative approach to size the GLHE and supplemental heat rejecter. The GLHE and supplemental heat rejecter were sized by limits on the maximum and the minimum heat pump EFTs for a specified duration of system operation. In theory, the supplemental heat rejecter was sized to balance the annual ground energy rejection with the annual ground energy extraction. In practice, a large cooling tower was initially selected for the HGSHP system. Then, the final required cooling tower capacity was determined by adjusting the cooling tower size and simulating the HGSHP system until the maximum-allowable peak EFT of heat pump occurs. This was done for each control strategy. Yavuzturk and Spitler were mainly concerned about the impact of various control strategies on the system performance. Therefore, they did not optimize the component sizes. As they mentioned, an optimal design procedure was highly recommended for future research.

A total of five cases and eight different control strategies were simulated for the example building in each location. The base case was a ground-source heat pump system with no supplemental heat rejecter. Case 2 was a ground-source heat pump system with an "undersized" ground loop heat exchanger. Case 3 through Case 5 were all hybrid ground-source heat pump system with identical component sizes but they had different control strategies. In Case 3, the cooling tower was controlled based on the set point control strategy. The tower was activated when ExFT > 96.5ºF (35.8ºC) for Case 3a and the tower was activated when EFT > 96.5ºF (35.8ºC) for Case 3b. In Case 4, the temperature difference between the fluid temperature entering heat pump and the ambient wet-bulb temperature was chosen to control the cooling tower. In case 4a, the tower was run when the temperature difference was greater than 3.6ºF (2ºC) and was switched off when the temperature difference was less than 2.7ºF (1.5ºC). In case 4b, the tower was run when the temperature difference was greater than 14.4ºF (8ºC) and was switched off when the temperature difference was less than 2.7ºF (1.5ºC). In case 4C, the tower was switched on when temperature difference was greater than 3.6ºF (2ºC) and was turned off when the temperature difference was less than 2.7ºF (1.5ºC). In Case 5, the cooling tower was activated based on preset schedule. In Case 5a, the cooling tower was run between 12:00 a.m. and 6:00 a.m. year-round. It was also run when the EFT exceeded 96.5ºF (35.8ºC). In Case 5b, the preset schedule was only used from January to March. In Case 5C, the preset schedule was used from June to August.

Yavuzturk and Spitler presented the energy consumption and the life-cycle cost of all the cases and control strategies over a 20-years period. In all different control strategies, Case 4 had the lowest life-cycle cost for the example buildings in both

locations. The reason was that this strategy had lower EFTs, giving better heat pump performance in cooling mode and a smaller cooling tower gives lower first cost.

In case 5, the cooling tower was forced to run in the preset schedule in addition to running it when the EFT exceeds the set point, as in case 3b. Comparing case 5 to case 3b, the operating cost of HGSHP system of case 5 is slightly higher than that of case 3b. However, the cooling tower size is much smaller in case 5, thus the life-cycle cost of case 5 is smaller than that of case 3b.

In Yavuzturk and Spitler's HGSHP system configuration, the PHE is piped in series with the ground heat exchanger. This system layout is suitable for the small HGSHP system in which the entire system flow passes through the boreholes and the pressure drop is still acceptable. Compared to the 100% geothermal system, Yavuzturk and Spitler noted that the pumping cost of the hybrid system attributed to the economic saving. In their scheme, a lower number of boreholes allowed lower flow rates, thus the pump energy consumption was reduced significantly.

Yavuzturk and Spitler compared several different control strategies and recommended the control strategies based on the difference between the ExFT of heat pump and the outside wet-bulb temperature. However, all these strategies were not optimized and may not be generally applicable to different building types and locations.

2.2.4.2 Ramamoorthy et al.'s Work on HGSHP System Optimal Design

For a cooling dominated building, a shallow pond can be added into the GSHP system as a supplemental heat rejecter. Chiasson et al. (2000) developed a shallow pond

model for simulation of a hybrid GSHP system. Based on Chiasson et al.'s shallow pond model (2000) and Yavuzturk and Spitler's GLHE model (1999), Ramamoorthy et al. (2001) aimed to optimize the size of the ground loop heat exchanger and the pond cooler of HGSHP system to minimize the system energy consumption.

This study used the same small office building and the same two locations as Yavuzturk and Spitler (2000). The ground loop heat exchanger and cooling pond were designed in series and a two-position valve was used to divert flow to pond heat exchanger. Both primary and secondary loop were designed with a constant flow pumping system.

Applying Yavuzturk and Spitler's (2000) result of the HGSHP system control strategies, the temperature difference between the average pond temperature and the heat pump exiting fluid temperature was used to control the cooling pond operation. In Ramamoorthy et al.'s study, the temperature differential selected was 8ºC(14.4ºF) with a dead band range of 5ºC (9ºF).

Following the same general approach of Yavuzturk and Spitler (2000), an iterative approach was used to size the GLHE and cooling pond. The GLHE and cooling pond were sized to maintain the heat pump entering fluid temperature between approximately -3.4ºC (25ºF) and 40.6ºC (105ºF), which came from the heat pump manufacturer's data. The lower limiting temperature of entering heat pump was suggested to be 18ºF (10ºC) higher than the freezing point of the antifreeze mixture.

Ramamoorthy et al. simulated a base case only with GLHE and four cases with different sizes of GLHE and cooling pond in each location. For the building in Houston, TX, as more pond heat exchanger coils were added into the system, the ground loop heat exchanger size was reduced. When the number of pond heat exchanger coils was 2, 4, 6 and 8, the total GLHE depth was 34.5%, 22.7%, 15.6% and 11.4% of the total depth of the base case. For the building in Tulsa, OK, when the number of pond slinky coils was 1, 2, 4 and 6, the total GLHE depth was 70.5%, 71.4%, 75.6% and 79.7% of the total depth of base case. In Tulsa, the effect of pong heat exchanger size on GLHE size showed an opposite trend with that of Houston. The reason is, in Tulsa, increasing the pond heat exchanger size required a larger size of GLHE to meet the minimum heat pump inlet fluid temperature because of the relatively higher peak heating load of the system.

Ramamoorthy et al. noted that the total HGSHP system energy consumption was decreased compared to the 100% geothermal system in both locations. The increased energy consumption of the pump for the secondary loop was offset by the energy savings of the heat pumps due to a lower inlet fluid temperature in cooling mode and the energy savings of the main circulation pump due to a smaller size of GLHE.

Ramamoorthy et al. presented the life-cycle cost of all the cases over a 20-year system simulation. The results showed that the HGSHP system with the largest pond coil size had the lowest life-cycle cost for Houston, which was 34.2% of the base case. And the hybrid system with 2 pond heat exchanger coils had the lowest life-cycle cost for Tulsa, 78.2% of the base case.

Ramamoorthy et al. investigated the impact of varying the dead band temperatures on the system life-cycle cost for the two HGSHP systems with lowest life cost in Houston and Tulsa. The life-cycle cost for the different control strategies varied within 1% for Houston and within 0.2% for Tulsa. Ramamoorthy et al. attributed the small changes of life cost to the fact that the system cost was mainly from the heat pump energy consumption and the changing of dead band temperatures would have little impact on the heat pump performance. However, another important reason Ramamoorthy et al. did not mention is that the hybrid systems were already optimized and there was not much possibility for changing the operating cost by changing the dead band temperatures. For those hybrid systems in which the component sizes have been not optimized, the impact of the control strategy on the system performance still needs to be investigated.

2.2.4.3 Khan's Work on GSHP System Optimal Design

A hydronic pavement heating system also can be used as a supplemental heat rejecter of the hybrid ground source heat pump system to reduce the required size the ground loop heat exchanger. Chiasson et al. (2000) developed a model for simulating the performance of a pavement heating system as a supplemental heat rejecter with GSHP system. Khan et al. (2003; 2004) tried to optimize the HGSHP system design with a pavement heating system.

Khan (2004) utilized GenOpt (Wetter 2000) coupled with HVACSIM+ to optimize the design of GSHP system. The eight optimized parameters in the design of the GSHP system included GLHE length, number of boreholes, U-tube diameter, borehole diameter, ground thermal conductivity, heat pump capacity, antifreeze type and concentration.

Khan developed a "Buffer Program", an interface between GenOpt and HVACSIM+. Together, the three programs would automatically adjust the parameter values, run the simulation and iterate to get the minimal life cost of the GSHP system. Due to the extremely expensive computational time for a 20-year simulation, Khan only ran the one-year optimization simulation. This was not successful, as it drove the loop size to be so small that it would be insufficient to run for more than a year. For a 20-year simulation, a varied time step was suggested by Khan to save simulation time, but he did not complete that method.

Khan et al. (2003) simulated two HGSHP systems with pavement heating system and compared them with the base case, which was a 100% geothermal system without any pavement heating system. The pavement heating system was in series with the ground loop heat exchanger. The temperature difference between the heat pump exiting fluid temperature and pavement exiting fluid temperature was used to control the secondary loop. The pavement heating system was activated when the temperature difference exceeds 5ºC (9ºF), and is turned off when the difference falls below 0ºC (0ºF).

The simulated results showed that life cost of the HGSHP system with the pavement heating was lower than the 100% geothermal system. However, in Khan et al.'s study, the sizes of GLHE and pavement were not optimized, neither is the control strategy of the pavement heating system.

2.3 Summary of the Literature

From the review of the literature discussed in the previous sections, the following conclusions can be drawn:

1. Analytical and numerical models have been developed for modeling and dimensioning vertical ground loop heat exchangers. The analytical GLHE models are usually used for long time period simulation and not suitable for the short time response calculation. Due to the computational time requirements, numerical models are not suitable for direct incorporation in a building simulation program with hourly or sub-hourly time steps.

2. Response factor models of GLHE with integrated short-time step and long time step response factor is able to simulate the heat transfer of ground loop heat exchanger in any time scale. Applying the load aggregation algorithm, the response factor model is computationally efficient, and it can be used to run an annual hourly (or shorter time-step) simulation of the GSHP system in a relatively short time.

3. The short-term behavior of ground loop heat exchangers is critical to the design and energy analysis of both the GSHP and HGSHP systems. In practical GSHP systems, the convection resistance varies due to changing flow rates and fluid temperatures and needs to be evaluated. However, the previous published GLHE models did not simultaneously account for these two phenomena.

Therefore, a more accurate GLHE model is highly desired for the HGSHP system simulation.

4. Heat pump models and open-circuit cooling tower models have been developed for the simulation of HGSHP systems. In the study of buildings with many heat pumps, it is difficult to model each heat pump independently. As an alternative, a new "gang-of-heat-pumps" model is desired. And also a closed-circuit cooling tower/fluid cooler model is required for the simulation of the HGSHP system.

5. Two HGSHP system configurations serial or parallel connection of the auxiliary heat rejecter device are in use now. However, strategies for controlling the distribution of flow between the cooling tower and the GLHE in parallel-connected HGSHP systems are not well-developed.

6. Several design procedures and software are available for sizing the vertical ground loop heat exchanger. Kavanaugh et al. (Kavanaugh and Rafferty 1997; Kavanaugh 1998) developed a procedure for sizing both GLHE and supplemental heat source or sink. But Kavanaugh's design procedure will tend to oversize the cooling tower and it is not suitable for the "retrofit design". An improved design procedure should be investigated.

7. Ramamoorthy et al. (2001) tried to optimized the design of HGSHP system with shallow pond to minimize the system energy consumption. Khan (2004)developed a "buffer" program for optimization of GSHP system.

However, optimization HGSHP systems with other types of heat source or sink have not been investigated.

8. Several control strategies of HGSHP are available now, including set point control, set temperature difference control and "preset schedule control". The temperature difference control strategy was recommended by Yavuzturk and Spitler (2000). However, since optimization of the HGSHP system control strategy has not been investigated, the currently available control strategies might be far from optimal and not generally applicable.

3 DEFINITION OF THE PROBLEM AND OBJECTIVES

3.1 Introduction

Ground-source heat pump systems are used for residential and commercial heating and cooling application because of their higher energy efficiency. However, the high first cost of the GSHP system has been a constraint for its wider application. Hybrid ground-source heat pump systems that incorporate a supplemental heat source or sink have been used to reduce the size of GLHE, and therefore the first cost the system.

Previous research has investigated evaluation of HGSHP systems, system component modeling, design procedures, control strategies, and energy consumption analysis. However, from the review of the literature in last chapter, control strategies of HGSHP systems are not well-developed. This research is aimed at developing optimal control strategies and set points for hybrid ground-source heat pump systems in order to improve the performance of HGSHP system.

3.2 Objectives

The main objective of this research is to develop optimal control strategies for HGSHP systems. Necessary sub-objectives to meet this objective include the following:

3.2.1 Developing HGSHP System Simulation and Requisite Component Models

Short-term response of the ground heat exchanger is an important aspect of HGSHP system performance. The thermal mass of the fluid can significantly dampen the short-term temperature response of the ground loop. In HGSHP systems, the convection resistance varies due to changing flow rates and fluid temperatures. The previously published GLHE models did not simultaneously account for these two phenomena. Therefore, an improved GLHE model, which simultaneously accounts for both phenomena will be developed. GEMS2D(Rees 2000) will be used as a reference model for validation of the new GLHE model.

Other system component models including heat pumps, cooling tower/fluid cooler and pumps model also will be developed or modified for simulation of HGSHP systems.

3.2.2 Validation of HGSHP System Simulation

HVACSIM+ is used as the testbed for the simulation of HGSHP systems. The simulation of component models and overall HGSHP systems is required to be validated against experimental data. The OSU hybrid ground source facility provided water temperature and flow rates at various points on the hydronic loop as well as power consumption for all loop equipment. This data set were sufficient to benchmark the accuracy of the simulation testbed. Therefore, the experimental validation of both component models and overall HGSHP systems was provided. Gentry et al. (2006) reported a 7 month period validation of HGSHP system simulation using the data from

the OSU HGSHP research facility. In this research, the validation will be extended to a 12 month period. Also as reported by Gentry et al. (2006) report, the heat pump model performed poorly with catalog data when the actual flow rates on both sides of the heat pump were larger than catalog data. For the extended validation, a parameter estimation-based heat pump model (Jin and Spitler 2002) will be investigated.

3.2.3 Developing Design Procedure of HGSHP System

Two HGSHP system configurations - serial or parallel connection of the auxiliary heat rejecter device - are in use now. Preliminary testing has shown that there are a large number of scenarios where the serial connection is infeasible. For an HGSHP system with large flow rate and a relatively small number of boreholes, all the system flow cannot feasibly pass through the GLHE without requiring excessive pumping power. In this research, a parallel-connected HGSHP system will be investigated. However, strategies for controlling the distribution of flow between the cooling tower and the GLHE in parallel-connected HGSHP systems are not well-developed. Therefore, strategies for controlling the distribution of flow in parallel-connected HGSHP systems will be developed.

Kavanaugh's (1998) design procedure has been developed for sizing the GLHE and supplemental heat source or sink. Kavanaugh's design procedure will tend to oversize the cooling tower and it is not suitable for the "retrofit design". Therefore, the existing design procedure of HGSHP system will be tested and, as needed, will be revised or new design procedures will be developed. GLHEPRO (Spitler 2006) is a tool for designing ground loop heat exchangers for use with ground source heat pump system. A

new version of GLHEPRO will be developed for designing HGSHP systems. The new version of GLHEPRO will work for designing a new HGSHP system and a "retrofit design". Also the new version of GLHEPRO will use a new algorithm to look for the right size of cooling tower.

3.2.4 Investigation and Optimization of HGSHP System Control

Several control strategies (Yavuzturk and Spitler 2000) have been developed for HGSHP systems, including set point control, set temperature difference control and "preset schedule control". Control strategies based on the difference between the ExFT of heat pump and the outside wet-bulb temperature were recommended. However, all these control strategies were not optimized and may not be generally applicable to different building types and locations. Therefore these three control strategies will be investigated. A wide range of new control strategies will also be developed for HGSHP systems.

All the control strategies of HGSHP system will be optimized. A "buffer program", an interface between GenOpt (Wetter 2000) and HVACSIM+ will be developed for the control strategies. For each of the specified HGSHP systems, the three programs would automatically adjust the parameter values (setpoint values), run the simulation and iterate to get the minimal operation cost of the HGSHP system. The purpose of running the optimization study is to search for the best setpoint value of each control strategy for each specified HGSHP system and try to find whether there is a common setpoint value which is generally applicable for all HGSHP systems. If so, generally applicable control strategies would be developed for all HGSHP systems.

Based on the parametric study and optimization work, generally applicable optimal control strategies will be developed.

4 Developing HGSHP System Simulation and Requisite Component Models

The main objective of this chapter is to develop an HGSHP system simulation and the requisite component models within HVACSIM+. Therefore, in this chapter, the component models requisite for HGSHP system simulation will be introduced first. In this research, for an optimization study, a large number of simulations are required. It is computationally expensive to run a large amount of 20-year simulation with hourly time step. Therefore, a new scheme for accelerating the multiyear simulation of HGSHP system is also developed in this chapter.

In this chapter, the primary work involves development of an improved GLHE model and development of a scheme for accelerating the multiyear simulation of the HGSHP system. The improved GLHE model accounts for the thermal mass of fluid and variable convective thermal resistance simultaneously and has a more accurate prediction of GLHE at short time steps. Other system component models including multiple heat pumps, closed-circuit cooling tower and variable speed pumps are developed or modified for the simulation of HGSHP systems. All these models are cast as HVACSIM+ component models. Some other system component models, including single heat pump, open-circuit cooling tower, plate heat exchanger and constant speed pump, have been

previously developed as HVACSIM+ component models and they will be introduced briefly here.

4.1 Vertical Ground Loop Heat Exchanger Model

Like the Yavuzturk and Spitler model (1999), the new ground loop heat exchanger model is an extension to the original long time-step Eskilson model (Eskilson 1987). However, whereas that model used a short time-step g-function to account for short time-step effects, the new model replaces the response function approach at short time-steps with a one-dimensional numerical model, which explicitly accounts for the thermal mass of the fluid and the convective resistance as a function of flow rate, fluid mixture, and fluid temperature.

4.1.1 Eskilson's Long Time-Step Temperature Response Factors Model

Eskilson (1987) developed an approach to determine the temperature response of a multiple borehole ground loop heat exchanger based on dimensionless temperature response factors. The calculation of response factors has three steps. Firstly, a two-dimensional numerical calculation is made to determine the temperature response of a single borehole to a unit step function heat pulse. Secondly, for multiple borehole systems, a spatial superposition method is applied to determine the temperature responses. Thirdly, the temperature response of the borehole wall vs. time response is nondimensionalized and the curves of dimensionless temperature response factors vs. dimensionless time for different configurations are called g-functions.

With the response factors of the borehole wall to a single step heat pulse, the response to any arbitrary heat rejection/extraction function can be determined by devolving the heat rejection/extraction into a series of step functions, and superimposing the response to each step function. (More details were given in Section 2.1.1.3). The borehole wall temperature at the end of the nth time period can be calculated as:

$$T_b = T_{ff} + \sum_{i=1}^{n} \frac{(q_i - q_{i-1})}{2\pi k_{ground}} g\left(\frac{t_n - t_{n-1}}{t_s}, \frac{r_b}{H}\right) \quad (4\text{-}1)$$

Where:

t = Time, (s)

t_s = Time scale, defined as $t_s = H^2 / 9\alpha$, (-)

H = Borehole depth, (m)

k_{ground} = Ground thermal conductivity, (W/m-K)

T_b = Average borehole temperature, (ºC)

T_{ff} = Undisturbed ground temperature, (ºC)

q = Heat rejection pulse, (W/m)

r_b = Borehole radius, (m)

i = The index to denote the end of a time step (the end of the 1st hour or 2nd month etc.)

The average fluid temperature can be calculated if the thermal resistance of borehole R_{BH} is known:

$$T_{fluid} = T_{ff} + \sum_{i=1}^{n} \frac{(q_i - q_{i-1})}{2\pi k_{ground}} g\left(\frac{t_n - t_{n-1}}{t_s}, \frac{r_b}{H}\right) + R_{BH} q_i \qquad (4\text{-}2)$$

The numerical model used in developing the time-step g-function approximates the borehole as a line source of finite length and it is only valid for times estimated by Eskilson to be greater than $5r_b^2 / \alpha$. For a typical borehole, that might imply times from 3 to 6 hours. However, much of the data developed by Eskilson does not cover periods of less than a month. When applied for a short-time system simulation, Eskilson's method cannot accurately model a system with transient operation and a short time-step response factor model is desired.

4.1.2 One-Dimensional Numerical Model for Short Time-Step Response

Yavuzturk and Spitler (1999; Yavuzturk et al. 1999) extended Eskilson's long time-step model to short time steps by developing short time-step g-functions with a two-dimensional (radial-angular) finite volume method, which utilized an automated gridding procedure and a "pie-sector" representation of the U-tubes. Because the short time-step g-function represented the response of the entire ground heat exchanger, it necessarily utilized a fixed convective resistance. The authors later found it necessary (Yavuzturk and Spitler 2001) to modify the model to include variable convective resistance, but this was done at the expense of modeling the thermal mass of the fluid in the borehole.

In order to simultaneously account for variable convective resistance and thermal mass in the borehole, a one-dimensional numerical model is used directly to compute the

short time-step response. This is integrated with Eskilson's long time-step model. By careful control of the one-dimensional model parameters, the model is able to give acceptably accurate short-term response, without the computational time that would be required to run such a model continuously throughout the simulation. The representation of a single U-tube ground heat exchanger with a one-dimensional model is illustrated in Figure 4.1. At short times, end effects can be neglected.

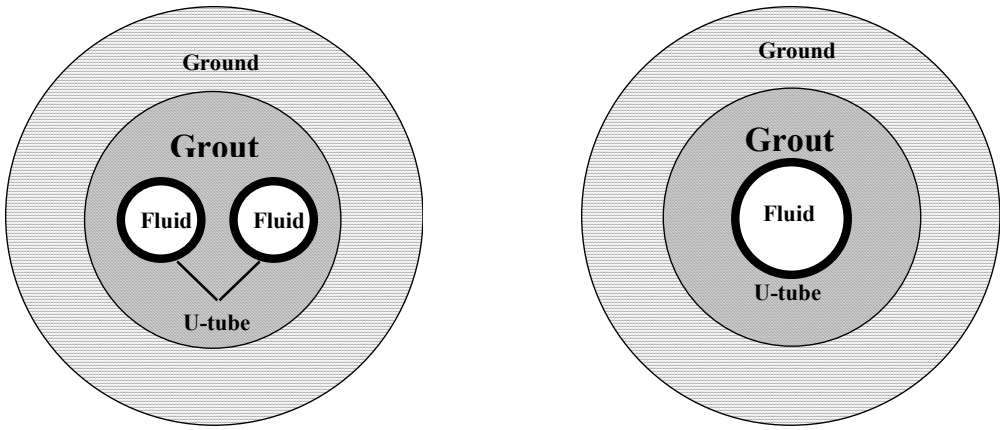

Figure 4.1 A schematic drawing of a borehole system (left) and a schematic drawing of the simplified one-dimension model (right).

The one-dimensional model has a fluid core, an equivalent convective resistance layer, a tube layer, a grout layer, and is surrounded by the ground. In order to get near-identical results to the more detailed two-dimensional model, it is important to specify the one-dimensional geometry and thermal properties in an "equivalent" manner:

- Equivalent volumetric thermal mass of fluid -- the cross-sectional area of the fluid multiplied by the density and specific heat in the 1-d model should be equivalent to the actual 2-d geometry. It is also possible to account for

additional fluid in the system outside of the borehole by increasing the thermal mass to account for the total volume of fluid in the system.

- The 1-d outer tube diameter is equal to $\sqrt{2}$ the outer diameter of the actual U-tube. This maintains the grout thermal mass and is also a standard approximation used for cylinder-source models of U-tubes.

- A thin artificial layer in the 1-d model between the fluid and grout represents the convective resistance. An equivalent conductivity is determined which gives the same resistance as the actual convection coefficient at the inside of the U-tube.

- The resistance between the inner tube wall and the borehole wall is determined with the multipole method (Bennet et al. 1987). A single equivalent conductivity for the tube layer and grout layer is based on this resistance. However, the tube grout layers have different thermal masses, set to match their actual individual thermal masses. The layer representing the tube wall in the 1-d model has the same thickness as the actual tube wall. The grout layer thickness is chosen to maintain the borehole diameter.

The gridding procedure and specification of the parameters are discussed in more detail below.

Governing Equation

The one-dimensional transient conduction equation in polar co-ordinates is expressed as:

$$\frac{1}{\alpha}\frac{\partial T}{\partial t} = \frac{\partial^2 T}{\partial r^2} + \frac{1}{r}\frac{\partial T}{\partial r} \tag{4-3}$$

This equation is discretized using a fully implicit volume approach (Patankar 1991).

Geometry and Gridding Procedure

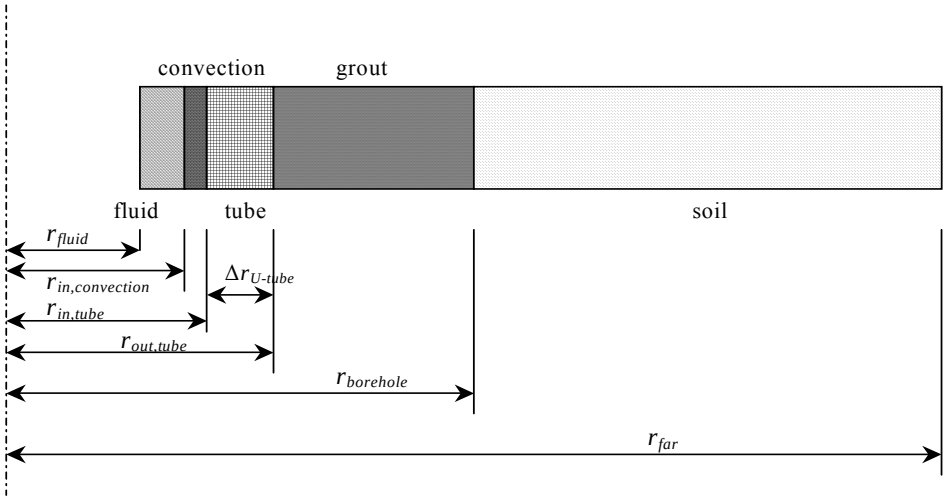

Figure 4.2 A schematic drawing of the simplified one-dimension model for the finite volume method

The geometry of the one-dimensional model is shown in Figure 4.2. Working from the outside in:

- r_{far} is the far-field radius and is set to 10 m; the soil region is represented by 500 cells.

- $r_{borehole}$ is set to the actual borehole radius; the grout region is represented by 27 cells.

- $r_{out,tube}$ is set to $\sqrt{2}$ times the outer radius of the actual U-tube; the tube region is represented by 4 cells.

- $r_{in,tube}$ is set to $r_{out,tube} - \Delta r_{U-tube}$, where Δr_{U-tube} is the actual U-tube wall thickness.

- $r_{in,convection}$ is set to $r_{in,tube} - \frac{1}{4}\Delta r_{in,tube}$; the artificial convection layer is represented by 1 cells.

- r_{fluid} is set to $r_{in,convection} - \frac{1}{4}\Delta r_{in,tube}$; the artificial convection layer is represented by 3 cells. The fluid is represented as an annulus because it is assumed to have very high thermal conductivity, i.e. a lumped capacitance for which the internal distribution of temperature is uniform, and the actual heat input is then represented as a heat flux boundary condition.

Equivalent Volumetric Thermal Mass of Fluid

In the ground loop heat exchanger system, fluid inside the U-tube and elsewhere in the system helps to damp the response to peak loads. Since this can be critical in the design of some systems, it is desirable to account for this in the model.

The equivalent thermal mass of the fluid can be calculated from:

$$\pi(r_{in,convection}^2 - r_{fluid}^2)C_{equiv,\,fluid} = 2\pi r_{actual,in,tube}^2 C_{fluid} \qquad (4\text{-}4)$$

Where:

$C_{equiv,\,fluid}$ = Equivalent volumetric thermal capacity of fluid, (kJ/m^3-K [Btu/ft^3-F]);

C_{fluid} = Volumetric thermal capacity of fluid, (kJ/m^3-K [Btu/ft^3-F]);

$r_{actual,in,tube}$ = Inner radius of the actual U-tube, (m [ft]).

The fluid at any cross-section in the U-tube is assumed to be at a uniform temperature. In the 1-d model, this is enforced by setting the thermal conductivity of the fluid to a high value (200 W/m-K). Finally, the fluid inside the system, but outside the U-tube may be accounted for by multiplying the $C_{equiv,\,fluid}$ by the "Fluid Factor". A typical value for an actual system is two.

Equivalent Thermal Conductivity of Tube and Grout

In order to get near-identical results with the two-dimensional model, the borehole thermal resistance in the simplified one-dimensional model should be exactly equal to the thermal resistance of the actual two-dimensional borehole. The multipole method (Bennet et al. 1987) is used to calculate the thermal resistance between the borehole wall and the convective resistance, accounting for the differing grout and U-tube thermal conductivities. The multipole method is a highly accurate analytical method and has compared very well to a two-dimensional boundary-fitted coordinate finite volume numerical model (Rees 2000).

The single equivalent conductivity assumed for the grout and tube layers can be calculated once the equivalent thermal resistance has been calculated with the multipole method:

$$k_{equiv,TG} = \frac{\ln(r_{borehole} / r_{in,tube})}{2\pi R_{equiv,TG}} \tag{4-5}$$

Where:

$k_{equiv,TG}$ = Equivalent conductivity of tube and grout layers, (W/m-K [Btu/hr-ft°F]);

$R_{equiv,TG}$ = Equivalent thermal resistance between the borehole wall and convective resistance, (m-K/W [hr-ft-°F/Btu]).

Equivalent Conductivity for Convection Layer

The multipole method is also used to calculate the thermal resistance between the borehole wall and the fluid, R_{BH} as before, except including a specific value of the convective resistance. Then the equivalent thermal resistance of the artificial convection layer is:

$$R_{equiv,convection} = R_{BH} - R_{equiv,TG} \tag{4-6}$$

The convective resistance is approximated as a conductive layer of thickness ¼ the U-tube wall thickness. The equivalent thermal conductivity of the convection layer, $k_{equiv,\ convection}$, can then be expressed as:

$$k_{equiv,convection} = \ln(r_{in,tube} / r_{in,convection}) / 2\pi R_{equiv,convection} \qquad (4\text{-}7)$$

The thermal mass of the convection heat transfer layer is set to a near-zero value, 1 J/m^3-K.

Currently, the multipole method is called at each time step to calculate the borehole thermal resistance after the convection coefficient has been calculated. Gnielinski's (Hellstrom 1991) correlation is used to calculate the Nusselt number when the flow in the U-tube is in turbulent:

$$Nu = \frac{(f/2)(\mathrm{Re}-1000)\,\mathrm{Pr}}{1+12.7(f/2)^{1/2}(\mathrm{Pr}^{2/3}-1)} \qquad (\mathrm{Re} > 2300) \qquad (4\text{-}8)$$

Where:

Re =Reynolds number, (-)

Pr = Prandtl number, (-)

f = Fanning friction factor, (-). f for smooth pipes is given by Petuhkov (Hellstrom 1991) as $f = [1.58\ln(\mathrm{Re}) - 3.28]^{-2}$.

The Nusselt number is set to 4.364 when the flow in the tube is in laminar, $\mathrm{Re} \le 2300$. Since this method will result in a discontinuity at the transition point, a linear correlation is used to smooth the Nusselt number when $2200 \le \mathrm{Re} \le 2400$.

4.1.3 One-Dimensional Numerical Model Validation and Error Analysis

Analytical solution, e.g. line source model (LSM), finite line source model (FLSM), and infinite cylindrical source model (CSM) are usually used for long time period simulation and are not suitable for the short time response calculation. As a result, the analytical solutions can not be used to validate the one-dimensional numerical model for short time-step response. In this research, the General Elliptical Multi-block Solver (GEMS2D) (Rees 2000) was used for the validation of the one-dimensional numerical model. As described in previous Section 2.1.1.2, GEMS2D is capable of dealing with both long time-step and short time-step simulation of the ground loop heat exchanger. Therefore, GEMS2D was used as a reference model for the other numerical models (Deng 2004; Young 2004).

Young (2004) used six sets of different test cases for the validation of his BFTM model for short time-step response. The same six sets of test cases were used for the comparison here between the one-dimensional numerical model and GEMS2D. The parameters varied between each of the test cases are given in Table 4.1. The test cases used a range of different borehole diameters, shank spacing, grout conductivities, soil conductivities, grout heat capacities and fluid factors. (Shank spacing is defined as the size of the gap between the pipes of the U-tubes.) These selected values included the common values used in vertical ground loop heat exchangers. The remaining parameters common to all test cases are given in Table 4.2.

Table 4.1 Input Data varied for model validation test cases

Test Case Group		Varied Properties	Test Case			
			A	B	C	D
1	Different borehole diameters	BH diameter mm (in)	76.2 (3)	114.3 (4.5)	152.4 (5)	190.5 (8)
		Shank Spacing mm (in)	3.127 (0.123)	15.83 (0.623)	28.52 (1.12)	41.23 (1.62)
		R_{bh} m-K/W (hr-ft-F/Btu)	0.1222 (0.2115)	0.183 (0.3167)	0.2232 (0.3862)	0.2523 (0.4366)
2	Different shank spacing	Shank Spacing mm (in)	3.18 (0.1252)	15.8 (0.6220)	28.6 (1.1260)	41.3 (1.6260)
		R_{bh} m-K/W (hr-ft-F/Btu))	0.2134 (0.3693)	0.183 (0.3167)	0.1568 (0.2713)	0.13 (0.2250)
3	Different grout conductivities	Grout Conductivity W/m-K (Btu/hr-ft-F)	0.25 (0.15)	0.7443 (0.43)	1.5 (0.87)	--
		R_{bh} m-K/W (hr-ft-F/Btu)	0.4400 (0.7614)	0.1822 (0.3153)	0.1158 (0.2004)	--
4	Different soil conductivities	Soil Conductivity W/m-K (Btu/hr-ft-F)	0.5 (0.29)	1.5 (0.87)	2.5 (1.45)	8 (4.62)
		R_{bh} m-K/W (hr-ft-F/Btu)	0.1868 (0.3232)	0.1841 (0.3186)	0.183 (0.3167)	0.1814 (0.3139)
5	Different grout volumetric heat capacities	Grout Volumetric Heat Capacity MJ/m^3-K (Btu/ft^3-F)	2 (29.8)	3.9 (58.2)	8 (119)	--
		R_{bh} m-K/W (hr-ft-F/Btu)	0.183 (0.3167)	0.183 (0.3167)	0.183 (0.3167)	--
6	Different fluid factor	Fluid factor (-)	1	2	4	--
		R_{bh} m-K/W (hr-ft-F/Btu)	0.183 (0.3167)	0.183 (0.3167)	0.183 (0.3167)	--

Table 4.2 Input data common to all validation test cases

Borehole Diameter	=	114 mm	4.5 in
Borehole Length	=	100 m	262.5 ft
U-tube Inside Diameter	=	27.44 mm	1.08 in
U-tube Outside Diameter	=	33.41 mm	1.32 in
Shank Spacing (m)	=	15.83 mm	0.62 in
Soil Conductivity	=	2.5 W/m-K	1.45 Btu/hr-ft-F
Grout Conductivity	=	0.7443 W/m-K	0.43 Btu/hr-ft-F
U-Tube Conductivity	=	0.3895 W/m-K	0.225 Btu/hr-ft-F
Soil Volumetric Heat Capacity	=	2.5 MJ/m^3-K	37.3 Btu/ft^3-F
Grout Volumetric Heat Capacity	=	3.9 MJ/m^3-K	58.2 Btu/ft^3-F
Tube Volumetric Heat Capacity	=	1.77 MJ/m^3-K	26.4 Btu/ft^3-F
Fluid Convection Coefficient	=	1690 W/m^2-K	298 Btu/hr-ft^2-F
Step pulse heat input	=	40.4 W/m	42.0 Btu/hr-ft
Fluid Type	=	Water	
Average Fluid Temperature	=	20 ºC	68 ºF
Fluid Factor	=	1	

The temperature predictions have been compared in terms of relative error where the error is scaled according to the difference between the GEMS2D determined fluid temperature and the far field (initial) temperature at each time step:

$$RelativeError = \frac{(T_{GEMS2D} - T_{One-D})}{(T_{GEMS2D} - T_{FarField})} \times 100\% \qquad (4\text{-}9)$$

Table 4.3 Relative error (%) between the GEMS2D and one-dimensional numerical results for each test case at 1 and 10 hours simulated time (1-min, time step)

Test Case Group		A		B		C		D	
Time		1 hr	10 hr	1 hr	10 hr	1 hr	10 hr	1 hr	10 hr
1	Different borehole diameters	5.12	0.07	3.53	-0.43	2.91	-0.37	0.85	-1.97
2	Different shank spacing	4.53	-0.56	3.53	-0.43	4.34	-0.33	7.83	-1.18
3	Different grout conductivities	-8.25	-2.53	3.53	-0.43	8.75	-0.26	--	--
4	Different soil conductivities	3.37	-0.33	1.57	-0.41	3.53	-0.43	3.50	-0.52
5	Different grout volumetric heat capacities	0.45	-0.37	1.60	-0.44	6.87	-0.62	--	--
6	Different fluid factor	3.53	-0.43	2.53	0.71	2.07	0.66	--	--

The resulting relative error found after one hour and 10 hours of simulation are given in Table 4.3. For most of cases, the relative errors are consistently less than 1% after 10 hours of simulation time. For the large borehole diameter case (Case 1D), the large shank spacing case (Case 2D) and the small grout conductivity case (Case 3A), the relative errors were larger than 1%.

Figure 4.3 illustrates for case 1A the predicted average fluid temperature given by one-dimensional model against that given by the GEMS2D model. In this case the relative error is less than 2% after the first hour of simulation and the decreases to a value of about -0.4% after 10 hours.

Figure 4.4 shows the same results plotted for the first hours. The absolute temperature error after the first minute is approximately 0.39ºC (0.7ºF) decreasing to 0.02ºC (0.36ºF) after thirty minutes. Similar behavior was observed in other cases, where the average relative error was found to be smaller than 1% of the temperature rise. (More validation results were given in Appendix A.)

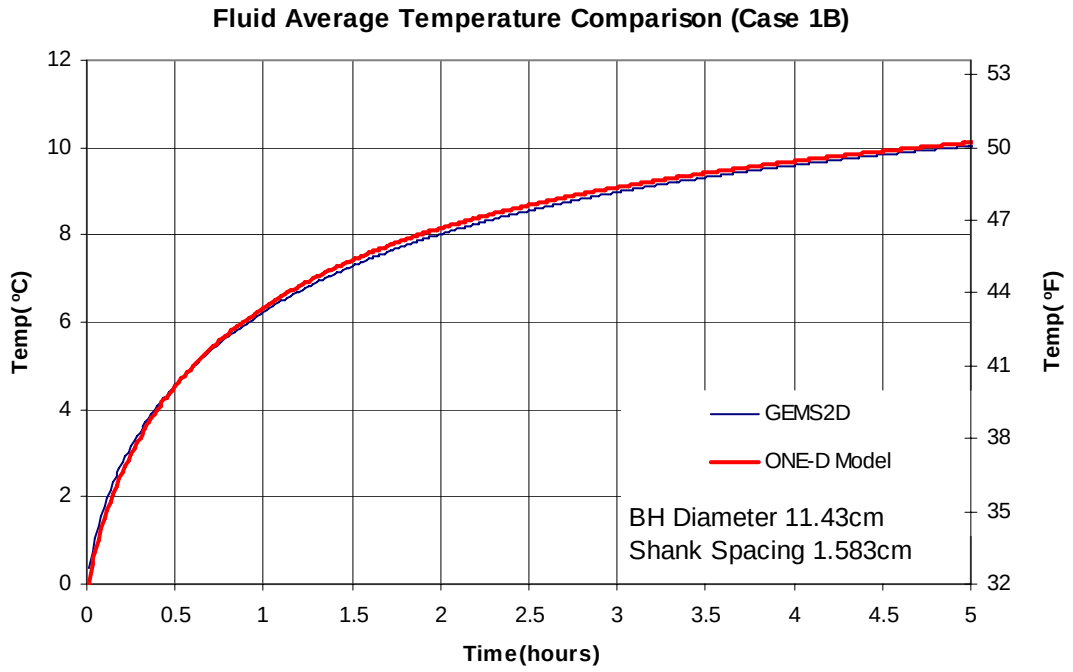

Figure 4.3 Comparison of the one-dimensional model and GEMS2D model temperature predictions for Test Case 1B.

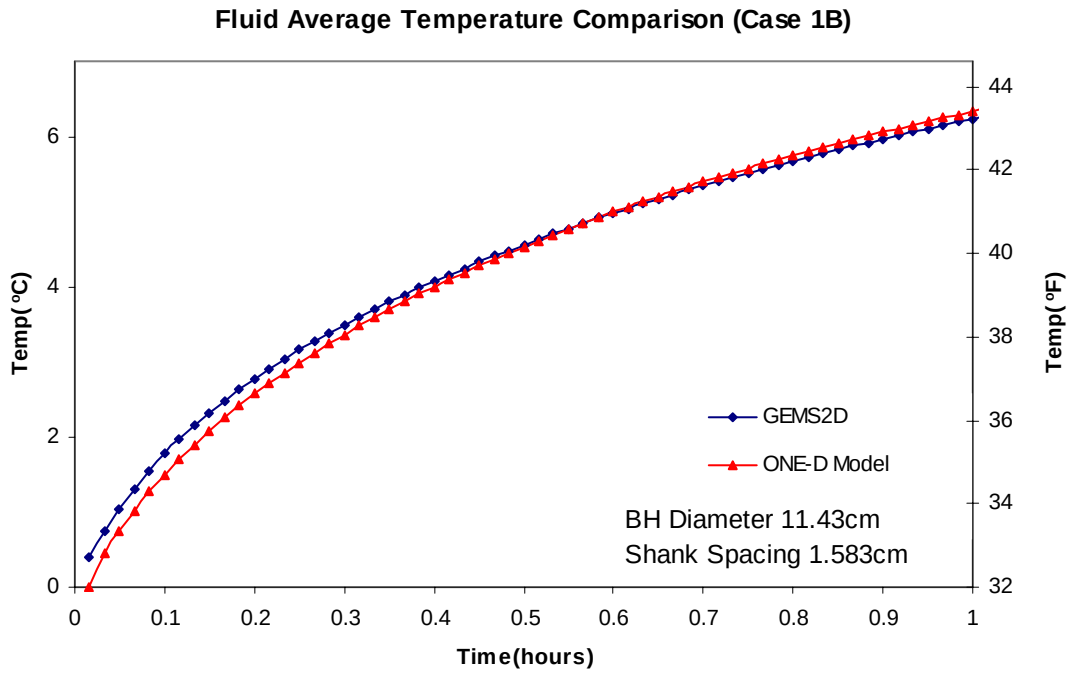

Figure 4.4 Comparison of the one-dimensional model and GEMS2D model temperature predictions over the first hour of simulation for Test Case 1B.

4.1.4 Summary of One-Dimensional Numerical Model

A short time-step model for vertical ground loop heat exchanger with variable convective resistance and thermal mass of the fluid was developed. The temperature response at short time-steps is calculated with a one-dimensional numerical model, which explicated accounts for the thermal mass of the fluid and the convective resistance as a function of flow rate, fluid mixture, and fluid temperature. In this model, the multipole method (Bennet et al. 1987) is used to calibrate the one-dimensional resistances so that they always match the total two-dimensional resistance. At the same time, the thermal mass of the individual components is maintained in the one-dimensional model. By

carefully controlling these parameters, the one-dimensional model compares very favorably to the detailed boundary-fitted coordinates finite volume model (GEMS2D).

4.1.5 Implementation as a Ground Heat Exchanger Model

In the Yavuzturk and Spitler (1999) model, the borehole wall temperature was determined by adding the temperature responses due to the heat inputs at different time steps, as described in Section 2.1.1.3. In the new GLHE model, the LTS g-function model is used to compute the borehole wall temperature due to excitations that occurred more than 24 hours ago. In turn, the fluid temperature due to excitations that occurred more than 24 hours ago is computed with the borehole resistance. Then, the STS model is used to determine the response of the fluid temperature to excitations that occurred less than 24 hours ago. Finally the two-responses are superimposed. On top of this, the model will iterate the current time step's heat extraction rate and fluid temperature.

4.1.5.1 Aggregation of Ground Loads and Yavuzturk and Spitler's (1999) Short Time Step Model

A load aggregation scheme for ground loop heat exchanger was applied for the Yavuzturk and Spitler's (1999) short time-step and Eskilson's (1987) long time-step response factor model. The loads on the ground loop heat exchanger were divided into the "lumped" and immediate thermal history.

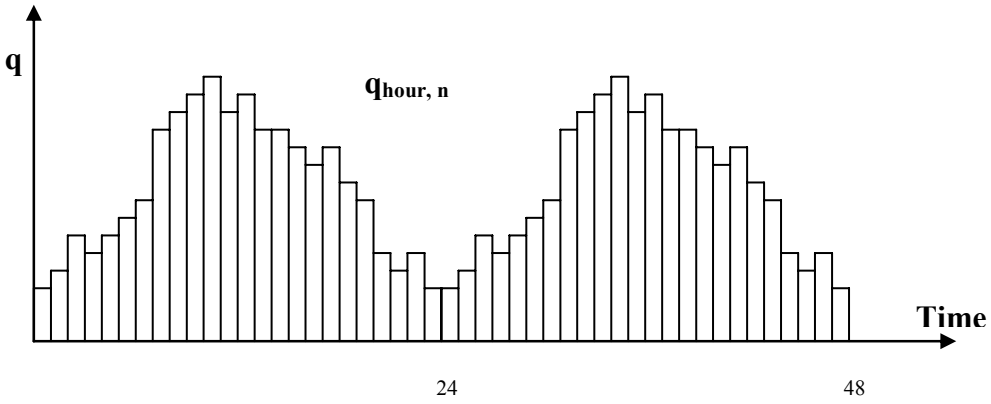

Figure 4.5 Hourly load of ground loop heat exchanger in 48 hours

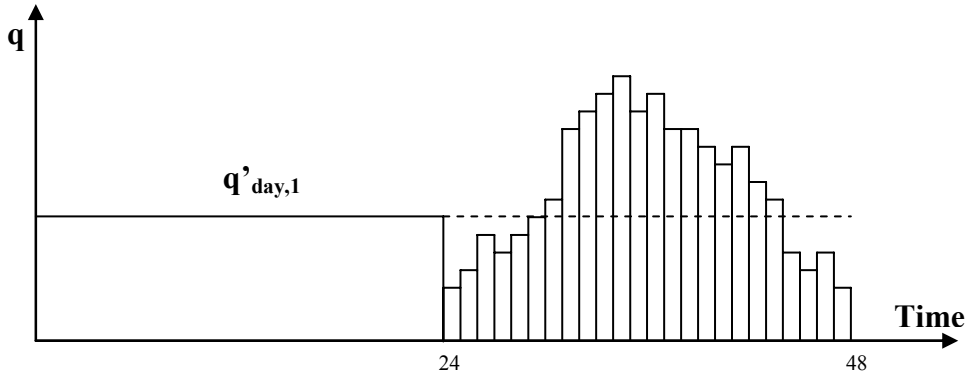

Figure 4.6 Average load of the first 24 hours and hourly loads in the next 24 hours

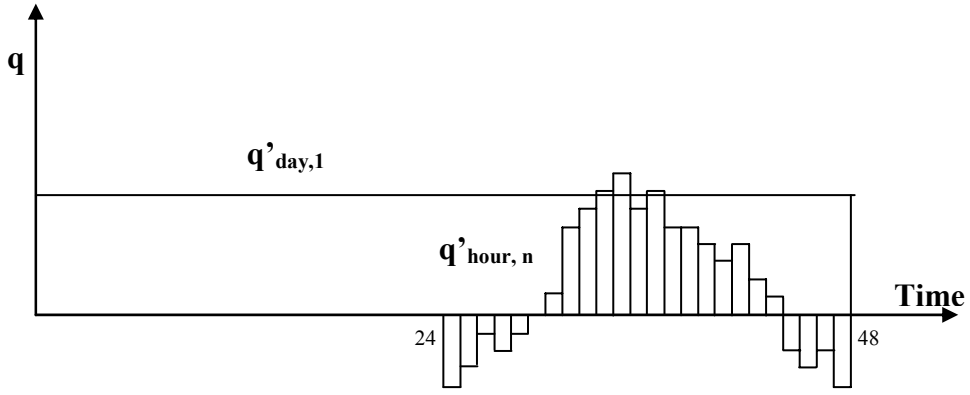

Figure 4.7 Lumped loads for LTS model and artificial hourly loads for STS model

For illustration purposes, assume the first 48-hour hourly loads ($q_{hour,n}$) of ground loop heat exchanger is illustrated as Figure 4.5. At the end of 48 hours, the loads that occur more than 24 hours ago are "lumped" together into a daily-averaged load ($q_{day,1}$), as shown in Figure 4.6. The subsequent 24-hour hourly loads are superimposed as artificial hourly loads ($q'_{hour,n}$), as shown in Figure 4.7.

Then the borehole wall temperature is computed by superposing the temperature changes from the "lumped" block loads and the temperature changes from the short time-steps loads. More details about the aggregation of ground loads and the short time-step model are given by Yavuzturk and Spitler's (1999).

To provide an example for the load aggregation and using Yavuzturk and Spitler's (1999) short time-step and long time-step response factor models, the borehole wall temperature for the 37th hour is calculated. For the 37th hour, the load is superposed by a daily-averaged load ($q_{day,1}$) and the artificial hourly loads ($q'_{hour,n}$). The daily-averaged load with the corresponding long time-step (daily step) g-functions yields the temperature response at the end of 37th hour. Then the artificial hourly loads ($q'_{hour,n}$) for the remaining 13 hours are superimposed in hourly steps with corresponding hourly g-function values to obtain the temperature at the 37th hour.

$$T_{fluid,37} = T_{ff} + \sum_{m=1}^{1} \frac{(q'_{day,m} - q'_{day,m-1})}{2\pi k_{ground}} g\left(\frac{t_{hour,n} - t_{hour,24m-24}}{t_s}, \frac{r_b}{H}\right) + \sum_{n=25}^{37} \frac{(q'_{hour,n} - q'_{hour,n-1})}{2\pi k_{ground}} g\left(\frac{t_{hour,n} - t_{hour,n-1}}{t_s}, \frac{r_b}{H}\right) + R_{BH} q_{hour,37} \tag{4-10}$$

Where:

m = Index for the load aggregated time blocks;

n = Index for the hourly time steps;

g = g-functions of borehole;

$T_{b,37}$ = Borehole wall temperature at the end of 37th hour, (ºC).

4.1.5.2 Implementation of One-dimensional Numerical Model and LTS Model

In the new GLHE model, a similar procedure is applied to couple the one-dimensional numerical model and LTS model to calculate the average fluid temperature.

In Yavuzturk and Spitler's (1999) procedure, the borehole wall temperature changes due to the short time-step loads are calculated using the short time-step g-function (the last term on the right side of Equation 4-10). In the new GLHE model, the temperature changes due to the short-time loads are calculated by the one-dimensional numerical model directly.

For the example in the last section, the borehole wall temperature at the 37th hour is then calculated by:

$$T_{b,37} = T_{ff} + \sum_{m=1}^{1} \frac{(q'_{day,m} - q'_{day,m-1})}{2\pi k} g\left(\frac{t_{hour,n} - t_{hour,24m-24}}{t_s}, \frac{r_b}{H}\right) + \Delta T_{short-term} + R_{BH} q_{hour,37} \quad (4\text{-}11)$$

Where:

$\Delta T_{short-term}$ = The temperature changes due to the recent artificial hourly loads ($q'_{hour,n}$) started at the 25th hour. It is calculated using the one-dimensional numerical model.

As presented in Equation 4-11, the borehole wall temperature at the 37th hour is calculated by superposing the temperature changes from the "lumped" block loads and the temperature changes from the short time-steps loads. When applying the one-dimensional numerical model to calculate the short time-step temperature response $\Delta T_{short-term}$ from the artificial hourly loads ($q'_{hour,n}$), the temperature changes from the "lumped" block loads ($q_{day,1}$) need to be considered.

4.1.6 Component Model for HVACSIM+

Using the one-dimensional numerical model and Eskilson's (1987) long time-step model, an HVACSIM+ component mode of the new ground loop heat exchanger (TYPE621) was developed. The diagram can be seen in Figure 4.8, showing all inputs, outputs and parameters needed to run the model.

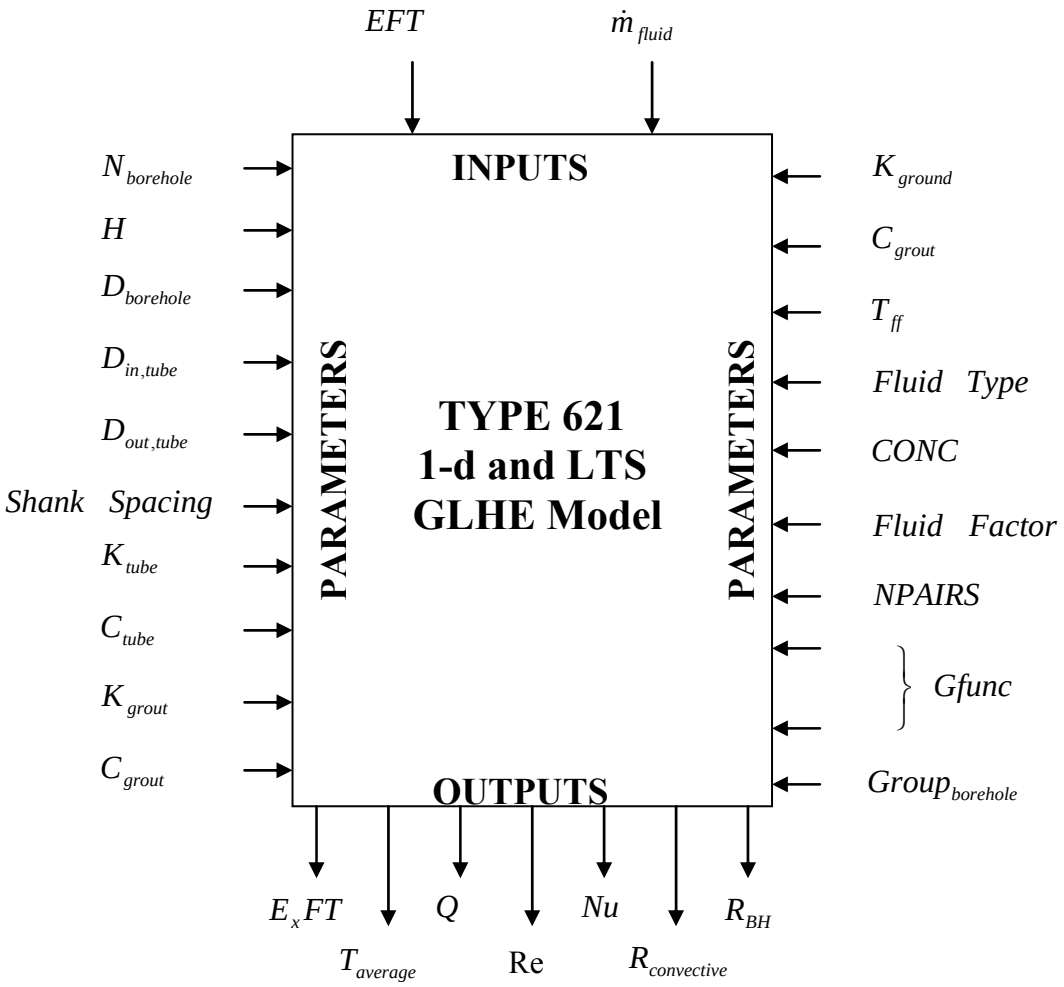

Figure 4.8 TYPE 621 1-d and LTS GLHE HVACSIM+ model diagram.

In the diagram:

EFT = Entering fluid temperature to the borehole, ºC;

$\dot{m}_{fluid}$ = Mass flow rate of fluid, kg/s;

ExFT = Exiting fluid temperature from the borehole, ºC;

$T_{average}$ = Average fluid temperature of ground loop heat exchanger, ºC;

Q = Heat transfer rate of the ground loop heat exchanger, W;

Re = Reynolds number;

Nu = Nusselt Number;

$R_{convective}$ = Convective thermal resistance, m-k/W;

R_{BH} = Thermal resistance of borehole, m-k/W;

$N_{borheole}$ = The number of borehole in each group;

H = Borehole length, m;

$D_{borehole}$ = Borehole diameter, m;

$D_{in,tube}$ = Inner diameter of the actual U-tube, m;

$D_{out,tube}$ =Outer diameter of the actual U-tube;

K_{tube} = Conductivity of tube, W/m-K;

C_{tube} = Volumetric thermal capacity of tube, J/m^3-K;

K_{grout} = Conductivity of grout, W/m-K;

C_{grout} = Volumetric thermal capacity of grout, J/m^3-K;

K_{ground} = Conductivity of ground, W/m-K;

C_{ground} = Volumetric thermal capacity of ground, J/m^3-K;

T_{ff} = Undisturbed ground temperature, ºC;

Fluid Type = The type of working fluid: (0 for water, 1 for propylene glycol, 2 for Ethylene glycol);

CONC = Weight of antifreeze concentration in solution;

$NPAIRS$ = Number of pairs of g-function data;

$Gfunc$ = G-functions;

$Group_{borehole}$ = Group number of borehole.

The one-dimensional numerical model and LTS model of ground loop heat exchanger was built into GLHEPRO (Spitler 2006). Using GLHEPRO, the parameter file for the TYPE621 model can be automatically generated.

4.1.7 Example Application for the GLHE Model

An example application is provided using an imaginary peak-load-dominant building in Birmingham, AL – a one-story, 547 m^2 church with a significant peak cooling or heating load of duration two hours occurring on a weekly basis. The building load was calculated using BLAST (1986) and the load profile is shown in Figure 4.9 (heating load is positive and cooling load is negative).

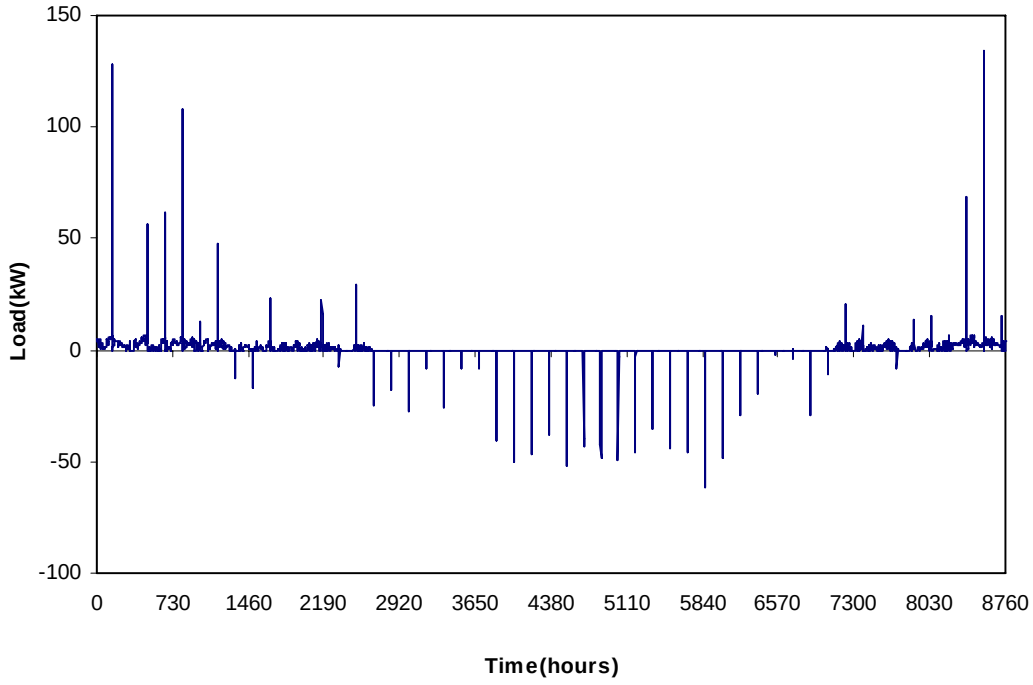

Figure 4.9 Annual hourly building load for the church building in Birmingham, AL.

Eight Climate Master GSV/H070 water-to-air heat pumps with a nominal cooling capacity of 21 kW are used, together capable of meeting the design requirement. The heat pumps are modeled within HVACSIM+ using a simple component model that determines the heat pump COP as a polynomial function of entering fluid temperature and mass flow rate. The model then returns the exiting fluid temperature, which is an input to the ground heat exchanger model.

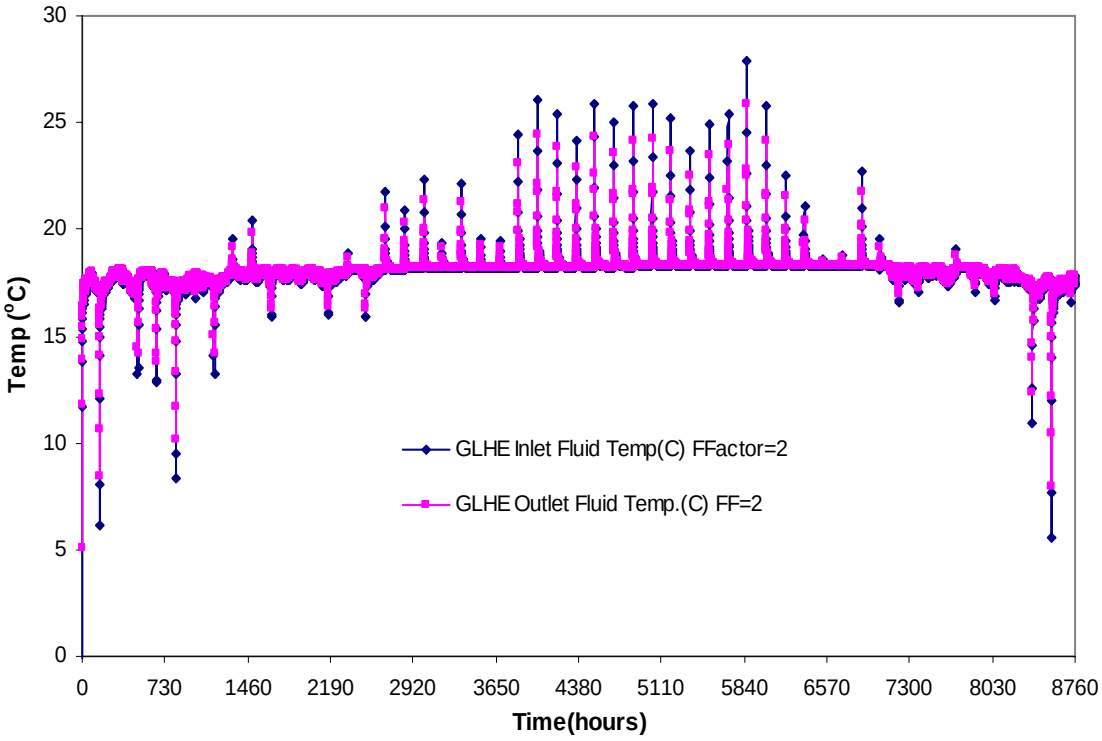

Figure 4.10 Hourly ground loop fluid temperature profiles for the church building in Birmingham, AL.

A 16-borehole ground heat exchanger, laid out in a 4x4 grid with boreholes 76.2 m deep, and other parameters shown in previously Table 4.2 is utilized. The total volumetric flow rate of the ground heat exchanger is 9.1 L/s. The undisturbed ground temperature in Birmingham is 18.3 ºC. In this system, the fluid factor of the GSHP

system is selected as 2 to account for the fluid in the distribution piping. The hourly entering and exiting fluid temperatures for the first year of operation are shown in Figure 4.10. The model is commonly used for multi-year simulations.

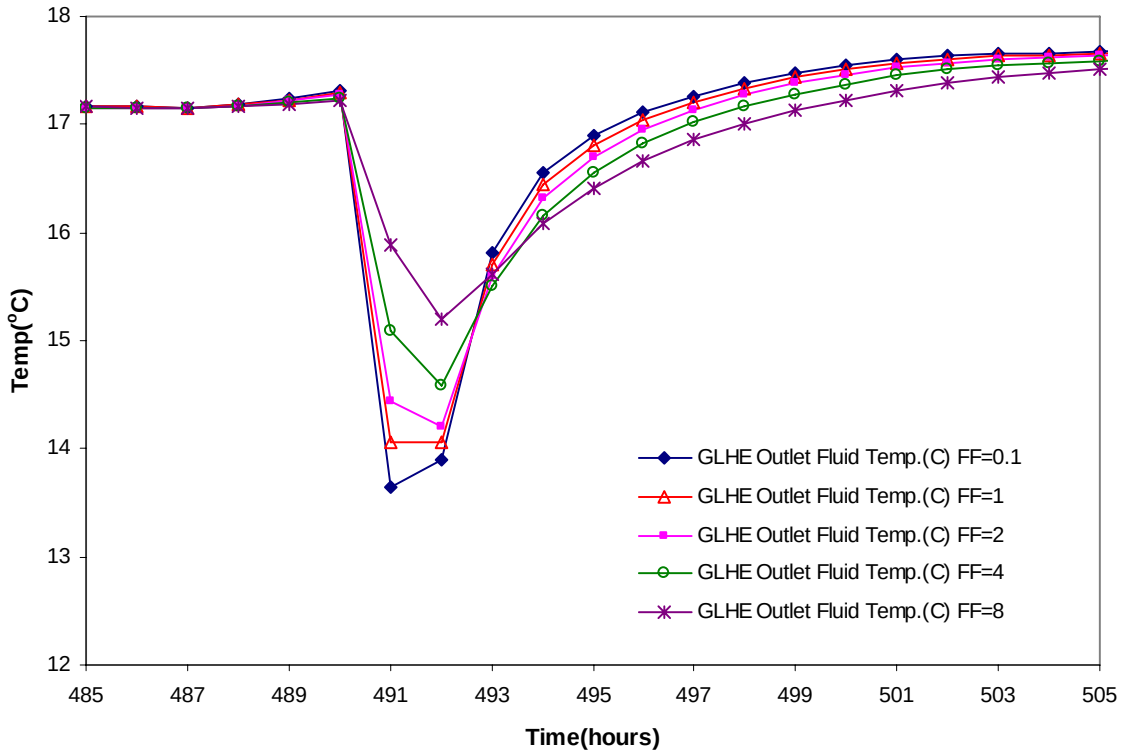

Figure 4.11 Detailed GLHE outlet temperatures for different fluid factors

The effect of different fluid factor values can be seen in Figure 4.11, which shows 21 hours of operation that includes a peak heating period. The 0.1 value of fluid factor would be representative of a simulation that did not include the effect of the thermal fluid mass; the value of 1 would account only for the thermal mass of fluid in the borehole; the value of 2 would be typical if the thermal mass of fluid in the distribution portion of the system is included; larger values might be representative of a system with long pipe runs or where additional fluid storage is intentionally included. The differences shown here

might be expected to give a relatively small difference in energy consumption prediction. However, as sizing of the ground heat exchangers can be highly sensitive to the peak temperature prediction, the difference in fluid factor can have a significant impact on the GLHE design. (Young 2004)

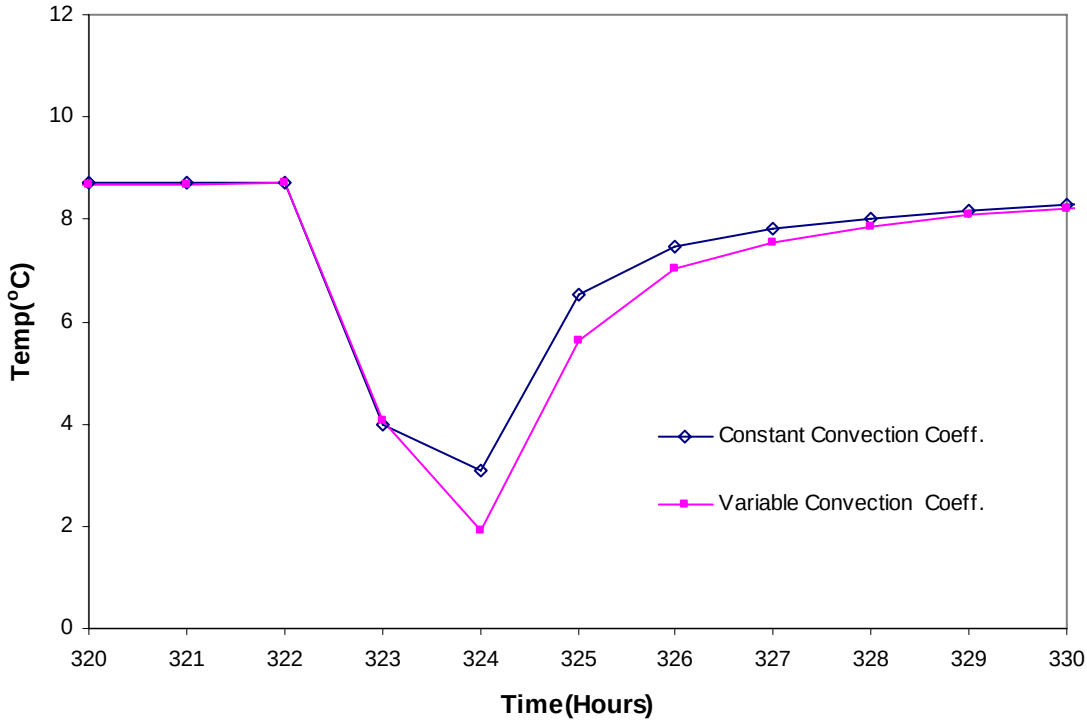

Figure 4.12 Detailed GLHE outlet fluid temperatures for different convection coefficient models.

To illustrate the use of the model in a situation where variable convective resistance may be important, the church building is modeled in Detroit, with 36 boreholes in a 6x6 grid, and a 30% by weight mixture of propylene glycol and water. Figure 4.12 shows a case where the flow transitions from turbulent (hour 322), Re=2428, to laminar (hour 324), Re=1893. As a result, the convection coefficient drops from 499 W/m^2-K to 69 W/m^2-K and the total borehole resistance increases from 0.193 W/m^2-K to 0.274 W/m^2-K. Table 4.4 summarizes the intermediate properties. In the constant convection

case, the fluid properties are determined at 10ºC. At this temperature, the flow remains turbulent (Re=2558) and the borehole resistance is 0.194 W/m^2-K. In practice, GLHE flow rates are usually designed to remain in the turbulent regime. So, for many cases, this feature is not needed and the extra computational effort is not justified. However, there is no evidence that keeping flow rates high enough so that the GLHE is always in the turbulent regime is universally a good practice. This model allows for further investigation of design practice.

Table 4.4 Comparison between the variable convection and constant convection cases

Hour	Variable Convection Case		Constant Convection Case
	322	324	
T_{mean} (C)	8.8	3.1	10
Viscosity (Pa·s)	0.005065	0.006502	0.004808
Density (kg/m^3)	1034	1035	1034
Volume heat capacity (kJ/m^3·K)	3935	3930	3936
Conductivity (W/m·K)	0.4315	0.4268	0.4326
Re	2428	1893	2558
Nu	31.2	4.4	33.1
Convective coefficient (W/ m^2·K)	499	69	530
Borehole resistance (m·K/W)	0.194	0.273	0.193

4.1.8 Simplified STS GLHE Model

For cases where the flow in the tube is always turbulent, the convective thermal resistance is much smaller relative to the thermal resistance of the grout and pipe.

Therefore, the changing of heat transfer rate of the ground loop heat exchanger brought by the variation of convective thermal resistance due to different fluid temperatures and flow rates can be negligible. A simplified GLHE model may then be developed without considering the variable convective thermal resistance but still accounting for the thermal mass of fluid.

This simplified short time-step model is similar to Yavuzturk and Spitler's (1999) short time-step model described in Section 4.1.5.1, but with a different approach for obtaining the short time-step g-functions. Using a one-dimensional numerical model, the temperature response of a single borehole to a unit step heat pulse at short time-steps can be obtained. Applying the same procedure to calculate the long time step response factors (Eskilson 1987), the temperature response of the borehole at the short time step vs. time response is nondimensionalized and the short time step response factors are obtained. This simplified model is referred to as the short time-step (STS) response factor model.

The resulting short time-step g-function values are plotted in Figure 4.13 side by side with the long time-step g-function values for a single borehole and an 8 x 8 borehole field calculated using GLHEPRO. The short time-step g-functions generated by one-dimensional numerical model line up very well with Eskilson' long time-step g-function.

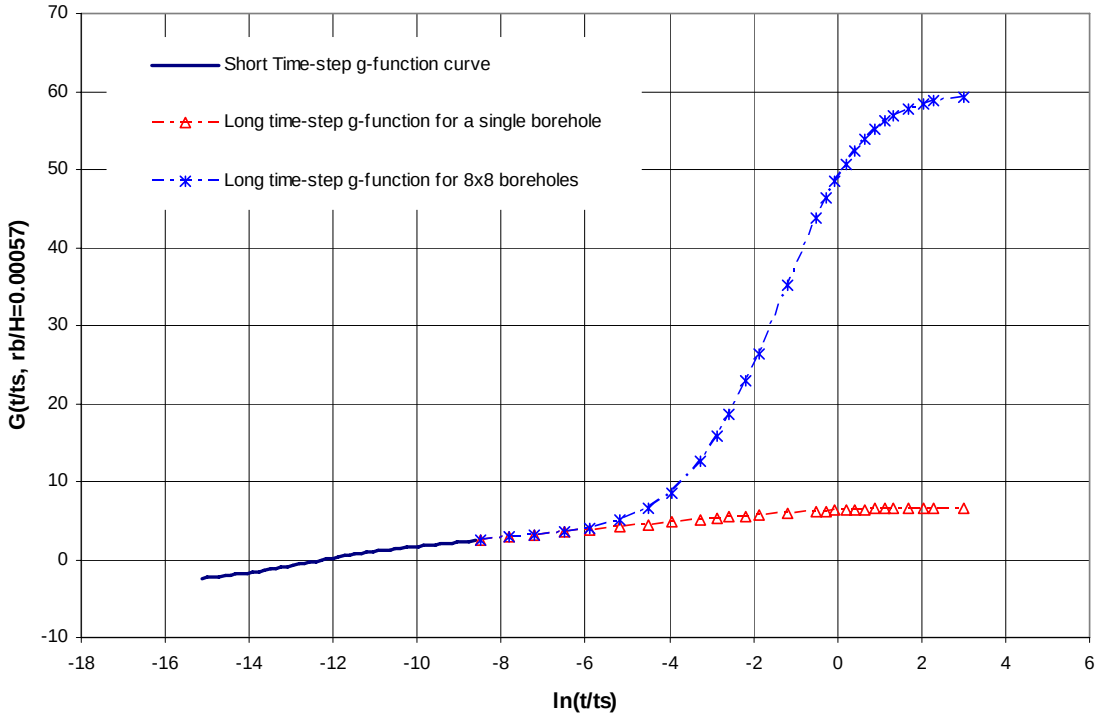

Figure 4.13 Short time-step g-function curve as an extension of the long time-step g-functions plotted for a single and a 8x8 borehole field.

Without applying the one-dimensional numerical model to calculate the temperature response at short time-steps, in the simplified GLHE model, the borehole wall temperature is calculated by adding the temperature response due to the heat inputs at different time steps, as illustrated in Equation 4-10.

Using the simplified model, an HVACSIM+ component model of the new ground loop heat exchanger (TYPE620) was developed. The diagram can be seen in Figure 4.14, showing all inputs, outputs and parameters needed to run the model.

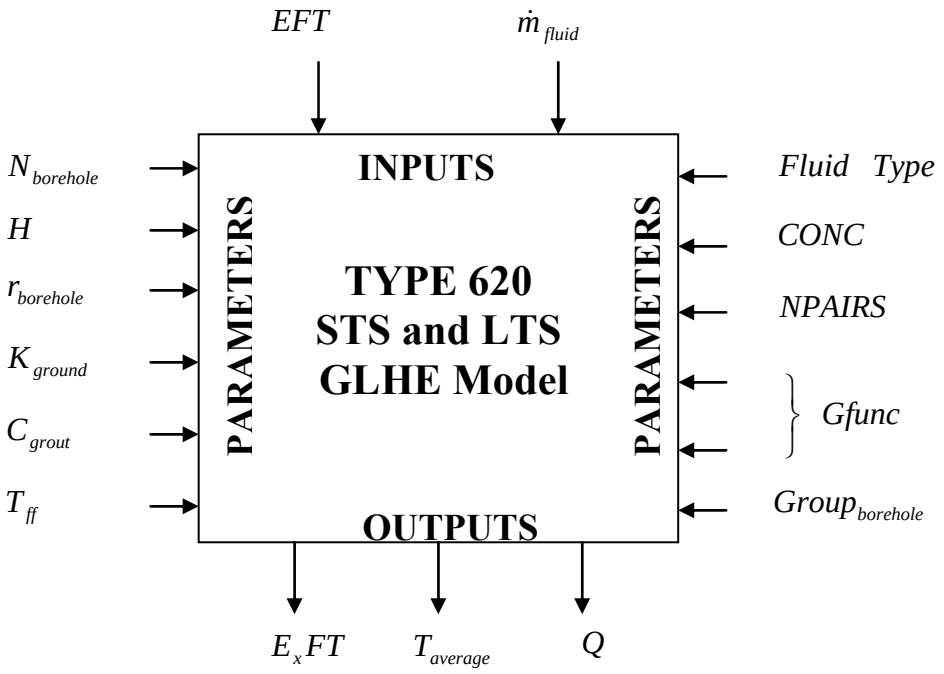

Figure 4.14 TYPE 620 New STS and LTS GLHE model diagram.

Using GLHEPRO (Spitler 2006), the parameter file for the TYPE620 model can be automatically generated.

4.1.9 Investigation of Simulation Time Step

During the simulation process of the GLHE model, it was found the GLHE model caused some errors when the time step was too small or the GLHE length was too large. Figure 4.15 and 4.17 show the GLHE fluid temperature comparison between the experimental data and simulation result with different simulation time steps. As shown in Figure 4.15, most of the time, the simulated GLHE outlet temperatures with 1-minute time steps match quite well with the experimentally measured temperatures. However, there are some points when the entering fluid temperature changes suddenly (heat pump switches on or off), the simulated GLHE temperatures showed quite a difference with the

measured data. Figure 4.16 shows the temperature comparison for a 30 minutes period. At time 12:55 PM, the entering fluid temperature of the GLHE decreased because the heat pump was off. Because of the thermal mass in the borehole and transport delay of the fluid flow, at short time steps, the simulated average GLHE temperature would not respond to the inlet fluid temperature changing instantly. Also in the GLHE model, there was an assumption that the fluid temperature changed linearly along the length of the borehole. Therefore, while the average fluid temperature at time 12:55 PM is higher than the EFT, it may be correct. However, the ExFT is higher than either the average fluid temperature or the EFT, and this is incorrect.

In the real heat transfer process of the borehole, the fluid temperature changes more like an exponential decay (representing long term temperature rise or fall). When the time step is big enough and the loop length is not too long, the impact of the thermal mass of the borehole on the fluid temperature changing would not be significant and the linear assumption would be acceptable for the GLHE model. The validity of the linear assumption depends on several parameters: the thermal mass of the borehole, the fluid factor, the borehole length and the simulation time step. Figure 4.17 shows the GLHE fluid temperature comparison at 5-minute time step. At 5-minute time step, the simulated GLHE outlet fluid temperatures matched quite well with the experimentally measured temperatures. To more accurately calculate the GLHE temperature sudden changing at small time step, a 3-d model or a 2-d radial-axial model which addresses the fluid temperature gradient along the borehole is required.

Also as shown in Figure 4.16, a phenomena of heat transport delay was observed. For the borehole of 75 m (258ft) deep, it took about 7 minutes for the fluid to pass through. In Figure 4.15, when the inlet fluid temperature suddenly changes, the outlet fluid temperature would not change significantly until 7 minutes later. However, the current GLHE model is not able to address the fluid transport delay issue. Again, a 3-d model or 2-d radial-axial model will help to address the fluid transport delay issue, which happens in the real borehole heat transfer process.

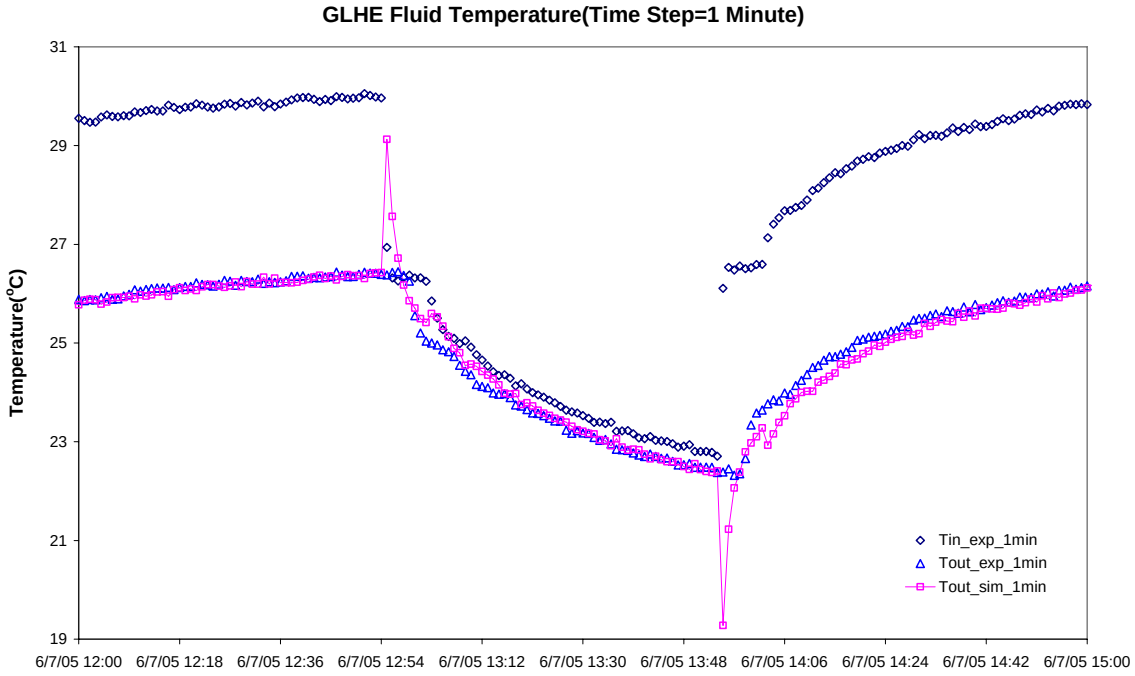

Figure 4.15 GLHE fluid temperatures at 1-minute time step in three hours

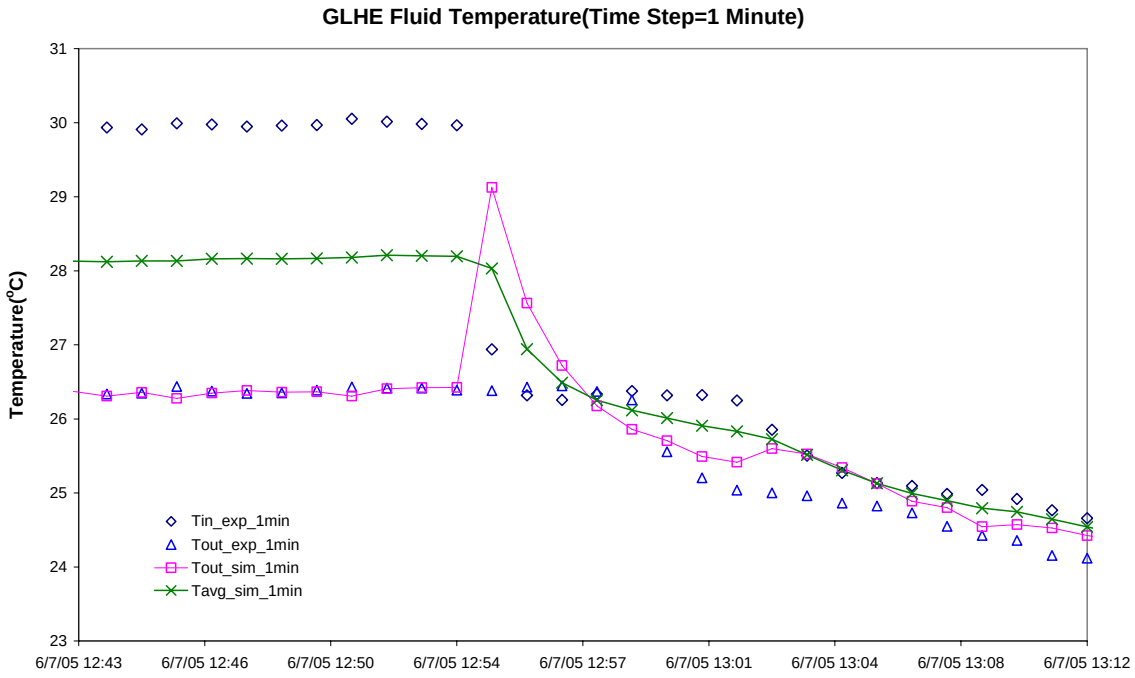

Figure 4.16 GLHE fluid temperatures at 1-minute time step in half an hour

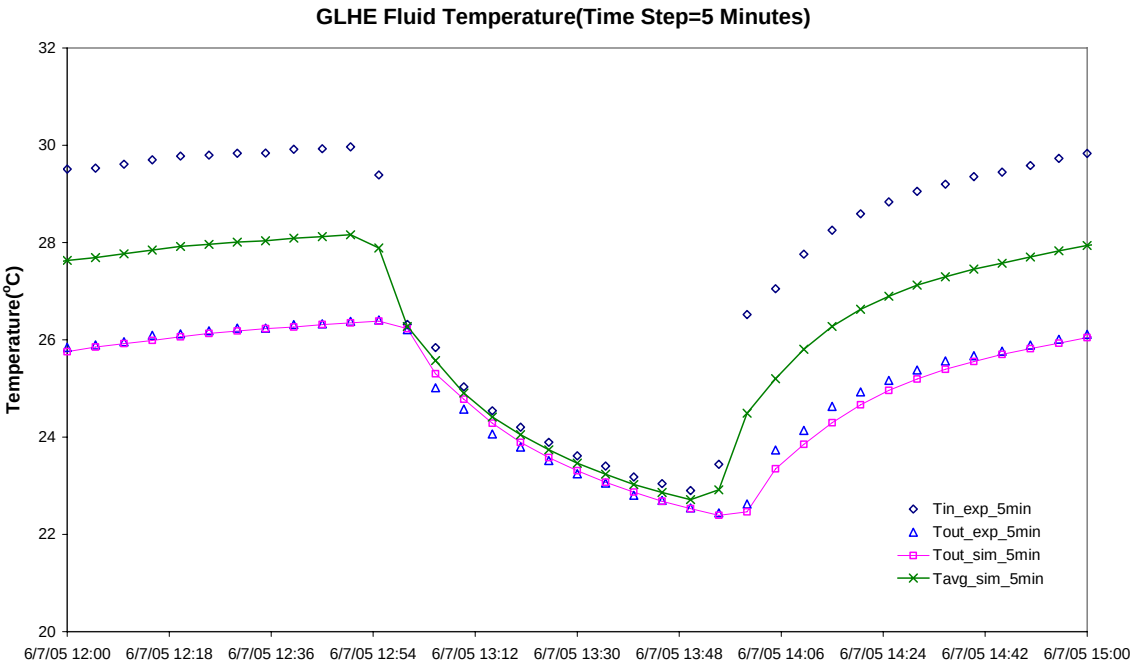

Figure 4.17 GLHE fluid temperatures at 5-minute time step

4.1.10 Summary of GLHE Model Results

Like the Yavuzturk and Spitler (1999) model, the one-dimensional numerical model and LTS GLHE model is an extension to the original long time-step Eskilson (1987) model. However, whereas that model used a short time-step g-function to account for short time-step effects, the new GLHE model uses a one-dimensional numerical model to calculate the borehole wall temperature at short time-steps directly. A new approach has been developed to couple the one-dimensional numerical and LTS response factor model together for modeling vertical GLHE.

The one-dimensional numerical model coupled with LTS model was cast as HVACSIM+ component model as TYPE621. An annual hourly simulation GSHP system in a church building was carried out to demonstrate this new GLHE model and illustrate the effect of thermal mass and variable convective resistance.

Generally, the flow rate in the ground loop heat exchangers is designed so as to ensure turbulent flow in the tube. In this case, the variation of convective thermal resistance due to fluid temperatures and flow rates has little effect on the heat transfer rate of the ground loop heat exchanger. Using one-dimensional numerical model, a new STS response factor model is then developed with fixed convective thermal resistance. The new STS and LTS model was cast as HVACSIM+ component model as TYPE620.

A validation for the new GLHE model is highly desirable. The one-dimensional numerical model has been verified using GEMS2D (Rees 2000). Additional experimental validation of the new GLHE model is provided in Chapter 5, using operating data

collected at from an HGSHP research facility (Hern 2004) located on the campus of Oklahoma State University.

Firstly, the verification of the effects of fluid thermal mass is carried out. An experimentally estimated fluid factor is used for the validation of the GLHE model. Comparison of the simulation results with different fluid factor values is presented in Chapter 5.

4.2 Heat Pump Models

In this research, two different heat pump models are used. Jin and Spitler's (2002) parameter estimation-based heat pump model is used for modeling a single heat pump. The parameter estimation-based heat pump model also is used in experimental validation of HGSHP system simulation (Chapter 5). This model is discussed briefly in Section 4.2.1 below.

In the study of buildings with many heat pumps, it is difficult to model each heat pump independently. As an alternative, a "gang-of-heat-pumps" model is developed as part of this work. This model considers, in aggregation, the behavior of all heat pumps in the building. This model is described in Section 4.2.2 below.

4.2.1 Parameter Estimation Heat Pump Model

The selected heat pump model, TYPE559, is based on a parameter estimation based model developed by Jin and Spitler (2002). The parameter estimation based model uses a thermodynamic analysis of the refrigeration cycle, simplified heat exchanger

models, and a detailed model of the refrigerant compressor. The parameters of the model are estimated from the manufacturer's catalog data using a multi-variable optimization procedure. This has better performance than equation-fit models for modeling heat pumps when the fluid temperatures and flow rates go beyond the catalog data.

The estimated parameters include piston displacement, clearance factor, load side heat transfer coefficient, source side heat transfer coefficient, a proportional loss factor accounting for the electromechanical loss of the compressor, constant part of the electromechanical loss, pressure drop across the suction and discharge valves, and superheat temperature. A detailed description of the model can be found in Jin and Spitler (2002; 2003).

In the parameter estimation-based heat pump model, the heating/cooling capacity is calculated based on the fluid inlet temperatures and flow rates on two sides of the heat pump. However, for this implementation the model has been cast to take loads as inputs, which are used when the heat pump runs with partial loads.

In Chapter 5, average experimental data of 5-minute time step was collected for validation and the heat pump might be switched on or off during the 5-minute time step of simulation. Therefore, an approach to deal with the heat pump partial duty at 5-minute time steps is described in Section 5.2.1.

The parameter estimation based heat pump model (TYPE559) diagram can be seen in Figure 4.18, showing all the inputs, outputs and parameters needed to run the

model. A multi-variable optimization procedure has been developed to generate these parameters from the heat pump manufacturer's catalog data.

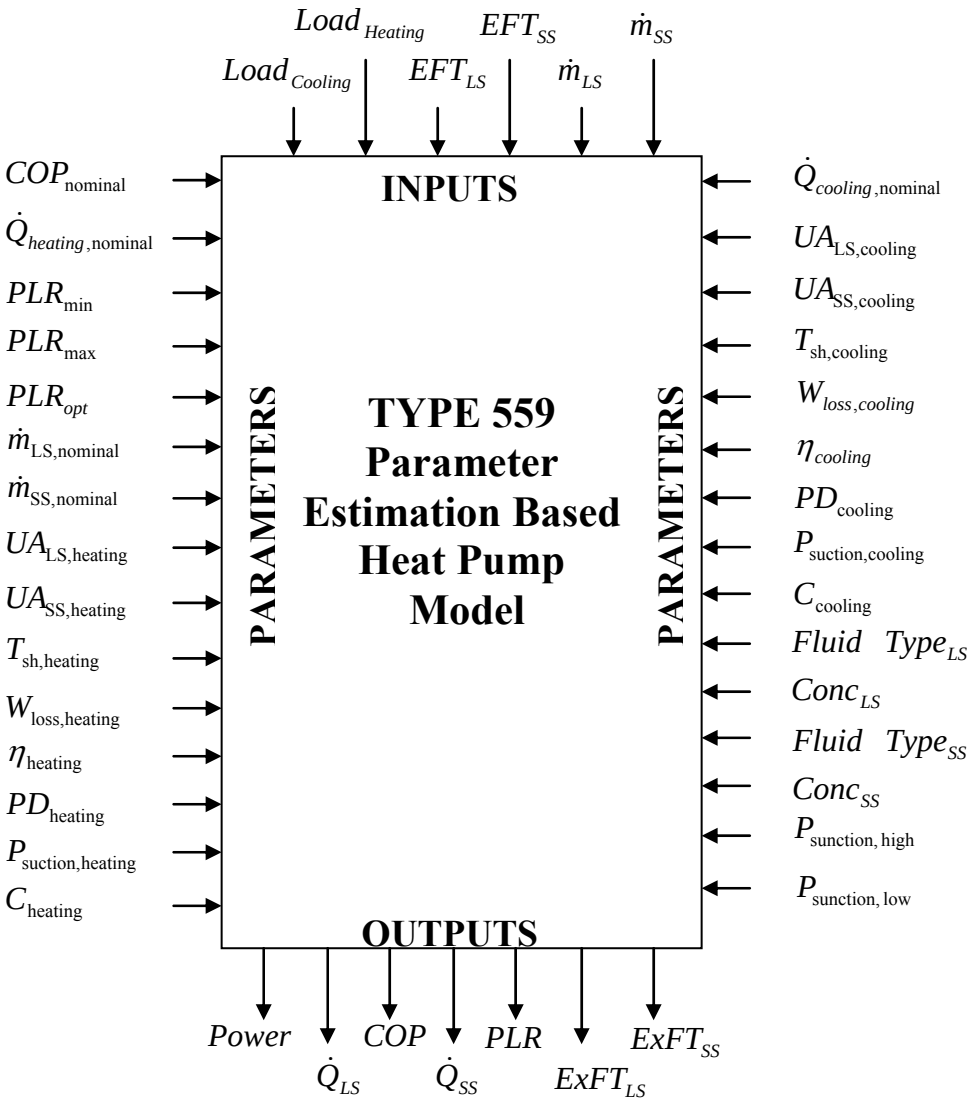

Figure 4.18 TYPE 559 parameter estimation based heat pump HVACSIM+ model diagram.

In the diagram:

$Load_{Cooling}$ = System required cooling load, (W);

$Load_{Heating}$ = System required heating load, (W);

EFT_{LS} = Entering fluid temperature of heat pump at load side, (ºC);

EFT_{SS} = Entering fluid temperature of heat pump at source side, (ºC);

$\dot{m}_{LS}$ = Mass flow rate at heat pump load side, (kg/s);

$\dot{m}_{SS}$ = Mass flow rate at heat pump source side, (kg/s);

$Power$ = Heat pump power consumption, (kW);

$\dot{Q}_{LS}$ = Heat pump total heating/cooling capacity, (kW);

COP = Heat pump COP, (-);

$\dot{Q}_{SS}$ = Heat pump source side heat transfer rate, (kW);

PLR = Heat pump part load ratio, (-);

$E_x FT_{LS}$ = Exiting fluid temperature on heat pump load side, (ºC);

$E_x FT_{SS}$ = Exiting fluid temperature on heat pump source side, (ºC);

COP_{nominal} = Nominal COP of heat pump, (-);

$\dot{Q}_{heating,\text{nominal}}$ = Nominal heating capacity of heat pump, (kW);

$PLR_{\min}$ = Minimal part load ratio of heat pump, (-);

$PLR_{\max}$ = Maximal part load ratio of heat pump, (-);

PLR_{opt} = Optimal part load ratio of heat pump, (-);

$\dot{m}_{\text{LS,nominal}}$ = Nominal volumetric flow rate at heat pump load side, (m^3/s);

$\dot{m}_{\text{SS,nominal}}$ = Nominal volumetric flow rate at heat pump source side, (m^3/s);

$UA_{\text{LS,heating}}$ = Load side heat transfer coefficient at heating mode, (kW/K);

$UA_{SS,heating}$ = Source side heat transfer coefficient at heating mode, (kW/K);

$T_{sh,heating}$ = Superheat temperature at heating mode, (ºC);

$W_{loss,heating}$ = Constant part of the electromechanical losses at heating mode, (kW);

$\eta_{heating}$ = Electromechanical loss factor proportional to power consumption at heating mode, (-)

$PD_{heating}$ = Piston displacement at heating mode, (m^3/s);

$P_{suction,heating}$ = Pressure drop across the suction valve at heating mode, (kPa);

$C_{heating}$ = Clearance factor at heating mode, (-);

$\dot{Q}_{cooling,nominal}$ = Nominal cooling capacity of heat pump, (kW);

$UA_{LS,cooling}$ = Load side heat transfer coefficient at cooling mode, (kW/K);

$UA_{SS,cooling}$ = Source side heat transfer coefficient at cooling mode, (kW/K);

$T_{sh,cooling}$ = Superheat temperature at cooling mode, (ºC);

$W_{loss,cooling}$ = Constant part of the electromechanical losses at cooling mode, (kW);

$\eta_{cooling}$ = Electromechanical loss factor proportional to power consumption at cooling mode, (-)

$PD_{cooling}$ = Piston displacement at cooling mode, (m^3/s);

$P_{suction,cooling}$ = Pressure drop across the suction valve at cooling mode, (kPa);

$C_{cooling}$ = Clearance factor at heating mode, (-);

$Fluid\ \ Type_{LS}$ = The type of working fluid at heat pump load side: (0 for water, 1 for propylene glycol, 2 for Ethylene glycol);

$Conc_{LS}$ = Weight of antifreeze concentration in solution at heat pump load side;

$Fluid\ \ Type_{SS}$ = The type of working fluid at heat pump source side: (0 for water, 1 for propylene glycol, 2 for Ethylene glycol);

$Conc_{SS}$ = Weight of antifreeze concentration in solution at heat pump source side;

$P_{\text{sunction, high}}$ = High pressure to shut off heat pump, (kPa);

$P_{\text{sunction, low}}$ = Low pressure to shut off heat pump, (kPa);

$Cycle\ \ Time$ = Heat pump unit cycle time, (s).

4.2.2 Gang-of-Heat-Pumps Model

The purpose of the "gang-of-heat-pumps" model is to represent multiple heat pumps without the need to have separate models for each individual heat pump. In particular, the total power consumption and heat transfer rate to/from the water loop are of interest for this work.

In addition, the model also determines the average number of heat pumps on in any time step and the required flow rate on the source side of heat pumps. Following ASHRAE Standard 90.1 the heat pumps are assumed to be equipped with two-way valve on the source water supply that opens only when the heat pump is on. When the total load seen by the building during any given time step is varied, the total number of heat pumps on is changed as well as the system flow rate at the source side of heat pumps.

In this model, the number of heat pumps and the system flow rate are determined first. At any given time step the number of heat pumps, in heating and cooling, is

determined by calculating the number that are needed to meet the required load, heating and cooling, with the nominal heating and cooling capacity (This is an approximation that all the heat pumps operate at the design conditions and provide the nominal heating and cooling capacity). Then, the system flow rate that corresponds to the number of heat pumps operation is also determined. This flow rate is output in order to be passed to the variable speed pump model, TYPE 592.

Variable speed pumping systems typically have a lower limit of about 30% of full flow rate. Since every heat pump is equipped with a two-way valve, a bypass is opened when less than 30% of full flow is required with the heat pumps on. When the calculated system flow rate is less than the minimal system flow rate, it will then be set as minimal system flow rate. In effect, the gang-of-heat-pumps model is also modeling the bypass control. The calculated system flow rate for that time step is then send to the variable speed pumping model, discussed in Section 4.4.2, where the pumping power is calculated.

An equation-fitting model was developed to calculate the heating and cooling COPs of heat pumps, as shown in Equation 4-12 and 4-13 below. Of particular interest are the effects of variation in entering fluid temperature and flow rates for this work.

$$COP_{heating} = C_1 + C_2 \cdot EFT + C_3 \cdot EFT^2 + C_4 \cdot \dot{m}_s + C_5 \cdot \dot{m}^2{}_s + C_6 \cdot EFT \cdot \dot{m}_s \quad (4\text{-}12)$$

$$COP_{cooling} = C_7 + C_8 \cdot EFT + C_9 \cdot EFT^2 + C_{10} \cdot \dot{m}_s + C_{11} \cdot \dot{m}^2{}_s + C_{12} \cdot EFT \cdot \dot{m}_s \quad (4\text{-}13)$$

Where:

$COP_{heating}$ = Heat pump coefficient of performance during heating mode, (-);

$COP_{cooling}$ = Heat pump coefficient of performance during cooling mode,(-);

EFT = Entering fluid temperature at the source side of heat pump, (ºC);

$\dot{m}_s$ = Mass flow rate of a single heat pumps, (kg/s);

C_{1-6} = Fitted coefficients for heating mode, (-);

C_{7-12} = Fitted coefficients for cooling mode, (-).

Once the heating and cooling COPs are calculated, the power consumption of heat pumps is calculated by dividing the load, heating and/or cooling, by the COP. The existing fluid temperature of heat pumps is calculated from the heat transfer rate on the heat pumps source side, the system flow rate and the entering fluid temperature.

The gang-of-heat-pumps model, TYPE557, diagram can be seen in Figure 4.19, showing all the inputs, outputs and parameters needed to run the model.

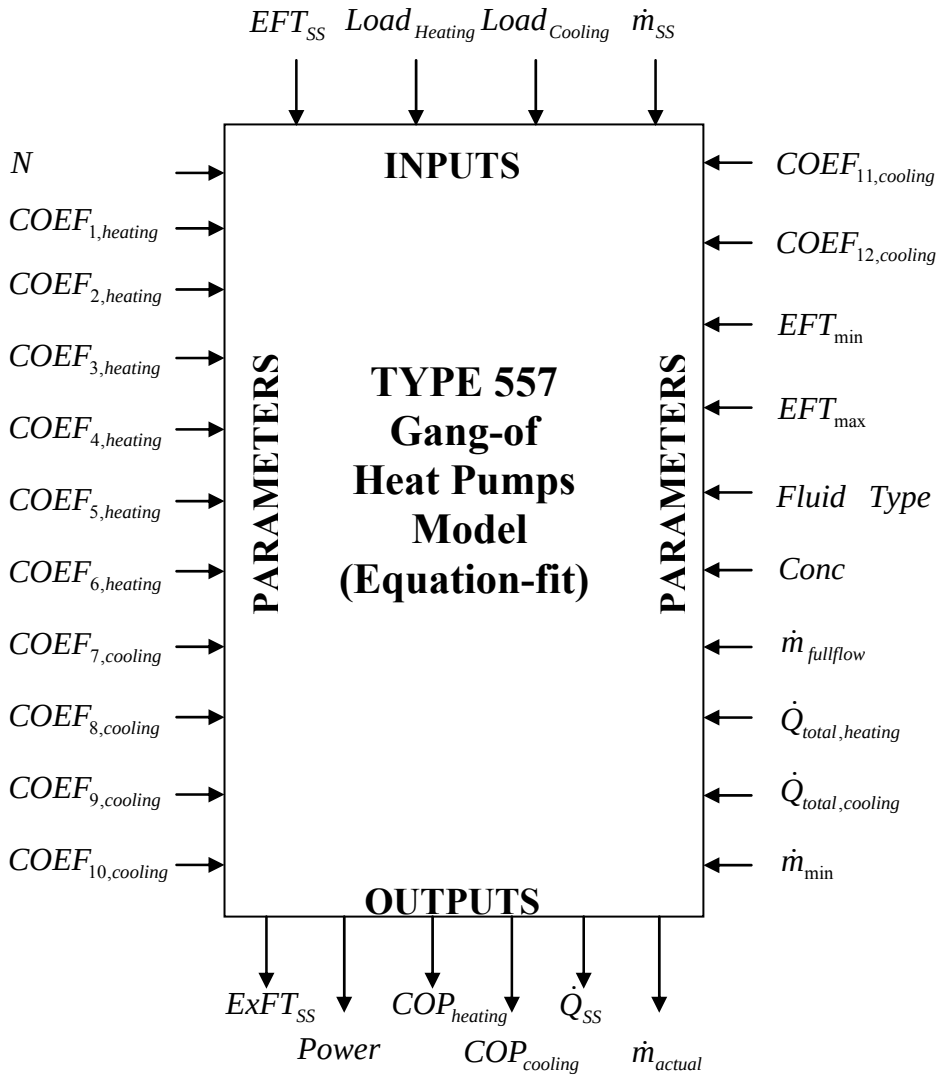

Figure 4.19 TYPE 557 gang-of-heat-pumps HVACSIM+ model diagram

In the diagram:

$\dot{m}_{ss}$ = Mass flow rate of fluid at heat pump source side, (kg/s);

$COEF_{1–12}$ = Coefficients corresponding to C_1 to C_{12};

$\dot{m}_{fullflow}$ = Mass flow rate of fluid at heat pump source side when all the pumps are on, (kg/s);

$\dot{m}_{\min}$ = Minimal flow rate of fluid at heat pump source side, usually set at 30% of $\dot{m}_{fullflow}$, (kg/s);

$\dot{m}_{actual}$ = Actual flow rate of fluid at heat pump source side, (kg/s);

$EFT_{\min}$ = Minimal entering fluid temperature at heat pump source side, (ºC);

$EFT_{\max}$ = Maximal entering fluid temperature at heat pump source side, (ºC);

$\dot{Q}_{total,heating}$ = Total heating capacity of heat pumps, (kW);

$\dot{Q}_{total,cooling}$ = Total cooling capacity of heat pumps, (kW).

A multi-variable optimization procedure has been developed to generate these parameters from the heat pump manufacturer's catalog data. This gang-of-heat-pumps model is used for the investigation of HGSHP system control strategy in Chapter 7.

4.3 Cooling Tower Models

In an HGSHP system, both open-circuit cooling towers and closed-circuit cooling towers maybe be used as supplemental heat rejecters. In this section, two existing open-circuit cooling tower models in HVACSIM+ are described briefly. A closed-circuit cooling tower model based on the Stabat and Marchio (2004) simplified indirect-contact evaporative cooling-tower model is developed. The model is cast as an HVACSIM+ component model and verified with manufacturer's catalog data.

4.3.1 Open-circuit Cooling Tower Models

Two open-circuit cooling tower models have been developed as HVACSIM+ component models: one is the fixed UA cooling tower model developed by Khan (2004)

and another is the variable UA cooling tower model based on Lebrun and Silva (2002). Applying the effectiveness-NTU method, the open-circuit cooling tower is modeled as a counter flow heat exchanger with water at one side and moist air treated as an equivalent ideal gas at the other side. Moist air enthalpy is used to calculate the heat transfer rate on the air side by assuming the enthalpy is a function of air wet bulb temperature. A detailed description of the effectiveness-NTU model can be found in Khan (2004).

4.3.1.1 Fixed UA Open-circuit Cooling Tower Model

The fixed UA open-circuit cooling tower model, TYPE 765, is based on a model developed by Khan (2004). The parameter UA is calculated from the manufacturer's catalog data.

The fixed UA open-circuit cooling tower model, TYPE765, diagram can be seen in Figure 4.20, showing all the inputs, output and parameters. This fixed UA open-circuit cooling tower model is used for the investigation of control strategies of HGSHP systems.

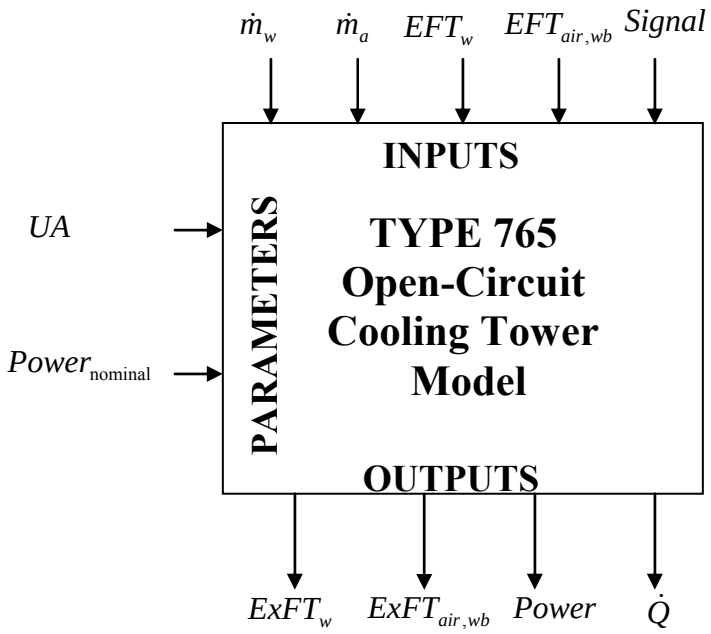

Figure 4.20 TYPE 765 fixed UA open-circuit cooling tower HVACSIM+ model diagram.

In the diagram:

Signal = Control signal of the cooling tower, 1: On and 0: Off.

4.3.1.2 Variable UA Open-circuit Cooling Tower Model

In the variable UA open-circuit cooling tower model, the UA value is calculated from Equation 4-14.

$$UA = [k\dot{m}_w^x \dot{m}_a^y] \frac{C_{pe}}{C_{p,moistair}} \tag{4-14}$$

Where:

UA = Cooling tower overall heat transfer coefficient times area, (W/K);

$\dot{m}_w$ = Mass flow rate of water, (kg/s);

$\dot{m}_a$ = Mass flow rate of air, (kg/s);

C_{pe} = Effective specific heat of moist air, (J/kg-K);

$C_{p,moistair}$ = Specific heat of moist air, (J/kg-K);

k, x, y = Coefficients to be fitted.

The coefficients k, x, y can be determined based on the experimentally measured data.

The variable UA open-circuit cooling tower model, TYPE768, diagram can be seen in Figure 4.21, showing all the inputs, output and parameters. This variable UA open-circuit cooling tower model is used for the experimental validation of HGSHP system simulation.

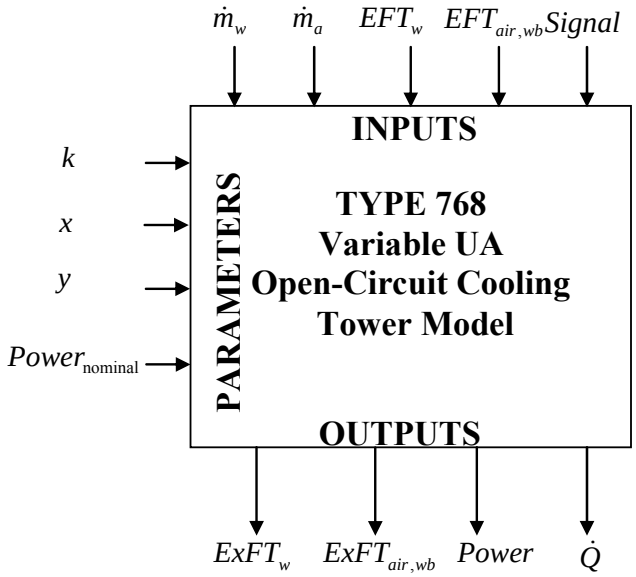

Figure 4.21 TYPE 768 variable UA open-circuit cooling tower HVACSIM+ model diagram.

4.3.2 Closed-circuit Cooling Tower Model

The closed-circuit cooling tower can operate at the wet or dry regime. The closed-circuit cooling tower model deals with both these two phenomena.

4.3.2.1 Theoretical Closed-circuit Cooling Tower Model

Using the Stabat and Marchio (2004) simplified indirect-contact evaporative cooling-tower model, a closed-circuit cooling tower model was developed. The heat exchange process of the closed-circuit cooling tower coils at wet regime is shown in Figure 4.22. The heat exchange of the closed-circuit cooling tower coil includes two parts: 1) the heat transfer between the air and the water film outside the tube; and 2) the heat transfer between the water in the tube and the water film outside the tube. The heat transfer between the water and the water film includes: the convection in the tube; the conduction through the tube and the heat transfer between the external surface and convection in the water film. The heat transfer between water and air can be represented by an overall heat transfer coefficient.

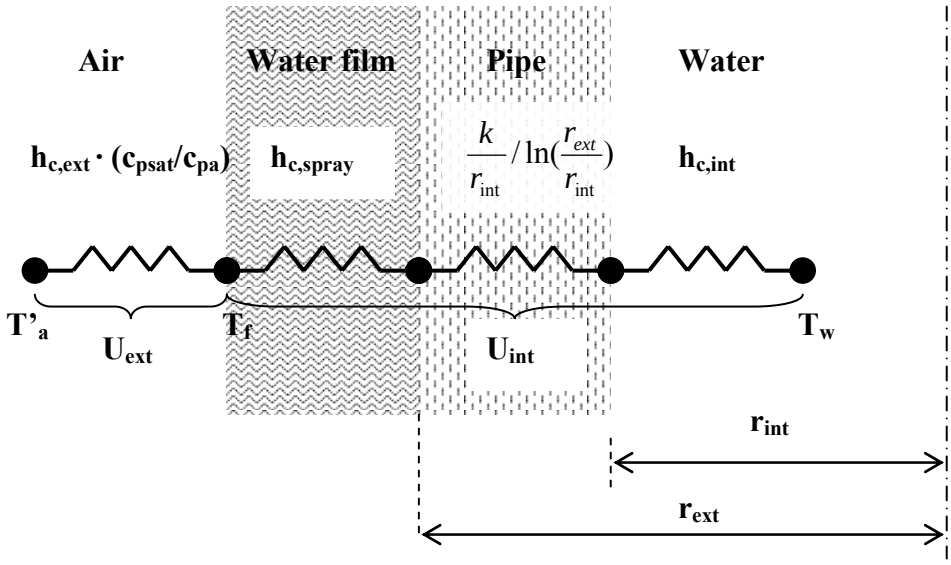

Figure 4.22 Heat exchanger scheme of closed-circuit cooling tower coils in wet regime.

Applying the Effectiveness-NTU method for a counter flow single pass heat exchanger, the effectiveness (ε) of a closed-circuit cooling tower is calculated and the equations are listed in Table 4.5. The calculation would have two different heat transfer coefficients ($U_t A_t$) based on the two different operating regimes.

Table 4.5 Effectiveness-NTU relations in wet and dry regimes

Wet regime	**Dry regime**
$\varepsilon = \dfrac{C_w(T_{wi} - T_{wo})}{C_{\min}(T_{wi} - T_{ai})}$	$\varepsilon = \dfrac{C_w(T_{wi} - T_{wo})}{C_{\min}(T_{wi} - T_{ai})}$
$\varepsilon = \dfrac{1-\exp[-NTU(1-C_r)]}{1-C\exp[-NTU(1-C_r)]}$ $(if \quad C_r < 1)$ $with \quad NTU = \dfrac{U_t A_t}{C_{\min}}$ $and \quad C_r = \dfrac{C_{\min}}{C_{\max}}$ $\varepsilon = \dfrac{NTU}{1+NTU}$ $(if \quad C_r = 1)$	
$C_a = \dot{m}_a c_{psat} \quad C_w = \dot{m}_w c_{pw}$	$C_a = \dot{m}_a c_{pa} \quad C_w = \dot{m}_w c_{pw}$
$C_{\min} = \text{minimum}(C_a, C_w) \quad C_{\max} = \text{maximum}(C_a, C_w)$	
$\dfrac{1}{U_t A_t} = \dfrac{1}{U_{ext}^{wet} A_{ext}} + \dfrac{1}{U_{\text{int}}^{wet} A_{\text{int}}}$	$\dfrac{1}{U_t A_t} = \dfrac{1}{U_{ext}^{dry} A_{ext}} + \dfrac{1}{U_{\text{int}}^{dry} A_{\text{int}}}$

Where:

ε = Effectiveness, (-);

T_{wi}, T_{wo} = Inlet and outlet water temperature, (ºC);

T_{ai}, T_{ao} = Inlet and outlet air dry-bulb temperature, (ºC);

$\dot{m}_a$ = Mass flow rate of air, (kg/s);

$\dot{m}_w$ = Mass flow rate of water, (kg/s);

c_w = Specific heat of water, (kJ/kg-K);

A_{ext}, A_{int} = Surface area at external side and internal side, (m^2);

$U_{ext}^{wet} A_{ext}$ = Air-side heat transfer coefficient in wet regime, (W/K);

$U_{ext}^{dry} A_{ext}$ = Air-side heat transfer coefficient in dry regime, (W/K);

$U_{\text{int}}^{wet} A_{\text{int}}$ = Water-side heat transfer coefficient, (W/K).

Air-side Heat Transfer Coefficient

On the air-side heat transfer, Stabat and Marchio (2004) correlated the air-side heat transfer coefficients as:

$$U_{ext}^{wet} A_{ext} = \beta_{ext,wet} c_{psat} \dot{m}_a^{0.8} \qquad \text{(wet regime)} \qquad (4\text{-}15)$$

$$U_{ext}^{dry} A_{ext} = \beta_{ext,dry} c_{pa} \dot{m}_a^{0.8} \qquad \text{(dry regime)} \qquad (4\text{-}16)$$

Where:

C_{psat} = Specified heat of saturated air, (J/kg-K);

c_{pa} = Specified heat of air, (J/kg-K);

$\beta_{ext,wet}$ = Constant to be fitted for wet regime.

$\beta_{ext,dry}$ = Constant to be fitted for dry regime.

Water-side Heat Transfer Coefficient

On the water-side heat transfer, the conductive resistance through the tubes is negligible compared to the convective resistance on both sides of the tube. The water-side heat transfer coefficient, $U_{ext}^{wet} A_{ext}$, can be decomposed as:

$$\frac{1}{U_{ext}^{wet} A_{ext}} = \frac{1}{h_c^w A_{\text{int}}} + \frac{1}{h_c^{film} A_{ext}} \qquad (4\text{-}17)$$

Where:

h_c^w = Convective heat transfer coefficient of water in the tube, (W/m^2-K);

h_c^{film} = Heat transfer coefficient between tube surface and water film, (W/m^2-K).

In the tube, the Dittus – Boelter correlation (Incropera and Dewitt (2002)) is used:

$$h_c^w = 0.023 \frac{k_w}{d_{\text{int}}} \text{Re}^{0.8} \text{Pr}^{0.3} \qquad (\text{Re} > 10^4) \tag{4-18}$$

Where:

k_w = Conductivity of water, (W/m-K);

d_{int} = Diameter of inner tube; (m).

Stabat and Marchio (2004) gave a general form for the correlation of h_c^{film} for the heat transfer coefficient between the tube surface and water film:

$$h_c^{film} = C(\frac{\dot{G}_{spray}}{d_{ext}})^n \tag{4-19}$$

Where:

$\dot{G}_{spray}$ = Flow rate of spray water per unit breadth, (kg/m^2-s);

d_{ext} = Diameter of outer tube; (m);

C, n = Constants to be fitted.

Then Equation 4-17 can be simplified as:

$$U_{\text{int}}^{wet} A_{\text{int}} \propto \text{Re}^{0.8}\,\text{Pr}^{0.3} = \beta_{\text{int},wet} \dot{m}_w^{\,0.8} \mu_w^{\,-0.5} \tag{4-20}$$

Where:

μ_w = Dynamic viscosity, (kg/m-s).

$\beta_{\text{int},wet}$ = Constant to be fitted.

When the cooling tower runs in the dry regime, neglecting the conductive resistance through the tubes, the water-side heat transfer coefficient, $U_{\text{int}}^{dry} A_{\text{int}}$, can be decomposed as:

$$\frac{1}{U_{\text{int}}^{dry} A_{\text{int}}} = \frac{1}{h_c^{w} A_{\text{int}}} \tag{4-21}$$

Applying the Dittus – Boelter correlation (Incropera and Dewitt (2002)), Equation 4-21 can be simplified as:

$$U_{\text{int}}^{dry} A_{\text{int}} \propto \text{Re}^{0.8}\,\text{Pr}^{0.3} = \beta_{\text{int},dry} \dot{m}_w^{\,0.8} \mu_w^{\,-0.5} \tag{4-22}$$

Where:

$\beta_{\text{int},dry}$ = Constant to be fitted.

Overall Heat Transfer Coefficient

The overall heat transfer coefficient of closed-circuit cooling tower can be expressed as:

$$\frac{1}{U_t^{wet} A_t^{wet}} = \frac{1}{\beta_{ext,wet} c_{psat} \dot{m}_a^{\,0.8}} + \frac{\mu_w^{\,0.5}}{\beta_{\text{int},wet} \dot{m}_w^{\,0.8}} \quad \text{(wet regime)} \tag{4-23}$$

$$\frac{1}{U_t^{dry} A_t^{dry}} = \frac{1}{\beta_{ext,dry} c_{pa} \dot{m}_a^{0.8}} + \frac{\mu_w^{0.5}}{\beta_{\text{int},dry} \dot{m}_w^{0.8}} \qquad \text{(dry regime)} \qquad (4\text{-}24)$$

The coefficients $\beta_{ext,wet}$, $\beta_{\text{int},wet}$, $\beta_{ext,dry}$ and $\beta_{\text{int},dry}$ are fitted using manufacturer's catalog data.

The variable UA open-circuit cooling tower model, TYPE768, diagram can be seen in Figure 4.23, showing all the inputs, output and parameters.

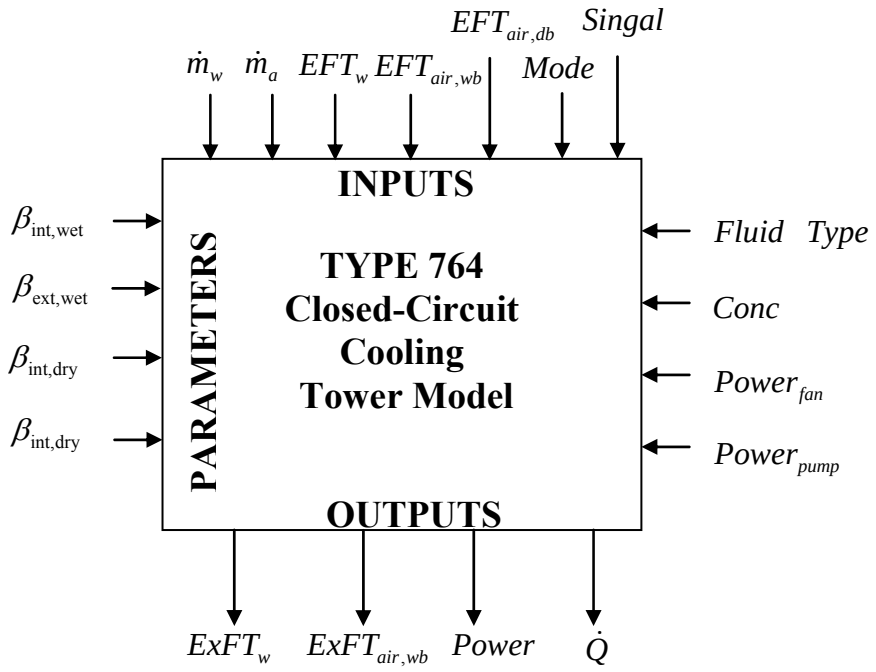

Figure 4.23 TYPE 764 closed-circuit cooling tower HVACSIM+ model diagram.

In the diagram,

$EFT_{air,db}$ = Entering air dry bulb temperature, (C);

Mode = Cooling tower mode, (0: dry regime; 1: wet regime);

$Power_{fan}$ = Fan power of cooling tower; (kW);

$Power_{pump}$ = Circulation pump power of cooling tower; (kW).

4.3.2.2 Verification of Closed-circuit Cooling Tower Model

The closed-circuit cooling tower model has been compared on the manufacturer's catalog data at different wet-bulb temperatures, inlet water temperatures and water flow rates for a selected closed-circuit cooling tower. (B.A.C. Model: VFL-024-22H). The estimated coefficients for the selected cooling tower in the wet regime are $\beta_{ext,wet} = 0.36$ and $\beta_{\text{int},wet} = 0.15$. The estimated coefficients for the selected cooling tower in dry regime are $\beta_{ext,dry} = 0.70$ and $\beta_{\text{int},dry} = 30.75$. As shown in Figure 4.24, the heat transfer rates predicted by the model match well with the manufacturer's catalog data, with all prediction within 5%. Also as shown in the figure, a closed-circuit cooling tower at wet regime has a much higher heat rejection rate than that when it operates at dry regime.

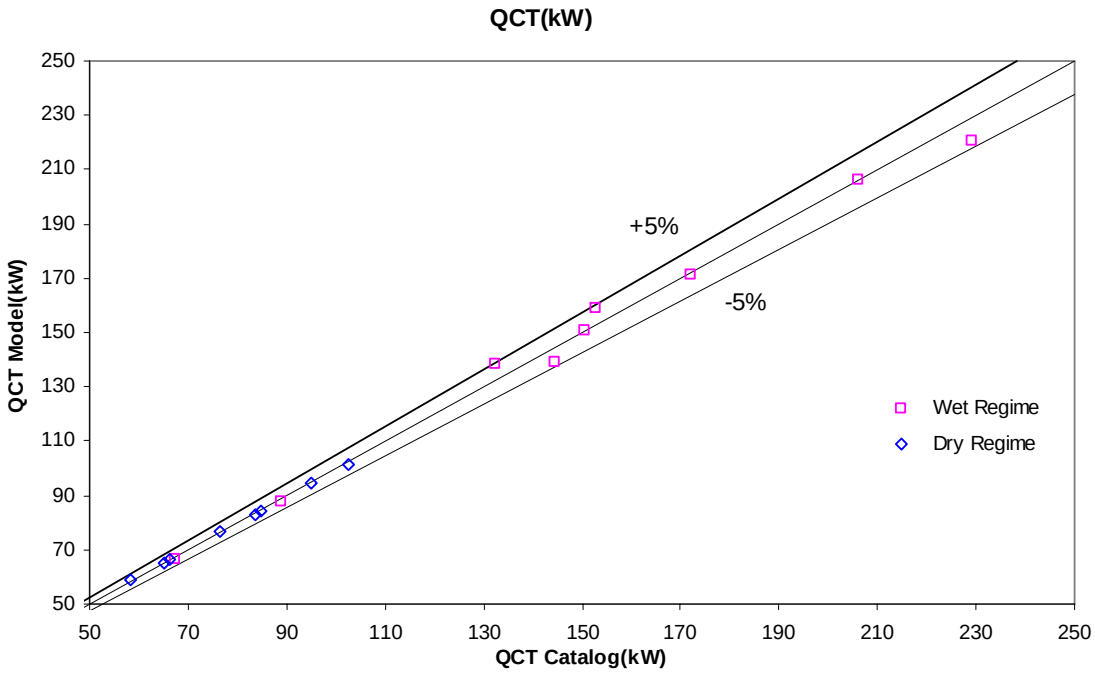

Figure 4.24 Calculated heat rejection rate vs. catalog heat rejection rate both at wet and dry regime.

4.4 Pump Models

In a variable flow pumping system, pump speed is adjusted to maintain a constant differential pressure across the heat pump unit loop supply and return headers. This insures adequate flow across the heat pump. When a heat pump is turned off, a two-way valve on the heat pump supply closes. As the number of closed valves increases, the pump's speed is reduced to maintain a constant differential pressure. Based on the physics of centrifugal pumps, the power required is approximately proportional to the cube of the flow rate in this scenario. As most buildings have a substantial number of low part-load hours, a significant amount of energy can be saved by using a variable speed drive (VSD). Therefore, a VSD pump model is developed.

A simple variable speed drive pump is also used in the secondary loop of HGSHP systems for the cooling tower. The simple variable speed drive pump mode has been developed as an HVACSIM+ component model and is described below.

4.4.1 A Simple Variable Speed Pumping Model

The selected simple variable speed pumping model is TYPE582. The simple variable speed pumping model calculates the pumping power using a cubic relationship between the fraction of full power (FFP) and fraction of full flow (FFF). Pump motor efficiency is not explicitly considered in the model, but can be included in the nominal efficiency.

The constant speed pump model, TYPE582, diagram can be seen in Figure 4.25, showing all the inputs, output and parameters.

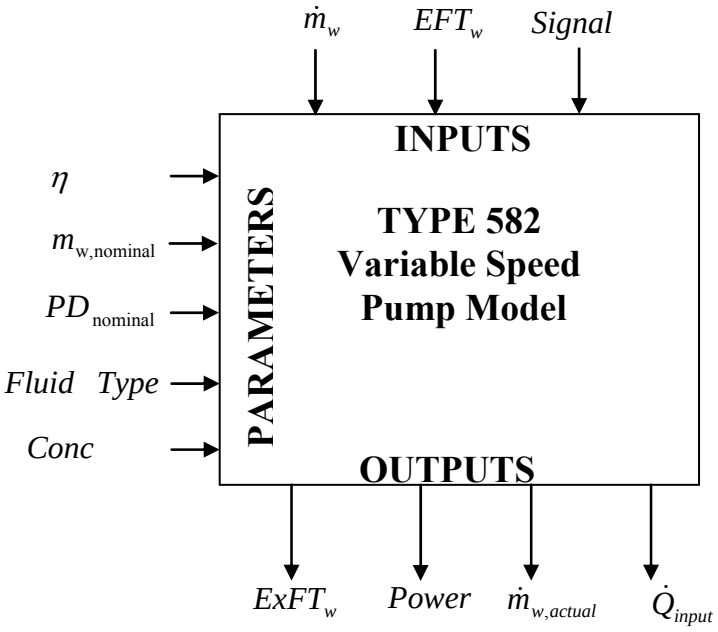

Figure 4.25 TYPE 582 constant speed pumping HVACSIM+ model diagram.

In the diagram:

$\dot{m}_w$ = Mass flow rate of pump, (kg/s);

η = Pump efficiency at the nominal flow rate, (-);

$\dot{m}_{\text{w,nominal}}$ = Pump nominal mass flow rate, (kg/s);

PD_{nominal} = Pressure drop at the nominal flow rate, (kPa);

$\dot{m}_{w,actual}$ = Pump actual mass flow rate with control, (kg/s);

$\dot{Q}_{input}$ = Heat input to the loop by the pump, (kW).

4.4.2 A Detailed Variable Speed Pumping Model

Relying on a user-precomputed curve for fraction of full power vs. fraction of full flow of the system, a dimensionless equation fit of fraction of full power against fraction of full flow will be developed for this VSD pump. Using user-specified full flow pumping power and the required flow from the "gang-of-heat-pumps" model (TYPE559), the energy consumption can be determined.

First the FFF is calculated, which is based on the ratio of actual flow rate to the design flow rate:

$$FFF = \frac{\dot{m}_{actual}}{\dot{m}_{design}} \tag{4-25}$$

Where:

FFF = Fraction of full flow, (-);

$\dot{m}_{actual}$ = Mass flow rate required by the heat pumps, (kg/s);

$\dot{m}_{design}$ = Mass flow rate of a system if all heat pumps are in operation, (kg/s).

Next, the FFP is computed using a polynomial with fitted coefficients:

$$FFP = C_0 + C_1 \cdot FFF + C_2 \cdot FFF^2 + C_3 \cdot FFF^3 \quad (4\text{-}26)$$

Where:

C_{0-3} = FFP coefficients.

To determine the coefficients in Equation 4.23 above, the total pressure drop at the full design flow rate is calculated for the system. A pump is selected to meet the flow rate and the pump head. Using data from the selected pump, non-dimensional equations of head vs. flow and efficiency vs. flow are obtained. An analysis is performed in a spreadsheet to determine pump speed, pressure drop, and pumping power over the full range of possible system flow rate (a lower limit of 30% of full flow rate). In this procedure, a strategy for controlling the distribution of flow to GLHE and PHE/cooling tower is required to calculate the system pressure drop at different system flow rates, which is provided in Chapter 6. Then, a polynomial equation of fraction of full power as a function of fraction of full flow is obtained. Figure 4.26 shows FFF vs. FFP for a HGSHP system.

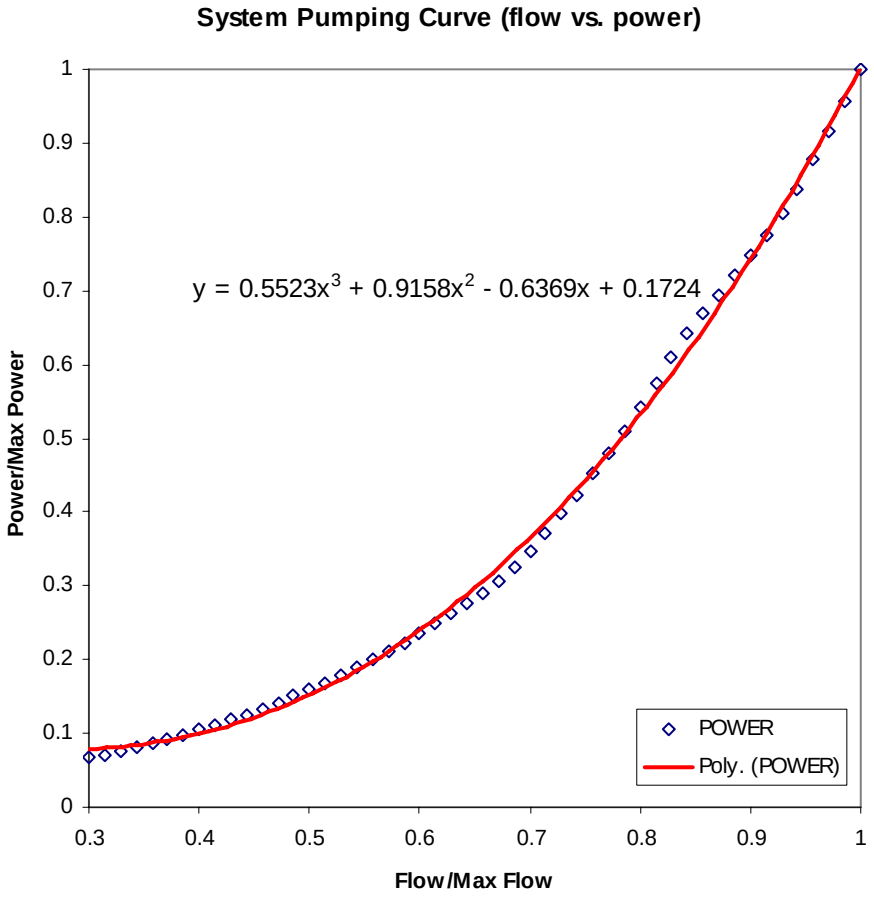

Figure 4.26 Fraction of Full Flow vs. Fraction of Full Power

Motor and drive losses are accounted for with a single efficiency number:

$$Power = FFP \cdot Power_{design} / \eta_{motor} \tag{4-27}$$

Where:

$Power_{design}$ = Power required by the pump at full flow, (W);

η_{motor} = Pump motor efficiency, (-).

By assuming all the pumping power is added into loop except the motor/drive losses, the exiting fluid temperature of pump is calculated:

$$T_{outlet} = T_{inlet} + \frac{\eta_{motor} Power}{\dot{m}_w c_{pw}} \tag{4-28}$$

Variable speed pumping systems typically have a lower limit of about 30% of full flow rate. Therefore, a minimum flow rate check $\dot{m}_{\min}$ is cast in the model to ensure the variable speed pump has a flow rate no less than 30% of full flow rate.

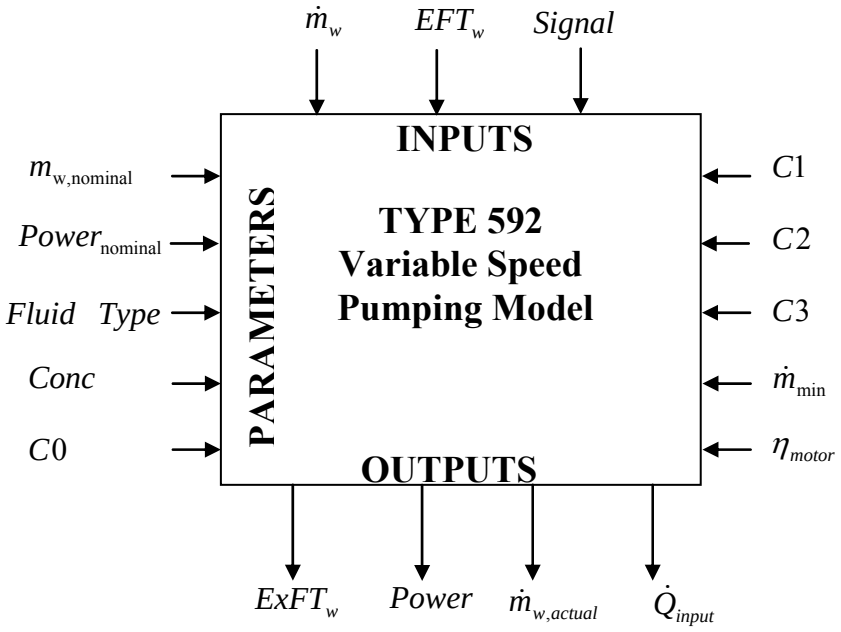

Figure 4.27 TYPE 592 constant speed pumping HVACSIM+ model diagram

The variable speed pumping model, TYPE592, diagram can be seen in Figure 4.27, showing all the inputs, output and parameters.

In the diagram:

$Power_{nominal}$ = Pump power at nominal flow rate, (kW);

$\dot{m}_{min}$ = Minimal mass flow rate requited by the variable speed drive, (kg/s).

4.5 Plate Heat Exchanger Models

HGSHP systems often use a plate frame heat exchanger to isolate the cooling tower from the rest of the system. The plate frame heat exchanger is modeled as a counter flow heat exchanger and the effectiveness-NTU method is applied. Three different ways have been developed to calculate the heat transfer coefficient UA: a fixed UA, a variable UA without fouling and a variable UA with fouling. These three methods are introduced in this section.

In this research, the plate frame heat exchanger model is intended for use in a large parametric study, where it is highly desirable to avoid having to select a specified heat exchanger from a manufacturer's catalog data, fit coefficients, etc. A simple approach has been developed by Gentry (2007) for modeling the plate frame heat exchange. This approach is also introduced in this section.

4.5.1 Effectiveness-NTU PHE Model

In the effectiveness-NTU method, the UA value is a key factor for the calculation of the heat transfer of the plate heat exchanger. Two methods have been developed for the calculation of UA. They are used for the validation of HGSHP system simulation in Chapter 5.

Variable UA Without Fouling Model

In the variable UA without fouling model, assuming that the conductive thermal resistance of plate is negligible, the UA may be calculated as the sum of the convective thermal resistances at two sides of plate heat exchanger and:

$$\frac{1}{U_t A_t} = \frac{1}{h_h A_h} + \frac{1}{h_c A_c} \tag{4-29}$$

Where:

$U_t A_t$ = Total heat transfer coefficient area product, (W/K);

h_h = Convective heat transfer coefficient on hot fluid side, (W/m^2-K);

h_c = Convective heat transfer coefficient on cold fluid side, (W/m^2-K);

A_h = Heat exchanger area on hot fluid side, (m^2);

A_c = Heat exchanger area on cold fluid side, (m^2).

Ayub (2003) reviewed more than forty reference for the plate heat exchanger model. Despite the differences, many of the models for convection with the plate heat exchanger fall into a general form as:

$$Nu_L = C_1 \, \mathrm{Re}^m \, \mathrm{Pr}^n \tag{4-30}$$

Where the coefficients C_1, m and n is determined based on the different geometry of the plate heat exchanger and the flow rate.

While Equation 4-30 might be evaluated with detailed knowledge of the plate heat exchanger geometry, this information is generally not available. Rather, only with catalog data for the plate heat exchanger, a model that gives heat transfer rate and ExFT with

EFT, $\dot{m}$ is desired. This can be done with the general approach described by Rabehl et al. (1999).

We are interested in finding *hA* on both sides of the heat exchanger, and both sides are assumed to have the same general form of the correlation. Applying the definition of Nusselt number, Reynolds number and Prandtl number, the equation for *hA* can be reduced to:

$$hA = C_1 \frac{Q^m}{\nu^m} \mathrm{Pr}^n k_{fluid} \tag{4-31}$$

Where:

Q = Volumetric flow rate of fluid, (m^3/s);

ν = Dynamic viscosity of fluid, (m^2/s);

k_{fluid} = Thermal conductivity of the fluid, (W/m-K);

C_1, m, n = Constants to be fitted.

A best estimate of the values of C_1, m, n for both hot fluid and cold fluid sides is determined from the plate heat exchanger manufacturer's catalog data by minimizing the sum-of-the-squares-of-the-error of the UA values.

Variable UA With Fouling Model

Fouling is always observed on the plate heat exchanger surface and reduces heat transfer and increases the resistance to fluid flow. Therefore, a variable UA with fouling

model is developed to represent the phenomena. The heat transfer performance of heat exchanger with fouling (Barrow and Sherwin 1994) can be calculated as:

$$(\frac{1}{UA})_{fouled} = R_{fouling} + (\frac{1}{UA})_{clean} \quad (4\text{-}32)$$

Where:

$(\frac{1}{UA})_{fouled}$ = Resistance with fouling, (K/W);

$(\frac{1}{UA})_{clean}$ = Resistance in the clean condition and determined by Equation 4-29, (K/W);

$R_{fouling}$ = Thermal resistance of fouling, (K/W).

The thermal resistance of fouling, $R_{fouling}$, is time related and can be developed in the form of (Knudsen 1984):

$$R_{fouling} = R_{\infty}(1 - e^{-Bt}) \quad (4\text{-}33)$$

The constant R_{∞} and B are obtained experimentally.

HVACSIM+ Component Model

A plate frame heat exchanger HVACSIM+ component mode, TYPE 666, is been developed for this effectiveness-NTU method. The UA value is input as a boundary condition of the model, which is user-precalculated based on the manufacturer's catalog data or experimental measurements.

The effectiveness-NTU PHE model, TYPE666, diagram can be seen in Figure 4.28, showing all the inputs, output and parameters.

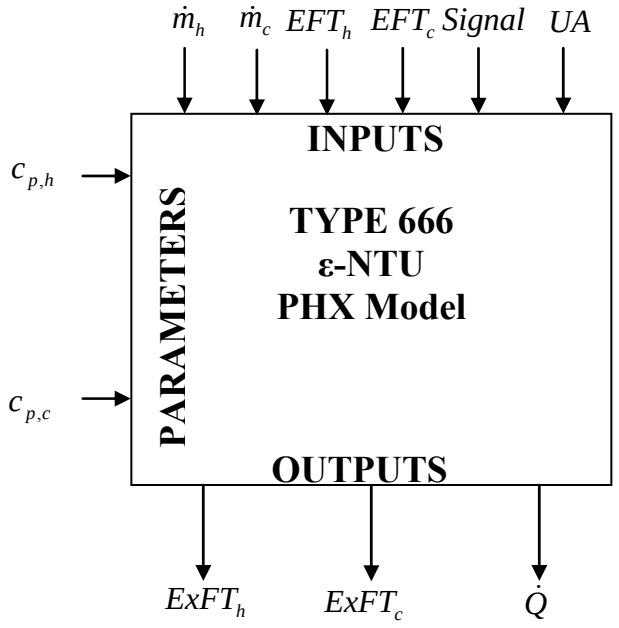

Figure 4.28 TYPE 666 effectiveness-NTU PHE HVACSIM+ model diagram.

In the diagram:

$c_{p,h}$ = Specific heat of hot fluid, (kJ/kg-K);

$c_{p,c}$ = Specific heat of hot fluid, (kJ/kg-K).

4.5.2 Variable Effectiveness PHE Model

In this research, the plate frame heat exchanger model is intended for use in a large parametric study, where it is highly desirable to avoid having to select a specified heat exchanger from a manufacturer's catalog data, fit coefficients, etc. A simplified effectiveness approach has been developed by Gentry (2007) for modeling the plate

frame heat exchanger. This approach has the advantage of being able to use the same model over a wide range of size and only the nominal needs to be specified uniquely to model a specific size of plate heat exchanger.

It was found from the plate frame heat exchanger manufacturer's catalog data that there is a generic polynomial relationship between the effectiveness of PHE and the fraction of full flow (FFF) at one side of PHE, as described in Equation 4-34:

$$\varepsilon = C_0 + C_1 \cdot EFF + C_2 \cdot EFF^2 + C_3 \cdot EFF^3 \qquad (4\text{-}34)$$

The values of coefficients C_{0-3} for the Mueller plate heat exchangers are listed in the following table. A detailed description of the variable effectiveness PHE model can be found in Gentry (2007).

Table 4.6 coefficients C_{0-3} for the Mueller plate heat exchangers

C_0	0.1839	C_2	-1.272
C_1	1.4249	C_3	0.4431

The variable effectiveness PHE model, TYPE665, diagram can be seen in Figure 4.29, showing all the inputs, output and parameters.

In the diagram:

$\varepsilon_{\text{nominal}}$ = Effectiveness of PHE at the nominal full flow rate, (-);

$\dot{m}_{\text{nominal}}$ = Nominal full flow rate of hot fluid in HGSHP systems, (kg/s).

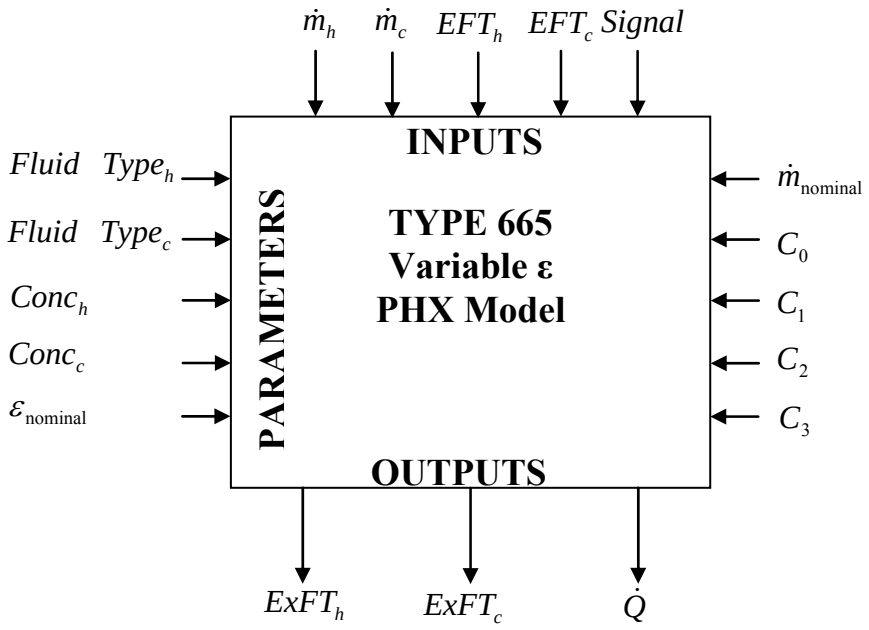

Figure 4.29 Type 665 variable effectiveness PHE HVACSIM+ model diagram.

4.6 HVACSIM+ System Simulation Implementation

An HGSHP system simulation in HVACSIM+ visual tool is shown in Figures 4.30 and 4.31. Figure 4.30 shows the full schematic with all system connections shown. Figure 4.31 shows the flow direction from component to component and the controller connection.

A parallel-connected HGSHP system as shown in Figure 2.8 is set up for the simulation. The main loop includes heat pumps, a variable speed circulation pump for the main loop, ground loop heat exchanger, a three-way valve, a mixing valve and a plate frame heat exchanger. The secondary loop includes a constant speed circulation pump for the secondary loop, an open-circuit cooling tower and the plate frame heat exchanger.

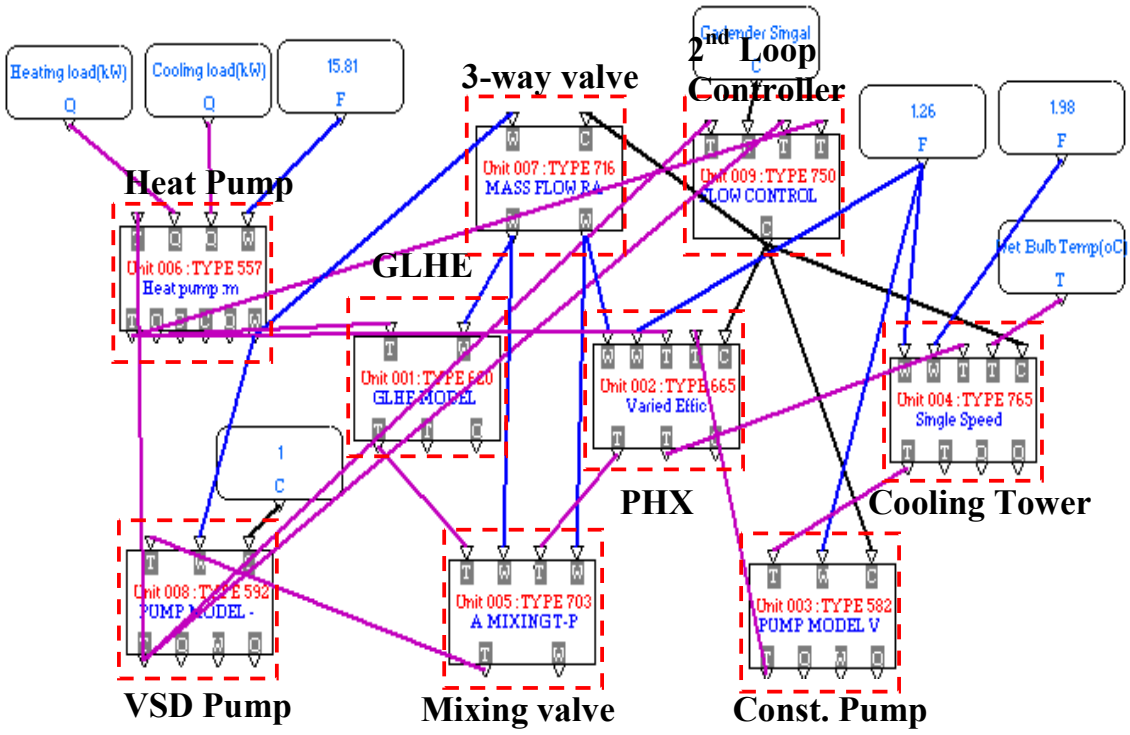

Figure 4.30 HVSCSIM+ visual tool model showing system connections.

A secondary loop controller is used to control the operation of cooling tower and circulation pump. Here, an EFT control strategy is used by the controller. When the EFT of the heat pumps exceeds an upper limit temperature, a control signal of "ON" is sent to the cooling tower and the secondary loop circulation pump. When the EFT of the heat pumps is below a lower limit temperature, a control signal of "OFF" is sent to the cooling tower and the secondary loop circulation pump to shut down the secondary loop.

In HVACSIM+, all the variables in one superblock are solved simultaneously. However, the sudden transients due to the controllers switching between on and off causes problems with the convergence of the entire system when trying to solve both control signals and temperatures used to drive the control signals, within the same time step. Therefore, in order to simulate the HGSHP system with a controller, two

superblocks are needed to handle the discontinuity caused by the controller. All the components except the controller are set in Superblock 1 and the controller is set in Superblock 2. At one time step, the temperatures and flow rates in Superblock 1 are solved simultaneously first, and then the temperatures are passed to the controller in Superblock 2. After getting the control signal, the simulation moves to the next time step. The control signal obtained from the last time step is then used to control the cooling tower, the secondary circulation pump, the plate frame heat exchanger and the three-way valve. Adding a superblock gives, in effect, a transit delay to the system and allows the control signal to be based on the previous time step's temperature values. Adding a superblock has an effect equivalent to adding a plug flow thermal mass to the loop. More discussion is given by Gentry (2007).

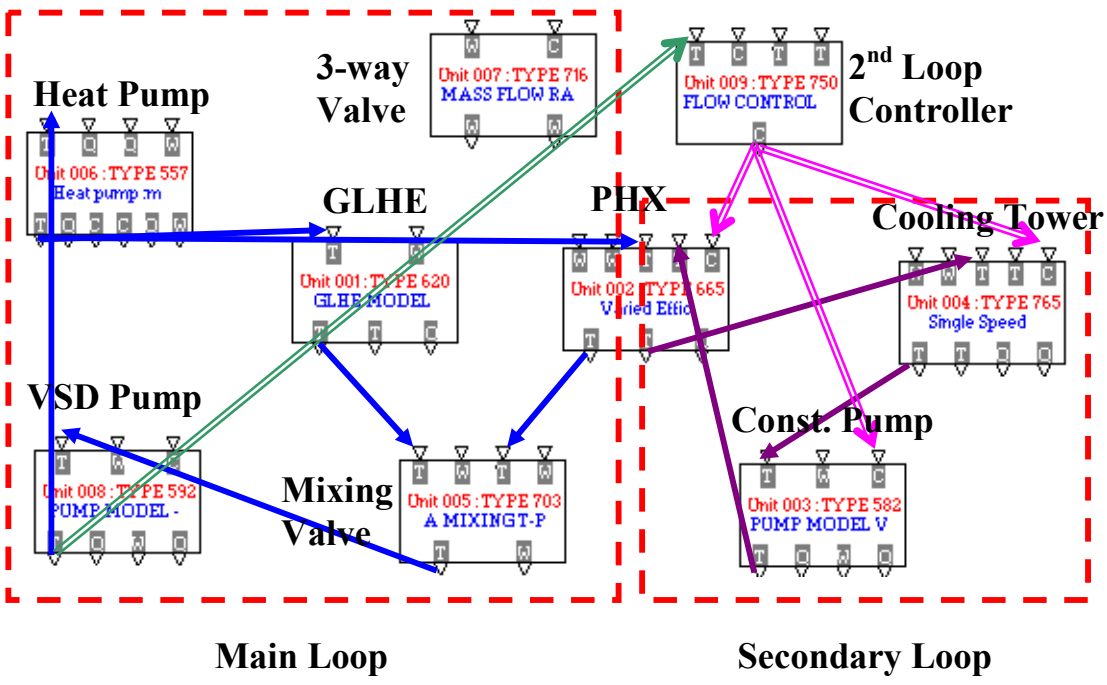

Figure 4.31 System flow direction and controller direction in HVACSIM+ visual tool.

4.7 Accelerating Multiyear Simulation of HGSHP Systems

In HGSHP systems, the ground temperature surrounding the GLHE can rise or fall over the system operation period depending on the heat imbalance of the ground. Therefore the GLHE performance and the heat pump energy consumption vary over the system operation period and usually a 20-year simulation will be carried out to evaluate the overall performance of the system. Applying the load aggregation algorithm, the new GLHE model is computationally efficient. However, for an optimization study, a large number of simulations – in the thousands – are required. It is still computationally expensive to run a large number of 20-year simulations with an hourly time step. Therefore, a new scheme is developed for accelerating the multiyear simulation of HGSHP system. The accelerated algorithm has two parts – a variable time step aspect

and a simplified life cycle cost calculation procedure. They are described in the following two sections.

4.7.1 Accelerating Multiyear Simulation Scheme

The scheme investigated here involves using large time steps for a significant part of the simulation in order to save computational time. Smaller time steps are used to improve accuracy for part of the simulation.

Preliminary testing shows the GLHE loop temperature over the 20-year operation period varies as shown in Figures 4.32, 4.33, and 4.44 covering a single week of operation, a single year, and 20 years respectively.

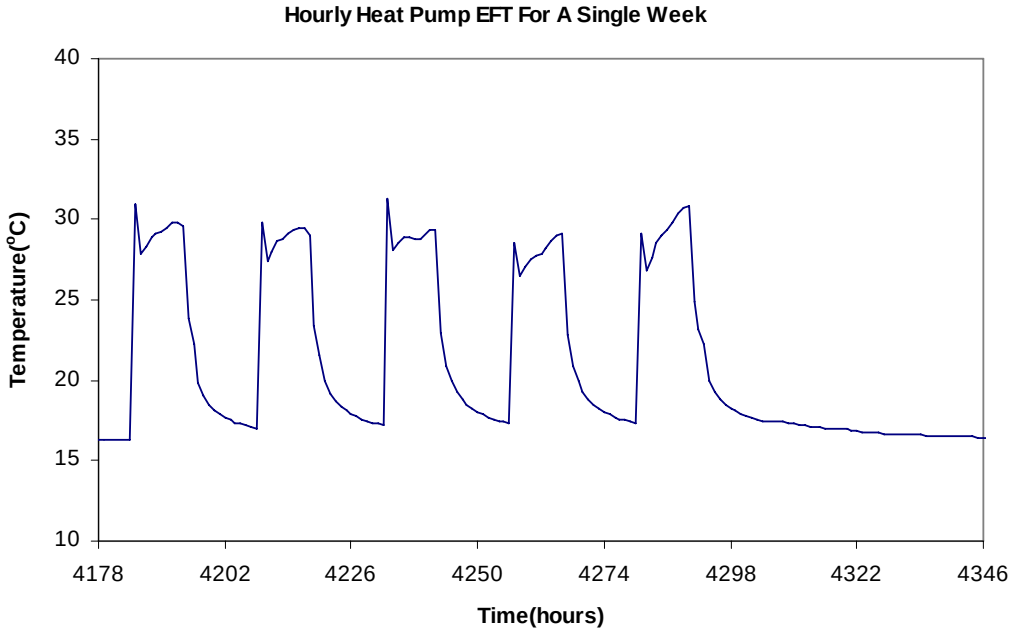

Figure 4.32 Hourly heat pump EFT of a HGSHP system for a single week

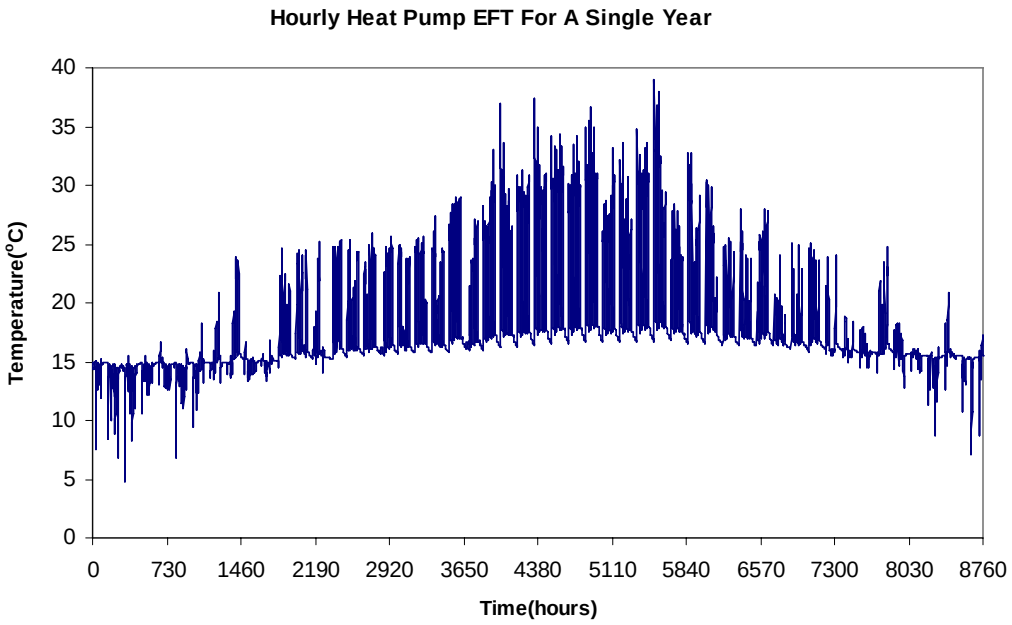

Figure 4.33 Hourly heat pump EFT of a HGSHP system for a single year

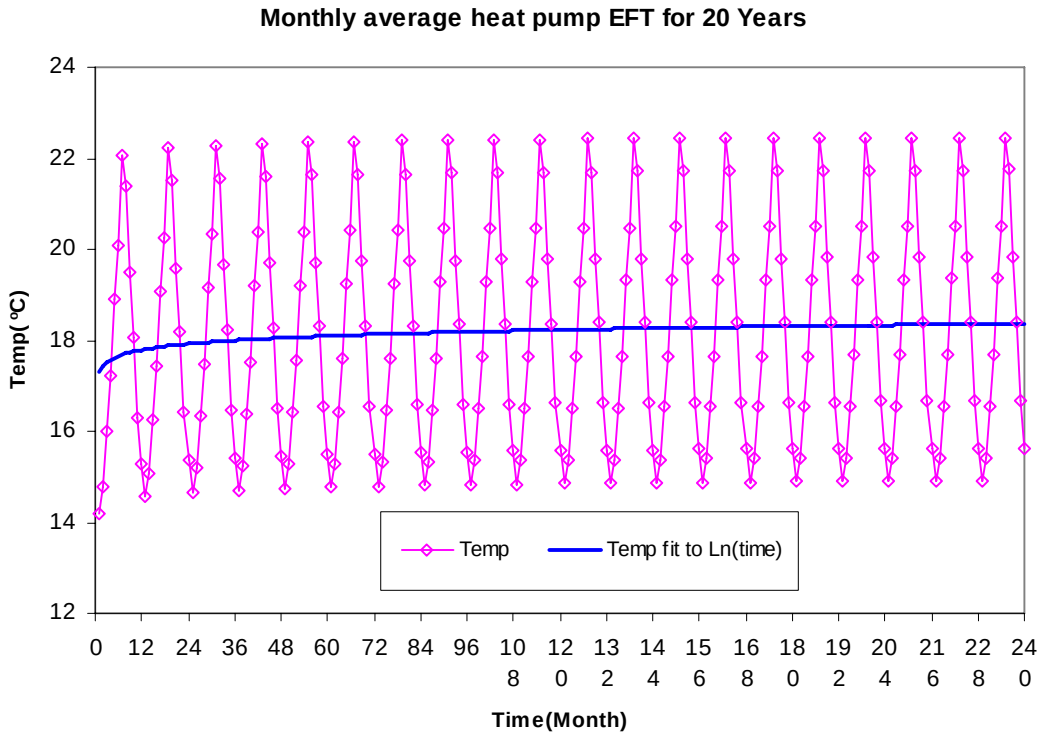

Figure 4.34 Monthly average heat pump EFT of a HGSHP system for 20 years

Overall, the 20 year heat pump EFT response loads are something like a superposition of:

- an exponential decay (representing long term temperature rise or fall)
- a sinusoid with period of one year
- diurnal variations with randomness caused by varying weather patterns

The scheme takes advantage of the fact that, for a well designed HGSHP system, the annual ground heat rejection and ground heat extraction are nearly balanced. In this case, the annual peak ground temperature remains almost unchanged over the operation time (20 years), especially over the later years of the system operation period, as shown in Figure 4.34. As a result, the 20-year HSGHP system energy consumption remains almost unchanged over the operation time (20 years), especially over the later years of the system operation period, as shown in Figure 4.35. Therefore, a shorter period simulation is possible for HGSHP systems without causing too much energy error in the consumption prediction. In this research, an 8-year simulation is carried out to represent the overall system performance over a 20-year period.

Also a variable time step scheme is developed for the 8-year simulation to accelerate the simulation. In the calculation of the life cycle cost of the system, only the operating cost of the first year and the 8^{th} year are required (Details are given in Section 4.7.2). Therefore, in the 8-year system simulation, these two years: 1^{st} and 8^{th} year, are simulated with hourly time step, which would provide a detailed and accurate hourly result. And the other years are simulated with 6-hour time step. In practice, the simulation

of other years with a large time step will bring an error of the 8th year result. Therefore, in order to minimize the error of the 8th year result caused by the variable time step, the 7th year is also simulated with hourly time step. And the years from 2nd to 6th are simulated with 6-hour time step.

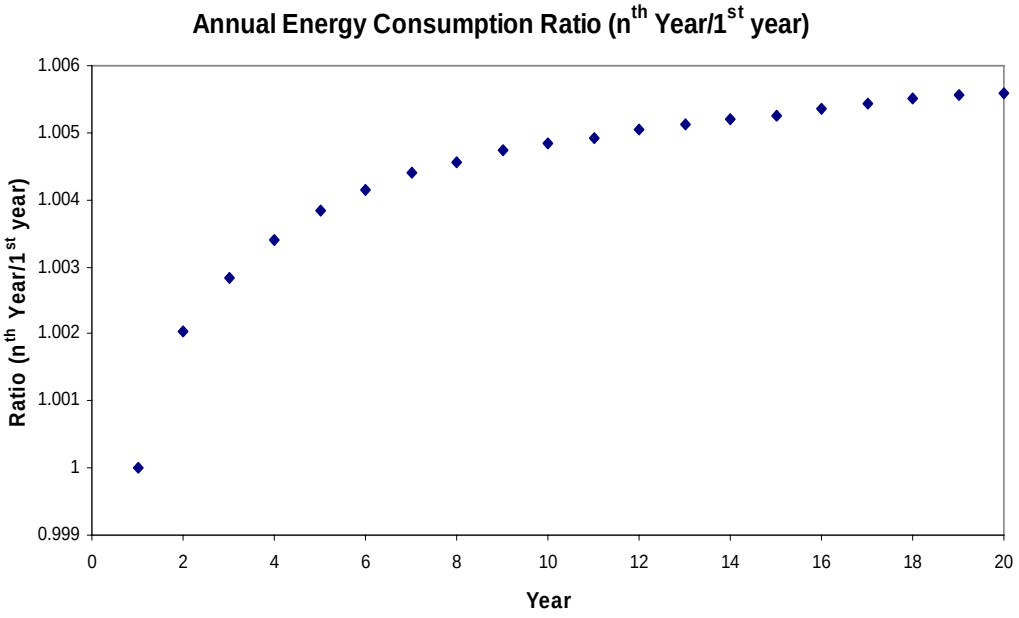

Figure 4.35 Annual HGSHP system energy consumption for 20 years.

Figure 4.36 shows the annual HGSHP system energy consumption between the detailed 20-year hourly simulation and the accelerating simulation for three years: 1st, 7th and 8th year. The system energy consumption at the 1st year is exactly same for the two methods. The relative error of the accelerating simulation at the 7th and 8th year is about 0.1%.

It takes 34 seconds to run an HGSHP system simulation with 8-year variable time steps scheme and 185 seconds to run the simulation with 20-year hourly time step scheme

on an AMD 2.10 GHz PC equipped with 1GB RAM and using Windows XP. For a large number of simulations, the computational time savings are significant.

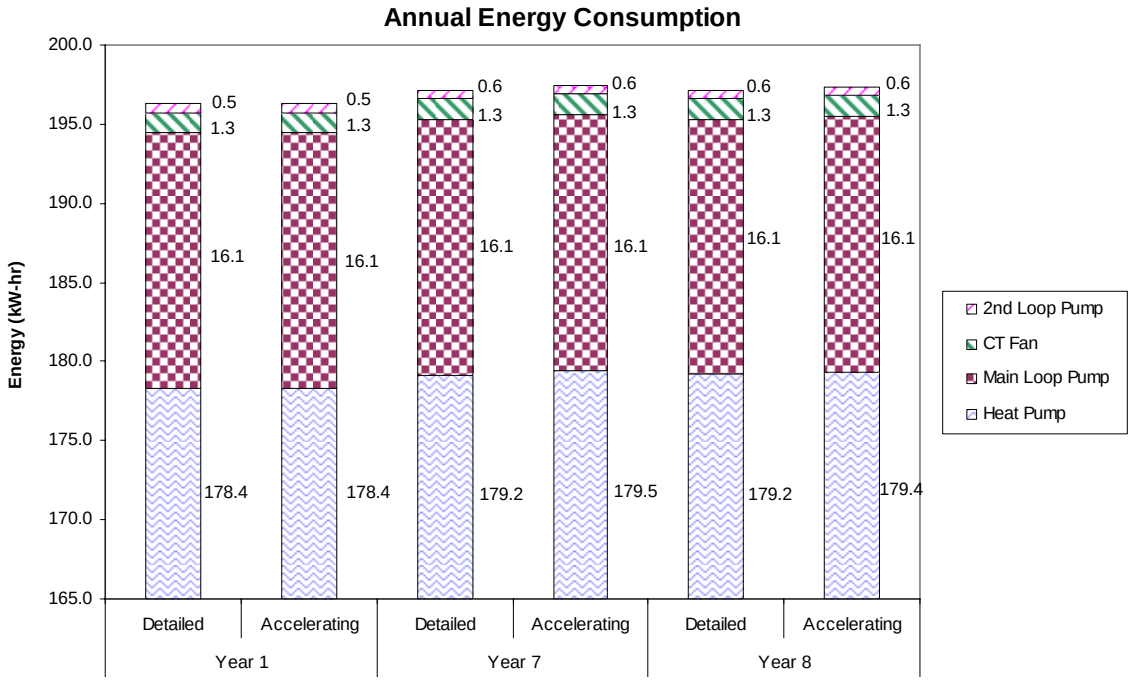

Figure 4.36 Annual energy consumption of HGSHP between the detailed 20-year hourly simulation and accelerating simulation.

4.7.2 Life Cycle Cost Analysis Methodology

In this section, a procedure is developed to estimate the overall system performance for the accelerating simulation.

The life cycle cost (LCC) of the HGSHP system is done on a representative value with an assumed life of 20 years and annual interest rate (IR) of 6%. The net present value (NPV) of a HGSHP system operating cost with 20-year hourly simulation can be represented as:

$$NPV = \sum_{n=1}^{20} OC_n /(1+IR)^n \tag{4-35}$$

Where:

OC_n = The system operation cost, ($).

If the system operation cost OC_n of each year is the same, then Equation 4-35 can be simplified as:

$$NPV = OC_{avg} \frac{(1+IR)^{20}-1}{IR(1+IR)^{20}} \tag{4-36}$$

Where:

OC_{avg} = Average operating cost of HGSHP system over 20 years.

As seen in Figure 4.35, the 20-year HSGHP system energy consumption remains almost unchanged over the operation time (20 years). Therefore, an average operating cost, OC_{avg}, is used to calculate the net present value (NPV) of a HGSHP system. The average operating cost of the HGSHP system OC_{avg} is calculated based on a weighted average of the 1st year and 8th year:

$$OC_{avg} = OC_{year,1} * ratio + OC_{year,8} * (1-ratio) \tag{4-37}$$

Where:

$OC_{year,1}$ = Operating cost of HGSHP system for the 1st year;

$OC_{year,8}$ = Operating cost of HGSHP system for the 8th year;

ratio = Weight ratio, here a value of 0.05 is selected, (-).

After getting the average operating cost of the HGSHP system, the NPV of the system is calculated by Equation 4.38.

For the HGSHP system shown in the Figure 4.35 and Figure 4.36, the net present value of system is listed in Table 4.7 with an electricity price of 7 ¢/kWh. Two approaches were applied for this calculation: 1) a 20-year simulation with hourly time step and the NPV is calculated by Equation 4-35; 2) an 8-year simulation with variable time step and the NPV is calculated by Equation 4-36. Applying the 8-year variable time steps simulation and the simplified NPV calculation, the relative error of the net present value of the HGSHP system operating cost is about 0.1%.

Table 4.7 Net present value of system operating cost over 20 years.

Case	CPU Time (second)	Net present value ($)
20-year hourly simulation	185	158,221
8-year variable time steps simulation	34	158,405

4.7.3 Verification of Multiyear Simulation Scheme for Optimization Study

One objective of this research is to develop the HGSHP system control strategy to optimize the operation of the HGSHP system. A buffer program developed in Chapter 7 is used to search for the best setpoint of each control strategy for different combinations

of system design, building type and location. In this buffer program, an accelerating simulation scheme is used to save the computational time. In this section, the influence of this accelerating simulation scheme on the optimization results of the HGSHP system control strategy is investigated.

Two different multiyear simulation approaches are used in the buffer program for the HGSHP system simulation and the net present value calculation: 1) a 20-year simulation with hourly time step and the NPV is calculated from each year result (Equation 4-36); 2) an 8-year simulation with variable time step and the NPV is calculated from 1^{st} and 8^{th} year result (Equation 4-36). Three control strategies developed by Yavuzturk and Spitler (2000) are be used for the investigation. Due to the expensive computational time for the optimization with a 20-year hourly time step simulation, only one location for the office building and the motel building case is chosen for the comparison. The details about the office building and the motel building are available in Section 7.1. For each building type, four different HGSHP systems with combination of different size of the GLHE and the cooling tower were designed. More details about the system component sizes are available in Section 7.3.

The optimized setpoint values of the three control strategies with the different simulation scheme are listed in Table 4.8 and plotted in Figure 4.37. The 20-years NPV of the system operation cost calculated by the different methods are listed in Table 4.8 and plotted in Figure 4.38. From the results in Figure 4.37 and 4.38, the optimal setpoint value estimated from the 20-year hourly simulation method and the optimal setpoint value estimated from the 8-year variable time step simulation method are nearly the

same, both for the office building and motel building cases. For the office building in "B-ExFT" case, the setpoint value difference is 0.6ºC and the NPV of the system 20-year operation cost difference is about 0.1%. For the motel building in "D-ExFT" case, the setpoint value difference is 0.8ºC and the NPV of the system 20-year operation cost difference is about 0.1%. However, the computational time of these two simulation schemes showed a huge difference. Using the 20-year hourly simulation scheme, it took about 552 minutes to run a single case. And using the 8-year variable time step simulation scheme, it only took about 77 minutes to run a single case.

In this Section 4.7, a new scheme was developed for accelerating the multiyear simulation of HGSHP system. An 8-year variable time step simulation scheme only took about one-fifth the computational time of a 20-year hourly time step simulation scheme. Applying the 8-year variable time step simulation and a simplified life cycle cost procedure, the relative error of the net present value of the HGSHP system operating cost is about 0.1%. The investigation of the optimization of the three old control strategies showed that the accelerating simulation scheme has a very small influence on the optimized setpoint result. Therefore, in this study, the accelerating simulation scheme is used for the investigation of the HGSHP system.

Table 4.8 Comparison of setpoint values and the Net present value of system operating cost between two different simulation schemes.

Case Description	Scheme	Office Building			Motel Building		
		Set Point (ºC)	20-years NPV operation cost($)	operation cost difference	Set Point (ºC)	20-years NPV operation cost($)	operation cost difference
A-EFT	Detailed	23.1	164,488		22.6	24,032	
	Accelerating	23.3	163,840	-0.4%	23.0	24,063	0.1%
B-EFT	Detailed	21.6	149,880		25.1	24,014	
	Accelerating	21.7	150,044	0.1%	24.6	24,003	0.0%
C-EFT	Detailed	23.1	166,711		22.2	22,124	
	Accelerating	23.2	165,642	-0.6%	22.2	22,140	0.1%
D-EFT	Detailed	22.4	147,781		24.6	22,143	
	Accelerating	22.4	147,932	0.1%	24.5	22,162	0.1%
A-ExFT	Detailed	26.3	164,081		31.2	24,028	
	Accelerating	26.5	163,408	-0.4%	30.6	24,029	0.0%
B-ExFT	Detailed	24.4	149,541		33.8	24,010	
	Accelerating	25.0	149,709	0.1%	33.6	24,013	0.0%
C-ExFT	Detailed	26.5	166,453		30.3	22,122	
	Accelerating	26.4	165,288	-0.7%	30.4	22,138	0.1%
D-ExFT	Detailed	24.8	147,310		33.2	22,141	
	Accelerating	24.9	147,453	0.1%	32.4	22,161	0.1%
A-Tdiff	Detailed	11.8	165,044		11.4	24,084	
	Accelerating	11.8	164,377	-0.4%	11.5	24,110	0.1%
B-Tdiff	Detailed	9.1	150,300		12.8	24,102	
	Accelerating	9.2	150,459	0.1%	12.9	24,124	0.1%
C-Tdiff	Detailed	10.8	168,381		11.2	22,229	
	Accelerating	10.8	167,300	-0.6%	11.3	22,246	0.1%
D-Tdiff	Detailed	8.9	148,334		12.4	22,242	
	Accelerating	9.0	148,464	0.1%	12.3	22,257	0.1%

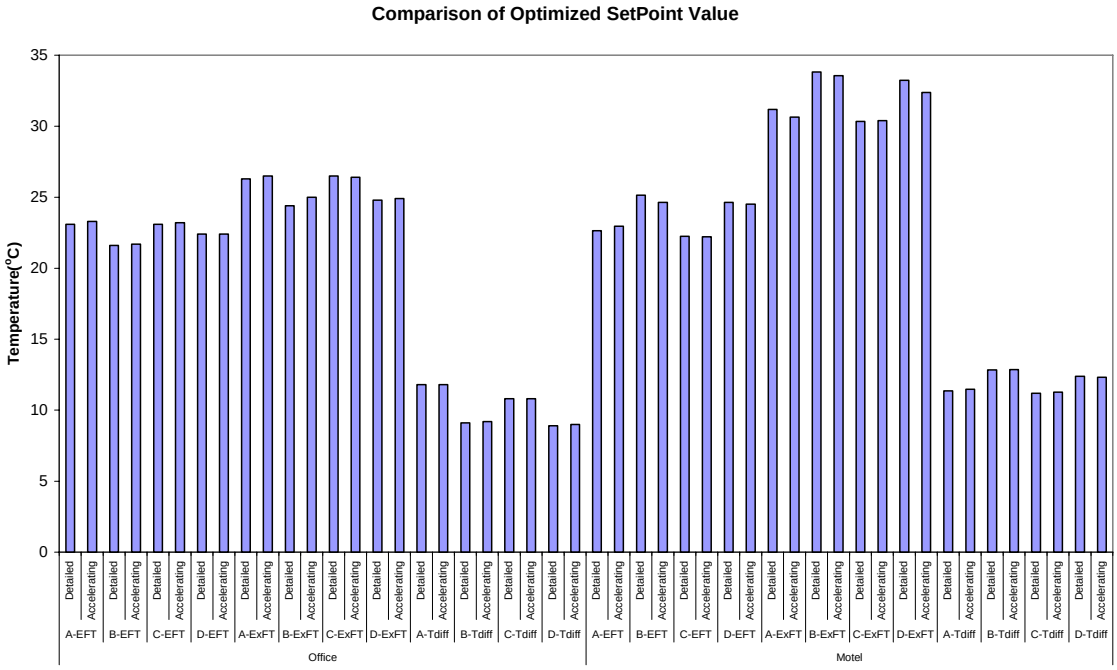

Figure 4.37 Comparison of setpoint values between two different simulation schemes

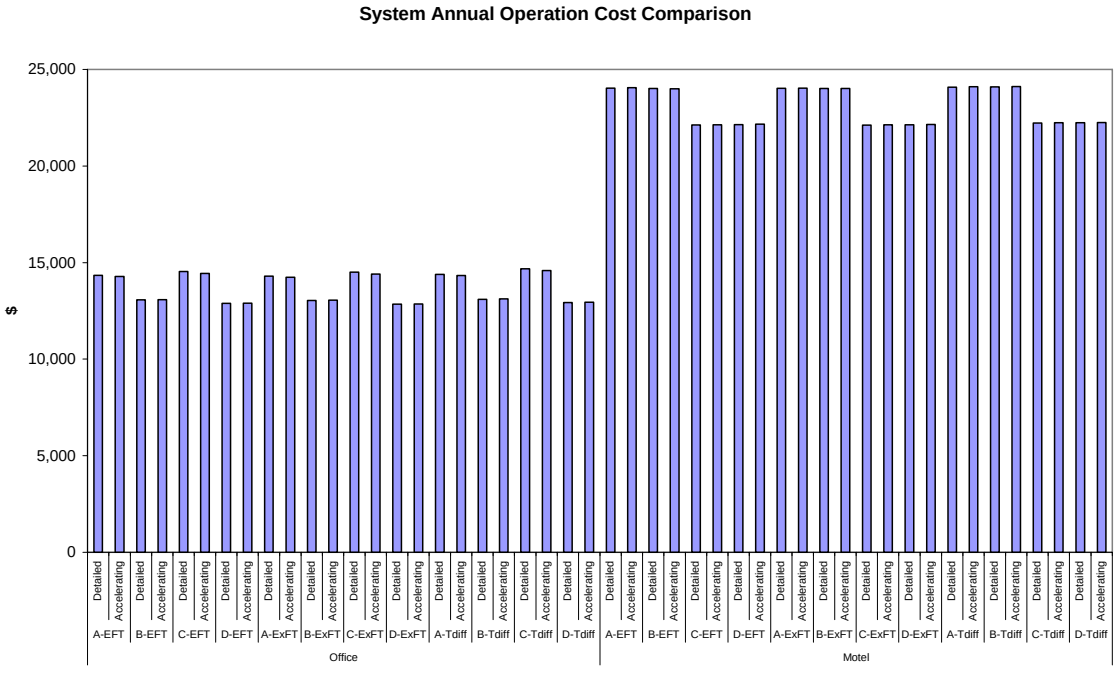

Figure 4.38 Comparison of the Net present value of system operating cost between two different simulation schemes

4.8 Summary

In this chapter, HGSHP system simulation and requisite component models were developed. A summary of the component models is listed in Table 4.9.

Table 4.9 A summary of the component models of HGSHP system simulation

Model	Type Number	Description	Author's work[1]
GLHE	TYPE 621	1-d and LTS model	Developing
	TYPE 620	New STS and LTS model	Developing
Heat Pump	TYPE 559	Parameter estimation based heat pump model	Applying
	TYPE 557	Gang-of-heat-pumps model	Developing
Open-circuit Cooling Tower	TYPE 765	Fixed UA model	Using
	TYPE 768	Variable UA model	Using
Closed-circuit Cooling Tower	TYPE 764	Variable UA model	Applying
Pump	TYPE 582	Simple variable speed pumping model	Using
	TYPE 592	Detailed variable speed pumping model	Developing
Plate frame heat exchanger	TYPE 665	Variable effectiveness model	Using
	TYPE 665	Variable UA model with/without fouling	Using/Developing

1: Author's work on the component model can be divided into three categories: developing, applying and using. Developing means author developed a new model and cast it as an HVACSIM+ component model; applying means author applied an existing model and cast it as an HVACSIM+ component model; using means author used a previously developed HVACSIM+ component model.

In this chapter, a one-dimensional numerical model and an LTS model of GLHE were developed. The new GLHE model used a one-dimensional numerical model to calculate the borehole wall temperature at short time-steps directly without using the superposition approach. Then a new approach was developed to couple the one-

dimensional numerical and the LTS response factor model together for modeling the vertical GLHE.

The one-dimensional numerical model was validated using the detailed boundary-fitted coordinates finite volume model (GSME2D).

The one-dimensional numerical model coupled with the LTS model was cast as HVACSIM+ component model as TYPE621. An annual hourly simulation GSHP system in a church building was carried out to demonstrate this new GLHE model and illustrate the effect of thermal mass and the variable convective resistance.

Generally, the flow rate in the ground loop heat exchangers is designed so as to ensure turbulent flow in the tube and the convective thermal resistance has little effect on the overall thermal resistance of borehole. Therefore, using the one-dimensional numerical model, a new STS response factor model is then developed with fixed convective thermal resistance. The new STS and LTS model was cast as HVACSIM+ component model as TYPE620.

Two heat pump models were developed in this chapter. A parameter estimation-based heat pump model was developed for a single heat pump and this model is used for the experimental validation of HGSHP system simulation in Chapter 5. A gang-of-heat-pump model based on equation-fit method was developed to represent multiple heat pumps and this model is used for the investigation of HGSHP system control strategy in Chapter 7.

Two open-circuit cooling tower models were briefly introduced in this chapter and they are used for the validation of HGSHP system simulation and the investigation of HGSHP system control strategy respectively in Chapter 7.

One variable UA model based on the effectiveness-NTU method for closed-circuit cooling tower was developed in this chapter. And this model is used for the validation of HGSHP system simulation in Chapter 5.

Two variable speed pump models were developed in this chapter. These two pump models are used for the HGSHP simulation and investigation of HGSHP system control strategy in Chapter 7.

An effectiveness-NTU method based plate frame heat exchanger model was developed. Three ways of calculating of UA values were introduced: fixed UA, variable UA without fouling model and variable UA with fouling model. This model is used for the experimental validation of HGSHP system simulation in Chapter 5. Also a previously developed plate frame heat exchanger using a variable effectiveness model was introduced. And this model is used for the investigation of HGSHP system control strategy in Chapter 7.

A new scheme was developed for accelerating the multiyear simulation of HGSHP system. An 8-year variable time step simulation only took about one-fifth computational time of a 20-year hourly time step simulation. The comparison between the 8-year variable time step simulation and the 20-year hourly time step simulation showed that the relative error of the net present value of the HGSHP system operating

cost is about 0.1% and the accelerating simulation scheme has a very small influence on the optimized setpoint value of the control strategies.

5 VALIDATION OF HGSHP SYSTEM SIMULATION

The validation of the HGSHP system simulation presented in Chapter 4 is highly desirable. In this chapter, the HGSHP system component models and system simulation will be validated against the experimental data from a HGSHP research facility. First, the experimental HGSHP research facility (Hern 2004) will be introduced. Second, the parameters of each component model for modeling the HGSHP system will be presented. Then the validation of each component model, individually and within the system simulation, will be presented. Finally, for the system validation, two variations of the system simulation approach will be investigated: 1) the cooling tower is modeled as a boundary condition taken from the experimental data, and 2) the cooling tower is modeled with a controller that mimicks the actual controller.

As a joint project, the author and Gentry (2007) worked together on the preliminary system simulation and validation. Gentry et al. (2006) presented a report on the validation of the HGSHP system simulation using seven months of data from the OSU HGSHP research facility. Therefore, in this chapter, some work overlaps with the Gentry (2007) work. However, compared to the Gentry work, significant additional work has been done for the validation of HGSHP system simulation. The main improvements include:

- In this research, the validation of HGSHP system simulation is extended to a 12 month period. It includes a continuous 7-month cooling season and portions of two heating seasons.

- As reported by Gentry et al. (2006), the equation-fit heat pump model performed poorly with catalog data when the actual flow rates on both sides of the heat pump were larger than catalog data. For the extended validation, a parameter estimation-based heat pump model (Jin and Spitler 2002) is utilized and performs well.

- In the simulation of the GLHE, Gentry et al. (2006) calibrated three parameters: the undisturbed ground temperature, the grout thermal conductivity and the ground thermal conductivity based on the measured experimental data. In this research, these parameters are recalibrated over a 12-month period.

  For the GLHE model presented in Chapter 4 (TYPE620), validation of the thermal mass effect case validation is carried out. An experimentally estimated fluid factor is used for the validation of the GLHE model. Comparison of the simulation results with different fluid factor values is also presented.

  Also for the validation of the variable convective thermal resistance aspect of the TYPE621 model, a planned experiment will be carried out in the HGSHP research facility. A variable flow rate experiment will be designed so as to transition from laminar flow to turbulent flow in the borehole U-tube. The

experiment will be used for the validation of the variable convective thermal resistance case.

- Instead of using a plate frame heat exchanger model, Gentry et al. (2006) used a generic heat exchanger model to simulate the plate heat exchanger. In this research, based on the literature summary of Ayub (2003), a general form of a plate heat exchanger convection correlation is integrated with the heat exchanger model. The correlations are fitted using catalog data.

  In the experimentation, fouling was observed on the cooling tower supply of the loop and the UA values of the plate heat exchanger decreased substantially. For lack of a method to predict the fouling, a heuristic approach was taken by Gentry et al. (2006) by adding a fouling factor that increased linearly with time. In this research, the heat exchanger model incorporates a fouling sub-model (Barrow and Sherwin 1994).

5.1 Experimental Facility

Both system component models and the entire HGSHP system simulation will be validated against the experimental data. The experimental data have been collected from an HGSHP research facility (Hern 2004) located on the campus of Oklahoma State University. The HGSHP system configuration is shown in Figure 5.1.

At the heat pumps' load side, chilled water and hot water generated by the HGSHP system serve two small buildings. The facility allows the source side of the heat pumps to be connected to a ground loop heat exchanger, an open-circuit cooling tower,

and/or a pond loop heat exchanger. These can be connected in any combination, but for the duration of these experiments, they were configured as a typical HGSHP system, with a GLHE and a cooling tower. The ground loop heat exchanger and the plate frame heat exchanger are placed in series in the system and a three-way valve is used to bypass the plate frame heat exchanger when the system runs in heating model. A variable speed pump was designed for the main loop of the heat pumps' source side. In the secondary loop, an open-circuit cooling tower is isolated from the ground loop heat exchanger with the plate frame heat exchanger. A constant speed pump was selected to serve the cooling tower loop. The cooling tower and secondary loop circulation pump were controlled with a programmable control system, which allowed a user-input control scheme. Brief descriptions of each component of the HGSHP system are given. A detailed description of the HGSHP research facility can be found in Hern (2004) and Gentry (2007).

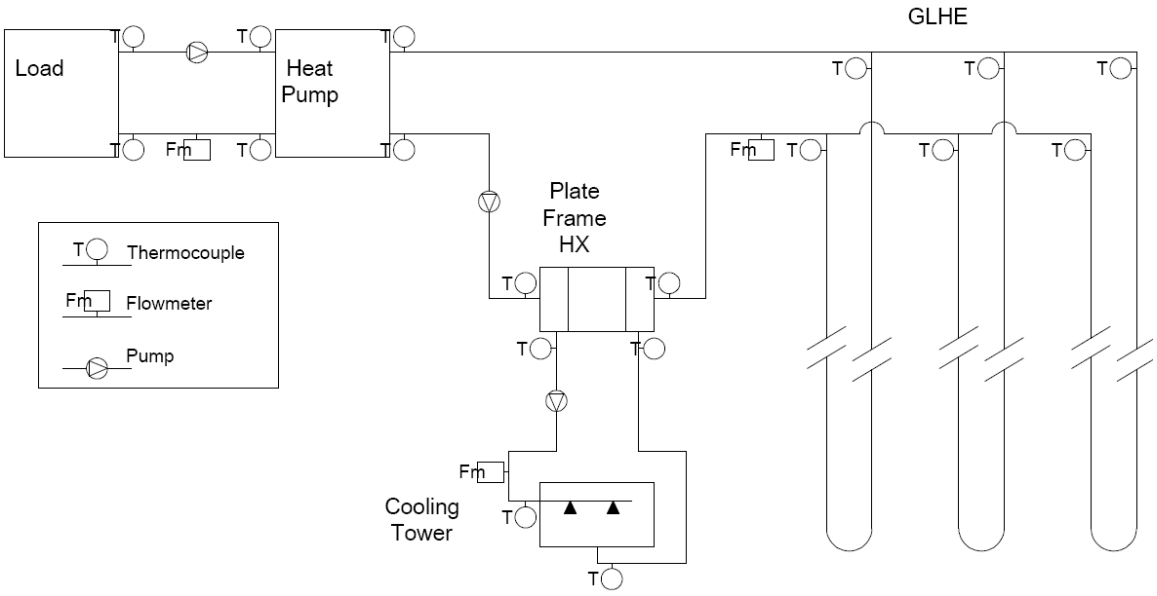

Figure 5.1 HGSHP configuration for validation (Gentry et al. 2006)

5.1.1 Heat Pumps

Two identical water-to-water heat pumps (Florida Heat Pump WP036-1CSC-FXX), of nominal capacity 10.6 kW are used to provide the chilled water and hot water. The load side of heat pumps consists of two 1.1m^3 water storage tanks that are used to serve two small buildings with hydronic heating and cooling systems. For the time period of interest in this simulation, only one heat pump is used at a time. In the 12-month operation from March 2005 to February 2006, cooling was provided between March 30 and November 27 of 2005; heating was provided for the other periods. The system was modeled with two heat pumps; one is for heating and the other is for cooling respectively. Catalog data – 35 points in cooling and 25 points in heating mode – at a range of flow rates and entering water temperatures on both the source side and load side are available from the manufacturer and are used to generate the heat pump model coefficients, as described in Section 5.2.1 below.

5.1.2 GLHE

The GLHE has, in total, 4 vertical boreholes and one horizontal loop. For these experiments, only 3 vertical boreholes are connected, as shown in Figure 4.32. The vertical boreholes are each approximately 75m (258ft) deep, 114 mm (4.5") in diameter and consist of a single HDPE U-tube of nominal diameter 19.05mm (3/4"), backfilled with bentonite grout. The ground thermal conductivity was estimated with an in-situ thermal conductivity test (Austin et al. 2000) and the volumetric specific heat was estimated from knowledge of the geology. The undisturbed ground temperature was

estimated with an in-situ water filled borehole temperature measurement. Comparisons of these in situ results with calibrated values are given in Section 5.2.2 below.

5.1.3 Cooling Tower

A direct-contact evaporative cooling tower (Amcot Model 5) with nominal capacity of 14.75kW (4.2 tons) (defined at a water flow rate of 0.63L/s (10gpm) being cooled from 35ºC (95ºF) to 29.4ºC (85ºF) with an outdoor wet bulb temperature of 25.6ºC (78ºF)) is connected to the source-side of the heat pumps via an isolation plate frame heat exchanger.

5.1.4 Plate Frame Heat Exchanger

The plate frame heat exchanger (Paul Mueller PHE AT4C-20) has a nominal capacity of 9.3 kW with flow rates of 0.5 L/s on both sides of the heat exchanger and a temperature difference of 19.4^{o}C between the inlet temperatures. The manufacturer gave an additional 15 data points at various flow rates and temperatures. The data are used to generate coefficients for the plate frame heat exchanger model described in Section 4.5.1.

5.1.5 Piping

In addition to the components that are shown explicitly in Figure 4.32, there is buried piping that connects the GLHE to the plant building (approximately 30 m in each direction), buried piping that connects the cooling tower to the plant building (approximately 31 m in each direction), and exposed (to the plant room environment) piping that connects the components inside the building (approximately 12 m in each

direction). Under many conditions, e.g. when the piping is insulated, heat losses and gains to/from the piping may be negligible. However, buried, uninsulated piping, as used to connect the cooling tower and GLHE may have a not-insignificant amount of heat transfer.

5.1.6 Experimental Measurement Uncertainty

A detailed uncertainty analysis was performed by Hern (2004). As can be seen from Figure 5.1, thermocouples after calibration, with an uncertainty of approximately ±0.11°C, were placed on the inlets and outlets of all components. Vortex and paddle wheel flow meters were utilized to measure flow through the heat pump – GLHE loop and through the cooling tower loop; expressions for their uncertainty were given by Hern (2004). The watt transducers are installed in the system to measure the power used by the cooling tower, circulating pumps, and heat pumps. This data set will be sufficient to benchmark the accuracy of the simulation model.

Heat transfer rates are determined as the product of the mass flow rate, specific heat and ΔT . Given the uncertainty in temperature measurement, the fractional uncertainty in the temperature difference measurement is:

$$e_{\Delta t} = \frac{\pm 0.16^{\circ} C}{\Delta T} \qquad 5\text{-}1$$

Then, the fractional uncertainty of the heat transfer rate may be given as:

$$e_{HTR} = \pm\sqrt{e_{\Delta t}^2 + e_{flow}^2} \qquad 5\text{-}2$$

Where:

e_{flow} = Fractional error in the flow rate.

This value changes throughout the experiment for each measurement, but typical values may be given, and for most components, the error bounds on the experimental measurement are also plotted.

5.2 Component Model and System Simulation Validation – Cooling Tower Operation Set with Boundary Condition

In this HGSHP system validation, two approaches to modeling the cooling tower control have been taken:

1. For the first set of simulations, cooling tower on/off operation is simply set as a boundary condition taken from the experiment. In this case, all control interactions are, in effect, treated as boundary conditions. The type of simulation was particularly useful as the first phase of the validation, in which the behavior of each component model was the first concern. In this set of simulations, the comparisons of interest include the fluid temperatures at any point in the loop and the heat transfer rates of the various components.

2. For the second set of simulations, a simple model of the cooling tower controller takes the difference between the outdoor ambient wet-bulb temperature, provided as a boundary condition, and the simulated exiting heat pump fluid temperature. When the difference exceeds a specified value, 3 ºC,

the cooling tower is switched on. When the difference falls below another specified value, 1 ºC, the cooling tower is switched off. The phase of the validation was primarily concerned with the behavior of the system as a whole. The validation of the HGSHP system simulation with cooling tower control simulated is presented in Section 5.3.

In this section, validation of each component model, individually and with the system simulation (cooling tower operation set with boundary condition) are presented. "Individually" means validation of the component model by itself where the input temperatures are taken from experimental data. "Within the system simulation" means validation of the component model where the input temperatures are computed by the system simulation, when all fluid temperatures are being solved simultaneously.

5.2.1 Heat Pumps

In this HGSHP system, the experimental entering fluid temperatures at the source side of heat pump were lower than the temperatures given by manufacturer's catalog. And the flow rates at both the load and source sides of the heat pumps were greater than the flow rates from the manufacturer's catalog. An equation-fit heat pump model was developed by Gentry (2007) and it performed poorly when one of the input variables fell outside the range of data which were used to fit the equations.

In this research, the parameter estimation-based heat pump model described in Section 4.2.1 is utilized. The parameter estimation-based heat pump model has a better

capability of modeling heat pump than the equation-fit model and allows some extrapolation beyond the catalog data.

As described in Section 4.2.1, the parameter estimation-based heat pump model has an algorithm to calculate the capacity approximately when the heat pump runs at partial load. In this experiment, average experimental data of 5-minute time step was colleted for validation and the heat pump might be switched on or off during the 5-minute time step of simulation. The heat pump model uses the load side experimental heat transfer rate as an input. First, the heat pump model calculates the heating/cooling capacity based on the inlet fluid temperatures and flow rates at both sides of the heat pump. Then the input load side heat transfer rate and the computed capacity are compared and when the partial load ratio (input load side heat transfer rate divided by the computed capacity) is less than 0.8, which indicates the heat pump is in partial duty, the input load side heat transfer rate is then used as the heat pump capacity. When the partial load ratio is greater then 0.8, which indicates the heat pump runs at full duty approximately, the model calculated heating/cooling capacity is used as the heat pump capacity.

The coefficients for the parameter estimation-based heat pump model descried in Section 4.2.1 were calculated with a program written by Tang (2005). The program read in the heat pump data (from manufacturer's catalog or from experimental measurements) and fitted the coefficients by using the generalized least-squares method. The coefficients for the heat pump models are listed in Table 5.1.

Table 5.1 Heat pump coefficients

Coefficient Name	Coefficients obtained based on manufacturer's data	Coefficients obtained based on experimental data
Heating Mode		
Load side heat transfer coefficient (kW/K)	2.029	1.898
Source side heat transfer coefficient (kW/K)	1.896	2.191
Superheat Temperature (ºC)	1.8	1.6
Constant part of the electromechanical power loss (kW)	0.784	1.400
Electromechanical loss factor (-)	0.78	1.11
Piston displacement (m^3/s)	0.003	0.002
Pressure drop across the suction valve (kPa)	0.92	1.04
Clearance factor (-)	0.153	0.051
Cooling Mode		
Load side heat transfer coefficient (kW/K)	2.503	2.932
Source side heat transfer coefficient (kW/K)	2.938	3.775
Superheat Temperature (ºC)	0.5	0.6
Constant part of the electromechanical power loss (kW)	1.399	0.817
Electromechanical loss factor (-)	1.14	0.87
Piston displacement (m^3/s)	0.003	0.002
Pressure drop across the suction valve (kPa)	0.87	0.95
Clearance factor (-)	0.161	0.005

Coefficients for the parameter estimation-based heat pump model were initially calculated using manufacturer's catalog data – the resulting model is labeled as "uncalibrated" in Figures 5.2-5.5. In Figures 5.2 and 5.3, the "uncalibrated" heat pump model gave quite good results in heating mode in spite of the fact that the actual flow

rates on both sides of the heat pump were larger than manufacturer's catalog data. In Figure 5.4-5.5, the "uncalibrated" heat pump model gave poor results in cooling mode. The reason was that the experimental data of heat pump did not have a heat balance in cooling mode but the coefficients for the heat pump were calculated from the catalog data in which the heat pump had a perfect heat balance.

Therefore, it was addressed in our case by using experimentally-measured data points in the data set and recalculating the model coefficients. The heat imbalance of heat pump also was considered in the recast heat pump model. Table 5.2, Figure 5.4 and Figure 5.5 show substantial improvements when this calibration is done.

Table 5.2 Summary of Uncertainties in HP model

Model	Source Side HTR RMSE (W)	Source Side HTR Mean Bias Error (W)	Load Side HTR RMSE (W)	Load Side HTR Mean Bias Error (W)	Power RMSE (W)	Power Mean Bias Error (W)	Source Side HTR Typical Uncertainty	Load Side HTR Typical Uncertainty	Power Typical Uncertainty
Simulated (calibrated system simulation)	360	-5	445	25	79	2	450 W	500 W	4.5 W
Simulated(calibrated component simulation)	482	-54	510	-19	87	6			
Simulated(uncalibrated component simulation)	642	-287	504	112	191	-74			

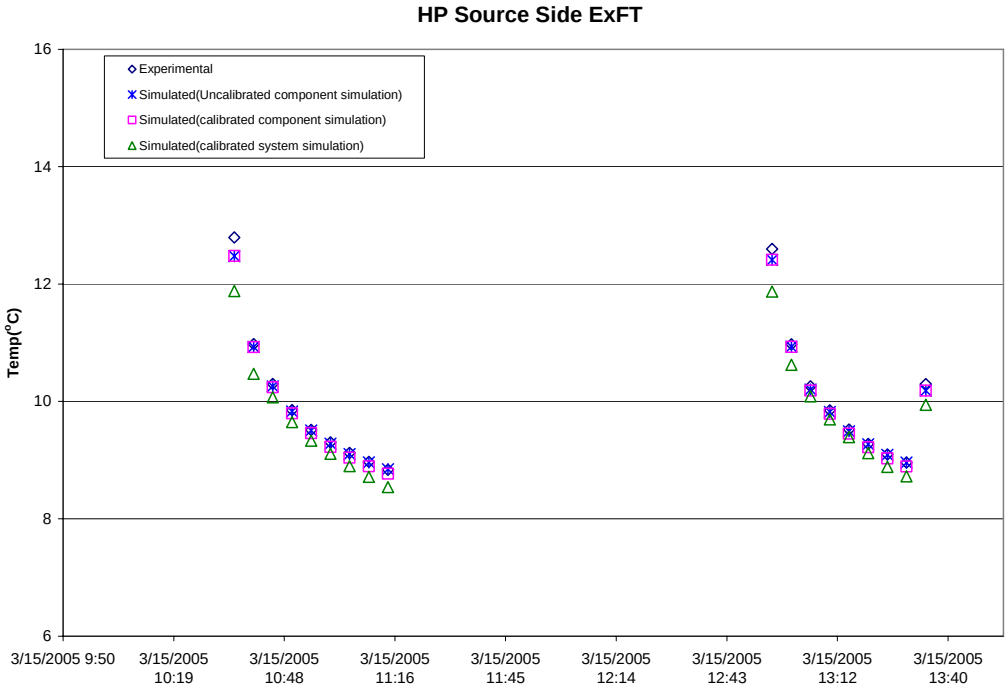

Figure 5.2 HP Source side ExFT for a typical heating day.

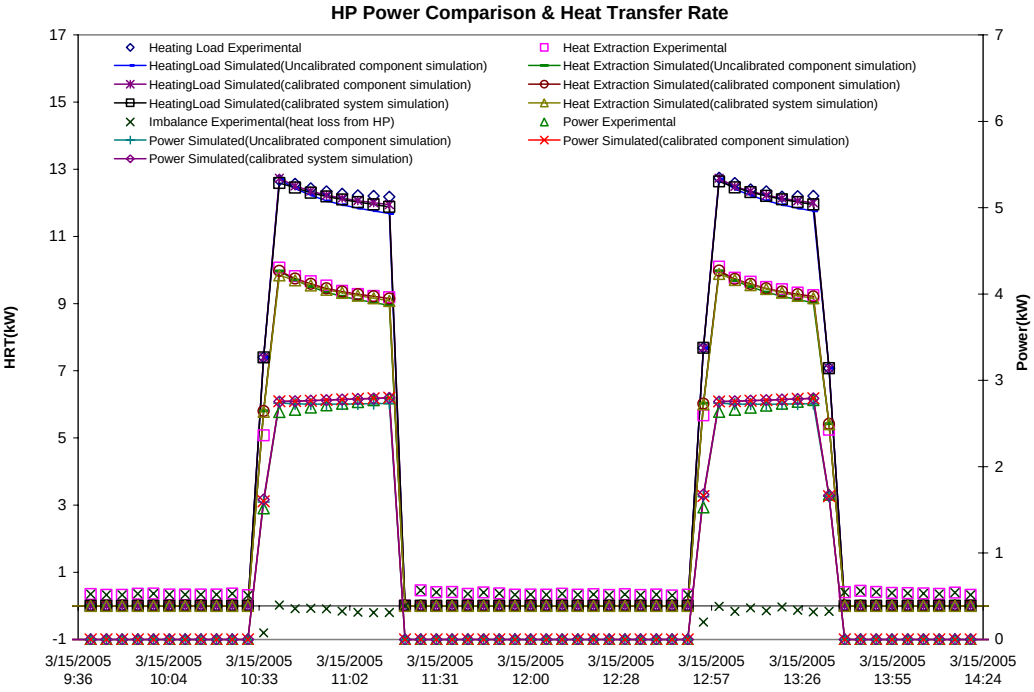

Figure 5.3 HP power consumption and heat transfer rate for a typical heating day.

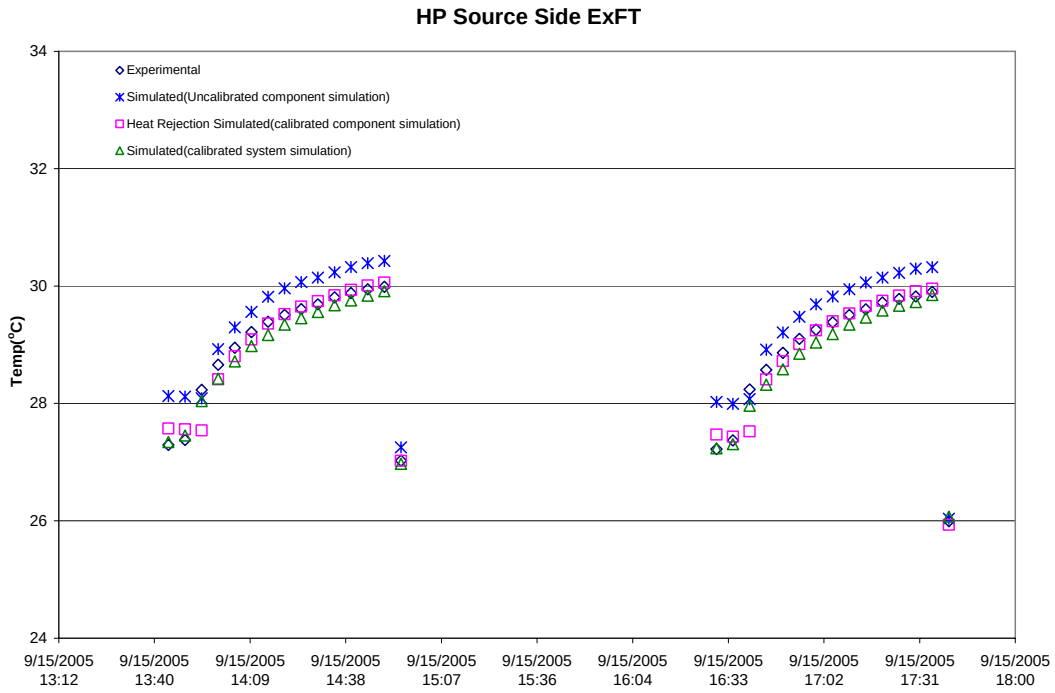

Figure 5.4 HP Source side ExFT for a typical cooling day.

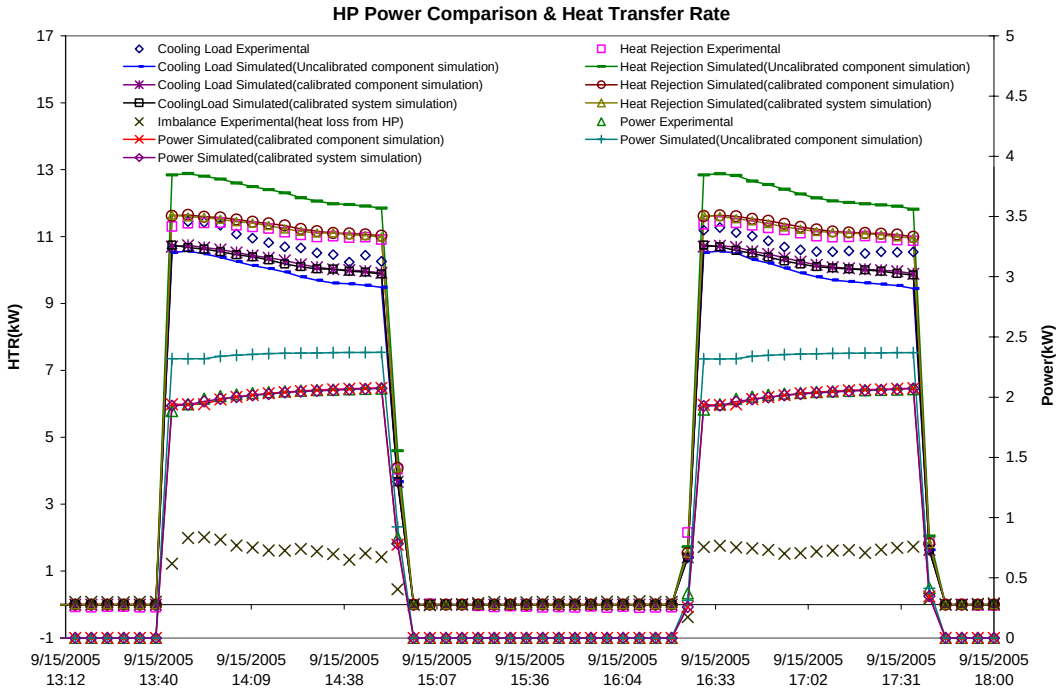

Figure 5.5 HP power consumption and heat transfer rate for a typical cooling day.

5.2.2 GLHE

In this section, validations of the ground loop heat exchanger model, individually and with the system simulation are presented, using the operating data collected from the HGSHP research facility. This is presented in Section 5.2.2.1.

Also in this section, verification of the effects of the thermal mass of fluid is presented. An experimental estimated fluid factor is used for the validation of the GLHE model in Section 5.2.2.1. In Section 5.2.2.2, different fluid factors are used and the comparison of the simulation results is presented.

5.2.2.1 Validation of GLHE of HGSHP System

As previously shown in Section 4.1.3, the heat transfer of the ground loop heat exchanger is related to the geometry of the borehole and thermal properties of the fluid, grout, and surrounding ground. After the borehole is installed, most of the borehole geometric parameters are determined except the shank spacing, which varies with the installation, but is typically new the "B" configuration specified in GLHEPRO. The GLHE simulation result depends on three parameters that are required to be estimated precisely: the undisturbed ground temperature, the effective grout thermal conductivity, and the effective ground thermal conductivity. The effective grout thermal conductivity is the grout conductivity, which gives the best approximation of the borehole thermal resistance assuming the "B" spacing. The effective ground thermal conductivity is the best overall value that represents all the layers of rock and soil intersected by the boreholes.

For large commercial systems, these parameters are typically estimated as part of an in-situ thermal conductivity test, which would be performed for one or a few test boreholes (Austin et al. 2000; Shonder and Beck 2000; Gehlin and Nordell 2003). Additional uncertainty, beyond sensor error, is introduced because of the nonhomogeneous nature of the ground; the time-varying nature of the undisturbed ground temperature, which is affected by seasonal changes near the surface; and downhole variations in the U-tube location and borehole diameters. Hern (2004) measured all these three parameters foe each of the three boreholes: the range of values and mean values are summarized in Table 5.3. The calibrated values shown in the last column of Table 5.3 are found by minimizing the sum-of-the-squares-of-the-error of the GLHE exiting fluid temperature for the 12 month period evaluated here. Because the parameters are interrelated, the calibration may find best-fit values that are outside the estimated uncertainty range of the experimental measurements, as found for the effective grout thermal conductivity.

Table 5.3 GLHE Parameters

Parameter	Range measured by Hern (2004)	Mean measured by Hern (2004)	Estimated Uncertainty	Calibrated Value
Undisturbed ground temperature (^{o}C)	17.1-17.4	17.25	± 1.0 ° C	18.2
Effective grout thermal conductivity (W/m-K)	1.07-1.09	1.08	± 15%	1.05
Effective ground thermal conductivity (W/m-K)	2.4-2.7	2.55	± 15%	2.8

Figure 5.6 compares experimental and simulated outlet temperature from the component GLHE simulation (calibrated and uncalibrated) as well as the system

simulation (calibrated only) for five hours of a typical cooling day. Figure 5.7 gives the heat transfer rates for the same time period. During these five hours, the heat pump went through two on/off cycles. During the off portion of the cycle, it may be noted that there is a small negative heat transfer rate. The circulation pump was operated continuously. Also, during this time period, the cooling tower was operated continuously, and heat was exchanged between the ground and the horizontal piping that runs between the plant and the cooling tower. The net effect is the small negative heat transfer rate; i.e. heat is being extracted from the ground, and is "pre-cooling" the ground during the heat pump off cycle.

For the component simulations, the experimental inlet temperature was used to drive the model. The results of the calibrated component model here did not bring much difference compared to those from the uncalibrated component model over this 12-month period simulation. It may be inferred from this that the thermal properties measured with the in situ test give adequate accuracy. The system simulation, which uses the inlet temperature calculated by the simulation, shows an increased amount of error.

For the uncalibrated component model simulation, the root mean square error (RMSE) of the heat transfer rate over the twelve month evaluation period is 605 W; the mean bias error (MBE) is 196 W, the simulation predicted, on average, 196 W more heat rejection than was experimentally measured. The calibrated component model simulation has a lower RMSE of 552 W; the MBE is -184 W, the simulation predicted, on average, 184 W less heat rejection than was experimentally measured. Finally, when the calibrated

model is run as part of the system simulation, the RMSE increases to 834 W, but the MBE is 31 W.

These errors should be compared to the experimental uncertainty of the heat transfer measurement. The uncertainty varies with flow rate and ΔT, but a typical value when the heat pump is operating is ±400 W. Figure 5.7 shows the upper and lower bounds on the experimental uncertainty. As shown, most of the calibrated component simulation and the system simulation results are within the bounds of experimental uncertainty.

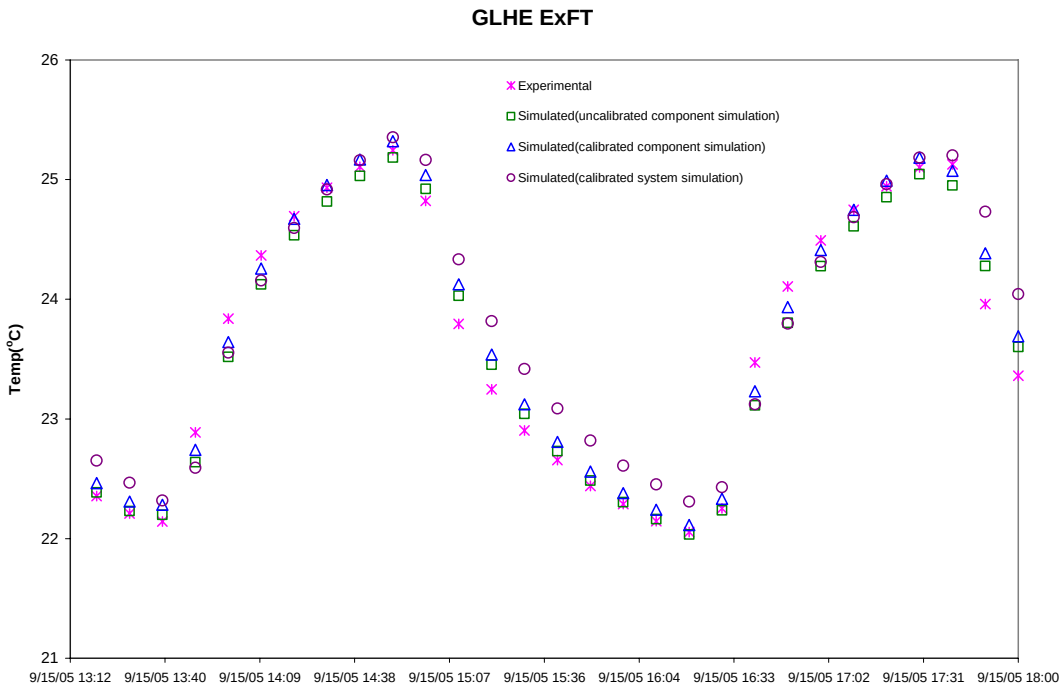

Figure 5.6 GLHE ExFTs for five hours of a typical cooling day

Figure 5.7 GLHE heat transfer (rejection) rates for five hours of a typical cooling day.

5.2.2.2 Verification of the Effects of Fluid Thermal Mass

In Section 5.2.2.1, an experimentally estimated fluid factor was used for the simulation of the ground loop heat exchanger. Calculation of the volume mass of the fluid in the ground loop heat exchanger and that outside the U-tube in the HGSHP system, a fluid factor value of 1.4 is estimated.

The thermal mass of the fluid inside and outside the U-tube dampens the temperature response of the ground loop heat exchanger. In this section, four different fluid factor values (0.1, 1, 1.4, 2) are selected for the ground loop heat exchanger simulation. The value 0.1 would be representative of a simulation that did not include the effect of the thermal fluid mass; the value of 1 would account only for the thermal mass of fluid in the borehole; the value of 1.4 was estimated based on the HGSHP system

layout; the value of 2 would be a typical value for a HGSHP system with a relatively large pipe layout. The simulated fluid exiting temperatures and the heat transfer rates against the experimentally measured data in a typical cooling day were presented in previously Figure 5.8 and Figure 5.9.

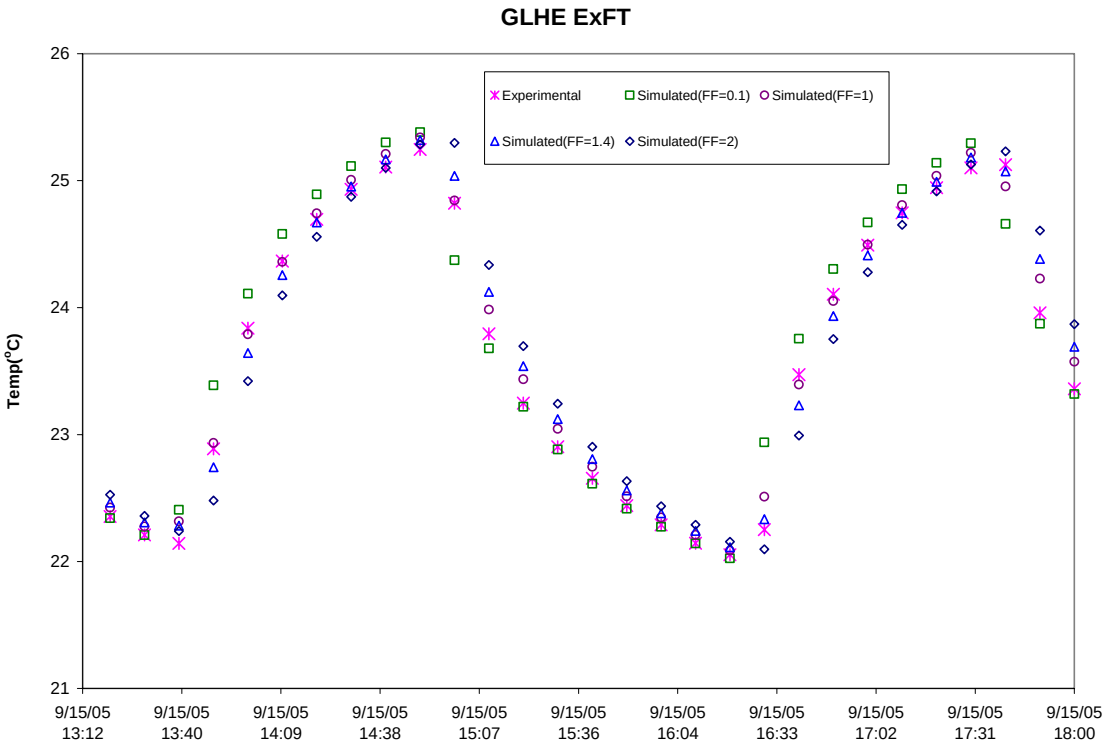

Figure 5.8 GLHE ExFTs for five hours of a typical cooling day

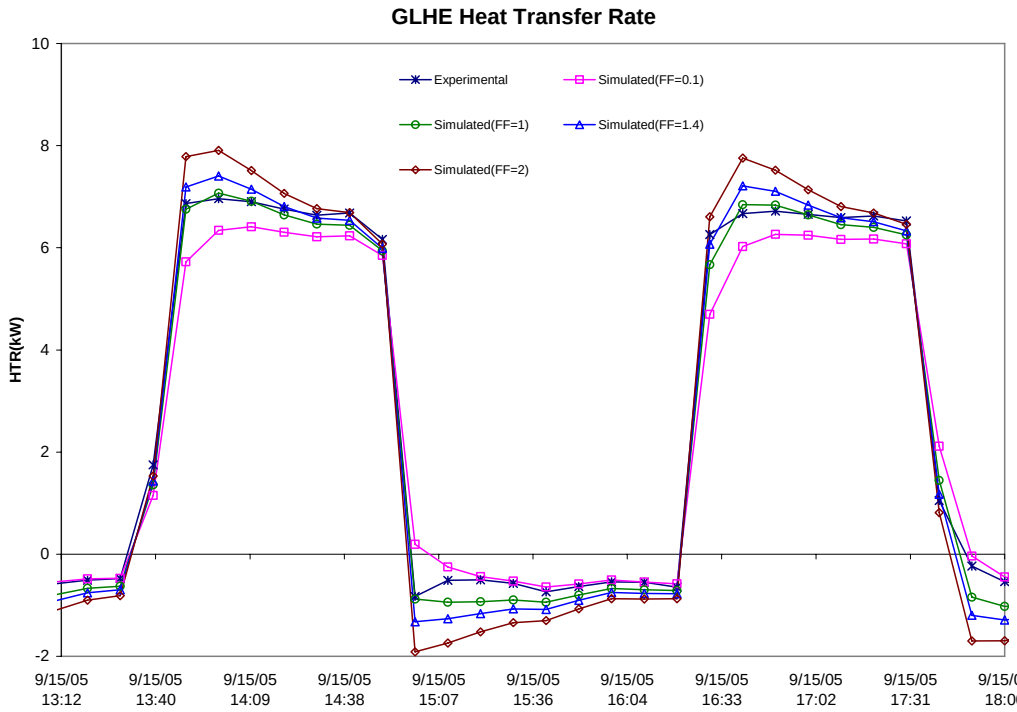

Figure 5.9 GLHE heat transfer (rejection) rates with different fluid factors for five hours of a typical cooling day.

In Figure 5.8, when the heat pump cycles on/off, the exiting fluid temperature of the small fluid factor case rises/drops much faster that that of the large fluid factor case. As a result, the heat transfer rate of the ground loop heat exchanger of the small fluid factor case is smaller than the heat transfer rate of the large fluid factor case, as shown in Figure 5.9.

Table 5.4 shows the root mean square error (RMSE) of the heat transfer rate over the twelve month evaluation period for different fluid factor cases. The case with fluid factor 1 had the relatively smallest RMSE. When the fluid factor became smaller or larger, the RMSE of heat transfer rate would increase. The case with the experimentally estimated fluid factor 1.4 had a larger RMSE of heat transfer rate than the case with fluid factor 1. The effect of the fluid thermal mass still needs to be checked.

Table 5.4 GLHE Parameters

Fluid Factor	RMSE(W)	MBE(W)
FF=0.1	662	-186
FF=1	502	-184
FF=1.4	552	-184
FF=2	746	-183

5.2.3 Cooling Tower

Two open-circuit cooling tower models previously descried in Section 4.3.1 are experimentally validated here.

The first model is a fixed UA model and the parameter UA is calculated from cooling tower manufacturer's catalog data. The cooling tower manufacturer (Amcot Model 5) gave only a single operating point as catalog data, as listed in Table 5.5. The estimated parameter UA value is 800 W/K.

Table 5.5 Cooling tower manufacturer's data (Amcot Model 5)

Model	Nominal Water Flow (GPM)	Air Volume (CFM)	Pump Head (FT.)	Fan Motor (HP)	EFT (F)	ExFT (F)	Entering Air Wet Bulb Temp (F)
5	10	2,100	5	0.167	95	85	78

The second model is variable UA model. The coefficients k, x, y in Equation 4-16 were estimated based on the experimentally measured data. The final variable UA model results in:

$$UA_e = \left[764\dot{m}_w^{1.11}\dot{m}_a^{0.41}\right]\frac{C_{pe}}{C_{p,moistair}} \qquad 5\text{-}3$$

Figures 5.10 and 5.11 show results for a five-hour of a typical cooling day, in which the cooling tower was on. Here, the uncalibrated component simulation represents the results from the fixed UA model; while the calibrated simulations represent results with the variable-UA model. The calibrated model gives a small improvement over the uncalibrated component model simulation. The RMSE in the heat transfer rate is 1553 W for the uncalibrated component simulation. Going to the calibrated variable UA model only reduces the RMSE to 1542 W. The MBE goes from 388 W to 480 W of overprediction by the simulation. When the calibrated model is simulated as part of the system, the RMSE is 1302 W and the MBE is 165 W of underprediction by the simulation.

The lower and upper bounds of the experimental uncertainty in the cooling tower heat transfer rate measurement are shown in Figure 5.9. In addition, the simulation has an experimental uncertainty component – the wet bulb temperature (an input) has a typical uncertainty of ± 0.5ºC – and this results in an uncertainty in the simulation results. Error bars are shown for a couple sample points in Figure 5.9. The uncertainty caused by the uncertainty in the wet bulb temperature appears to be the limiting factor in the simulation. This also suggests that, in practice, caution is warranted in using a control based on wet bulb temperature.

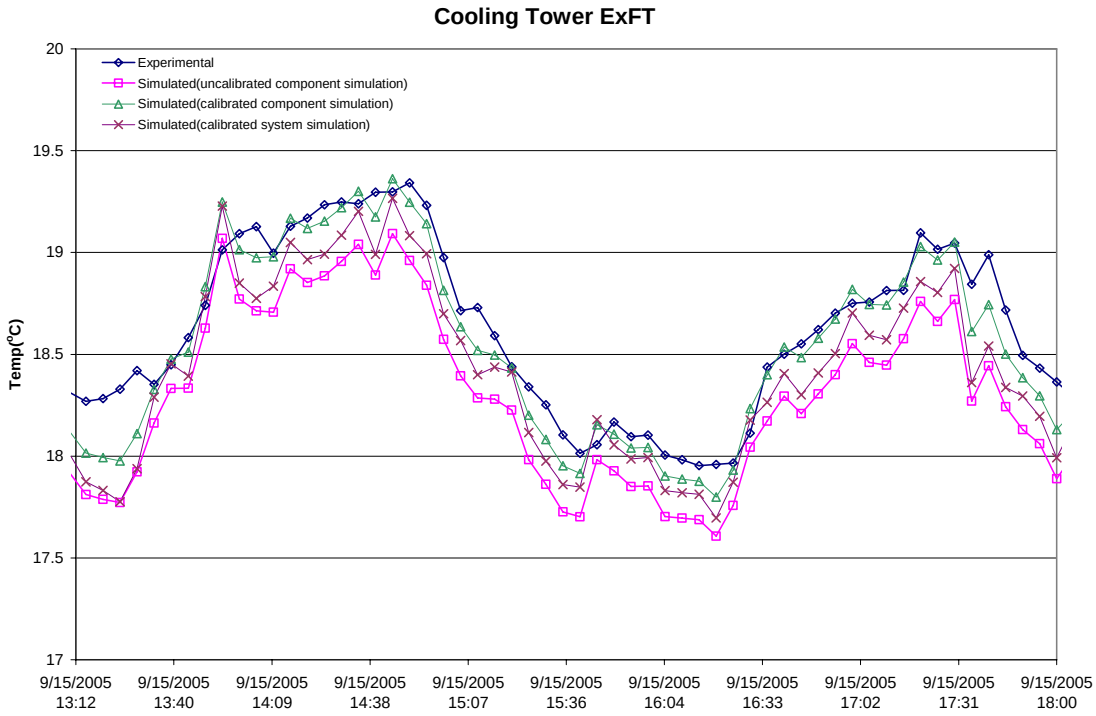

Figure 5.10 Cooling tower ExFTs for a typical cooling day

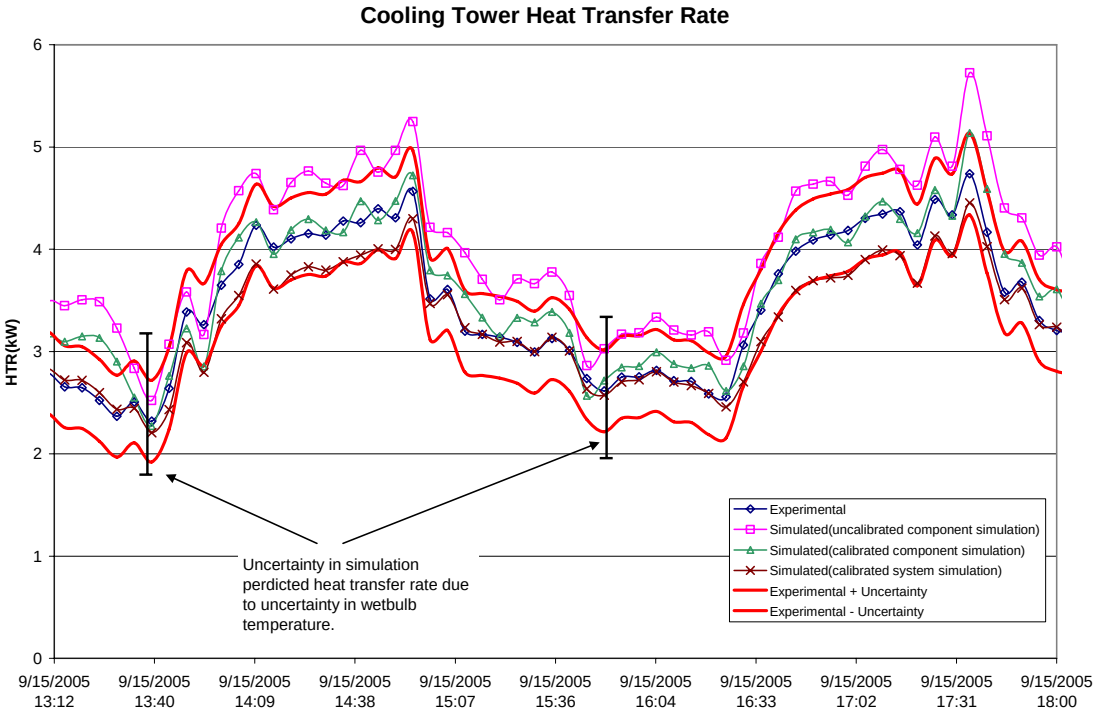

Figure 5.11 Cooling tower heat transfer rates for a typical cooling day.

5.2.4 Plate Frame Heat Exchanger

The two variable UA with/without fouling plate frame heat exchanger models previously descried in Section 4.5.1 are validated here.

Initially, the variable UA without fouling model was utilized for the simulation. Sixteen data points were available from the manufacturer of the plate frame heat exchanger model (Paul Mueller PHE AT4C-20), which are listed in Table 5.6.

Table 5.6 Plate frame heat exchanger manufacturer's data (Gentry 2007).

Loop Side (Hot)		CT Side (Cold)					
EFT (^oF)	Flow rate (GPM)	EFT (^oF)	Flow rate (GPM)	HTR (Btu/hr)	LMTD (^oF)	U (Btu/ft2-hr-^oF)	Heat Transfer Area (ft2)
100	6	75	6	21,448	17.8	405	3
120	6	85	6	23,737	27.0	296	3
140	6	95	6	35,467	33.0	361	3
100	8	75	8	28,597	17.8	540	3
120	8	85	8	31,650	27.0	394	3
140	8	95	8	47,289	33.0	482	3
100	12	75	12	41,703	18.0	779	3
120	12	85	12	47,474	27.0	591	3
140	12	95	12	70,934	33.0	723	3
100	14	75	14	47,262	18.2	874	3
120	14	85	14	55,387	27.0	690	3
140	14	95	14	82,756	33.0	843	3
140	6	95	10	56,200	29.7	638	3
140	12	95	8	70,934	30.0	797	3
140	14	95	6	62,046	29.7	704	3
120	10	85	14	59,368	24.7	809	3
120	6	85	14	44,540	24.0	624	3
120	8	85	12	51,457	24.1	718	3

The manufacturer's data were used to estimate the parameters C_1, m, n in Equation 4.31 at both sides of plate frame heat exchanger. In this application, based on Ayub (2003) summary of plate frame heat exchanger model, the parameter m was set as 0.667 and the parameter n was set as 0.33. The parameter C_1 at both sides of the plate frame heat exchanger is estimated as shown in Table 5.7.

Table 5.7 The parameters for the plate frame heat exchanger model

Parameter	m	n	C_1 of heat pump side	C_1 of cooling tower side	R_∞ (K/W)	B (hours)
Value	0.667	0.333	23.50	18.52	0.00186	2655

However, the calculation of the UA value at every time step based on experimental measurements revealed two phenomena:

1. In the first six month cooling period of experimentation (April- September), significant fouling was observed on the cooling tower supply of the loop and the UA decreased substantially.

2. From October, bleach was added in the cooling tower circulation loop and the cooling tower loop was cleaned almost every two days. As a result, the UA remained relatively stable in the following two months (October-November).

Therefore, two different models were utilized for modeling these two phenomena:

1. For the first six month cooling period, the variable UA with Knudsen's fouling model (1984) was used for modeling the plate frame heat exchanger. The constant R_∞ and B were addressed based on experimentally measured data, which were listed in Table 5.7.

2. In the next two cooling month period, the variable UA without fouling model was used.

Figure 5.12 shows a comparison of the various simulations with the experimental results. Clearly, the original approach, without the fouling model, yields large errors. With the fouling model the system simulations give heat transfer rates that are substantially improved. The RMSE of the heat transfer rate prediction is 694 W for the uncalibrated model; 415 W for the calibrated model; and 625 W for the model in the system simulation. The MBE is 285 W of overprediction for the uncalibrated model; 20 W of overprediction for the calibrated model; and 160 W of overprediction for the model in the system simulation.

The parameters of the plate frame heat exchanger model with fouling R_∞ and B were addressed based on experimental measurements and the model performed well. However, without having experimental measurements in advance of operation, the inherently unpredictable nature of fouling leaves a difficulty for the system designer.

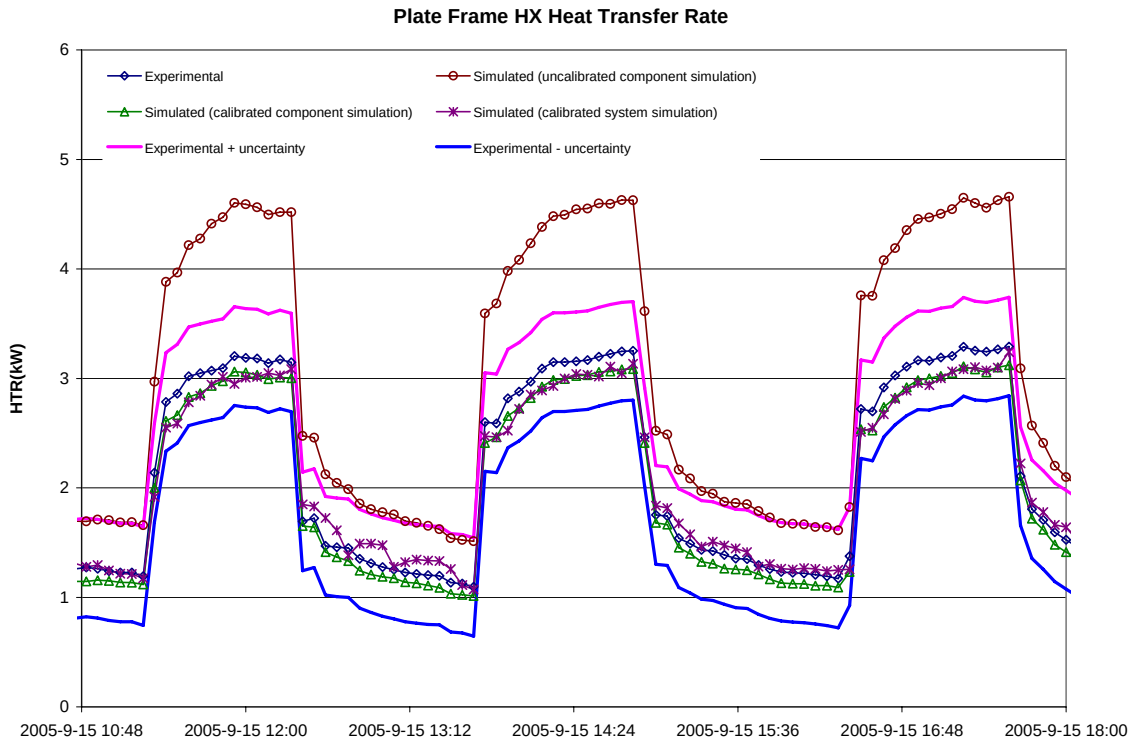

Figure 5.12 Plate frame heat exchanger heat transfer rate for a typical cooling day.

5.2.5 Pipe

As described above in the "Experimental Facility" section, the uninsulated piping, either exposed to the environment or buried in the ground, has some not insignificant heat losses or gains. These heat transfers vary significantly over time. For example, the heat loss from the buried pipe leading to the cooling tower will be high (say 650 watts on average for the first 10 minutes) when the cooling tower is first switched on. After, say, an hour of cooling tower run time, the heat loss may drop to 350 watts.

As buried horizontal piping is a common feature of ground source heat pump systems, it would be useful to develop a component model that predicts the heat losses or gains. However, at present, no such model is available, and another approach was taken. A simple component model was developed that took the measured heat gain or loss as an input provided as a boundary condition, and computed the outlet temperature as:

$$T_{out} = T_{in} + \frac{Q_s}{\dot{m} C_p} \qquad 5\text{-}4$$

Where:

T_{out} = The temperature of the water leaving the pipe, (ºC);

T_{in} = The temperature of the water entering the run of pipe, (ºC);

Q_s = The measured heat transfer rate, (W).

This approach worked satisfactorily when the cooling tower control was treated as a boundary condition so that the simulated cooling tower on/off operation matched the experiment well. For cases where the cooling tower control was simulated, the short time variations in the empirical pipe heat losses or gains for the piping running to and from the cooling tower are no longer meaningful. Instead, a new boundary condition was developed that used the average heat gain/loss during cooling tower runtime for each component for each day. This was set as the boundary condition for every time step of the day, and maintained the heat loss or gain approximately correctly to the extent that the simulated daily cooling tower runtime matched the actual daily runtime.

5.3 System Simulation Validation – Cooling Tower Control Simulated

After adjusting component models and their parameters while setting the cooling tower operation to exactly match the experimental data, attention may be turned to the broader question of how the model performs with the cooling tower control explicitly modeled. Again, this is the simulation that is of interest for validation from a designer's perspective. In addition to looking at the final calibrated simulation, the intermediate steps between the starting case and the final calibrated simulation will also be examined. Three results are of primary interest: system energy consumption, cooling tower run time, and maximum entering fluid temperature to the heat pump.

Starting with the system energy consumption, Figure 5.13 shows the component-by-component energy consumption over the entire period, starting with the completely uncalibrated mode case, then showing each incremental improvement. Clearly, the improved cooling tower model and ground loop heat exchanger model bring little difference in total energy consumption of system. The improved heat pump model has a significant improvement of heat pump energy consumption. By way of explanation, energy consumption by the heat pump is the largest component of the system energy and is about 57% of total system energy consumption. While there is definitely a relationship between entering fluid temperature and energy consumption, a few degrees Celsius error does not make a significant difference in energy consumption, so small errors in the GLHE model or cooling tower are not as important as errors in the heat pump model.

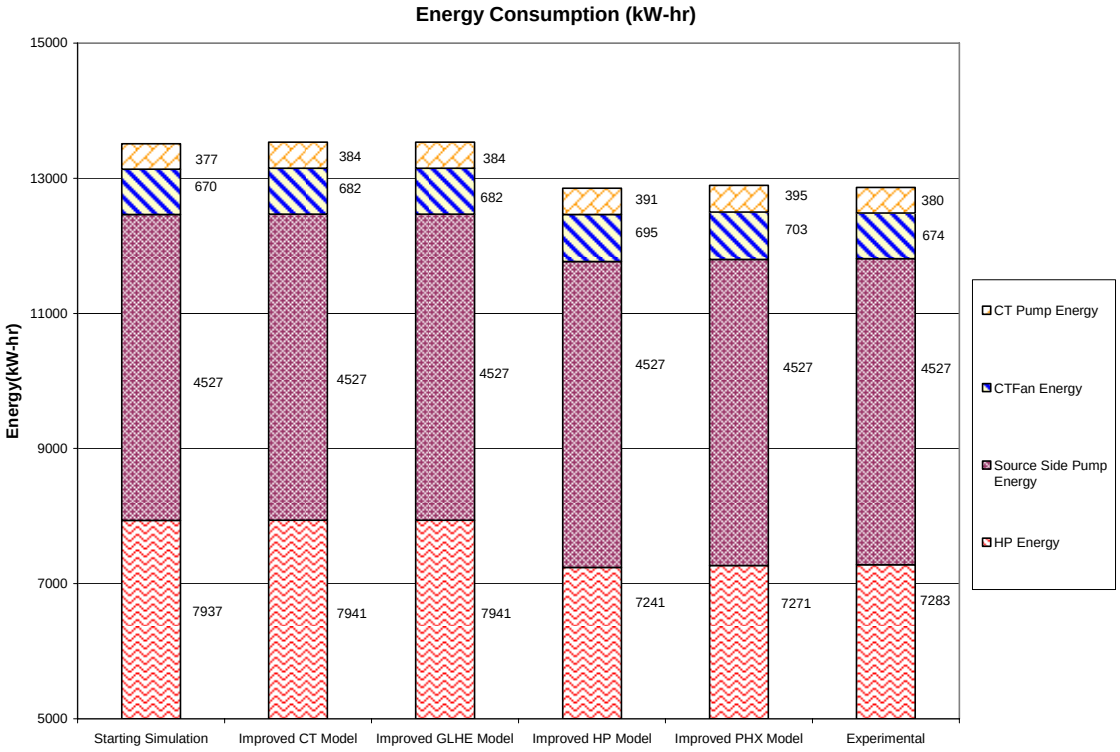

Figure 5.13 System energy consumption – incrementally improved simulations vs. experimental measurements. Note: Y-axis begins at 5000 kW-hr

The monthly energy consumption for the final calibrated simulation and the experiment is shown in Figure 5.14. There is quite a good match between the simulated energy consumption and the experimental measurements.

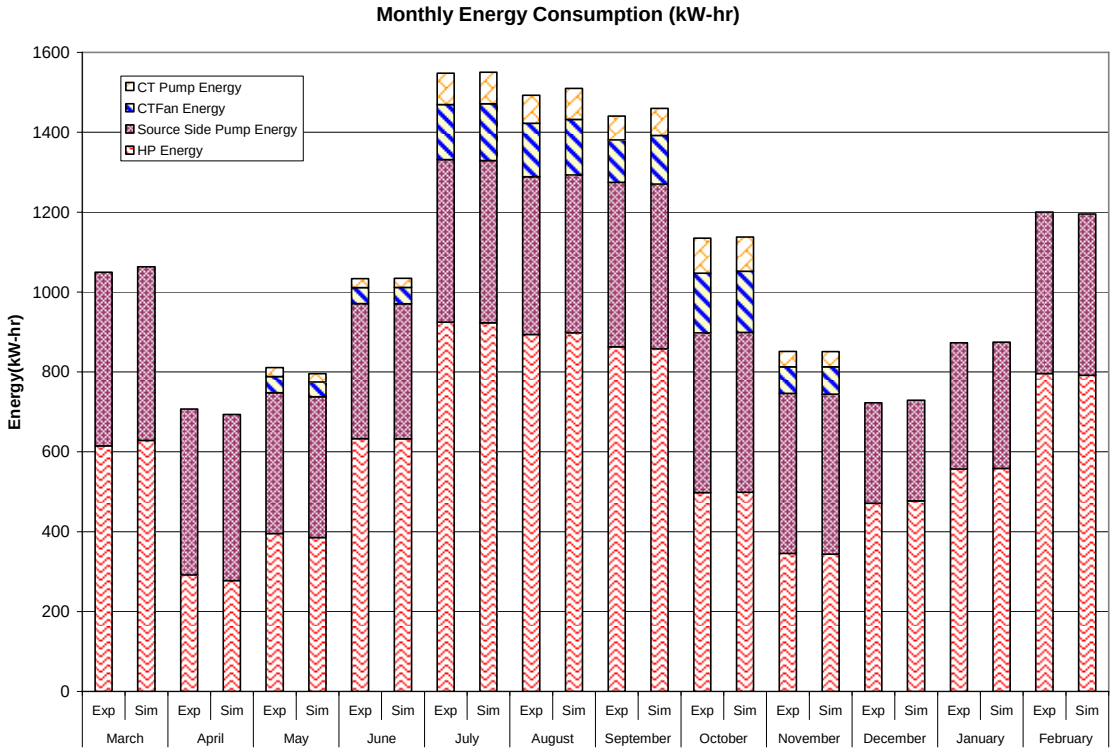

Figure 5.14 Experimental vs. simulated monthly energy consumption

The cooling tower run times predicted by each model variation and the experiment are summarized in Table 5.8. Again, all variations of the model fall within a few percent of the experimental results, and this accuracy should be quite adequate for any design simulation.

Table 5.8 Cooling tower run times

	Starting Case	Improved CT Model	Improved GLHE Model	Improved HP Model	Improved PHE Model	Experimental
Cooling Tower Run Time (Hours)	2793	2843	2843	2896	2929	2809

A final parameter of interest is the predicted maximum entering fluid temperature. Ground loop heat exchangers serving cooling-dominated buildings are generally sized to not exceed a maximum entering fluid temperature, so this parameter is of particular interest. Also the minimum entering fluid temperature of the heat pump is compared. As shown in Table 5.9, all of the simulations overpredict the maximum entering fluid temperature and underpredict the minimum entering fluid temperature.

Table 5.9 Maximum and minimum heat pump entering fluid temperatures.

	Starting Case	Improved GLHE Model	Improved CT Model	Improved HP Model	Improved PHE Model-Final Simulation	Experimental
Max HP EFT (ºC)	30.7	30.9	30.9	31.0	31.2	30.1
Min HP EFT (ºC)	10.0	10.0	10.0	10.4	10.4	10.7

5.4 Conclusions

This chapter described a validation of a hybrid ground source heat pump system simulation. The experimental data were collected from the OSU HGSHP research facility (Hern 2004). The validation coved a 12 month period, including a continuous 7-month cooling season and portions of two heating seasons.

In this HGSHP system validation, two approaches were used for the simulation. First, the HGSHP system was simulated with the cooling tower on/off operation set as a boundary condition taken from the experiment. The type of simulation provided insight into the nature of the each component model performance while the cooling tower

operation schedule is forced to match the experiment. After the validation of each component model, the HGSHP system was simulated with a temperature difference control strategy. When the difference exceeds a specified value, 3 ºC, the cooling tower is switched on. When the difference falls below another specified value, 1 ºC, the cooling tower is switched off. With cooling tower control simulated, the simulated operation of the cooling tower drifts from the actual operation. Hence, only energy consumption can be feasibly compared. Although the unclibrated system simulation energy consumption matched the actual system energy consumption within 6%, a serial of calibrations were applied to the simulation.

- A parameter estimation-based heat pump model (Jin and Spitler 2002) was utilized and performed well when the actual flow rates on both sides of the heat pump were larger than catalog data.

- For the simulation of GLHE, three parameters: the undisturbed ground temperature, the grout thermal conductivity and the ground thermal conductivity had been recalibrated based on the measured experimental data and the GLHE model performed well.

- In the validation of GLHE, an experimentally estimated fluid factor was used for the validation of the GLHE model. For purpose of validation of thermal mass of fluid of GLHE model, several other fluid factor values had been selected for the simulation of GLHE and comparison of the simulation results was presented.

- In the experimentation, fouling was observed on the cooling tower supply of the loop and the UA values of the plate heat exchanger decreased substantially. In this research, a new plate frame heat exchanger model with fouling model (Barrow and Sherwin 1994) was used and performed well.

After the validation of each component model, the HGSHP system was simulated with a temperature difference control strategy and compared against the experimentally measured data. The simulation gave total energy consumption about 0.2% higher than the experiment.

6 DEVELOPING DESIGN PROCEDURE OF HGSHP SYSTEMS

The main objective of this chapter is to develop a new design procedure for HGSHP systems. The design of an HGSHP system involves specifying the system configuration (parallel or serial) and sizing the system components. Therefore, in this chapter, issue related to HGSHP system configuration will first be summarized. In this research, a parallel-connected system will be investigated. The control of distribution of flow to the GLHE and PHE/cooling tower will be then discussed. A new design procedure-GLHEPRO will be developed for sizing the HGSHP system components. The new design procedure is capable of being used for both a new HGSHP and a "retrofit" HGSHP system. A new algorithm in the design procedure will be presented to determine the right size of cooling tower. Finally, an example of designing an HGSHP system will be presented.

6.1 HGSHP System Configuration

The design of an HGSHP system has many degrees of freedom and there are many possible configurations of HGSHP systems. According to the layout of the supplemental heat rejecter and the ground loop heat exchanger, the system can be divided into two categories: 1) parallel-connected system, and 2) serially-connected system. In the parallel-connected HGSHP system, the ground loop heat exchanger and

PHE/cooling tower are placed in parallel. In the serially-connected HGSHP system, the ground loop heat exchanger and PHE/cooling tower are placed in series. More details were given in Section 2.2.1.

The parallel-connected system layout is suitable for an HGSHP system with large flow rate and a relatively small number of boreholes. In this case all system flow cannot feasibly pass through the GLHE without requiring excessive pumping power. A three-way valve is used to control the fluid flow through these two components. However, no recommendation for distribution of the flow between the GLHE and the PHE/cooling tower is given in the literature.

The serially-connected system layout is suitable for the system with a relatively small cooling tower and large number of boreholes. In this case, the entire system flow can pass through the boreholes and the pressure drop will still be acceptable.

Serial and parallel configurations are possible. However, preliminary testing has shown that there are a large number of scenarios where the serial connection is infeasible. For an HGSHP system with large flow rate and a relatively small number of boreholes, all the system flow cannot feasibly pass through the GLHE without requiring excessive pumping power. A possibility for the serially-connected layout is that the diverter valves are added into the system and help to control the flow rate though the GLHE and the PHE/cooling tower in order to avoid the excessive pressure drop through each component. However, no recommendation for the control of these diverters is given in the literature. When variable flow pumping is designed for the HGSHP system, control of

the diverter for each component becomes more difficult. Therefore, in this research, a parallel-connected HGSHP system will be investigated.

6.2 Flow Control

In a variable flow pumping system, the pump speed is controlled to maintain a constant pressure difference across the heat pumps. This results in the system flow being scaled to the peak flow rate according to the ratio of the current number of heat pumps in operation to the total number of heat pumps. Variable speed pumping systems typically have a lower limit of about 30% of full speed and this limit has been assumed here. When the system flow rate varies, the distribution of flow to the GLHE and PHE/cooling tower may also change, though how this should be controlled is not immediately apparent. Therefore, a strategy for controlling the distribution of flow to the GLHE and PHE/cooling tower is developed. The general guidelines for developing the flow distribution control strategy are as follows: a) the control strategy is physically possible; b) flow is able to pass through each component without requiring excessive pumping power; c) some flow always passes through the GLHE when the cooling tower is running to allow for the possibility of cooling down the ground. The following two section describe the control strategy as applied to the bypass valve and GLHE/PHE distribution valve.

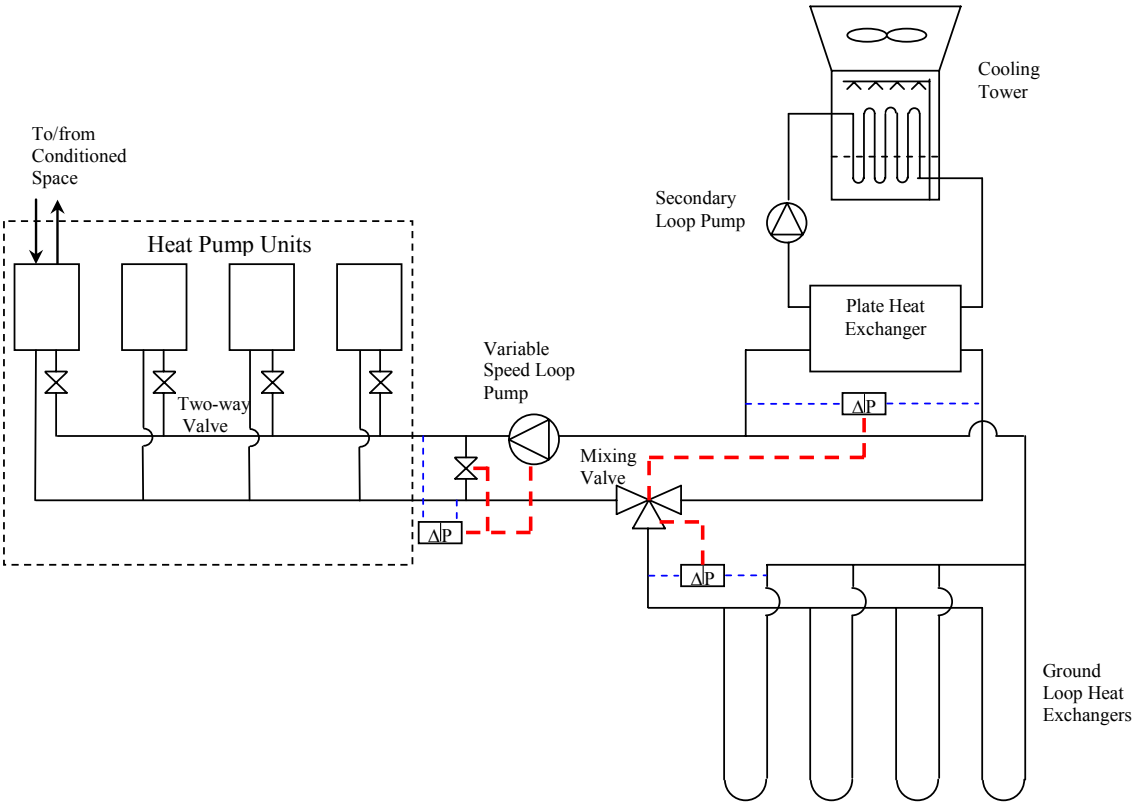

Figure 6.1 A schematic of a parallel-connected HGSHP system with flow distribution control.

6.2.1 Control of Two-way Valve for Bypass

In a variable flow pumping system, pump speed is adjusted to maintain a constant differential pressure across the heat pump unit loop supply and return headers. This insures adequate flow across the heat pump. When a heat pump is turned off, a two-way valve on the heat pump supply closes. As the number of closed valves increases, the pump's speed is reduced to maintain a constant differential pressure. In this case, a significant amount of energy can be saved by using a variable speed drive.

The variable speed drive pump has a lower limit of 30% of full flow rate. As the number of closed two-way valves increases, a total flow rate to the heat pumps may

become less than 30% of the system full flow rate. As a result, the differential pressure across the heat pump unit loop supply and return headers will be larger than a preset value (differential pressure at 30% of the system full flow rate) and a control signal will be sent to the two-way valve to turn on the bypass. This two-way valve control strategy ensures that the variable speed drive pump does not go below the limit of 30% of the system full flow rate.

6.2.2 Control of Three-way Valve for Flow Distribution

As shown in Figure 6.1, a three-way valve is used to control flow distribution between the GLHE and PHE/cooling tower. Two differential pressures are used to control this three-way valve: 1) differential pressure across the GLHE loop supply and return headers, ΔP_{GHE} ; and 2) differential pressure across the PHE loop supply and return headers, ΔP_{PHE} .

Based on the state of the cooling tower, the HGSHP system has two different flow distribution control strategies, which are illustrated in Figure 6.2 and Figure 6.3.

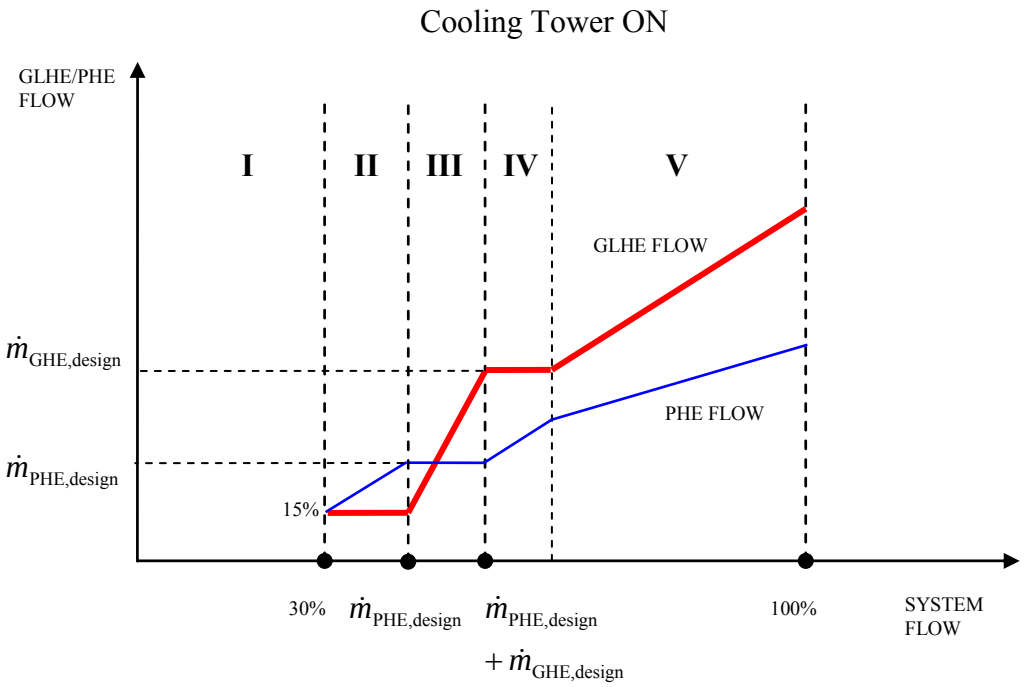

Figure 6.2 A schematic of flow distribution control strategy when cooling tower is on.

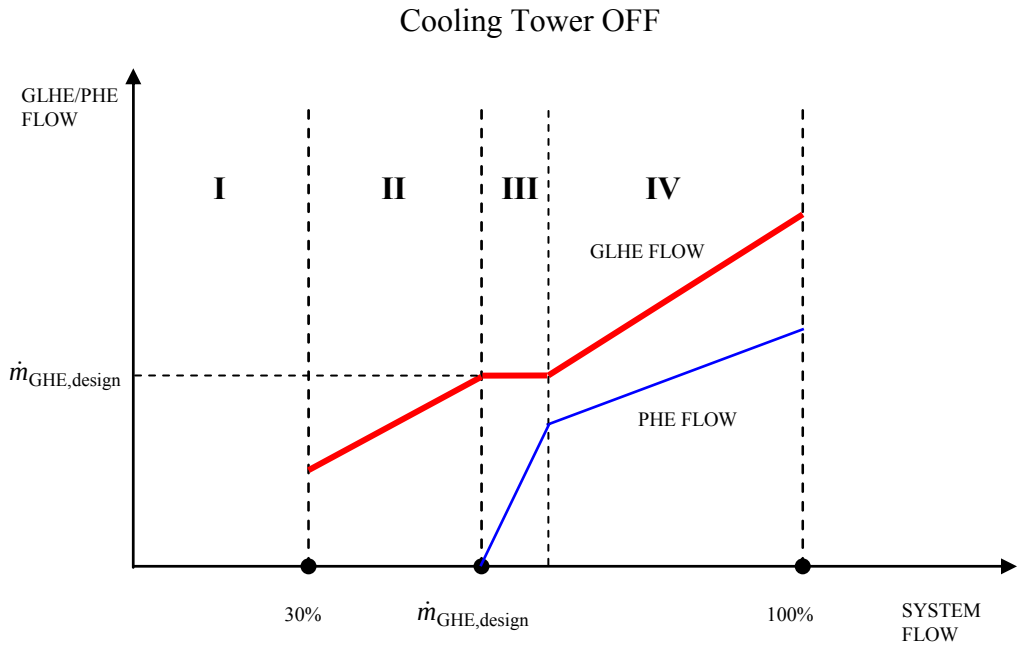

Figure 6.3 A schematic of flow distribution control strategy when cooling tower is off.

In the Figure 6.2 and Figure 6.3, $\dot{m}_{\text{GHE,design}}$ is the design mass flow rate through the ground loop heat exchanger, which is determined by assuming each borehole has a design flow rate (e.g. 3 gpm/per borehole). $\dot{m}_{\text{PHE,design}}$ is the design mass flow rate through the plate heat exchanger, which is the same as the flow rate of the cooling tower.

Cooling Tower ON

When the cooling tower is on, the control strategy of flow distribution is described as follows:

1. The HGSHP system has a lower limit of 30% of system full flow rate. When this low limit is reached and the cooling tower is on (Area I in Figure 6.2), 15% of the system full flow goes through the GLHE loop and 15% of the system full flow goes through the PHE/cooling tower loop. This setting ensures that some flow always passes through the GLHE when the cooling tower is running to allow for the possibility of cooling down the ground.

2. When the HGSHP system has a flow rate greater than $\dot{m}_{\text{PHE,design}} + \dot{m}_{\text{GHE,design}}$ (Area IV and V in Figure 6.2), the flow is distributed between the GLHE and PHE to ensure the system has a minimal pressure drop and only requires the least amount of circulation pumping power.

   The differential pressures across the two loops at their design flow rate are usually not the same. Therefore, in order to have the same differential pressure across the GLHE loop and the PHE loop, the flow rate of the loop with a

larger differential pressure (the GLHE loop in Figure 6.2) remains unchanged and the flow rate of the loop with a smaller differential pressure (the PHE loop in Figure 6.2) increases until it has a same differential pressure as the other loop. This process is illustrated as Area IV in Figure 6.2.

When the differential pressures across the two loops are the same and the system flow rate keeps increasing, the system flow is distributed between the two loops to ensure the two loops have a same differential pressure across the loop. This process is illustrated as Area V in Figure 6.2.

3. When the HGSHP system has a flow rate between the 30% lower limit of the system full flow rate and the design flow of $\dot{m}_{\text{PHE,designl}} + \dot{m}_{\text{GHE,design}}$ (Area II and III in Figure 6.2), the additional flow goes through the PHE loop prior to the GHE loop and the GLHE loop remains at 15% of the system full flow until the PHE loop has the design flow rate of $\dot{m}_{\text{PHE,designl}}$. This process is illustrated as Area II in Figure 6.2.

   As the system flow rate increases further, the PHE loop remains at the design flow rate of $\dot{m}_{\text{PHE,designl}}$ and the additional flow goes through the GLHE loop until the loop has the design flow rate of $\dot{m}_{\text{GHE,design}}$. This process is illustrated as Area III in Figure 6.2.

   This setting ensures that when the cooling tower is on, some flow always passes through the plate heat exchanger.

Cooling Tower OFF

When the cooling tower is off, the control strategy of flow distribution is described as follows:

1. When the HGSHP system has a lower limit of 30% of the system full flow rate (Area I in Figure 6.3), all 30% of the system full flow goes to the GLHE loop and no flow goes through the PHE/cooling tower loop.

2. When the HGSHP system has a flow rate greater than $\dot{m}_{\text{GHE,design}}$ (Area III and IV in Figure 6.3), the flow is distributed between the GLHE and PHE to ensure the system has a minimal pressure drop and has a minimal circulation pumping power.

   As described previously, the differential pressures across the two loops are not usually the same with their design flow rates. Therefore, in order to have the same differential pressure across the GLHE loop and the PHE loop, the same control strategy described previously is applied to distribute the flow between the GLHE loop and PHE loop. The flow rate of the GLHE loop with the larger differential pressure remains unchanged and the flow rate of the PHE loop with a smaller differential pressure increases until the PHE loop has a same differential pressure as the GLHE loop. This process is illustrated as Area III in Figure 6.3.

   When the differential pressures across the two loops are equal and the system flow rate keeps increasing, the system flow is distributed between the two

loops to ensure the two loops have a similar differential pressure across the loop. This process is illustrated as Area IV in Figure 6.3.

3. When the HGSHP system has a flow rate between the lower limit of 30% of the system full flow rate and the design flow of $\dot{m}_{\mathrm{GHE,design}}$ (Area II in Figure 6.3), all the flow goes through the GLHE loop and no flow goes through the PHE/cooling tower loop.

To implement the control strategy described above, the differential pressure across the GLHE loop, ΔP_{GHE}, and the differential pressure across the PHE loop, ΔP_{PHE}, are used to control the three-way valve to distribute flow to these two components.

$\Delta P_{GHE,dsn}$ is the differential pressure across the GLHE loop supply and return headers when the GLHE loop has a design mass flow rate $\dot{m}_{\mathrm{GHE,design}}$. $\Delta P_{PHE,dsn}$ is the differential pressure across the PHE loop supply and return headers when the PHE loop has a design mass flow rate $\dot{m}_{\mathrm{PHE,designl}}$. $\Delta P_{GHE,15\%}$ is the differential pressure across the GLHE loop supply and return headers when the GLHE loop has 15% of the system full flow rate. $\Delta P_{PHE,15\%}$ is the differential pressure across the GLHE loop supply and return headers when the GLHE loop has a 15% of the system full flow rate.

The pressure drop through the GLHE loop, ΔP_{GHE}, and the PHE loop ΔP_{PHE} is measured and used to control the three-way valve that splits the flow through these two components. When the system flow is determined, the three-way valve can always reach a steady-state position and realize the flow control strategy above. All possible control

states are listed in Table 6.1 and Table 6.2, which are for cooling tower on and off, respectively.

Table 6.1 Control process of three-way valve when cooling tower is on (assuming that $\Delta P_{GHE,dsn} > \Delta P_{PHE,dsn} > \Delta P_{PHE,15\%}$)

	$\Delta P_{PHE} < \Delta P_{PHE,15\%}$	$\Delta P_{PHE} = \Delta P_{PHE,15\%}$	$\Delta P_{PHE,15\%} < \Delta P_{PHE} < \Delta P_{PHE,dsn}$	$\Delta P_{PHE} = \Delta P_{PHE,dsn}$	$\Delta P_{PHE,dsn} < \Delta P_{PHE} < \Delta P_{GHE,dsn}$	$\Delta P_{PHE} = \Delta P_{GHE,dsn}$	$\Delta P_{PHE} > \Delta P_{GHE,dsn}$
State			(A)	(B)	(C)	(D)	(E)
$\Delta P_{GHE} < \Delta P_{GHE,15\%}$	--	--	**Adjust Valve to:** ↓ ΔP_{PHE}; ↑ ΔP_{GHE} **Aim:** State (F) or (G)	**Adjust Valve to:** ↓ ΔP_{PHE}; ↑ ΔP_{GHE} **Aim:** State (F) or (G)	**Adjust Valve to:** ↓ ΔP_{PHE}; ↑ ΔP_{GHE} **Aim:** State (F), (G), (H), (O), or (W)	**Adjust Valve to:** ↓ ΔP_{PHE}; ↑ ΔP_{GHE} **Aim:** State (F), (G), (H) (O), (V), or (W)	**Adjust Valve to:** ↓ ΔP_{PHE}; ↑ ΔP_{GHE} **Aim:** State (F), (G), (H), (O), (V), (W), (Z) or (AF)
State		(F)	(G)	**(H)**	(I)	(J)	(K)
$\Delta P_{GHE} = \Delta P_{GHE,15\%}$	--	Steady-state Remain the valve position	Steady-state Remain the valve position	Steady-state Remain the valve position	**Adjust Valve to:** ↓ ΔP_{PHE}; ↑ ΔP_{GHE} **Aim:** State (O), (V), or (W)	**Adjust Valve to:** ↓ ΔP_{PHE}; ↑ ΔP_{GHE} **Aim:** State (O), (V), or (W)	**Adjust Valve to:** ↓ ΔP_{PHE}; ↑ ΔP_{GHE} **Aim:** State (O), (V), (W), (Z) or (AF)
State	(L)	(M)	(N)	**(O)**	(P)	(Q)	(R)
$\Delta P_{GHE,15\%} < \Delta P_{GHE} < \Delta P_{GHE,dsn}$	**Adjust Valve to:** ↑ ΔP_{PHE}; ↓ ΔP_{GHE} **Aim:** State (F), (G), (H), or (O)	**Adjust Valve to:** ↑ ΔP_{PHE}; ↓ ΔP_{GHE} **Aim:** State (G), (H), or (O)	**Adjust Valve to:** ↑ ΔP_{PHE}; ↓ ΔP_{GHE} **Aim:** State (G), (H), or (O)	Steady-state Remain the valve position	**Adjust Valve to:** ↓ ΔP_{PHE}; ↑ ΔP_{GHE} **Aim:** State (O), (V), or (W)	**Adjust Valve to:** ↓ ΔP_{PHE}; ↑ΔP_{GHE} **Aim:** State (O), (V), or (W)	**Adjust Valve to:** ↓ ΔP_{PHE}; ↑ ΔP_{GHE} **Aim:** State (O), (V), (W), (Z) or (AF)
State	(S)	(T)	(U)	**(V)**	**(W)**	**(Z)**	(Y)
$\Delta P_{GHE} = \Delta P_{GHE,dsn}$	**Adjust Valve to:** ↑ ΔP_{PHE}; ↓ ΔP_{GHE} **Aim:** State (F), (G), (H), or (O)	**Adjust Valve to:** ↑ ΔP_{PHE}; ↓ ΔP_{GHE} **Aim:** State (G), (H), or (O)	**Adjust Valve to:** ↑ ΔP_{PHE}; ↓ ΔP_{GHE} **Aim:** State (G), (H), or (O)	Steady-state Remain the Valve Position	Steady-state Remain the Valve Position	Steady-state Remain the Valve Position	**Adjust Valve to:** ↓ ΔP_{PHE}; ↑ ΔP_{GHE} **Aim:** State (W), (Z) or (AF)
State	(Z)	(AA)	(AB)	(AC)	(AD)	(AE)	**(AF)**
$\Delta P_{GHE} > \Delta P_{GHE,dsn}$	**Adjust Valve to:** ↑ ΔP_{PHE}; ↓ ΔP_{GHE} **Aim:** State (F), (G), (H), (O), (V), (W), (Z) or (AF)	**Adjust Valve to:** ↑ ΔP_{PHE}; ↓ ΔP_{GHE} **Aim:** State (G), (H), (O), (V), (W), (Z) or (AF)	**Adjust Valve to:** ↑ ΔP_{PHE}; ↓ ΔP_{GHE} **Aim:** State (G), (H), (O), (V), (W), (Z) or (AF)	**Adjust Valve to:** ↑ ΔP_{PHE}; ↓ ΔP_{GHE} **Aim:** State (O), (V), (W), (Z) or (AF)	**Adjust Valve to:** ↑ ΔP_{PHE}; ↓ ΔP_{GHE} **Aim:** State (W), (Z) or (AF)	**Adjust Valve to:** ↑ ΔP_{PHE}; ↓ ΔP_{GHE} **Aim:** State (AF)	If($\Delta P_{PHE} = \Delta P_{GHE}$) Steady-state Elseif($\Delta P_{PHE} < \Delta P_{GHE}$) Adjust Valve to: ↑ ΔP_{PHE}; ↓ ΔP_{GHE} Till: $\Delta P_{PHE} = \Delta P_{GHE}$ Elseif($\Delta P_{PHE} > \Delta P_{GHE}$) Adjust Valve to: ↓ ΔP_{PHE}; ↑ ΔP_{GHE} Till: $\Delta P_{PHE} = \Delta P_{GHE}$ Endif

Table 6.2 Control process of three-way valve when cooling tower is off (assume that $\Delta P_{GHE,dsn} > \Delta P_{PHE,nor}$)

	$\Delta P_{PHE} = 0$	$\Delta P_{PHE} \leq \Delta P_{GHE,dsn}$	$\Delta P_{PHE} > \Delta P_{GHE,dsn}$
State	**(A)**	(B)	(C)
$\Delta P_{GHE} \leq \Delta P_{GHE,dsn}$	Steady-state Remain the Valve Position	**Adjust Valve to:** $\downarrow \Delta P_{PHE}$; $\uparrow \Delta P_{GHE}$ **Aim:** State (A), (D) or (E)	**Adjust Valve to:** $\downarrow \Delta P_{PHE}$; $\uparrow \Delta P_{GHE}$ **Aim:** State (A), (D), (E) or (I)
State	**(D)**	**(E)**	(F)
$\Delta P_{GHE} = \Delta P_{GHE,dsn}$	Steady-state Remain the Valve Position	Steady-state Remain the Valve Position	**Adjust Valve to:** $\downarrow \Delta P_{PHE}$; $\uparrow \Delta P_{GHE}$ **Aim:** State (I)
State	(G)	(H)	**(I)**

$\Delta P_{GHE} > \Delta P_{GHE,dsn}$	**Adjust Valve to:**
	$\uparrow \Delta P_{PHE}$; $\downarrow \Delta P_{GHE}$
	Aim:
	State (E) or (I)
		Adjust Valve to:
		$\uparrow \Delta P_{PHE}$; $\downarrow \Delta P_{GHE}$
		Aim:
		State (E) or (I)
			If($\Delta P_{PHE} = \Delta P_{GHE}$)
			Steady-state
			ElseIf($\Delta P_{PHE} < \Delta P_{GHE}$)
			Adjust Valve to: $\uparrow \Delta P_{PHE}$; $\downarrow \Delta P_{GHE}$
			Till: $\Delta P_{PHE} = \Delta P_{GHE}$
			ElseIf($\Delta P_{PHE} > \Delta P_{GHE}$)
			Adjust Valve to: $\downarrow \Delta P_{PHE}$; $\uparrow \Delta P_{GHE}$
			Till: $\Delta P_{PHE} = \Delta P_{GHE}$
			EndIf

As shown in Table 6.1, when the cooling tower is on, the three-way valve has a total of thirty-two states according to the different values of ΔP_{GHE} and ΔP_{PHE}. However, following the instructions in Table 6.1, the three-way valve position is adjusted and it is always able to reach one of the eight steady states (State F, G, H, O, V, W, Z, or AF), which is the gray cell in Table 6.1.

For an example, when $\Delta P_{PHE} < \Delta P_{PHE,15\%}$ and $\Delta P_{GHE} < \Delta P_{GHE,15\%}$, the state of the three-way valve is State A. In this case, the flow rate of the GLHE is less than 15% of the system full flow rate and the flow rate of the PHE is greater than 15% of the system full flow rate but less than the nominal flow rate of the PHE, $\dot{m}_{PHE,design}$. From Figure 6.2, the mass flow rate of the PHE falls in Area II and the mass flow rate of the GLHE falls into Area I. Therefore, the three-way valve is adjusted to increase the mass flow rate of the GLHE and accordingly the mass flow rate of the PHE decreases. As a result, the three-way valve position could be at the state (F), where the $\Delta P_{GHE} = \Delta P_{GHE,15\%}$ and $\Delta P_{PHE} = \Delta P_{PHE,15\%}$. Or three-way valve position could be at the state (G), where the $\Delta P_{GHE} = \Delta P_{GHE,15\%}$ and $\Delta P_{PHE,15\%} < \Delta P_{PHE} < \Delta P_{PHE,nor}$. These two states are both possible and steady.

Also as shown in Table 6.2, when the cooling tower is off, the three-way valve has a total of nine states according to the different values of ΔP_{GHE} and ΔP_{PHE}. Following the instructions in Table 6.2, the three-way valve position is adjusted and it is always able to reach one of the three steady states (State D, E, or I), which is the gray cell in Table 6.2.

In summary, this section developed a strategy for controlling the distribution of flow to GLHE and PHE/cooling tower in the parallel-connected HGSHP system. The control strategy is based on the two differential pressures of the GLHE and PHE loops and is physically feasible. By carefully controlling the flow through each component, the HGSHP system has a minimal pressure drop and therefore requires a minimum circulation pumping power. While the application of this control strategy, some flow always passes through the GLHE when the cooling tower is running to allow for the possibility of cooling down the ground.

6.3 HGSHP System Design Procedure

In this section, a new design procedure implemented in GLHEPRO is developed for sizing the HGSHP system components. GLHEPRO (Spitler 2006) is a tool for designing ground loop heat exchangers for use with ground source heat pump systems. The new version of GLHEPRO allows the sizing a new HGSHP system and a "retrofit design". Before the design procedure for the HGSHP system is introduced, a discussion of heating/cooling dominated systems and heating/cooling constrained system is presented first.

6.3.1 Heating/Cooling Dominated Systems vs. Heating/Cooling Constrained Systems

Usually, when a GSHP system is referred to as a cooling dominated system, it means that the ground loop heat exchanger of the GSHP system will reject more heat to the ground than it extracts on an annual basis. As a result, the ground temperature

surrounding the heat exchanger will rise over the system operation period. When a GSHP system is referred to as a heating dominated system, it means that the ground loop heat exchangers of the GSHP system extract more heat from the ground than it rejects on an annual basis. As a result, the ground temperature surrounding the heat exchanger will fall over the system operation period. However, a cooling dominated system does not necessarily mean that the required borehole length for cooling is greater than the required length for heating. The required borehole length for cooling/heating not only depends on the system heat rejection/extraction demand, but also on the potential ability of the ground loop heat exchanger for heat rejection/extraction. The latter is determined by the allowed heat pump entering fluid temperature (EFT) and by the undisturbed ground temperature. It is entirely possible that, due to a small difference between the temperature limits on the heat pump and the ground temperature, a GSHP system design may be constrained by one mode of operation (heating or cooling), while the "dominant" mode is the opposite. For this reason, two new terms are introduced: "heating constrained" and "cooling constrained"; these terms describe systems whose designs are driven by the system heat extraction or rejection, respectively.

For instance, for one model of commercial heat pump, the allowed minimum EFT is -6.7ºC (20ºF) and the allowed maximum heat pump EFT is 43.3ºC (110ºF). When pure water is used as the working fluid, to prevent the fluid from freezing, the allowed minimum heat pump EFT is set to 6ºC (42.8ºF). These two temperature limits are used to size the borehole to ensure that the GLHE exiting fluid temperature will not exceed either of them. The undisturbed ground temperature is about 15ºC (59ºF) in Tulsa, OK and is about 10ºC (50ºF) in Chicago, IL. So, the allowed temperature difference is 28.3ºC for

GLHE heat rejection and 9ºC for GLHE heat extraction in Tulsa, while the allowed temperature difference is 33.3ºC for GLHE heat rejection and 4ºC for GLHE heat extraction in Chicago. These temperature differences drive the sizing of the GLHE. In other words, although a system (like the building in Chicago) may have more demand for heat rejection than heat extraction, it is not necessarily true that the required borehole length for cooling will be larger than that for heating. In Figure 6.4, the heat pump EFTs of two different GSHP systems are shown, one in Tulsa, and another in Chicago, but otherwise identical. Both GSHP systems have more cooling demand than heating demand, and the heat pump EFTs rise over the system operation period. In the Tulsa case, the maximum heat pump EFT is 43.3ºC (110ºF) in the 236th month and the minimum heat pump EFT is 10.6ºC (51.1ºF) in the 1st month. In the Chicago case, the maximum heat pump EFT is 22.8ºC (73ºF) in 235th month and the minimum heat pump EFT is 6ºC (42.8ºF) in the 1st month. Thus, even though both systems are cooling dominated, the small difference between the heat pump minimum allowed fluid temperature and the undisturbed ground temperature in Chicago causes this system to be sized based on heating. The Chicago system is heating constrained, while the Tulsa system is cooling constrained. However, in the Chicago, if a 20% propylene glycol/water solution is used as the working fluid, the freezing point of the fluid is -8.1ºC (17.4ºF). When sizing the borehole length, the lower temperature limit of heat pump EFT can now be set as -4.1ºC (24.6ºF). Therefore, the allowed temperature difference is 33.3ºC for GLHE heat rejection and 14.1ºC for GLHE heat extraction. As a result, the maximum heat pump EFT is 43.3ºC (110ºF) in the 235th month and the minimum heat pump EFT is -3ºC (27.2ºF) in the 1st month. By adding antifreeze to the working fluid and thereby lowering the

lower temperature limit on the heat pump, the heating constrained system can be transformed into a cooling constrained system.

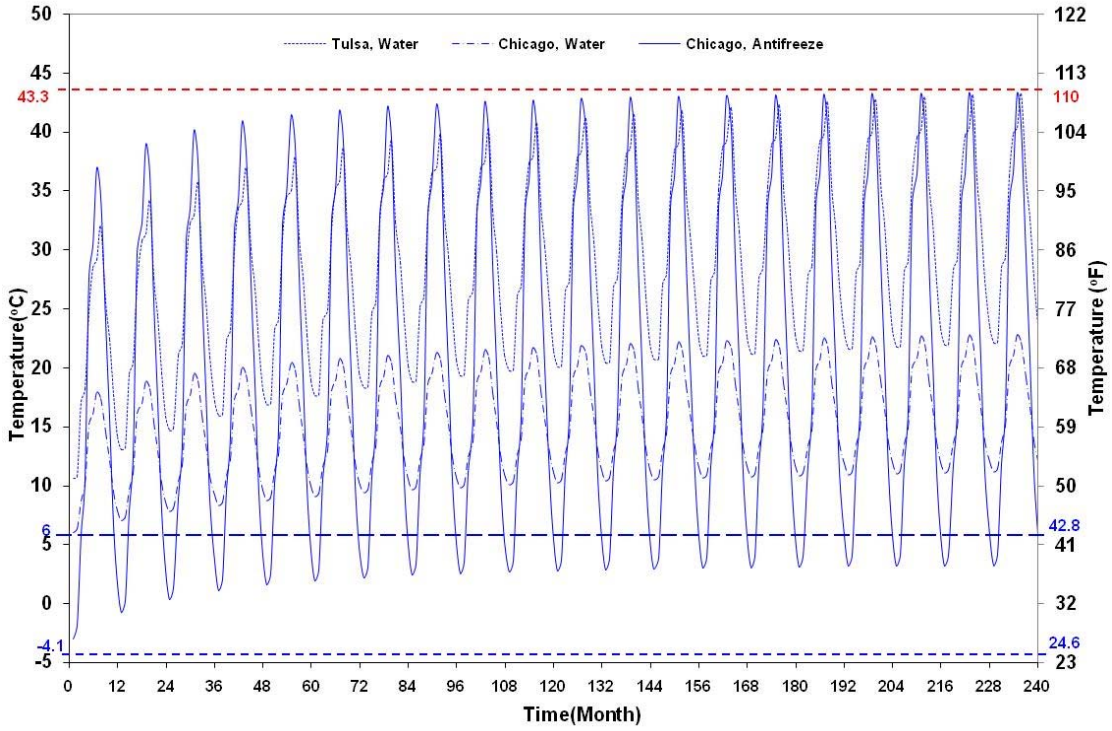

Figure 6.4 Heat pump entering fluid temperatures for different system designs

In this research, the study mainly focus on the the HGSHP system for the cooling constrained system is and the HGSHP system design and control strategy for the cooling constrained system are investigated.

6.3.2 Design GLHE for GSHP Systems

Before the design procedure for the HGSHP system is presented, the methodology of GLHEPRO for designing ground loop heat exchangers for use with GSHP systems is introduced here first. GLHEPRO (Spitler 2000) is a tool originally developed for

designing ground loop heat exchangers for use with ground source heat pump systems. The methodology of GLHEPRO to size GLHE of GSHP systems is summarized below. More details are given by Spitler (2000).

1. Input all the necessary data, including:

    - Monthly heating and cooling loads on the heat pump or heat pumps;
    - Monthly peak heating and cooling loads on the heat pump or heat pumps;
    - Information about the heat pump or heat pumps, from which the relationship between the entering fluid temperature to the heat pump and the heat rejected to the ground for a given cooling load and the heat extracted from the ground for a given heating load can be determined;
    - Thermal properties of the ground;
    - Geometric configuration of the ground loop heat exchanger;
    - Borehole diameters, U-tube diameter, grout thermal properties.

2. Calculate the borehole thermal resistance and then g-functions of the borehole are automatically updated.

3. Specify the minimum and maximum entering fluid temperature of the heat pump and length of the design period.

The minimum and maximum entering fluid temperature of heat pump are very important to the outcome of the design. Either the minimum or maximum entering fluid temperature will control the borehole depth, while also affecting the overall energy consumption. For cooling dominated buildings, the annual heat rejection exceeds the annual heat extraction. When this occurs, the entering fluid temperature rises from year to year. Therefore, a maximum entering fluid temperature (EFT) into the heat pump is used to control the borehole depth. The a minimum heat pump EFT controls the borehole depth for heating dominated buildings.

For example, using the ClimateMaster Genesis Heat Pump, a maximum EFT of 43.33 ºC (110 ºF) is allowed. The minimum EFT is selected based on the freezing point of the working fluid. If water is used a margin of safety might be incorporated by choosing a minimum EFT of 6 ºC (42.8 ºF).

4. Run GLHE sizing function and output the design results.

   The sizing function iteratively adjusts the borehole depth, for each iteration, recomputing the STS g-functions, and running the simulation until the borehole depth that satisfied the temperature constraints is found.

   After the program gets the desired borehole length, a summary of GSHP system design is presented. Additional results are provided in an output file.

Usually, the annual heat rejection and the annual heat extraction of the GLHE are not balanced. Depending on the imbalance, the heat pump entering fluid temperatures of

rise or drop over the system operation period. When the heat pump entering fluid temperature just reaches the user-specified maximum or minimum entering fluid temperature, while not exceeding the other limit, the size of the ground loop heat exchanger is the right size for the GSHP system.

6.3.3 Design New HGSHP Systems

In HGSHP systems, a supplemental heat source or sink into the system is added into the system to handle some portion of the system loads, therefore reducing the size of the GLHE and the first cost of the system. In this section, a new design procedure is implemented in GLHEPRO for sizing the HGSHP system components.

Kavanaugh and Rafferty (1997) gave a design procedure for sizing the GLHE and supplemental heat source or sink and later Kavanaugh (1998) revised the design procedure. Firstly, Kavanaugh and Rafferty developed a procedure to calculate the required borehole lengths for cooling and heating respectively. In this procedure, the annual equivalent heating and cooling hours are required for the calculation of the GLHE system heat extraction/rejection rate, which is done with a spreadsheet procedure. The effects of annual, monthly, daily, and peak (four hour block load) heat pulses are used to compute the required borehole length for both heating and cooling. Secondly, the size of supplemental heat source or sink is sized from the difference of the two required borehole lengths. For a cooling constrained building, by assuming that the fluid has a 10ºF temperature change through the heat pump condenser and cooling tower, the capacity of the cooler is specified in terms of the fluid flow rate, shown in Equation 2-14. For further information on this procedure, see Section 2.2.2.2.

One possibility for specifying the design of a HGSHP system is to describe it on the basis of the GSHP system that could be designed to account for the entirety of the system heating and cooling loads; this is shown in Figure 6.5. Point 1 in this figure represents the base GSHP system, with no supplemental heating or cooling. As supplemental heating or cooling is added to the system, the design moves to the left or right on the figure, respectively. Additionally, since the system now has a higher capacity for heating or cooling, a smaller borehole length can be used—a downward movement on the figure. The other points on the figure represent both a heating (point 2') and cooling (point 2) HGSHP system design; the task is to find just how far to move within this domain to find the optimum system design.

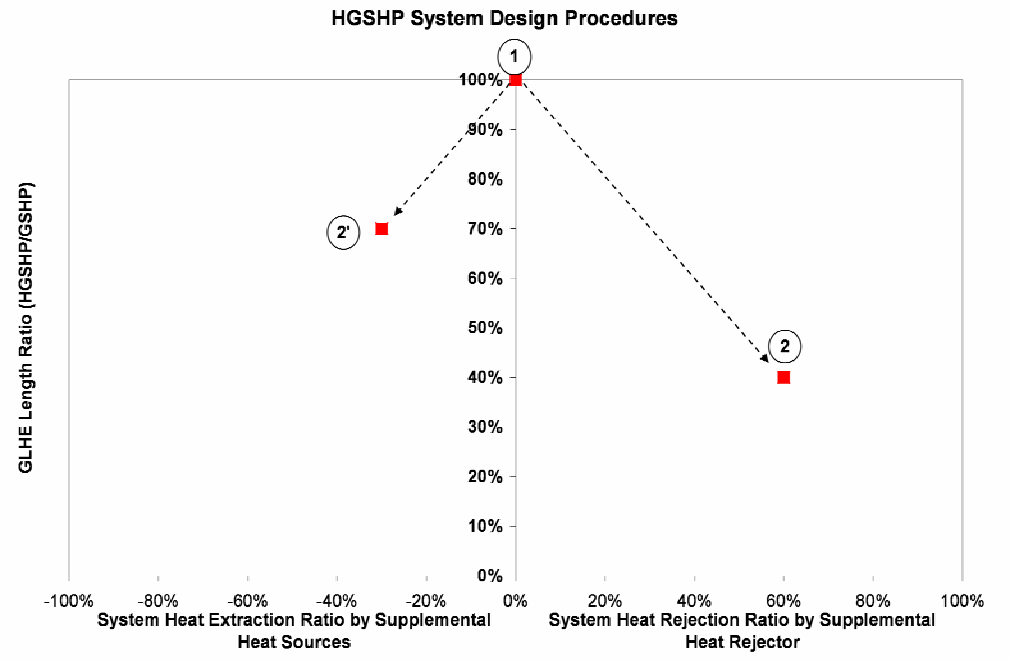

Figure 6.5 Conceptual diagram of HGSHP system design procedure

Following the idea above, a temperature limit-optimized simulation-based design method is developed to size the borehole length and supplemental sink or source

simultaneously. For a standard GSHP system without a supplemental heat source or sink, the GLHE of the system is sized to ensure than heat pump EFT will not exceed either the lower or the upper temperature limit. The size of the GLHE will be such that the heat pump EFT will just meet either the maximum or the minimum temperature limit, in which cases the system is said to be cooling constrained or heating constrained, respectively. The heat pump EFTs of a cooling constrained and heating constrained GSHP system are shown in Figure 6.6. The basic idea of this HGSHP system design method comes from the fact that for a cooling/heating constrained GSHP system, a supplemental heat sink or source can be added into the system to decrease the borehole length. In a cooling constrained GSHP system, an upper temperature limit is used to control the borehole length. If some portion of the cooling loads is removed by the supplemental cooler, the borehole length can be reduced until the heat pump EFT meets the lower temperature limit in addition to the upper temperature limit. In that case, the borehole length can not be reduced any further since the GLHE could no longer meet the system heating demand. The same principles can be applied to a heating constrained GSHP system. In a heating constrained GSHP system, the lower temperature limit is used to control the borehole length. If some portion of the heating loads is met by a supplemental heat source, the borehole length can be reduced until the heat pump EFT also meets the upper temperature limit. In that case, the borehole length can not be reduced any further since the GLHE could no longer meet the system cooling demand. The desired outcome of this method—meeting both temperature limits simultaneously—is shown as the HGSHP system data plotted in Figure 6.6; the detailed design procedure is described below.

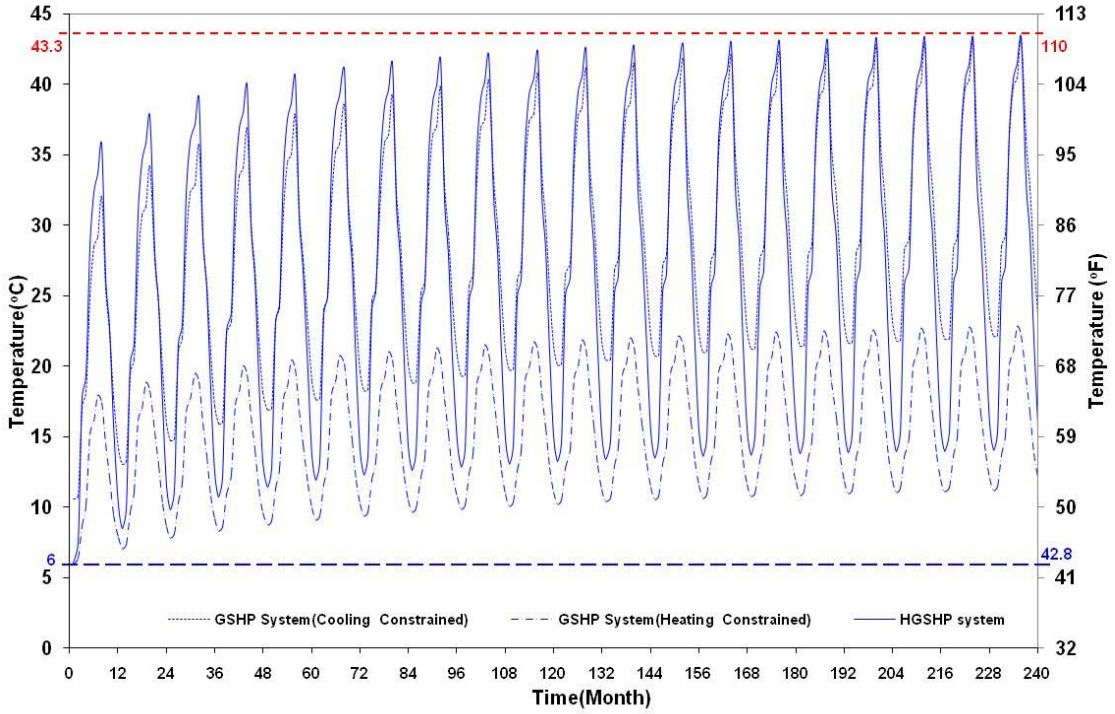

Figure 6.6 Heat pump EFTs of an HGSHP system at the different design stages

1. Calculate the borehole length of a GSHP system. For this procedure, two new factors, $Ratio_{Loads}$ and $Ratio_{Length}$, are introduced. The definitions of the two factors are given by Equations 1 and 2. $Ratio_{Loads}$ is introduced to adjust the monthly cooling or heating loads so that some portion of the loads is assumed to be handled by the supplemental device. The value of $Ratio_{Loads}$ is between -1 and 1; a negative value means the GSHP system is heating advanced, while a positive value indicates that the system is cooling advanced. $Ratio_{Length}$ is adjusted to get the borehole length of the HGSHP system so that, with the adjusted borehole length and loads, the calculated heat pump maximum EFT will equal the upper temperature limit and the heat pump minimum EFT will

equal the lower temperature limit. The value of $Ratio_{Length}$ is between 0 and 1, with a value of 1 indicating that the length is the same as for the GSHP system. The Nelder-Mead simplex method (Nelder and Mead 1965) is used to search for the value of $Ratio_{Length}$ and $Ratio_{Loads}$ that minimizes the objective function developed for the HGSHP simulation. The objective function is the sum of the squares of the error (SSQE) of the calculated heat pump minimum and maximum temperature compared to the heat pump temperature limits, as shown in Equation 3. After the optimization, the borehole length is, then, the minimum required borehole length for the HGSHP system. The adjusted loads are the loads which will be removed by the GLHE of the HGSHP system.

$$Ratio_{length} = \frac{GLHE \quad Length \quad of \quad HGSHP \quad System}{GLHE \quad Length \quad of \quad GSHP \quad System} \tag{6-1}$$

$$Ratio_{loads} = \frac{Cooling\ /\ Heating\ Loads\ met\ by\ supplemental\ device(s)}{Total \quad Cooling\ /\ Heating \quad Loads \quad of \quad System} \tag{6-2}$$

$$SSQE = (MaxEFT_{cal} - MaxEFT_{set})^2 + (MinEFT_{cal} - MinEFT_{set})^2 \tag{6-3}$$

2. Calculate the capacity of the supplemental heat sink/source component. Once the GLHE length of the HGSHP system and the loads met by the GLHE are determined, the peak heat rejection and peak heat extraction of the GLHE can be calculated. In this way, the capacity of the supplemental heat rejection or extraction component can be obtained.

$$\dot{Q}(Supplemental)_{rejection} = \dot{Q}(GLHE)_{peak,rejection,GSHP} - \dot{Q}(GLHE)_{peak,rejection,HGSHP} \tag{6-4}$$

$$\dot{Q}(Supplemental)_{extraction} = \dot{Q}(GLHE)_{peak,extraction,GSHP} - \dot{Q}(GLHE)_{peak,extraction,HGSHP} \tag{6-5}$$

Where:

$\dot{Q}(Supplemental)_{rejection}$: the capacity of the supplemental heat rejecter, (kW);

$\dot{Q}(GLHE)_{peak,rejection,GSHP}$: the peak heat rejection of the GLHE in a GSHP system, (kW);

$\dot{Q}(GLHE)_{peak,rejection,HGSHP}$: the peak heat rejection of the GLHE in an HGSHP system, (kW).

$\dot{Q}(Supplemental)_{extraction}$: the capacity of the supplemental heat source, (kW);

$\dot{Q}(GLHE)_{peak,extraction,GSHP}$: the peak heat extraction of the GLHE in a GSHP system, (kW);

$\dot{Q}(GLHE)_{peak,extraction,HGSHP}$: the peak heat extraction of the GLHE in an HGSHP system, (kW).s

3. Calculate the nominal size cooling tower at the nominal design conditions.

   Once the capacity of the cooling tower of the HGSHP system is obtained by the program, following the procedure described by Kavanaugh (1998), the size of the cooling tower can be specified in terms of the nominal water flow rate, which is determined from the cooling tower capacity as the flow rate of water cooled from 35ºC (95ºF) to 29.4ºC (85ºF) with a 25.6ºC (78ºF) wet bulb temperature.

   However, this procedure described by Kavanaugh (1998) will tend to oversize the cooling tower/fluid cooler. A new algorithm to size cooling tower is based on the local peak wetbulb temperature and the peak ExFT of heat pump. It will be discussed in Section 6.3.5.

6.3.4 Procedure of GLHEPRO for Designing "Retrofit" HGSHP Systems

The procedures described in Section 6.3.3 size the GLHE and cooling tower simultaneously and they are intended for design of a new HGSHP system. In some existing GSHP systems, an improperly-sized GLHE can not meet the cooling/heating loads of the system. In this case, a supplemental heat source or sink is added into the system to help meet loads of the system. This might be referred to as a "retrofit design". The design procedure for a "retrofit" HGSHP system is presented in this section.

For a cooling dominated building, the GLHE size, L_{given}, is given, then the capacity of the cooling tower is calculated by being scale to the maximum capacity of cooling tower of a new HGSHP system:

$$Q_{CT} = Q_{CT,\max} \frac{L_{\max} - L_{given}}{L_{\max} - L_{\min}} \tag{6-6}$$

Where:

$L_{\max}$ = The maximum required GLHE length, obtained from a GSHP system, (m);

$L_{\min}$ = The shortest desired GLHE length, obtained for a new HGSHP system, (m);

$Q_{CT,\max}$ = The maximum capacity of the cooling tower, for a new HGSHP system, (W).

The procedure for sizing the cooling tower for a "retrofit" HGSHP system is described as follows.

1. Run GLHE sizing function for GSHP system to determine the GLHE size, $L_{\max}$. The GLHE sizing procedures are previously described in Section 6.3.2.

2. Run GLHE sizing function for a HGSHP system to get the shortest length of GLHE, $L_{\min}$. Also the capacity of cooling tower, $Q_{CT,\max}$, is available. The procedures are previously described in Section 6.3.3.

3. Calculate the capacity of the cooling tower desired for the "retrofit" HGSHP system. The capacity of the cooling tower is calculated by Equation 6.8.

6.3.5 Sizing Cooling Tower

The new version of GLHEPRO gives the required size of the cooling tower for a HGSHP system in terms of heat rejection capacity. It also specifies the cooling tower size in terms of the nominal water flow rate (Kavanaugh 1998), which is determined from the cooling tower capacity as the flow rate of water cooled from 35ºC (95ºF) to 29.4ºC (85ºF) with a 25.6ºC (78ºF) wet bulb temperature.

In an actual HGSHP system, the peak inlet water temperature of cooling tower might be higher than 35ºC (95ºF) (perhaps as high as 43.3ºC (110ºF)) and the local wet bulb temperatures may often be lower than 25.6ºC (78ºF). As a result, the cooling tower design procedure described by Kavanaugh (1998) will tend to oversize the cooling tower/fluid cooler. Therefore a new algorithm is developed here more accurately to determine the required size of cooling tower.

A possible algorithm for sizing cooling tower is based on the local peak wetbulb temperature and the peak ExFT of heat pump. Assuming peak heat pump ExFT (on the order of 100ºF - 115ºF) coincident with local peak wetbulb temperature, the practical cooling capacity of cooling tower for the HGSHP system can be calculated, which will be greater than the cooling capacity of cooling tower at the nominal design conditions. Then looking at the cooling tower manufacturer's catalog data, a smaller size of cooling tower will be chosen for the HGSHP system. The detailed procedure is as follows:

1. Select the local outdoor peak wetbulb temperature.

   There are several possibilities to determine the local peak wetbulb temperature. The website of the U.S. Department of Energy (DOE 2007) provides the Typical Meteorological Year (TMY) weather data of more than 250 cities in North American. The local outdoor peak wetbulb temperature can be calculated. Also the local outdoor peak wetbulb temperature can be obtained from ASHRAE Standard weather data (ASHRAE 2005). In this research, the local outdoor peak wetbulb temperature is calculated from the Typical Meteorological Year (TMY) weather data.

2. Select the peak inlet fluid temperature of cooling tower.

   At this point, the peak heat pump ExFT is selected as the peak inlet fluid temperature of the cooling tower. Knowing the heat pump rejection rate and the fluid flow rate, the peak heat pump ExFT can be determined from user-specified maximum heat pump EFT. Some heat pump manufacturers give an

allowable ExFT of heat pump as 110ºF - 120ºF. In this research, a temperature of 115ºF is selected as the peak inlet fluid temperature of cooling tower.

3. Choose a cooling tower from a database of cooling towers to meet the required capacity of the cooling tower. Although cooling tower capacities can be represented in more than one way, it is convenient to use the fixed-UA model in Section 4.3.1.1 to determine UA values for a range of cooling tower and place than in a database, as shown in Table 6.3.

Table 6.3 User-precalculated database of cooling towers from the manufacturer (ArctiChill)

CT Nominal Capacity kW(tons)	$\dot{m}_{water}$ kg/s(GPM)	$\dot{m}_{air}$ kg/s(CFM)	UA W/K(Btu/h-ºF)	Fan Power kW(HP)
10.6(3)	0.38(6)	0.49(870)	420(222)	0.124(1/6)
17.6(5)	0.63(10)	1.19(2,100)	648(342)	0.124(1/6)
28.1(8)	1.01(16)	1.48(2,620)	1,086(573)	0.124(1/6)
35.2(10)	1.26(20)	1.98(3,500)	1,139(601)	0.186(1/4)
52.8(15)	1.89(30)	2.66(4,700)	2,058(1,086)	0.186(1/4)
70.3(20)	2.52(40)	3.57(6,300)	2,740(1,446)	0.373(1/2)
87.9(25)	3.15(50)	3.96(7,000)	3,529(1,862)	0.559(3/4)
106(30)	3.85(61)	4.59(8,100)	4,371(2,306)	0.746(1)
141(40)	5.24(83)	5.55(9,800)	6,183(3,262)	1.119(1.5)
176(50)	6.62(105)	6.51(11,500)	8,068(4,257)	1.119(1.5)
211(60)	7.89(125)	8.32(14,700)	9,243(4,877)	1.119(1.5)
246(70)	9.15(145)	9.91(17,500)	10,717(5,654)	1.119(1.5)
281(80)	10.6(168)	10.7(18,900)	12,715(6,709)	1.491(2)
352(100)	13.12(208)	13.87(24,500)	15,368(8,108)	2.237(3)
440(125)	16.53(262)	16.46(29,060)	19,987(10,545)	2.237(3)
528(150)	20.06(318)	18.83(33,260)	25,122(13,255)	3.729(5)
615(175)	23.28(369)	22.79(40,250)	28,419(14,994)	3.729(5)
703(200)	26.88(426)	24.78(43,760)	33,278(17,558)	3.729(5)
791(225)	29.02(460)	34.7(61,270)	37,566(19,820)	5.593(7.5)
879(250)	32.81(520)	34.7(61,270)	44,964(23,723)	5.593(7.5)
1055(300)	39.12(620)	43.61(77,020)	58,466(30,847)	7.457(10)
1231(350)	46.94(744)	43.61(77,020)	64,794(34,186)	7.457(10)
1407(400)	53.31(845)	51.55(91,030)	99,366(52,426)	11.186(15)
1758(500)	70.22(1,113)	51.55(91,030)	114,391(60,354)	11.186(15)

2110(600)	80.63(1,278)	70.79(125,000)	172,226(90,868)	14.914(20)
2462(700)	97.54(1,546)	70.79(125,000)	140,737(74,254)	14.914(20)
2813(800)	107.44(1,703)	99.1(175,000)	134,286(70,850)	22.371(30)
3517(1000)	142.14(2,253)	99.1(175,000)	221,942(117,099)	22.371(30)
4396(1250)	178.17(2,824)	123.96(218,900)	269,798(142,348)	29.828(40)
5275(1500)	213.24(3,380)	149.95(218,900)	315,644(166,537)	37.285(40)

Then, given the peak outdoor wetbulb temperature and peak cooling tower inlet fluid temperatures, the database can be searched to find the smallest UA cooling tower that meets the required heat rejection rate.

In summary, by assuming peak heat pump ExFT (on the order of 100ºF - 115ºF) coincident with local peak wetbulb temperature, a smaller size of cooling tower will be chosen for the HGSHP system. A demonstration case of design a new HGSHP system and a "retrofit" HGSHP system for an office building will be presented in the next section. In this case, the procedure of sizing the cooling tower will also be presented.

6.4 Example of Designing HGSHP Systems

In this section, an example application of designing a HGSHP system is provided using an office building in Tulsa, Oklahoma. Three different systems are designed for this office building: 1) 100% GSHP system; 2) a new HGSHP system; and 3) a "retrofit" HGSHP with given GLHE size.

6.4.1 Office Building

The test building was based on a typical floor plan from the Bank of Oklahoma (BOK) Tower in Tulsa, OK. The office building has 52 stories, of which only three

stories with 7,144m^2 floor area are modeled for this work. The building was modeled and simulated using DesignBuilder (2006) and the building load profile is shown in Figure 6.7. The office building has more cooling loads than heating loads in Tulsa, OK (a warm-humid climate zone). For further information on this building, see Section 7.1.1.

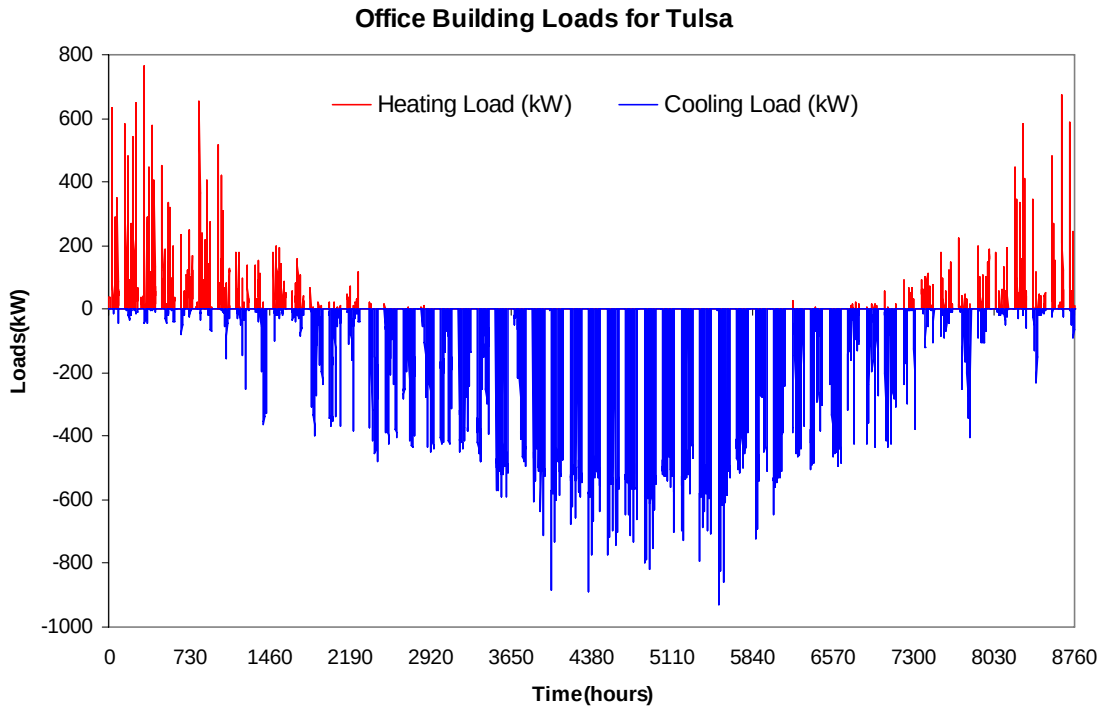

Figure 6.7 Annual hourly building load for the office building in Tulsa, OK.

6.4.2 System Design

The office building has 30 zones and two Climate Master GSH/SCS 060 water-to-water heat pumps with a nominal cooling capacity of 17.5 kW are used for each zone. The system has a total 42.8 kg/s (680gpm) of full flow rate.

Since the office building has more cooling requirement than heating in this case, the HGSHP system with an open-circuit cooling tower was designed for this building. To

demonstrate the design procedures of HGSHP systems, two different HGSHP systems were designed for this office building: 1) a new HGSHP system; and 2) a "retrofit" HGSHP with given GLHE size. But first, a 100% GSHP system will be designed for this building.

6.4.2.1 Design a GSHP system

GLHEPRO was used for designing ground loop heat exchangers for the GSHP system. The program is controlled from the main dialog box shown in Figure 6.8.

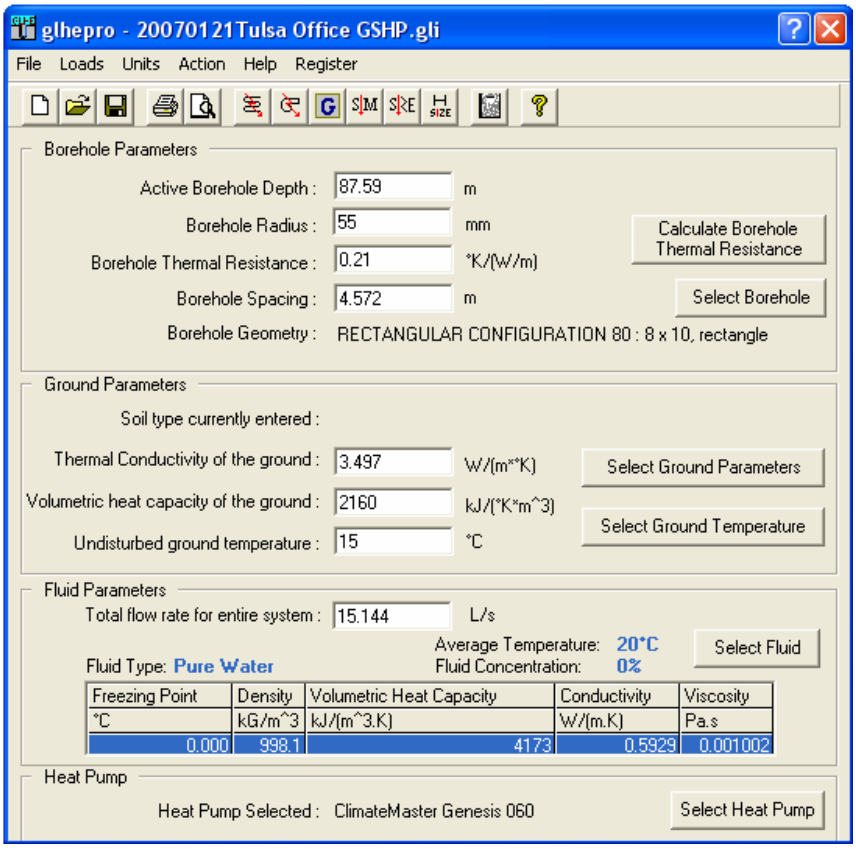

Figure 6.8 Main dialog box of GLHEPRO

1. Following the procedures described in Section 6.3.2, firstly, input all the necessary data.

In this case, most of the information requires by the program is shown in Figure 6.5. Details such as borehole radius, borehole spacing, undisturbed ground temperature, and flow rate were entered here. Borehole geometry and heat pump were both selected from a library. An initial guess of borehole depth is required.

The loads were determined with EnergyPlus and pasted from a spreadsheet into the heat pump loads dialog box, shown in Figure 6.9. In this case, because the building loads were too big for the allowed size of GLHE in the program library, only half of the building loads were used.

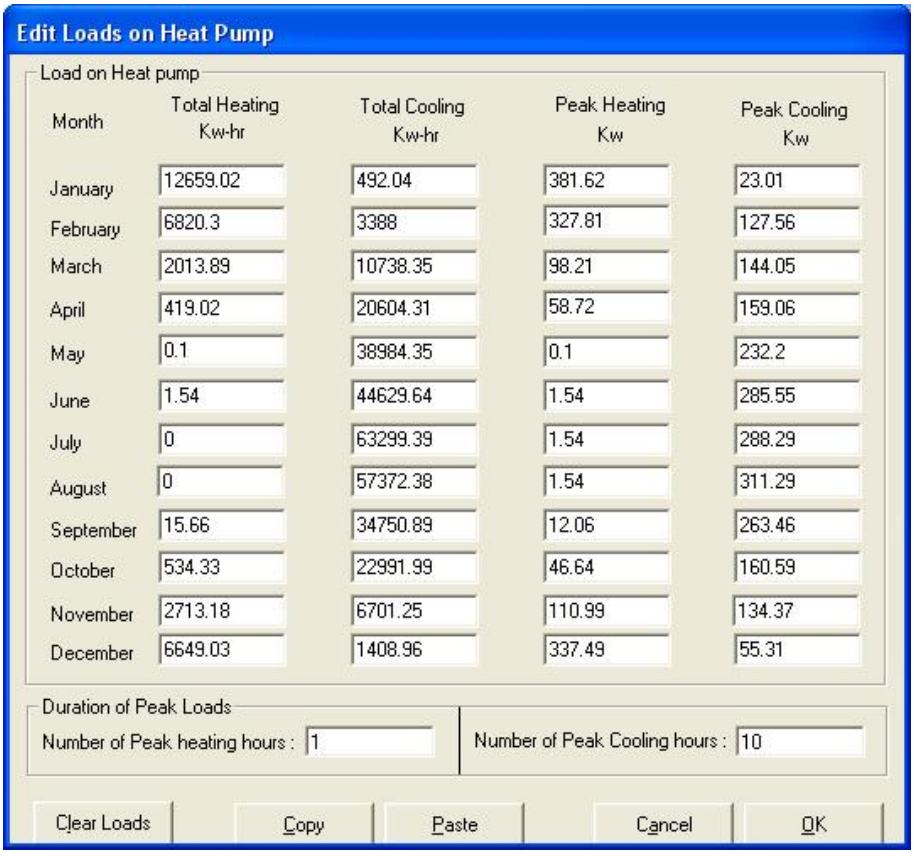

Figure 6.9 Heat Pump Loads Dialog Box

The GLHEPRO program uses a simple approximation for the peak loads. They are represented by the user as a square-wave type pulse, specified by giving the peaking cooling and heating load for each day, and the number of hours for which the peak applies. More details about the approximation for the peak loads are given by Spitler (2000).

2. Calculate the borehole thermal resistance and update g-functions of the borehole.

   The borehole thermal resistance is determined using the borehole thermal resistance calculator, shown in Figure 6.10. Most entries are close to self-explanatory. In this dialog box, user can choose different types of borehole: single U-tube, double U-tube and concentric tube. Details such as tube diameters, shank spacing, fluid factor, thermal properties of soil, grout and pipe are entered here. The fluid convection coefficient can be specified by giving the value directly or using Equation 4-8, which is implemented in GLHEPRO. When the borehole thermal resistance is calculated the g-functions of the borehole are automatically updated.

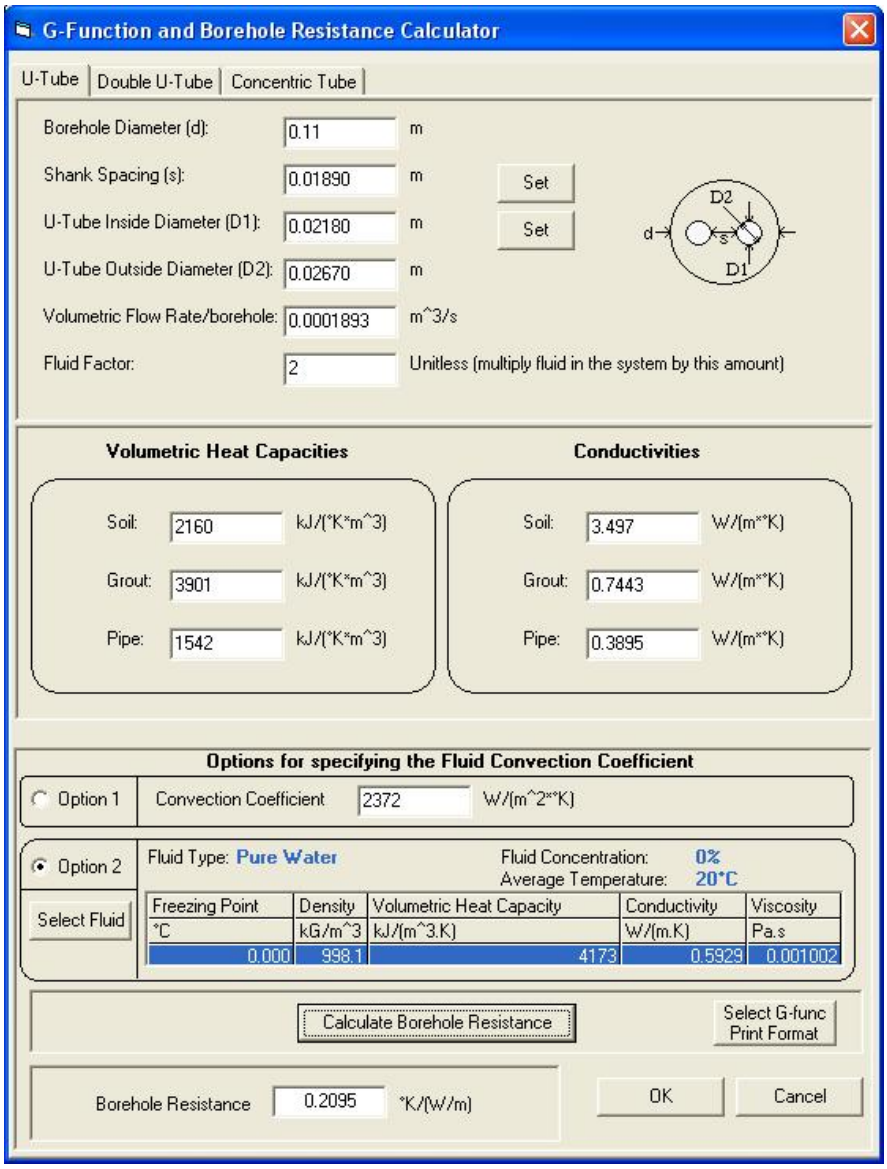

Figure 6.10 G-function and borehole resistance calculator dialog box.

3. Specify the minimum, maximum entering fluid temperature of heat pump and length of the design period. Run GSHP system GLHE sizing function.

   Once all necessary input data have been entered, the user can proceed with the design. In GLHEPRO this is done by choosing the GLHE size option. The GLHESize control dialog box is shown in Figure 6.11.

Using the ClimateMaster GSH/SCS 060 Heat Pump, a maximum entering fluid temperature (EFT) of 43.33 ºC (110 ºF) to the heat pump is allowed. Here the working fluid was water and a minimum EFT of 6 ºC (42.8 ºF) was selected. For this system design, a 20-year design period was selected.

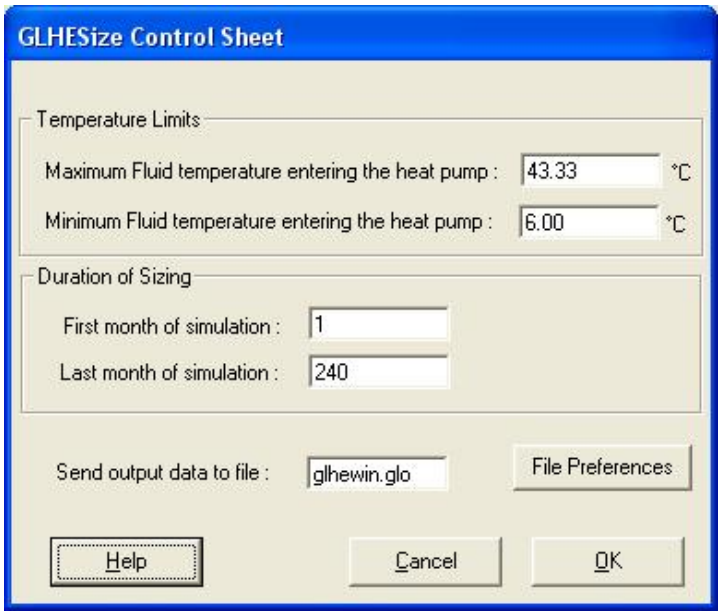

Figure 6.11 GLHE size dialog box.

The GLHEPRO Size program gave a depth of 87.6 m for the 80 boreholes that serve half of the loads of the office building, as shown in Figure 6.12. Therefore a GSHP system with total 160 boreholes, 87.6 m deep would be an adequate design for the office building in Tulsa, OK.

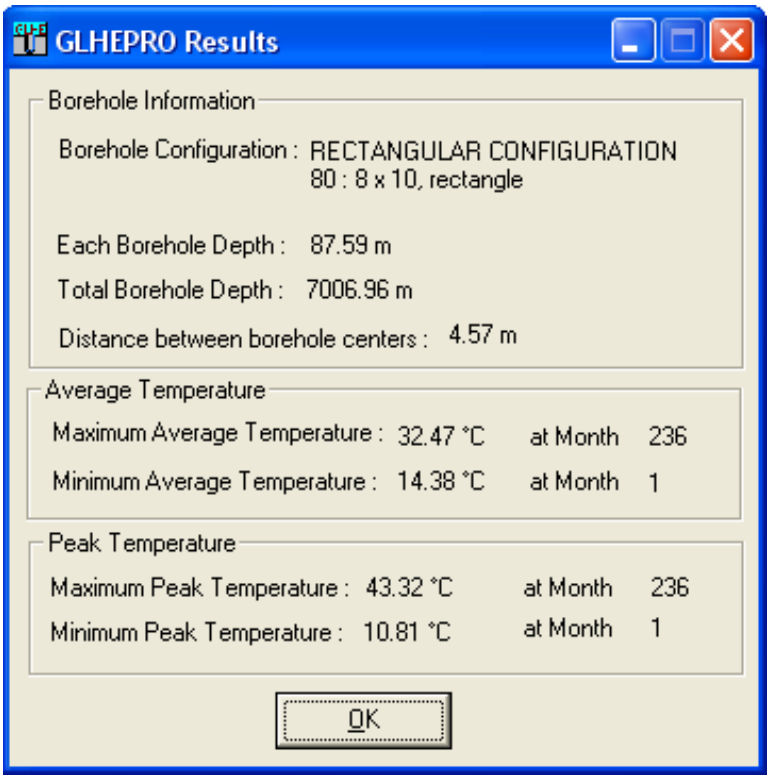

Figure 6.12 Summary of results for GSHP system design

6.4.2.2 Design a new HGSHP system

Next, an HGSHP system with an open-circuit cooling tower was designed.

The procedures described in Section 6.3.3, are implemented in GLHEPRO and run by selected HGSHP GLHE/CT Sizing function as shown in Figure 6.13. The resulting depth for the 80 boreholes is 49.5 m, and an open-circuit cooling tower with capacity of 119.9 kW was recommended for the half loads of the office building, as shown in Figure 6.14. The additional of the cooling tower allows on 40% reduction in required GLHE size compared to the GSHP system. Therefore, an HGSHP system with total 160 boreholes, 49.5 m deep, and an open-circuit cooling tower with capacity of 239.8 kW are suitable for the office building in Tulsa, OK.

Figure 6.13 HGSHP GLHE/CT sizing function in GLHEPRO.

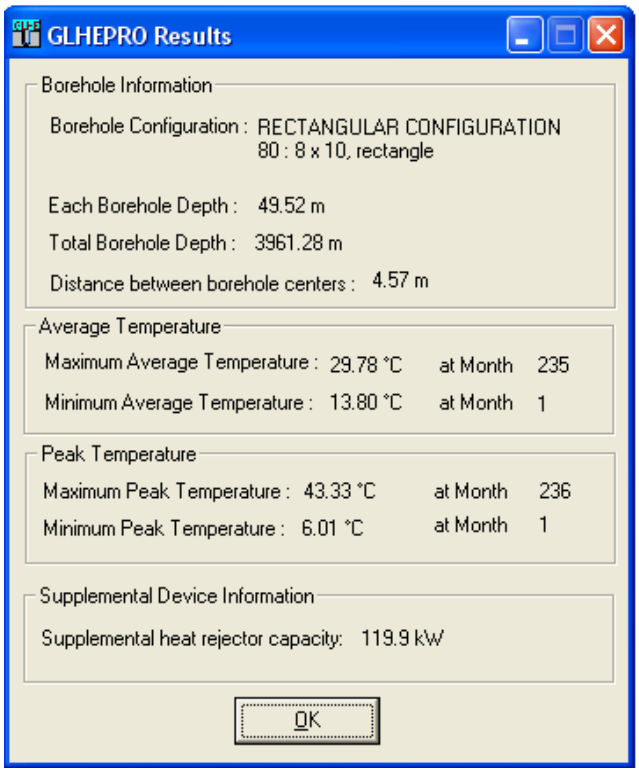

Figure 6.14 Main dialog box of GLHEPRO

Then, outside of GLHEPRO, procedures described in Section 6.3.5 were used to select a cooling tower from the cooling tower manufacturer database in Table 6.3.

1. From the Typical Meteorological Year (TMY) weather data (DOE 2007), a temperature of 26.7ºC(80.1ºF) was select as the local outdoor peak wetbulb temperature in Tulsa, OK.

2. Using the ClimateMaster GSH/SCS 060 Heat Pump, a maximum allowed ExFT of heat pump is about 50ºC (122ºF). In this case, a temperature of 115ºF was selected as the peak inlet fluid temperature of cooling tower.

3. The desired capacity of open-circuit cooling tower is 239.8 kW. Applying the fixed-UA open-circuit cooling tower model in Section 4.3.1.1, after several tries, an ACT-50 Model from Table 6.3 was selected for the new HGSHP system. The cooling tower has a nominal capacity of 50tons (176 kW), but at the conditions described in Steps 1 and 2, it can provide a capacity of 284kW.

Applying the procedure described by Kavanaugh (1998) to select the cooling tower, the flow rate of water is cooled from 35ºC (95ºF) to 29.4ºC (85ºF) with a 25.6ºC (78ºF) wet bulb temperature. This corresponds to an ACT-100 Mode from Table 6.3 was selected in order to meet the desired capacity of 239.8 kW. The selected cooling tower has double the capacity determined in Step 3. This is because, with a higher inlet fluid temperature of the cooling tower and a slightly higher local wetbulb temperature, the cooling tower is able to provide more heat rejection than its nominal capacity.

6.4.2.3 Design a "Retrofit" HGSHP system

In this section, a "retrofit" HGSHP system was designed for the office building. It was assumed that there was an existing GSHP system with total 160 boreholes, 68.6 m

deep had been designed for this office building. This GLHE would be 20% undersized compared to the system designed in Section 6.4.2.1. The improperly-sized GLHE would not meet the cooling loads of the office building and would overheat over time. In this case, an open-circuit cooling tower was added into the system to help meet loads of the system. The problem, then, is to find the cooling tower size that will fix the probslem.

Following the design procedures in Section 6.3.4, the capacity of the cooling tower is calculated outside of GLHEPRO by hand.

$$Q_{CT} = 239.9kW \times \frac{14014 - 10969}{14014 - 7923} = 120kW$$

Applying the same procedure as in the last section, an ACT-30 Model from Table 6.3 was selected for the "retrofit" HGSHP system. If the procedure described by Kavanaugh (1998) was applied, an ACT-40 Model from Table 6.3 would be selected for the "retrofit" HGSHP system. The selected cooling tower has much larger capacity than that of the ACT-30 Model.

Therefore, a "retrofit" HGSHP system with total 160 boreholes, 68.6 m deep, and an ACT-30 Model cooling tower with nominal capacity of 120 kW was designed for the office building in Tulsa, OK.

6.4.3 Discussion of System Design Results

Three different systems were designed for this cooling dominated office building: 1) 100% GSHP system; 2) a new HGSHP system; and 3) a "retrofit" HGSHP with given GLHE size. The designed results are listed in Table 6.4.

Table 6.4 System design results for the office building in Tulsa, OK.

System	GLHE size	Cooling tower Size	Cooling tower Model	
		Capacity (kW)	New procedure	Kavanaugh procedure
100% GSHP system	$160 borehole \times 87.6m = 14{,}014m$	--	--	--
New HGSHP system	$160 borehole \times 49.5m = 7923m$	240	ACT-50	ACT-100
"Retrofit" HGSHP system	$160 borehole \times 68.8m = 10969m$	120	ACT-30	ACT-40

These three systems are all workable for the office building in Tulsa, OK. However, the design of a GSHP/HGSHP system depends on various factors, considering the investment budget, building layout, available layout of borehole field, geological conditions, etc. Therefore, performance simulation will be helpful to determine which system is the best choice.

6.5 Comparison Study of HGSHP System Design Methods

Currently, there are two approaches can be used to design HGSHP system: the Kavanaugh and Rafferty (1997) procedure and the new procedure developed in this chapter. Also the Buffer Program, an interface between GenOpt (Wetter 2000) and HVACSIM+, developed in Chapter 7 can be used to optimize the design of HGSHP systems. In this section, a small study for a few building types and locations is carried out to compare these two design procedures' results to optimized design results.

6.5.1 GenOpt Design Method

The Buffer Program developed in Chapter 7 can be used to optimize the design of HGSHP systems. When the control strategy is specified, the buffer program can automatically adjust the design parameters (GLHE length and cooling tower size), run the simulation and iterate to get the minimal life cycle cost of the HGSHP system.

The flow diagram of the program is shown in Figure 6.15. Details about the aspects of the HVACSIM+ simulation and GenOpt are discussed in Section 7.2. It should be noted that this is only a reference procedure. While life cycle cost is, of course, a good way to optimize any system, this method requires far too much computation time to be practical. While either of the first two methods take just a few minutes to complete, this method may take several hours to complete.

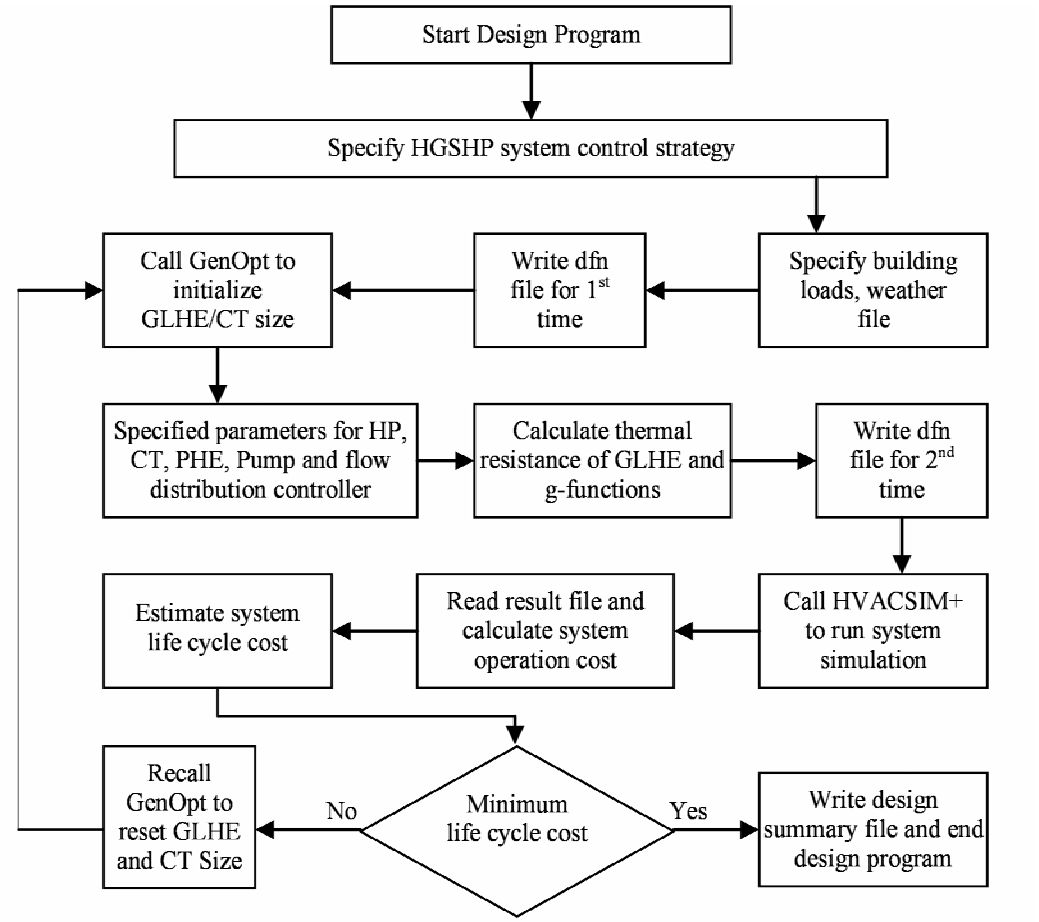

Figure 6.15 Optimization methodology flow diagram.

6.5.2 Methodology for System Simulation and Analysis

6.5.2.1 Example HGSHP Application System Description

Two different building types: office building and motel building are chosen for the comparison study. The test office building was based on a typical floor plan from the Bank of Oklahoma (BOK) Tower in Tulsa, OK. The office building is 52 stories, of which only three stories with a total area of 7,144m2 are modeled for this work. The test motel building was based on an actual motel in Tulsa, Oklahoma as described by Chen (1996). The motel building is a 2-story building with 1,037m^2. For this research a

building with a load ranging from 100 to 500-tons was desired. Therefore the motel building was modeled as three identical buildings having ten floors with the same floor plan by Gentry (2007). The detail information of the office building and motel building are available in Section 7.1.1 and 7.1.2.

6.5.2.2 Climatic Consideration – Building Loads

Briggs et al. (2002) presented climate classification for building energy codes and standards on the basis of heating degree days, cooling degree days, and humidity. For each climate zone, Briggs et al. provided a representative U.S. city (More details are available in Section 7.1.3). In this study, six representative cities were chosen for considering multiple different climate zones. The cities are: Memphis, TN, representing a warm-humid climate zone; El Paso, TX, representing a warm-dry climate zone; Albuquerque, NM, representing a mixed-dry climate zone; Baltimore, MD, representing a mixed-humid climate zone; and Houston, TX, representing a hot-humid climate zone. Together with the city of Tulsa, OK, which also represents a warm-humid climate zone and was used since it is the actual location of the building used, the building loads for these six cities were calculated with EnergyPlus. Peak loads and annual equivalent full-load hours (EFLH) for all citied are summarized in Table 6.5.

As expected based on building locations, the office building has higher cooling loads than heating loads in all six climate zones and is therefore cooling-dominated in each location. Additionally, the GSHP systems for the office building in all six climate zones are all cooling constrained. Therefore, a HGSHP system with an open-circuit

cooling tower as the supplemental heat rejecter is designed for the building in six difference climate zones.

Table 6.5 Summary of design data for each simulation case

	Tulsa, OK	El Paso, TX	Albuquerque, NM	Memphis, TN	Baltimore, MD	Houston, TX
Office Building Loads Summary						
$q_{peak,heating}$ kW(MBTU/h)	763(2,603)	433(1,477)	607(2,071)	694(2,368)	739(2,521)	730(2,091)
$q_{peak,cooling}$ kW(MBTU/h)	931(3,176)	910(3,105)	788(2,689)	936(3,139)	897(3,060)	819(2,794)
Annual EFLH - heating	89	36	71	48	118	20
Annual EFLH - cooling	660	1009	898	797	599	1121
Annual heat rejection/annual heat extraction	10.8	70.5	19.5	26.5	7.3	75.9
Motel Building Loads Summary						
$q_{peak,heating}$ kW(MBTU/h)	459(1,918)	173(725)	282(1,178)	320(1,338)	404(1,692)	288(1,206)
$q_{peak,cooling}$ kW(MBTU/h)	729(3,049)	776(3,244)	740(3,097)	687(2,874)	685(2,863)	663(2,773)
Annual EFLH - heating	195	64	227	142	338	55
Annual EFLH - cooling	1330	1589	1380	1639	1013	2003
Annual heat rejection/annual heat extraction	6.8	111.1	10	14.6	3.2	60.6
Ground Thermal Properties						
k_{soil} W/m-K(Btu/h-ft-ºF)	3.5(2.02)	3.5(2.02)	3.5(2.02)	3.5(2.02)	3.5(2.02)	3.5(2.02)
T_{ground} ºC(ºF)	15(59)	17.8(64)	13.9(57)	15.6(60)	13.9(57)	23.5(74)
ρc_p kJ/ m^3-K(Btu/ºF-ft^3)	2,160(32.21)	2,160(32.21)	2,160(32.21)	2,160(32.21)	2,160(32.21)	2,160(32.21)
GLHE Design Summary						
$r_{borehole}$ m(in)	0.055(2.17)	0.055(2.17)	0.055(2.17)	0.055(2.17)	0.055(2.17)	0.055(2.17)
$R_{borehole}$ m-K/W(h-ft-ºF/BTU)	0.209(0.363)	0.209(0.363)	0.209(0.363)	0.209(0.363)	0.209(0.363)	0.209(0.363)

6.5.2.3 Thermal Mass of System

In the HVACSIM+ simulation, the only component model that explicitly accounts for thermal mass effects is the GLHE model. In the simulation, two thermal storage tanks

were added into the system simulation to account for the thermal mass of the equipment (i.e., heat pumps) and the thermal mass in the pipe system.

To determine the thermal mass of the heat pumps in the system, a simplified methodology based on the dynamic heat pump model (Didion and Mulroy 1983) was developed. In the Didion and Mulroy model, a time constant, τ_1 , was used to account for the heat storage dynamics of heat pump. The time constant τ_1 was experimentally identified and a reasonable value of τ_1 typically falls in a range between 60s and 180s.

By applying the energy balance on the fluid in the system, the time constant τ_1 can be deduced in terms of $\tau = m/\dot{m}$, where m is the equivalent volume of the fluid caused by the heat pump, and $\dot{m}$ is the system flow rate, m^3/s. Knowing values of the time constant, which was determined from experimental data, and the system flow rate, the equivalent volume of the fluid caused by the heat pumps can be determined.

To determine the fluid thermal mass in the pipe system, the pipe layouts were designed for the office building and the motel building. The fluid volumes in two building pipe systems were calculated.

6.5.2.4 Operating and Control Strategies

The objective of this comparison is to investigate the impact of each design procedure on the system operation rather than develop an optimal control strategy for the HGSHP system. Yavuzturk and Spitler (2000) investigated several different control strategies for the HGSHP system. The study showed that the best results were achieved when the cooling tower is controlled based on the difference between the heat pump

entering fluid temperature and the outside wet-bulb temperature. In this present study, a similar temperature difference control strategy was adopted, as well as an additional strategy for comparison

- Control 1. When the difference between the heat pump exiting fluid temperature and the outside ambient air-wet-bulb temperature is greater than 2ºC (3.6ºF), the cooling tower fan and the secondary fluid circulation loop pump are activated. When the temperature difference is less then 1ºC (1.8ºF), the cooling tower fan and the secondary fluid circulation loop pump are turned off.

- Control 2. Another control strategy using the heat pump entering fluid temperature (Yavuzturk and Spitler 2000) was also utilized for the comparison. When the heat pump entering fluid temperature is greater than 32.2ºC (90ºF), the cooling tower fan and the secondary fluid circulation loop pump are activated. When the temperature is less then 27.2ºC (81ºF), the cooling tower fan and the secondary fluid circulation loop pump are turned off.

A parallel-connected HGSHP system is set up for the simulation in HVACSIM+. More details about the system simulation in HVACSIM+ are available in Section 4.6.

6.5.3 Comparison Results and Discussion

6.5.3.1 Office Building System Design Results

The three different HGSHP system design methods described previously were used to design the HGSHP system for the office building in six different climate zones. The design results, including the open-loop cooling tower size, the number of boreholes, and the depth of each borehole, are summarized in Table 6.6. In the table, the Kavanaugh and Rafferty design method is labeled as Method 1; the new GLHEPRO design method is labeled as Method 2 and the GenOpt design method is labeled as Method 3. Using Method 3, the choice of control strategy will affect the system operation cost, and, additionally, the optimal system design results. Therefore, Table 6.6 lists the two different results of Method 3; these are shown as Methods 3-1 and 3-2, for the two control strategies described above. Also shown in the table is, for Methods 1 and 2, the ratio of the total borehole length of the HGSHP system to that of the GSHP system; it should be noted that the number of boreholes is not necessarily the same between the two. Also, there is no ratio data for Method 3, as this procedure does not involve first designing a GSHP system as a base.

Table 6.6 Summary of design results for each simulation case

Cities	**Tulsa, OK**				**El Paso, TX**			
Design Method	1	2	3-1	3-2	1	2	3-1	3-2
Number of Boreholes	100	100	100	100	24	48	56	56
Borehole depth, m (ft)	98.45 (323.00)	79.23 (259.94)	73.53 (241.24)	72.56 (238.06)	128.25 (420.77)	82.35 (270.18)	45.04 (147.77)	67.45 (221.29)
Borehole depth ratio, HGSHP/GSHP	0.443	0.565	---	---	0.099	0.171	---	---
Capacity of cooling tower, kW (tons)	383.7 (109)	154.9 (44)	59.8 (17)	59.8 (17)	464.6 (132)	246.4 (70)	383.7 (109)	306.2 (87)
Cities	**Albuquerque, NM**				**Memphis, TN**			
Design Method	1	2	3-1	3-2	1	2	3-1	3-2
Number of Boreholes	64	100	100	100	64	100	100	100
Borehole depth, m (ft)	117.02 (383.92)	72.99 (239.47)	55.44 (181.89)	52.16 (171.13)	116.92 (383.60)	76.11 (249.70)	56.44 (185.17)	53.25 (174.70)
Borehole depth ratio, HGSHP/GSHP	0.368	0.508	---	---	0.302	0.445	---	---
Capacity of cooling tower, kW (tons)	306.2 (87)	123.2 (35)	183.0 (52)	183.0 (52)	464.6 (132)	183.0 (52)	211.2 (60)	211.2 (60)
Cities	**Baltimore, MD**				**Houston, TX**			
Design Method	1	2	3-1	3-2	1	2	3-1	3-2
Number of Boreholes	120	120	120	120	42	60	60	60
Borehole depth, m (ft)	97.15 (318.73)	73.12 (239.90)	64.78 (212.53)	63.97 (209.88)	156.57 (513.68)	87.18 (286.02)	67.97 (223.00)	54.72 (179.53)
Borehole depth ratio, HGSHP/GSHP	0.697	0.710	---	---	0.132	0.196	---	---
Capacity of cooling tower, kW (tons)	183.0 (52)	73.9 (21)	42.2 (12)	42.2 (12)	464.6 (132)	306.2 (87)	246.4 (70)	383.7 (109)

Tulsa, OK. For the HGSHP system in Tulsa, OK, Method 1 gave the largest GLHE length while Method 3 gave the smallest GLHE length. The GLHE size from the Method 2 (7,923m) was fairly close to the GLHE length from Method 3 (7,256m and 7,353m for the two control strategies). The cooling tower size from Method 1 was much larger than that from the other two methods. The reason is that, in the design procedures of both Method 2 and Method 3, the cooling tower was sized based on the local outdoor peak wetbulb temperature, 26.7 ºC (80 ºF) and the heat pump peak exiting fluid temperature, 46.1ºC (115ºF). However, in Method 1, the cooling tower was sized by assuming that the fluid was cooled from 35ºC (95ºF) to 29.4ºC (85ºF) with a 25.6ºC (78ºF) wet bulb temperature. This method tends to oversize the cooling tower.

For the HGSHP system design using Method 3, using the different control strategies did not cause a significant change in the system design results. The cooling tower sizes were the same and the difference in GLHE length was within 7%.

El Paso, TX. For the HGSHP system in El Paso, TX, the three design procedures gave out quite different design results. Method 2 gave out the largest GLHE size (3,953m). Using Method 3, the results varied greatly between the two control strategies—3,777m for the set EFT control strategy and 2,522m for the set Tdiff control strategy. Using Method 3, the HGSHP system with a larger GLHE size had a relatively smaller cooling tower size and, similarly, the HGSHP system with a smaller GLHE size had a relative larger cooling tower size. Because of using the different control strategies, the fraction of system cooling loads removed by the cooling tower was different (horizontal position of Point 2 in Figure 6.5). This difference can be seen from the Average Annual Energy Consumption for Cooling Tower Fan entry in Table 6.7. The fan power of these two sizes of cooling tower were the same, but the average annual energy comsumption of the cooling tower fan in Method 3-1 (8,135kWh), the set Tdiff control case, was much higher than the energy consumption in Method 3-2 (1,428kWh), the set EFT control case, which means the cooling tower in the set Tdiff control case ran more hours and rejected more heat from the loop than the cooling tower in the set EFT control case.

Albuquerque, NM. and Memphis, TN. For the HGSHP systems in Albuquerque, NM and Memphis, TN, Methods 1 and 2 gave similar GLHE lengths, but the cooling tower sizes from the Method 2 were again much smaller than the cooling tower sizes from Method 1. Method 3 gave out the smallest GLHE length for both of the

climate zones; the different control strategies did not cause a significant difference in the system design result. The cooling tower sizes were also the same. The difference in GLHE length was within 5% in the Albuquerque case and within 6% in the Memphis case.

Baltimore, MD. For the HGSHP system in Baltimore, MD, Methods 2 and 3 gave similar GLHE lengths and cooling tower sizes. Method 1 gave out a much larger GLHE length and larger cooling tower size than from the other two methods. In Table 6.7, the HGSHP system with set EFT control strategy results (Control 2) shows that the cooling tower fan power and the annual run time of the cooling tower was zero. That means the cooling tower has not been turned on because with a relatively large GLHE length the loop temperature does not reach the 32.2ºC (90ºF) design temperature, above which the cooling tower is turned on. The GLHE is oversized due to the closer balance between heating and cooling loads and the low ground temperature, as shown in Table 2; both of these factors combine to create the oversizing in Method 1. Additionally, the large cooling tower is specified because this design method is equation-based, not simulation-based. Since no simulation is ever performed, the method has no way of knowing that the EFT will never exceed the cooling tower set point—in other words, that a cooling tower is not needed with the specified GLHE length. This is a substantial flaw in this particular design method.

Houston, TX. For the HGSHP system in Houston, TX, the three design procedures gave out quite different design results. Like the system in El Paso, using the different control strategies, the systems designed with Method 3 had quite different

GLHE lengths and cooling tower sizes for the same building. The HGSHP system with a larger GLHE had a relatively smaller cooling tower size, and the HGSHP system with a smaller GLHE had a relatively larger cooling tower size.

Using the GLHE and cooling tower size from each design method, the HGSHP system with the two control strategies described earlier for each climate zone was simulated using the HVACSIM+ modeling environment. Pure water was utilized as the working fluid of the system. Based on common manufacturer specifications, a maximum entering fluid temperature of 43.33ºC (110ºF) was specified; the minimum exiting fluid temperature was set at 2ºC (35.6ºF) to prevent freezing in the water loop. For each simulation case, the heat pump maximum entering fluid temperature and the minimum exiting fluid temperature are listed in Table 6.7. In most of the simulation cases, the heat pump entering and exiting fluid temperatures were within the allowed temperature range. In some HGSHP system simulation cases, though, the minimum exiting fluid temperature of the heat pump could be lower than the design temperature limit (2ºC); the average number of hours that the heat pump fluid temperature exceeded the design temperature limits in one year are listed in Table 6.7.

In the Tulsa cases with the GLHE and cooling tower size from Method 2, for both control strategies, the simulated minimum heat pump exiting fluid temperature was 1.5ºC (34.7ºF). The heat pump exiting fluid temperature was lower than 2ºC in only one hour per year. In the simulation cases with the Method 3 design results, the minimum heat pump exiting fluid temperature was as low as 0.8ºC (33.4ºF) in Memphis, and the total hours that the heat pump exiting fluid temperature was lower than 2ºC in one year

averaged 2.3 hours. In these cases, the minimum heat pump exiting fluid temperatures were lower than the allowed temperature, but the temperature was still within an acceptable region and would not cause a freezing problem. The total hours that the temperature went out of range in one year was about one to two hours. Therefore, all these design methods gave a feasible HGSHP system design.

6.5.3.2 Analysis of Office System Performance

For each combination of HGSHP system design and control strategy, the annual system component energy consumptions, as obtained from the HVACSIM+ simulation, are listed in Table 6.7 and shown in Figure 6.16. As can be seen in Figure 6.16, in the HGSHP system, 80%-90% of energy was consumed by the heat pump, and 5%-8% of energy was by the primary circulation pump. The cooling tower fan and the secondary loop circulation pump consume about 2%-10% of total system energy depending on system design and control strategy.

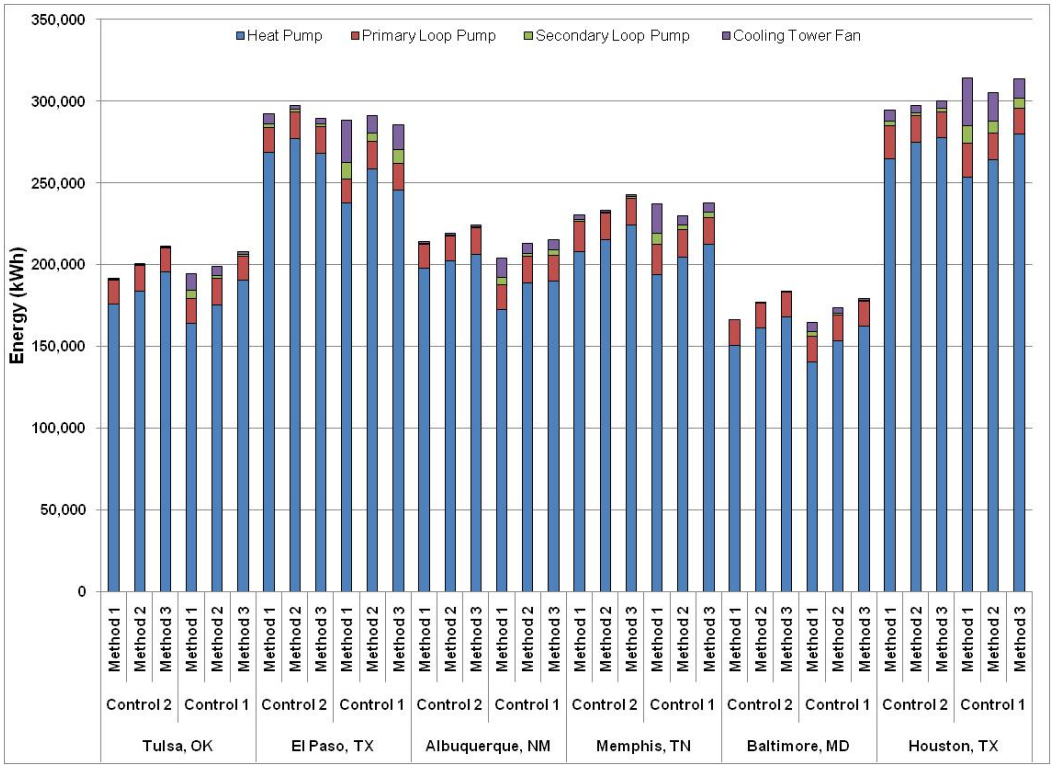

Figure 6.16 HGSHP system annual energy consumption in each office building simulation case

With different HGSHP system component sizes, the system energy consumption was different. In Figure 6.16, for each climate zone and control strategy, the system with a relatively larger GLHE length and cooling tower size would have a relatively smaller total system energy consumption. With a larger GLHE length and cooling tower size, the system was able to reject the same amount of system cooling loads with relative lower fluid temperatures. As a result, the heat pump had higher COPs in cooling mode and consumed less energy. For example, in the Tulsa set EFT control case, the system designed with Method 1 had larger GLHE and cooling tower sizes than the system designed with Method 2. As a result, this system had a lower annual energy consumption.

For systems designed with either Method 1 or Method 2, the systems had identical GLHE and cooling tower sizes. Applying the different control strategies, the run time of

the cooling tower, the cooling tower fan power, the circulation pump energy consumption and the heat pump energy consumption were different. For example, the system designed from Method 2 in Tulsa had an annual cooling tower run time of 595 hours in the set EFT case as opposed to 4,669 hours in the set Tdiff case. Because, in the latter case, the cooling tower ran more hours and rejected more heat from the system loop, the heat pump had higher COPs and lower energy consumption. Although in the set Tdiff control case, the cooling tower fan and the secondary loop circulation pump consumed more energy than the fan and pump in the set EFT case, the annual total system energy of the set Tdiff case (198,738kWh) was less than the energy consumption in the set EFT case (200,669kWh). For the system designed with the Method 1 in Tulsa using the set Tdiff control strategy, the cooling tower ran more hours and rejected more heat than the cooling tower in the set EFT case. As a result, the heat pump had a smaller annual energy consumption. However, because the cooling tower and secondary loop circulation pump were much larger than those from Method 2 and therefore consumed more energy, the heat pump energy savings brought by running the cooling tower for more hours could not make up for the extra energy consumed by running the cooling tower fan and secondary loop pump. In this case, the annual total system energy consumption using the Tdiff control strategy was higher than the system using the EFT control strategy.

The choice of control strategy will obviously affect the performance of the HGSHP system. However, the total system energy consumption also depends on the climate zone, system design, etc. In this study, we have not attempted to investigate the optimum control strategy for the HGSHP system but note that such a development is a highly desirable topic for further research.

6.5.3.3 Office System Installation and Operating Cost Analysis

A 20-year life-cycle cost analysis was performed to evaluate the various cases from different HGSHP design methods. A net present value (NPV) was selected to compare the different simulation cases. The present value of the system operating costs and the system first costs are calculated based on series of assumptions. In this study, issues related to the maintenance of supplemental heat rejecters and related equipment were not considered.

- The cost of the ground heat exchanger is calculated at $6.00 per foot ($19.67/m) of the borehole (Kavanaugh 1998). This amount includes the horizontal runs and connections.

- The first cost of the cooling tower, including the isolation plate heat exchanger, is calculated at $275.00 per ton ($78.13/kW) of cooling tower capacity (Means 2006). This amount includes other equipment and apparatus required for controls.

- The cost of auxiliary equipment and materials for the cooling tower and the plate heat exchanger is estimated to be 10% of the first cost.

- The cost of electricity is assumed to be $0.07 per kWh.

- A 6% annual percentage rate is used for the present value analysis. Annual compounding is used for the 20-year analysis.

Table 6.8 summarizes the open-loop cooling tower size, the number of and depth of borehole, the first cost of the system, the average annual system component operating cost, the net-present value for 20-year system operating cost and the system life cycle cost for each simulation case. The HGSHP system life cycle cost of each simulation case is shown in Figure 6.17.

As can be seen in Figure 6.17, the HGSHP system designed from Method 3 produced the minimum system life cycle cost. The reason is quite obvious. In this method, the program automatically adjusts the GLHE size and cooling tower size, runs the HGSHP system simulation, and iterates to determine the minimum life cycle cost of the HGSHP system; in other words, the method is supposed to produce the system with the lowest life cycle cost. In most cases, the systems designed with Method 2 had a lower system life cycle cost than the system designed with Method 1 except for the systems in El Paso, TX..

The different control strategies also caused a difference in the system life cycle cost. Yavuzturk and Spitler (2000) investigated several control strategies for the HGSHP system in a small office building. In their study, they found the system with the set Tdiff control strategy had the smallest system life-cycle cost. However, in this study, this conclusion is not always true. For the system designed with Method 1 in Tulsa, the system with the set EFT control strategy had a lower life-cycle cost than the system with the set Tdiff control strategy. Again, the HGSHP system life-cycle cost not only depends the control strategy but also depends on the climate zone and the system design. As discussed previously, the purpose of this paper is to compare the different HGSHP

system design procedures but not to investigate the best choice of control strategy for the HGSHP system. Further research about HGSHP system control is highly desired.

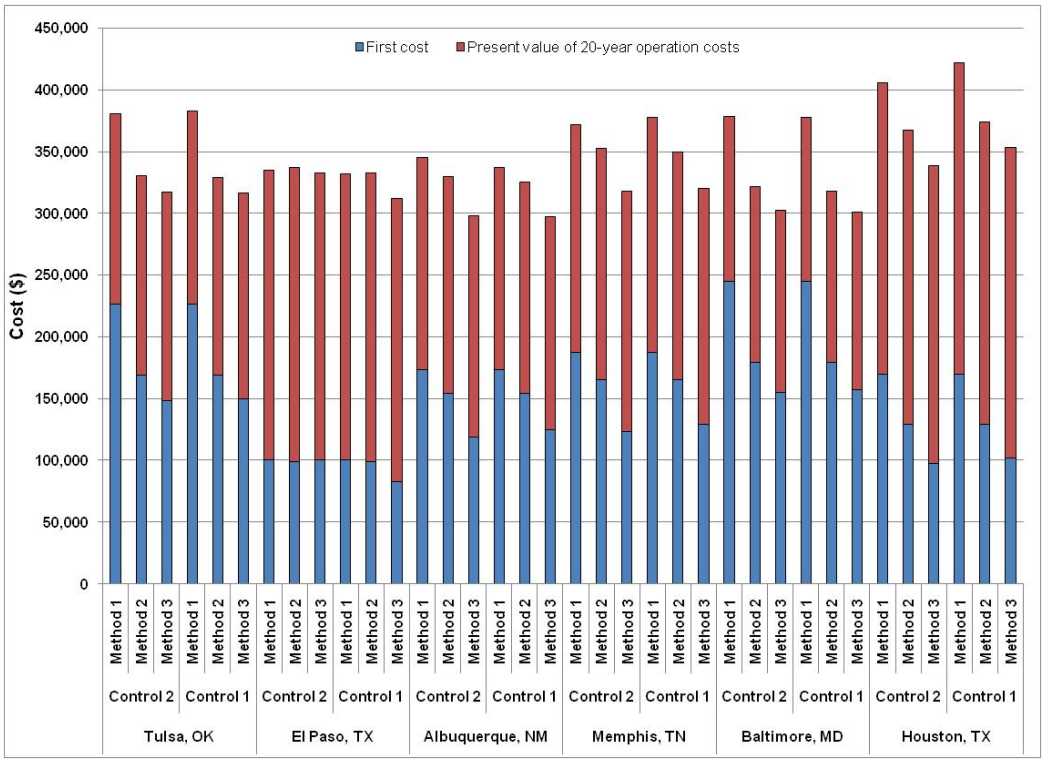

Figure 6.17 HGSHP system life cycle cost in each office building simulation case

Table 6.7 Summary of energy consumption and fluid temperature for each office building simulation case

Control Strategy	**Set EFT (Control 2)**			**Set T_{diff} (Control 1)**			**Set EFT (Control 2)**			**Set T_{diff} (Control 1)**		
Design Method	**1**	**2**	**3**	**1**	**2**	**3**	**1**	**2**	**3**	**1**	**2**	**3**
Cities	**Tulsa, OK**						**El Paso, TX**					
Average Annual Energy Consumption Heat Pump (kWh)	175,601	183,704	195,748	163,985	175,296	190,409	268,672	276,990	267,717	237,363	258,497	245,769
Primary Loop Pump (kWh)	15,365	16,018	14,800	15,365	16,018	14,788	14,987	16,520	16,656	14,987	16,520	16,043
Cooling Tower Fan (kWh)	259	281	134	5,098	2,199	897	2,276	1,191	1,428	9,849	5,291	8,135
Secondary Loop Pump (kWh)	491	666	279	9,702	5,225	1,866	5,943	2,351	3,419	25,753	10,465	15,485
Total annual energy consumption (kWh)	191,716	200,669	210,961	194,150	198,738	207,961	291,878	297,052	289,220	287,952	290,773	285,433
Average CT run time (hours)	220	595	748	4,337	4,669	5,003	1,594	1,577	1,528	6,906	7,019	6,922
HP EFT Max, 8 years operation (ºC/ºF)	34.1/93.4	35.0/95.0	42.6/108.7	28.0/82.4	34.4/93.9	42.1/107.1	46.7/116.1	42.3/108.1	42.5/108.5	32.8/91.0	40.0/104.0	35.5/95.9
HP ExFT Min, 8 years operation (ºC/ºF)	3.8/38.8	1.5/34.7	0.9/33.6	3.3/37.9	1.5/34.7	1.0/33.8	4.9/40.8	7.3/45.1	7.4/45.3	5.4/41.7	4.2/39.6	1.5/34.7
Hours EFT/ExFT out of range in a year	0	1	1.3	0	1	1.3	0	0	0	0	0	0.7
Cities	**Albuquerque, NM**						**Memphis, TN**					
Average Annual Energy Consumption Heat Pump (kWh)	197,751	201,996	206,431	172,508	188,984	189,759	208,038	214,942	224,357	193,988	204,593	212,239
Primary Loop Pump (kWh)	14,855	15,965	15,991	14,855	15,965	16,037	18,298	16,724	16,327	18,298	16,724	16,394
Cooling Tower Fan (kWh)	401	263	530	4,905	2,049	3,067	1,047	470	718	6,784	2,775	3,312
Secondary Loop Pump (kWh)	959	789	1,054	11,766	6,154	6,117	2,730	934	1,231	17,734	5,533	5,693
Total annual energy consumption (kWh)	213,966	219,013	224,007	204,034	213,152	214,980	230,112	233,069	242,633	236,804	229,625	237,638
Average CT run time (hours)	429	705	942	5,260	5,500	5,466	732	835	1,100	4,756	4,944	5,088
HP EFT Max, 8 years operation (ºC/ºF)	35.2/95.4	36.2/97.2	37.3/99.1	28.0/82.4	35.7/96.3	36.1/97.0	37.6/99.7	36.0/96.8	39.2/102.6	30.2/86.4	35.8/96.4	38.4/101.1
HP ExFT Min, 8 years operation (ºC/ºF)	4.1/39.4	3.838.8	1.3/34.3	2.7/36.9	3.5/38.3	1.4/34.5	2.6/36.7	3.7/38.7	0.8/33.4	2.5/36.5	3.6/38.5	1.2/34.2
Hours EFT/ExFT out of range in a year	0	0	1.7	0	0	1	0	0	2.3	0	0	1
Cities	**Baltimore, MD**						**Houston, TX**					
Average Annual Energy Consumption Heat Pump (kWh)	150,434	161,371	168,191	140,274	153,494	162,132	264,401	274,816	277,392	253,473	264,311	279,515
Primary Loop Pump (kWh)	15,800	15,659	15,389	15,800	15,659	15,405	20,406	15,952	15,678	20,406	15,952	16,027
Cooling Tower Fan (kWh)	0	53	56	2,857	1,198	729	2,686	1,814	2,443	11,184	7,384	6,024
Secondary Loop Pump (kWh)	0	131	78	5,699	2,990	1,009	7,007	4,338	4,640	29,218	17,689	11,905
Total annual energy consumption (kWh)	10,530	11,296	11,773	9,819	10,745	11,349	18,508	19,237	19,417	17,743	18,502	19,566
Average CT run time (hours)	0	234	418	5,093	5,349	5,427	1,879	1,939	4,146	7,835	7,907	7,984
HP EFT Max, 8 years operation (ºC/ºF)	31.8/89.2	34.1/93.4	39.1/102.4	25.8/78.4	33.6/92.5	38.4/101.1	40.5/104.9	40.5/104.9	41.4/106.5	32.6/90.7	37.8/100.0	42.6/108.7
HP ExFT Min, 8 years operation (ºC/ºF)	4.2/39.6	2.2/36.0	1.1/34.0	4.2/39.6	2.2/36.0	1.2/34.2	6.7/44.1	6.0/42.8	0.8/33.4	5.0/41.0	4.5/40.1	1.7/35.1
Hours EFT/ExFT out of range in a year	0	0	1.3	0	0	1	0	0	1.3	0	0	0.7

Table 6.8 Summary of Net Present Value and system first costs for each office building simulation case

Control Strategy	**Set EFT (Control 2)**			**Set T_{diff} (Control 1)**			**Set EFT (Control 2)**			**Set T_{diff} (Control 1)**		
Design Method	**1**	**2**	**3**	**1**	**2**	**3**	**1**	**2**	**3**	**1**	**2**	**3**
Cities	**Tulsa, OK**						**El Paso, TX**					
Total Length of Loop Installation (m)	9,845	7,923	7,256	9,845	7,923	7,353	3,078	3,953	3,777	3,078	3,953	2,522
Total Cost of Loop Installation ($)	193,848	155,995	142,876	193,848	155,995	144,783	60,606	77,840	74,359	60,606	77,840	49,653
First Cost of Cooling Tower + PHX incl. Control ($)	29,980	12,006	4,577	29,980	12,006	4,577	36,382	19,225	23,800	36,382	19,225	29,979
Cost of Auxiliary Equipment ($)	2,998	1,201	458	2,998	1,201	458	3,638	1,922	2,380	3,638	1,922	2,998
Total First Cost of Equipment ($)	226,826	169,202	147,910	226,826	169,202	149,818	100,626	98,987	100,539	100,626	98,987	82,630
Average Annual Operating Cost ($)	13,420	14,047	14,767	13,591	13,912	14,558	20,431	20,793	20,245	20,159	20,354	19,980
Present Year of 20-year-Operation ($)	153,928	161,116	169,379	155,882	159,565	166,971	234,348	238,502	232,213	231,195	233,460	229,173
Present Value of Total Cost ($)	380,754	330,318	317,290	382,708	328,768	316,788	334,973	337,489	332,752	331,821	332,447	311,803
Cities	**Albuquerque, NM**						**Memphis, TN**					
Total Length of Loop Installation (m)	7,489	7,299	5,216	7,489	7,299	5,544	7,483	7,611	5,325	7,483	7,611	5,644
Total Cost of Loop Installation ($)	147,458	143,712	102,696	147,458	143,712	109,156	147,340	149,861	104,849	147,340	149,861	111,125
First Cost of Cooling Tower + PHX incl. Control ($)	23,795	9,504	14,310	23,795	9,504	14,310	36,382	14,310	16,591	36,382	14,310	16,591
Cost of Auxiliary Equipment ($)	2,380	950	1,431	2,380	950	1,431	3,638	1,431	1,659	3,638	1,431	1,659
Total First Cost of Equipment ($)	173,633	154,166	118,436	173,633	154,166	124,897	187,360	165,601	123,100	187,360	165,601	129,376
Average Annual Operating Cost ($)	14,978	15,331	15,680	14,823	14,921	15,049	16,108	16,315	16,984	16,576	16,074	16,636
Present Year of 20-year-Operation ($)	171,792	175,844	179,854	163,818	171,139	172,606	184,756	187,130	194,809	190,129	184,364	190,798
Present Value of Total Cost ($)	345,425	330,010	298,290	337,451	325,305	297,503	372,116	352,731	317,909	377,489	349,966	320,174
Cities	**Baltimore, MD**						**Houston, TX**					
Total Length of Loop Installation (m)	11,658	8,774	7,676	11,658	8,774	7,774	6,576	5,231	3,283	6,576	5,231	4,078
Total Cost of Loop Installation ($)	229,546	172,752	151,145	229,546	172,752	153,065	129,481	103,000	64,645	129,481	103,000	80,298
First Cost of Cooling Tower + PHX incl. Control ($)	14,310	5,713	3,428	14,310	5,713	3,428	36,382	23,795	29,980	36,382	23,795	19,225
Cost of Auxiliary Equipment ($)	1,431	571	343	1,431	571	343	3,638	2,380	2,998	3,638	2,380	1,922
Total First Cost of Equipment ($)	245,287	179,036	154,916	245,287	179,036	156,836	169,502	129,175	97,622	169,502	129,175	101,446
Average Annual Operating Cost ($)	11,636	12,405	12,859	11,524	12,134	12,549	20,614	20,785	21,010	21,999	21,374	21,943
Present Year of 20-year-Operation ($)	133,469	142,284	147,503	132,181	139,175	143,940	236,451	238,395	240,992	252,335	245,153	251,684
Present Value of Total Cost ($)	378,755	321,320	302,419	377,467	318,211	300,775	405,953	367,570	338,614	421,836	374,328	353,129

6.5.3.4 Motel Building System Design Results

The three different HGSHP system design methods were used to design the HGSHP system for the motel building in the same six different climate zones. The design results, are summarized in Table 6.9. The definition of the design method labels are the identical with the definition in Table 6.6.

Table 6.9 Summary of design results for each motel building simulation case

Cities	**Tulsa, OK**				**El Paso, TX**			
Design Method	1	2	3-1	3-2	1	2	3-1	3-2
Number of Boreholes	300	144	144	144	40	40	40	40
Borehole depth, m (ft)	72.68 (238.46)	67.47 (221.34)	67.60 (221.78)	69.16 (226.90)	87.63 (287.48)	75.03 (246.15)	38.85 (127.46)	43.78 (143.62)
Borehole depth ratio, HGSHP/GSHP	0.952	0.493	---	---	0.114	0.104	---	---
Capacity of cooling tower, kW (tons)	306.2 (87)	154.9 (44)	154.9 (44)	73.9 (21)	542.1 (154)	383.7 (109)	383.7 (109)	383.7 (109)
Cities	**Albuquerque, NM**				**Memphis, TN**			
Design Method	1	2	3-1	3-2	1	2	3-1	3-2
Number of Boreholes	150	64	64	64	200	128	128	128
Borehole depth, m (ft)	82.68 (271.26)	96.47 (316.5)	38.34 (125.8)	40.34 (132.36)	67.74 (222.24)	65.88 (216.15)	45.97 (150.82)	46.97 (154.1)
Borehole depth ratio, HGSHP/GSHP	0.613	0.308	---	---	0.656	0.400	---	---
Capacity of cooling tower, kW (tons)	306.2 (87)	246.4 (70)	383.7 (109)	383.7 (109)	383.7 (109)	183.0 (52)	246.4 (70)	183.0 (52)
Cities	**Baltimore, MD**				**Houston, TX**			
Design Method	1	2	3-1	3-2	1	2	3-1	3-2
Number of Boreholes	200	150	150	150	64	48	48	48
Borehole depth, m (ft)	99.57 (326.66)	65.47 (214.79)	68.97 (226.29)	69.72 (228.74)	92.30 (302.81)	84.33 (276.68)	64.98 (213.19)	66.40 (217.83)
Borehole depth ratio, HGSHP/GSHP	0.902	0.626	---	---	0.149	0.107	---	---
Capacity of cooling tower, kW (tons)	123.2 (35)	88.0 (25)	10.6 (3)	42.2 (12)	542.1 (154)	383.7 (109)	246.4 (70)	246.4 (70)

For each simulation case, the annual system component energy consumptions are listed in Table 6.10 and shown in Figure 6.18. A 20-year life-cycle cost analysis was performed to evaluate the each case. The present value of the system operating costs, the

system first costs and the system life cycle costs are listed in Table 6.11 and shown in Figure 6.19.

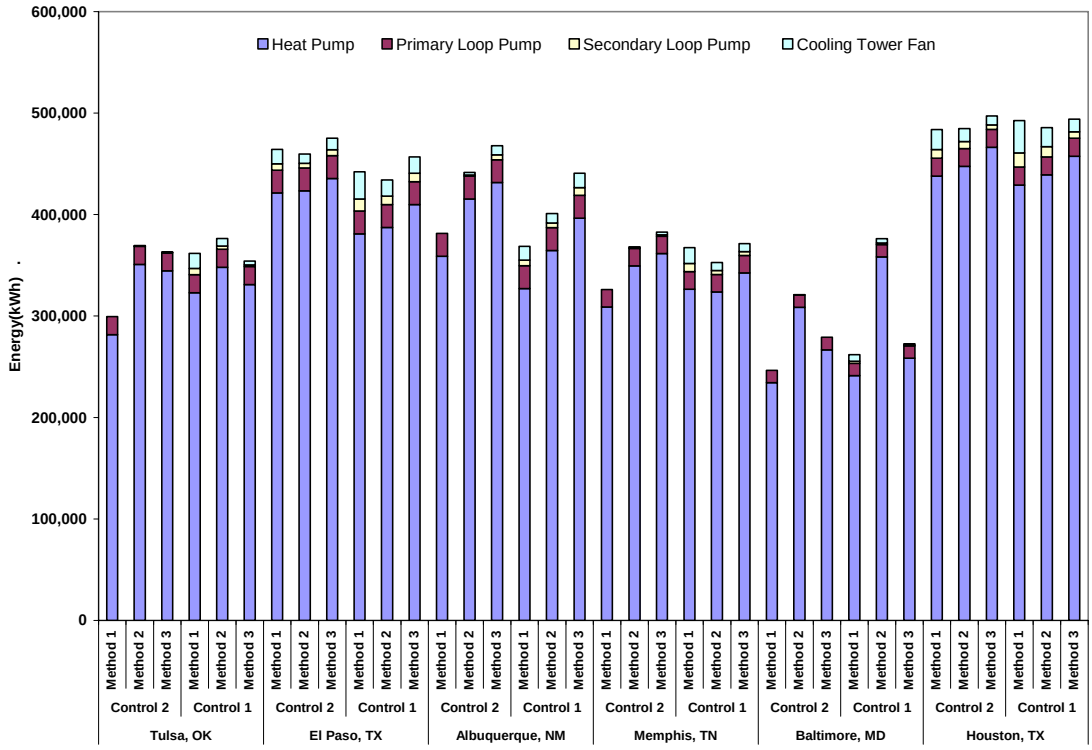

Figure 6.18 HGSHP system annual energy consumption in each motel building simulation case

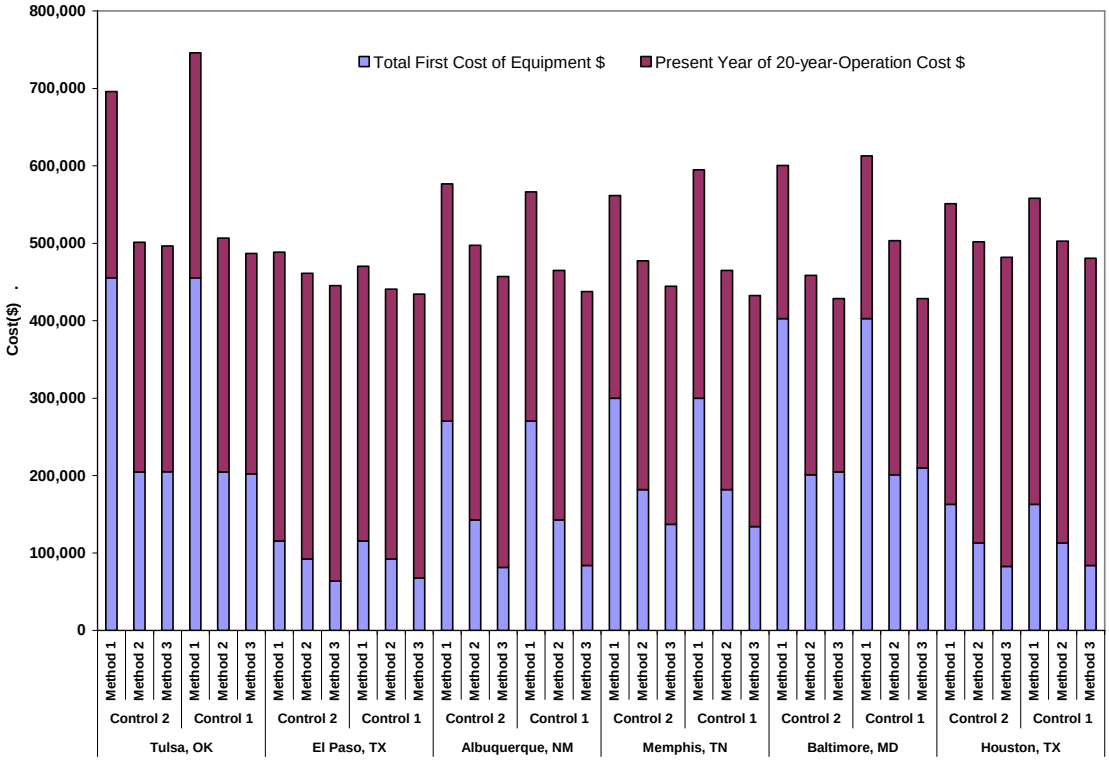

Figure 6.19 HGSHP system life cycle cost in each motel building simulation case

Table 6.10 Summary of energy consumption and fluid temperature for each motel building simulation case

Control Strategy	**Set EFT (Control 2)**			**Set T_{diff} (Control 1)**			**Set EFT (Control 2)**			**Set T_{diff} (Control 1)**		
Design Method	**1**	**2**	**3**	**1**	**2**	**3**	**1**	**2**	**3**	**1**	**2**	**3**
Cities	**Tulsa, OK**						**El Paso, TX**					
Average Annual Energy Consumption Heat Pump (kWh)	281,494	350,710	344,524	322,920	348,124	331,070	421,284	423,341	435,557	381,006	387,261	409,872
Primary Loop Pump (kWh)	17,851	17,852	17,852	17,855	17,847	17,847	22,453	22,453	22,453	22,453	22,453	22,453
Cooling Tower Fan (kWh)	0	242	243	6,152	3,113	1,487	6,350	4,788	5,952	11,889	8,439	8,464
Secondary Loop Pump (kWh)	0	574	576	14,743	7,395	3,708	14,295	9,103	11,320	26,783	16,059	16,105
Total annual energy consumption (kWh)	299,345	369,377	363,195	361,669	376,479	354,112	464,382	459,685	475,283	442,131	434,213	456,893
Average CT run time (hours)	0	513	515	6,590	6,608	6,633	3,834	4,069	5,061	7,182	7,179	7,199
HP EFT Max, 8 years operation (ºC/ºF)	24.1/75.4	34.2/93.6	34.2/93.6	29.8/85.6	32.8/91	36.1/97	36.8/98.2	36.7/98.1	36.9/98.4	30.2/86.4	33.8/92.8	36.1/97
HP ExFT Min, 8 years operation (ºC/ºF)	6.7/44.1	1/33.8	1/33.8	3.2/37.8	1/33.8	1.2/34.2	7/44.6	6.1/43	1.8/35.2	6.2/43.2	5.3/41.5	1.8/35.2
Hours EFT/ExFT out of range in a year	0	5.7	5.7	0	5.7	4.3	0	0	2	0	0	0.7
Cities	**Albuquerque, NM**						**Memphis, TN**					
Average Annual Energy Consumption Heat Pump (kWh)	358,845	415,357	431,505	327,074	364,572	396,506	308,906	349,482	361,512	326,461	323,753	342,459
Primary Loop Pump (kWh)	22,453	22,453	22,453	22,461	22,452	22,452	17,169	17,169	17,169	17,169	17,160	17,160
Cooling Tower Fan (kWh)	42	1,251	4,804	5,615	4,719	7,541	0	523	1,377	8,221	3,929	3,932
Secondary Loop Pump (kWh)	101	2,468	9,131	13,463	9,329	14,344	0	1,039	2,718	15,638	7,831	7,836
Total annual energy consumption (kWh)	381,440	441,529	467,893	368,613	401,072	440,843	326,075	368,213	382,776	367,489	352,674	371,388
Average CT run time (hours)	45	1,655	4,082	6,018	6,257	6,412	0	929	1,823	6,990	6,998	5,256
HP EFT Max, 8 years operation (ºC/ºF)	33/91.4	36/96.8	36.7/98.1	25.9/78.6	35.2/95.4	36.2/97.2	31.5/88.7	33.6/92.5	35/95	31.2/88.2	32.6/90.7	37.3/99.1
HP ExFT Min, 8 years operation (ºC/ºF)	6.9/44.4	5.9/42.6	1.2/34.2	6.9/44.4	5.9/42.6	1.6/34.9	7/44.6	4.2/39.6	1.1/34	4.5/40.1	4/39.2	1.3/34.3
Hours EFT/ExFT out of range in a year	0	0	3.3	0	0	2	0	0	6.3	0	0	5
Cities	**Baltimore, MD**						**Houston, TX**					
Average Annual Energy Consumption Heat Pump (kWh)	234,307	308,600	266,737	241,130	358,189	258,406	437,807	447,434	466,247	429,082	439,184	457,547
Primary Loop Pump (kWh)	12,243	12,245	12,245	12,246	12,243	12,243	17,713	17,713	17,713	17,713	17,713	17,713
Cooling Tower Fan (kWh)	0	18	1	2,136	1,570	771	8,687	6,762	4,503	14,069	9,929	6,338
Secondary Loop Pump (kWh)	0	48	5	6,416	4,278	1,067	19,538	12,849	8,889	31,669	18,878	12,522
Total annual energy consumption (kWh)	16,401	21,602	18,672	16,879	25,073	18,088	30,646	31,320	32,637	30,036	30,743	32,028
Average CT run time (hours)	857	857	857	857	857	857	1,240	1,240	1,240	1,240	1,240	1,240
HP EFT Max, 8 years operation (ºC/ºF)	22.9/73.2	33.5/92.3	35.7/96.3	22.4/72.3	31.4/88.5	32.7/90.9	34.5/94.1	35.5/95.9	42.5/108.5	33.5/92.3	34.7/94.5	42.4/108.3
HP ExFT Min, 8 years operation (ºC/ºF)	5.6/42.1	0.9/33.6	1.4/34.5	1.8/35.2	0.9/33.6	1.5/34.7	9.8/49.6	5.5/41.9	1.7/35.1	9.6/49.3	5.2/41.4	1.7/35.1
Hours EFT/ExFT out of range in a year	0	19	11.3	0.7	20.3	10	0	0	1.7	0	0	1.7

Table 6.11 Summary of Net Present Value and system first costs for each motel building simulation case

Control Strategy	Set EFT (Control 2)			Set T_{diff} (Control 1)			Set EFT (Control 2)			Set T_{diff} (Control 1)		
Design Method	1	2	3	1	2	3	1	2	3	1	2	3
Cities	**Tulsa, OK**						**El Paso, TX**					
Total Length of Loop Installation (m)	21,805	9,715	9,734	21,805	9,715	9,959	3,505	3,001	1,554	3,505	3,001	1,751
Total Cost of Loop Installation ($)	429,344	191,297	191,653	429,344	191,297	196,083	69,017	59,095	30,593	69,017	59,095	34,482
First Cost of Cooling Tower + PHX incl. Control ($)	23,795	12,006	12,006	23,795	12,006	5,713	42,222	29,980	29,980	42,222	29,980	29,980
Cost of Auxiliary Equipment ($)	2,380	1,201	1,201	2,380	1,201	571	4,222	2,998	2,998	4,222	2,998	2,998
Total First Cost of Equipment ($)	455,519	204,504	204,860	455,519	204,504	202,367	115,461	92,073	63,571	115,461	92,073	67,460
Average Annual Operating Cost ($)	19,705	24,550	24,117	22,604	24,369	23,175	29,490	29,634	30,489	26,670	27,108	28,691
Present Year of 20-year-Operation ($)	240,342	296,571	291,607	290,382	302,273	284,314	372,850	369,078	381,602	354,985	348,627	366,837
Present Value of Total Cost ($)	695,861	501,075	496,467	745,901	506,777	486,682	488,311	461,151	445,173	470,446	440,700	434,297
Cities	**Albuquerque, NM**						**Memphis, TN**					
Total Length of Loop Installation (m)	12,402	6,174	2,454	12,402	6,174	2,582	13,548	8,433	5,884	13,548	8,433	6,012
Total Cost of Loop Installation ($)	244,203	121,562	48,319	244,203	121,562	50,840	266,768	166,042	115,856	266,768	166,042	118,376
First Cost of Cooling Tower + PHX incl. Control ($)	23,795	19,225	29,980	23,795	19,225	29,980	29,980	14,310	19,225	29,980	14,310	14,310
Cost of Auxiliary Equipment ($)	2,380	1,922	2,998	2,380	1,922	2,998	2,998	1,431	1,922	2,998	1,431	1,431
Total First Cost of Equipment ($)	270,378	142,709	81,297	270,378	142,709	83,817	299,746	181,783	137,003	299,746	181,783	134,117
Average Annual Operating Cost ($)	25,119	29,075	30,205	22,895	25,520	27,755	21,623	24,464	25,306	22,852	22,663	23,972
Present Year of 20-year-Operation ($)	306,256	354,501	375,669	295,958	322,018	353,951	261,804	295,636	307,329	295,055	283,160	298,185
Present Value of Total Cost ($)	576,634	497,211	456,966	566,336	464,728	437,768	561,550	477,419	444,332	594,801	464,942	432,302
Cities	**Baltimore, MD**						**Houston, TX**					
Total Length of Loop Installation (m)	19,913	9,820	10,346	19,913	9,820	10,458	5,907	4,048	3,119	5,907	4,048	3,187
Total Cost of Loop Installation ($)	392,079	193,352	203,703	392,079	193,352	205,914	116,313	79,713	61,404	116,313	79,713	62,762
First Cost of Cooling Tower + PHX incl. Control ($)	9,504	6,983	689	9,504	6,983	3,428	42,222	29,980	19,225	42,222	29,980	19,225
Cost of Auxiliary Equipment ($)	950	698	69	950	698	343	4,222	2,998	1,922	4,222	2,998	1,922
Total First Cost of Equipment ($)	402,533	201,033	204,461	402,533	201,033	209,685	162,757	112,691	82,552	162,757	112,691	83,909
Average Annual Operating Cost ($)	16,401	21,602	18,672	16,879	25,073	18,088	30,646	31,320	32,637	30,036	30,743	32,028
Present Year of 20-year-Operation ($)	197,954	257,658	223,998	210,301	302,113	218,779	388,396	389,209	399,321	395,452	389,968	396,726
Present Value of Total Cost ($)	600,487	458,690	428,459	612,834	503,146	428,464	551,153	501,900	481,873	558,209	502,659	480,634

6.5.4 Comparison Conclusions and Recommendations

This section provides a comparative study of three HGSHP system design method for commercial applications: a required borehole length difference equation-based method (Kavanaugh and Rafferty method), a temperature limit-optimized simulation-based method (GLHEPRO method), and a life cycle cost-optimized simulation-based method (GenOpt method). An office building and a motel building was used as the test building and modeled using EnergyPlus for six U.S. cities: Tulsa, OK; El Paso, TX; Albuquerque, NM; Memphis, TN; Baltimore, MD; and Houston TX. The HGSHP system is modeled and simulated using the HVACSIM+ modeling environment. Overall system performance was evaluated using a 20-year life-cycle cost analysis.

Some specific conclusions of this study are as follows:

1. In the required borehole length difference equation-based method, the cooling tower was sized by assuming that the fluid was cooled from 35ºC (95ºF) to 29.4ºC (85ºF) with a 25.6ºC (78ºF) wet bulb temperature. In the design procedures of the two simulation-based methods, the cooling tower was sized based on the local outdoor peak wetbulb temperature and the heat pump peak exiting fluid temperature. These methods consistently gave out a smaller cooling tower size.

2. All three HGSHP system design methods presented in this paper gave feasible HGSHP system designs for the office building in the six different climate zones. Although, in some cases, there were a few hours each year in which the

simulated heat pump exiting fluid temperatures exceeded the allowed temperature limits of the heat pump, the temperature would not cause freezing. For different building locations and system control strategies, the three design methods gave different system component sizes.

3. For the Baltimore case, the equation-based method produced both a very large GLHE and cooling tower. When a simulation was performed, it was determined that the cooling tower would never turn on, as the ground loop was more than capable of handling the load. This is a substantial flaw in this particular design method, as it resulted in unnecessary equipment, and therefore a higher total cost.

4. The HGSHP system designed from the life cycle cost-optimized simulation-based method had the minimum system life cycle cost, as anticipated. In most cases, the systems designed with the temperature limit-optimized simulation-based method had a lower system life cycle cost than the systems designed with the required borehole length difference equation-based method, except for the systems in El Paso, TX.

6.6 Conclusions

In this chapter, a design procedure was developed for sizing the HGSHP system components. The design of an HGSHP system has many degrees of freedom and there are many possible configurations of HGSHP systems. Therefore, in this chapter, the configurations of HGSHP systems were investigated firstly. In HGSHP systems, the

GLHE and PHE/cooling tower can be placed in serial or in parallel. However, preliminary testing has shown that there are a large number of scenarios where the serial connection is infeasible. Therefore, in this research, a parallel-connected HGSHP system is investigated.

In HGSHP systems, variable flow pumping system will likely be utilized save pumping energy. When the system flow rate varies, the distribution of flow to GLHE and PHE/cooling tower may also change. A strategy for controlling the distribution of flow between GLHE and PHE/cooling tower was developed. This flow distribution control strategy is physically feasible. Applying this flow distribution control strategy, flow is able to pass through each component without requiring excessive pumping power.

A new design procedure, implemented in GLHEPRO, was developed for sizing the HGSHP system components. The new design procedure is capable of being used for both a new HGSHP and a "retrofit" HGSHP system. For a new HGSHP system, GLHEPRO gives out the size of GLHE and open-circuit cooling tower simultaneously. For designing a "retrofit" HGSHP with giving GLHE size, GLHEPRO gives out the required capacity of the cooling tower, which is added into the system to help meet loads of the system.

In Kavanaugh's (1998) design procedure, the cooling tower is sized at the nominal design conditions: the cooling tower capacity as the flow rate of water cooled from 35ºC (95ºF) to 29.4ºC (85ºF) with a 25.6ºC (78ºF) wet bulb temperature. This cooling tower design procedure will tend to oversize the cooling tower/fluid cooler because of a possibly higher entering fluid temperature and a possibly lower local peak

wetbulb temperature. In this chapter, a new algorithm was developed to size cooling towers based on the local peak wetbulb temperature and the peak ExFT of heat pump. This procedure gives a much smaller cooling tower size than that from Kavanaugh (1998) design procedure.

An example of design a HGSHP system for a cooling dominated office building in Tulsa, OK, was presented in this chapter. Three different systems were designed for office building: 1) 100% GSHP system; 2) a new HGSHP system; and 3) a "retrofit" HGSHP with given GLHE size.

A comparative study of three hybrid ground source heat pump system design procedures is presented. The three design procedures are: the Kavanaugh and Rafferty (1997) procedure, the new procedure developed in this chapter and the GenOpt design procedure. An actual office building and a motel building is used as the test building and modeled using EnergyPlus for six U.S. cities: Tulsa, OK; El Paso, TX; Albuquerque, NM; and Memphis, TN. The HGSHP system is modeled and simulated using the HVACSIM+ modeling environment. Overall system performance was evaluated using a 20-year life-cycle cost analysis. In general, the HGSHP designed from the new GLHRPRO design procedure would have a smaller GLHE and cooling tower size and a smaller system initial cost and the life cycle cost than the system designed from the Kavanaugh and Rafferty procedure.

7 INVESTIGATION AND OPTIMIZATION OF HGSHP SYSTEM CONTROLS

In this chapter, controls of HGSHP systems will be investigated. The study aims to develop generally applicable optimal control strategies. Three different building types and 16 U.S. cities are chosen to provide different building load profiles for the investigation of HGSHP system controls. Firstly, three control strategies previously developed (Yavuzturk and Spitler 2000) will be optimized. Optimal setpoints of the three control strategies are investigated to try to find common setpoint values which are generally applicable for all HGSHP systems. Then a range of new control strategies will be investigated for HGSHP systems. Two current ideas to be tested are described in Section 7.4. Finally, recommendations about generic control strategies for HGSHP systems will be presented.

7.1 Test Buildings and cities

For the purpose of estimating control strategies of HGSHP systems under different conditions, different building types and building locations are chosen to provide different building loads profile.

Test building types will include:

- Office building
- Motel building

7.1.1 Office Building

The test office building was based on a typical floor plan from the Bank of Oklahoma (BOK) Tower in Tulsa, OK. The office building is 52 stories, of which only three stories with 7,144m^2 are modeled for this work. The building glazing area is 60%-70% of the exterior envelope. More details about the BOK building are readily available in Feng's M.S. thesis (1999).

Each of the three floors has ten zones, 6 perimeter zones and 4 core zones. The building was modeled and simulated using DesignBuilder (DesignBuilder 2006) and EnergyPlus by Gentry (2007). The following assumptions have been used to determine the annual building loads.

- Office occupancy of 1 person per 5 m^2 (54 ft^2).
- Equipment heat gains of 10 W/m^2 (0.9 W/ft^2).
- Lighting heat gains of 13.13 W/m^2 (1.18 W/ft^2).
- Minimum fresh air per person of 9.4 L/s-person (20 ft^3/min-person).
- Infiltration of 0.5 ACH.

- Day time (7am-6pm, Monday-Friday), night time and weekend thermostat setting are specified for each zone. During the day, the temperature set point is 20.0 ºC (68 ºF) for heating and 24 ºC (75.2 ºF) for cooling. A night and weekend setback has been set for 5 ºC (41 ºF) for heating and 30 ºC (86 ºF) for cooling.

The calculated office building loads for El Paso, TX are shown in Figure 7.1. Additional results for other locations are available in Appendix B.

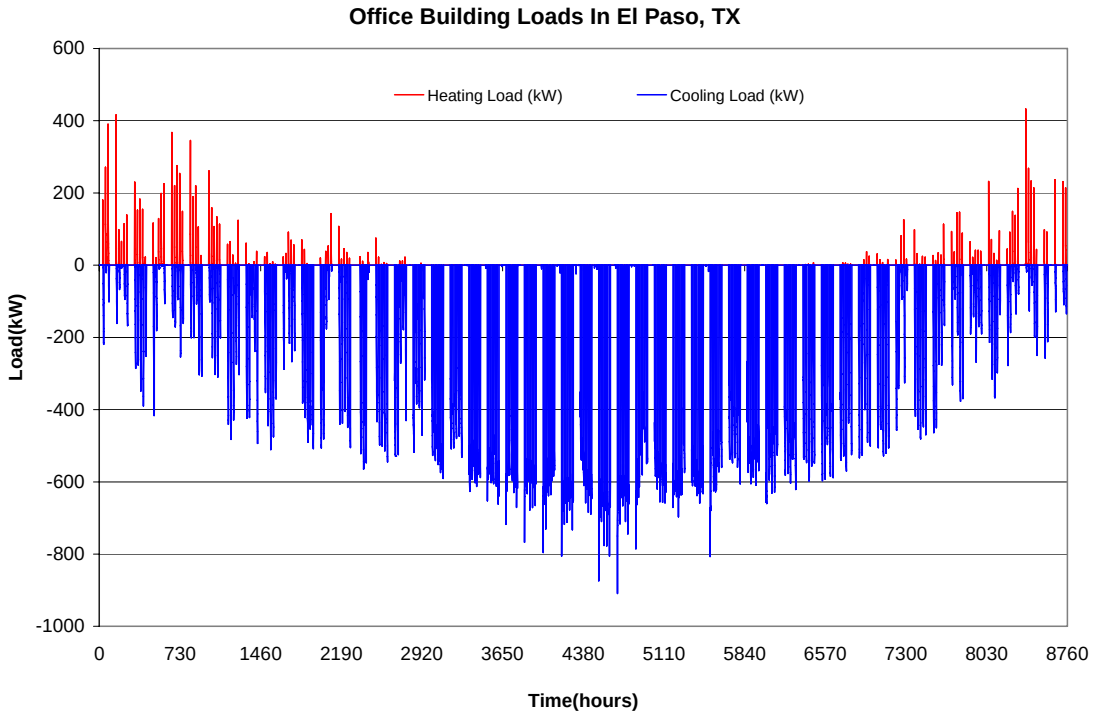

Figure 7.1 Office building loads for El Paso, TX.

7.1.2 Motel Building

The test motel building was based on an actual motel in Tulsa, Oklahoma as described by Chen (1996). The motel building is a 2-story building with 1,037m^2. For this research a building with a load ranging from 100 to 500-tons was desired. Therefore the motel building was modeled as three identical buildings having ten floors with the same floor plan by Gentry (2007). (This did not include the swimming pool in Chen's (1996) motel) The building was modeled and simulated using DesignBuilder (DesignBuilder 2006) and EnergyPlus (Gentry 2007). The following assumptions have been used to the annual building loads calculation.

- Motel occupancy of 1 person per 36.23 m^2 (390 ft^2).
- Equipment heat gains of 3.33 W/m^2 (0.3 W/ft^2).
- Lighting heat gains of 7.76 W/m^2 (0.7 W/ft^2).
- Minimum fresh air per person of 7 L/s-person (15 ft^3/min-person).
- Infiltration of 0.2 each.
- Thermostat settings are specified for each zone. The temperature set point is 20.0 ºC (68 ºF) for heating and 24 ºC (75.2 ºF) for cooling. There is no setback.

The calculated motel building loads for Tulsa, OK are shown in Figure 7.2. Motel building loads in other locations are available in Appendix B.

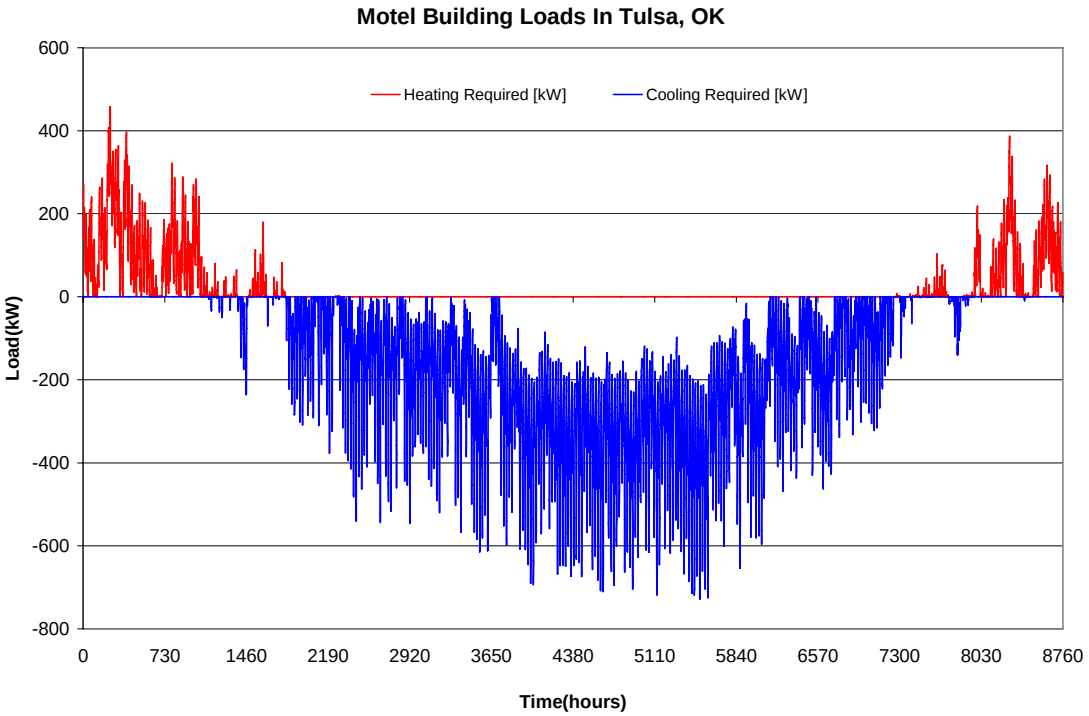

Figure 7.2 Motel building loads for Tulsa, OK.

7.1.3 Test Cities

Briggs et al. (2002) presented climate classification for building energy codes and standards on the basis of heat degree days, cooling degree days, and humidity. Figure 7.3 shows a map of the climate zone of the U.S. and Table 7.1 gives their description. Of the 17 climate zones, representative cities are given for those 15 zones that exist within the U.S.

It should be noted that the main objective of this research is to investigate and optimize HGSHP systems control strategies. Specifically, this means a control strategy for operation of the supplemental heat rejecter. Therefore, only those cities in which the buildings are cooling constrained will be chosen for the investigation of controls. After

the load investigation, GSHP system design investigation, 5 cities together with Tulsa, OK, in total 6 cities, are chosen for the study of control strategies of HGSHP system. The six cities are: Tulsa, OK; El Paso, TX; Albuquerque, NM; Memphis, TN; Baltimore, MD; and Houston, TX. The office building and motel building in Miami, FL. and Phoenix, AZ has little demand for heating. For these two climate zones, a water loop heat pump system would be a better choice than the HGSHP system.

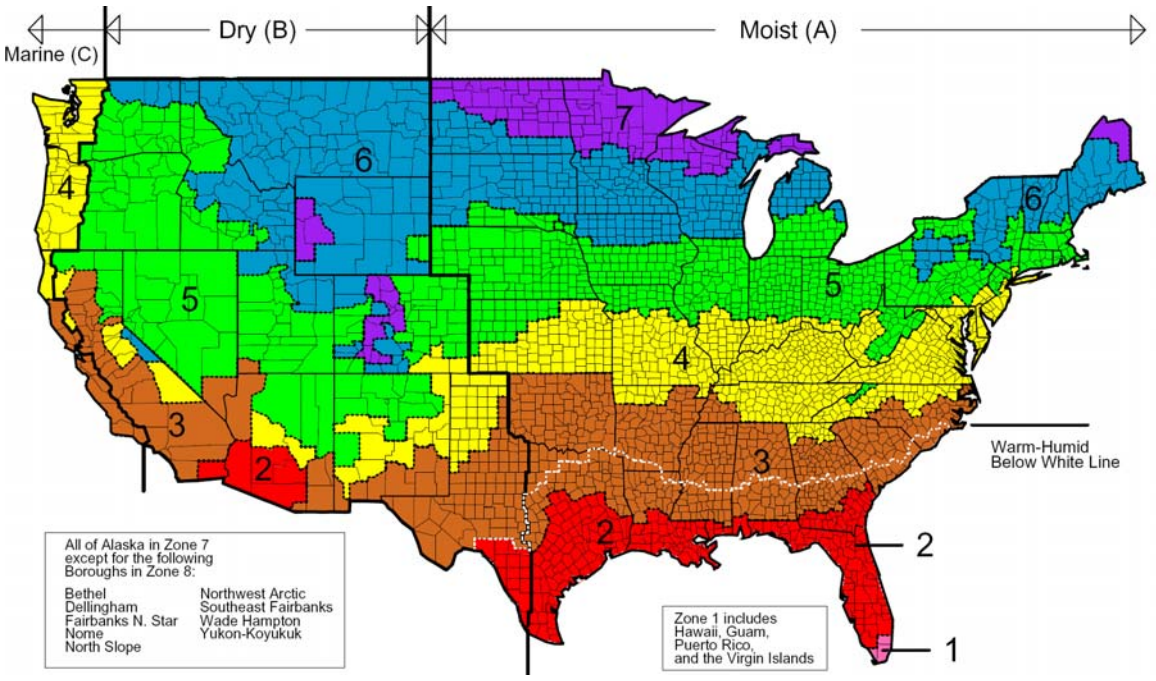

Figure 7.3 Map of Briggs et al.'s proposed climate zones (2002).

Table 7.1 Description of climate zones (Briggs et al. 2002)

Zone No.	Climate Zone Name and Type	Representative U.S. City
1A	Very Hot-Humid	Miami, Fl
1B	Very Hot-Dry	- - -
2A	Hot-Humid	Houston, TX
2B	Hot-Dry	Phoenix, AZ
3A	Warm-Humid	Memphis, TN
3B	Warm-Dry	El Paso, TX
3C	Warm-Marine	San Francisco, CA
4A	Mixed-Humid	Baltimore, MD
4B	Mixed-Dry	Albuquerque, NM
4C	Mixed-Marine	Salem, OR
5A	Cool-Humid	Chicago, IL
5B	Cool-Dry	Boise, ID
5C	Cool-Marine	- - -
6A	Cold-Humid	Burlington, VT
6B	Cold-Dry	Helena, MT
7	Very Cold	Duluth, MN
8	Subarctic	Fairbanks, AK
3A	Warm-Humid	Tulsa, OK

7.2 Methodology

Yavuzturk and Spitler (2000) developed three control strategies for HGSHP system, including set point control, set temperature difference control and "preset schedule control". Optimization of these three control strategies has not been investigated and the best set point values for these control strategies are unknown. Therefore, these control strategies might or might not be generally applicable for all HGSHP systems. Therefore, additional control strategies will be developed and investigated.

In this section, a general approach has been developed to optimize the best set point value of the candidate control strategy. The general procedure is as follows:

1. Choose a candidate control strategy.

This could be any control strategy with setpoints to be determined.

2. Optimize the setpoints for a range of building types and climates.

Using the buffer program developed in this chapter, the optimization program searches to find the best setpoint values for the candidate control strategy with different combinations of the HGSHP system designs, building types and climates.

3. Formulate generic control strategy

The results from step 2 are reviewed. A generic control strategy, i.e. based on a single set of setpoints for all system variations/buildings/climates, is sought. Alternatively, two or three sets of setpoints might be utilized, if the choice of which set to use can be readily correlated to climate or chosen based on other objective criteria. The generic control strategy is not expected to perform as well as the individually-optimized setpoints developed in step 2. However, what is sought is a control strategy with generic setpoints for which the performance approaches that of the individually-optimized setpoints. It is expected that some control strategies, e.g adaptive control strategies, will be more suitable as generic control strategies than others.

4. Test the generic control strategy against the individually-optimized control strategies.

For a range of system variations/buildings/climates, the performance of the generic control strategy will be compared against the performance of the

individually-optimized control strategy. Generic control strategies that compare favorably to the individually-optimized control strategies may be recommended for use. It is expected that the insights gained will lead to synthesis of new candidate control strategies and the process will be repeated, starting with step 1.

7.2.1 Different HGSHP System Designs

The main objective of this research is to investigate and optimize HGSHP systems control strategies. Specifically, this means a control strategy for operation of the supplemental heat rejecter. However, the design of the HGSHP system has an impact on both HGSHP system performance and the control strategy. Therefore, in the investigation of HGSHP system control strategies, the influence of different HGSHP system designs will be considered.

For a new HGSHP system, a properly-sized GLHE and cooling tower will be designed. In some existing GSHP systems, a larger size of GLHE than that of new HGSHP system is designed but it can not meet the cooling loads of the system. Therefore a supplemental cooling tower is added into the system to help meet the loads of the system, which is referred to as a "retrofit design". Both the new HGSHP system and "retrofit design" HGSHP system work well but they have different sizes of GLHE. For sizing the cooling tower, Kavanaugh's design procedure (1998) tends to oversize the cooling tower and the new version of GLHEPRO gives out a smaller size of cooling tower that that from Kavanaugh's design procedure. More details about sizing the GLHE and cooling tower are given in Chapter 4.

Therefore, in this research, HGSHP systems with combination of different sizes of GLHE and cooling tower are designed for investigation of control strategy. The different combinations represent designs of new systems with Kavanaugh's procedure and the new GLHEPRO procedure and designs of "retrofit" systems with different amount of GLHE undersizing.

In practice, a new HGSHP system with shortest size of GLHE and a "retrofit design" HGSHP system with a larger size of GLHE are used. The GLHE size of the "retrofit design" HGSHP system, $L_{retrofit}$, is determined from the GLHE size of a new HGSHP system and the GLHE size of a GSHP system.

$$L_{retrofit} = \frac{1}{2}(L_{\max} + L_{\min}) \qquad 7\text{-}1$$

Where:

$L_{\min}$ = The minimum length of GLHE, which is calculated from a new HGSHP system, (m);

$L_{\max}$ = The maximum length of GLHE, which is calculated from a GSHP system, (m).

For each size of GLHE, two different sizes of cooling tower are designed. One cooling tower is sized from the new procedure described in Section 6.3.4 and the other cooling tower is sized from Kavanaugh's design procedure. Therefore, for a particular building type and location, four different HGSHP systems are designed for the investigation of the control strategies, which are listed in Table 7.2.

Table 7.2 HGSHP systems with different sizes of GLHE and cooling tower

System Case	GLHE size	Cooling tower Size
A	$L_{\min}$	CT_{New} for $L_{\min}$
B	$L_{\min}$	CT_{Kava} for $L_{\min}$
C	$L_{\max}$	CT_{New} for $L_{\max}$
D	$L_{\max}$	CT_{Kava} for $L_{\max}$

7.2.2 Methodology for Optimizing Control Strategies

An approach has been developed to optimize the best set point values of the candidate control strategies for the three building types in 16 U.S. locations. There are three main components of the optimization methodology:

1. Buffer Program
2. HVACSIM+
3. GenOpt

A "buffer program", an interface between GenOpt (Wetter 2000) and HVACSIM+ is developed for these three control strategies. For each of the specified HGSHP systems, the three programs would automatically adjust the parameter values (setpoint values), run the simulation and iterate to get the minimal operation cost of the HGSHP system. The three work together as shown below in the flow diagram in Figure 7.4. Each of the three main optimization components will be discussed in mode detail in the following sections.

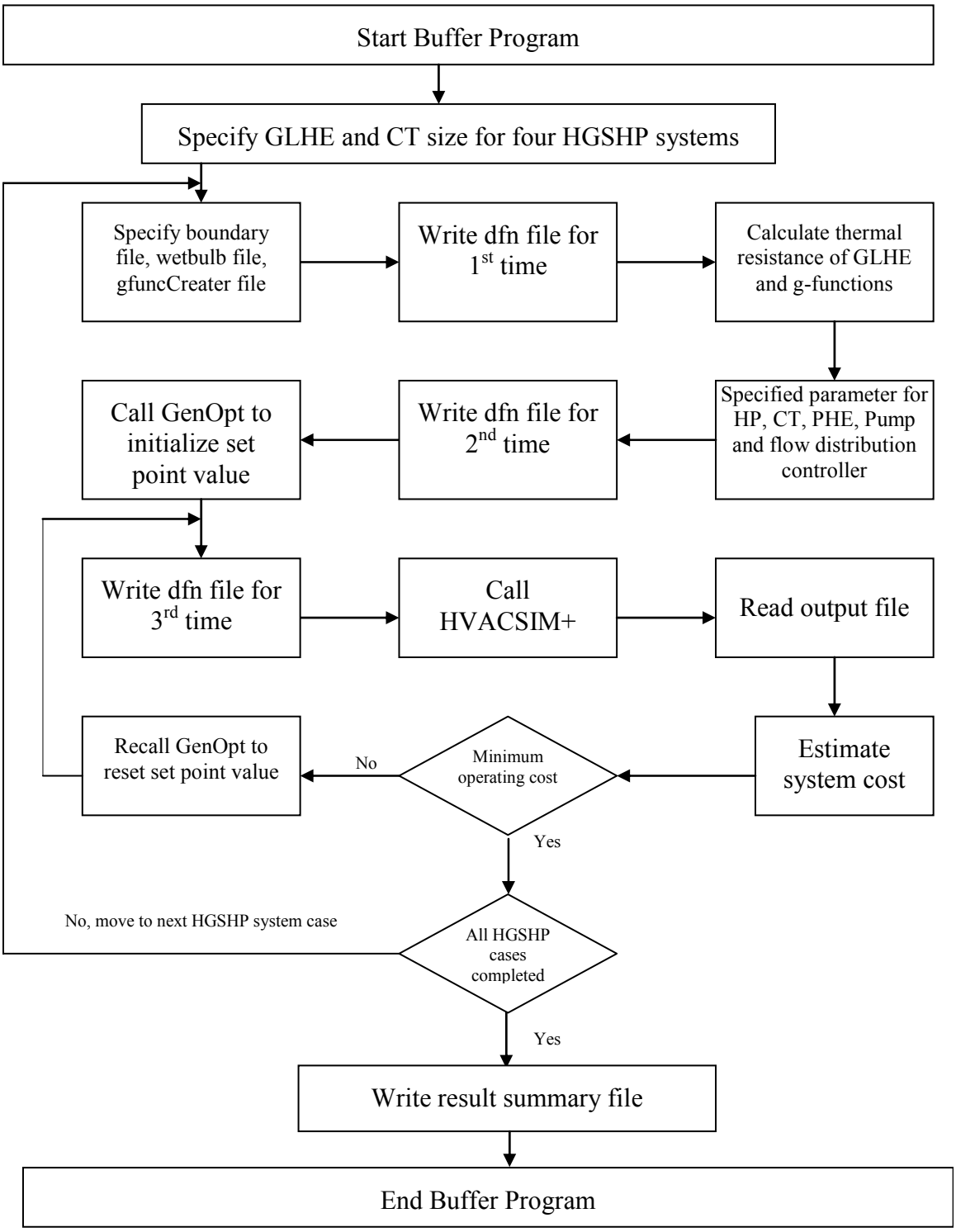

Figure 7.4 Optimization methodology flow diagram.

7.2.3 HVACSIM+

The HVACSIM+ HGSHP system model is comprised of six different component models that are connected together to form a HGSHP system. The component models are listed below along with the section number where more detailed information can be found on each model.

1. GLHE model – Section 4.1.7.

2. Heat pump model – Section 4.2.2.

3. Open-circuit cooling tower model – Section 4.3.1.1.

4. Main loop variable speed circulation pump model – Section 4.4.2.

5. Secondary loop variable speed circulation pump model – Section 4.4.1.

6. Plate frame heat exchanger model – Section 4.5.2.

The HVACSIM+ model was formed from the HGSHP schematic that is shown in Figure 6.1, and is discussed in more details in Chapter 4.

In order to perform a simulation for a specified HGSHP system, building type, location and control strategy, HVACSIM+ needs five files:

1. Input file (INPUTFILE.dat), which specified the names of the boundary file, definition file and output file.

2. The boundary file (*.bnd), which contains site-specified weather data and building site-specified heating and cooling loads.

3. The definition file (*.dfn), which describes the system configuration and parameter site-specific parameter values.

4. The wetbulb temperature file (Wetbulb.txt), which contains site-specified outdoor air wetbulb temperature and is used for the variable time step scheme for the multiyear simulation in Section 4.7.1.

5. The timestep file (TIMESTEP.txt), which contains information about the variable time step scheme for the multiyear simulation in Section 4.7.1.

All these five files are created by buffer program for each HGSHP system, building type, location and control strategy. Details are presented in Section 7.2.5.

7.2.4 GenOpt

GenOpt (Wetter 2000), a generic optimization program, minimizes an objective function by adjusting the interested parameters. GenOpt can be coupled to any simulation program that has text-based I/O. Khan (2004) utilized GenOpt (Wetter 2000) coupled with HVACSIM+ to optimize the design of GSHP system. In this research, GenOpt (Wetter 2000), coupled with HVACSIM+, is used to optimize the setpoint of the three control strategies for each building type and each location.

In GenOpt, the Nelder Mead ONeill algorithm is used to optimize the setpoint of the three control strategies. More details about the optimization algorithms are available in Wetter (2000).

The way that GenOpt works together with the buffer program and HVACSIM+ is presented in the next section.

7.2.5 Buffer Program

The "buffer program" is an interface between GenOpt (Wetter 2000) and HVACSIM+ and runs the optimization for these three control strategies automatically, as shown in Figure 7.5.

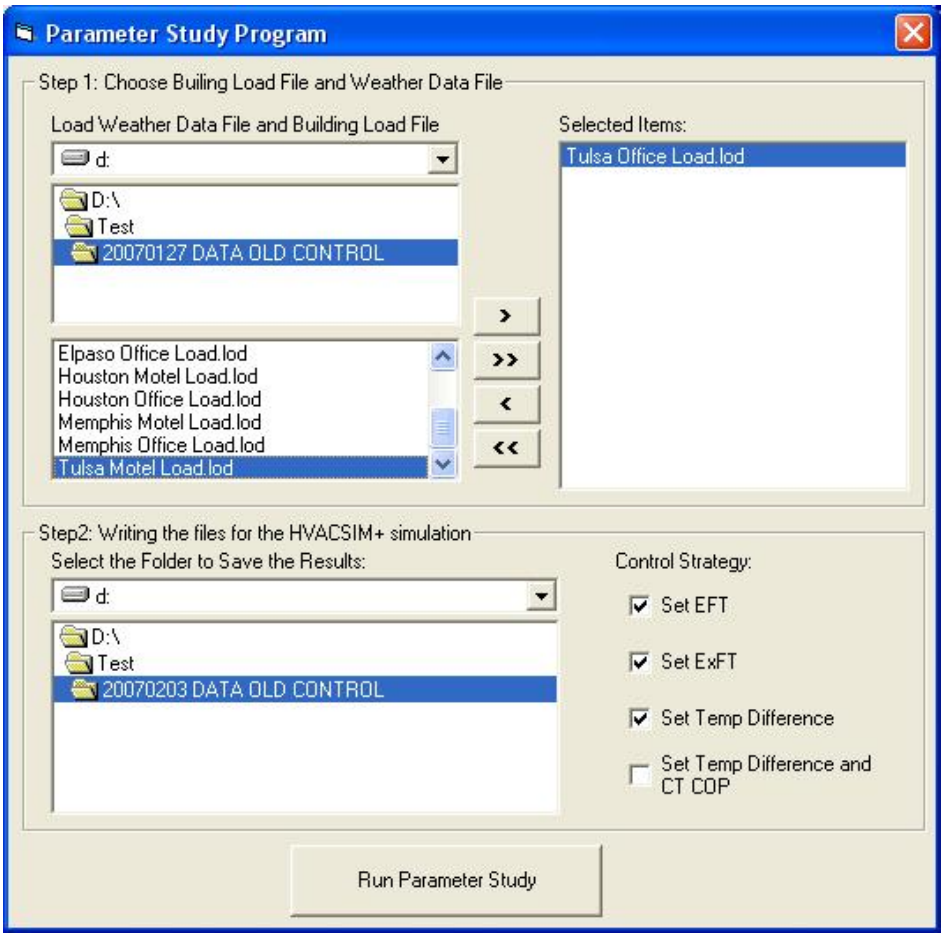

Figure 7.5 Buffer program dialog box.

As illustrated in Figure 7.4, the procedure of the buffer program is described as follows:

1. For the building type and location, the buffer program designs four HGSHP systems with combination of different sizes of GLHE and cooling tower. Details are available in Section 7.2.1. For each HGSHP, all the selected control strategies will be applied. Here, three control strategies will be investigated: 1) set EFT; 2) set ExFT; and 3) set T_{diff}.

2. For each building type, location and the specified control strategy, the buffer program generates three files: 1) the wetbulb temperature file; 2) boundary file; and 3) gfuncCreater file. The first two files are required for running an HGSHP system simulation in HVACSIM+. The gfuncCreater.dat file contains the information of the GLHE and will be read by the buffer program to calculate the thermal resistance of borehole and g-functions of the GLHE without calling GLHEPRO. This is calculated in Step 4.

3. Update the dfn file from a template file for the first time. In the dfn file, the size of GLHE and cooling tower is updated.

4. For each HGSHP system with the specified size of the GLHE, the buffer program calculates the thermal resistance of boreholes and the g-functions of GLHE. The required GLHE information is read from the gfuncCreater.dat file from Step 2. Details about the calculation of the thermal resistance of boreholes and the g-functions of the GLHE are available in Section 4.1.

5. For each HGSHP system, the buffer program calculates the parameters for heat pumps, cooling tower, plate frame heat exchanger, circulation pumps and flow distribution controller. Details are available in Chapter 4.

6. Update the dfn file for the second time. In the dfn file, the parameters of GLHE, heat pumps, cooling tower, plate frame heat exchange, circulation pumps and flow distribution controller will be updated. Till now, all the

parameters of the HGSHP system are ready except for the set point value of the selected control strategy.

7. Call GenOpt to initialize the set point value of the selected control strategy.

8. Update the dfn file for the 3rd time. In the dfn file, the set point value of the selected control strategy will be updated.

9. Call HVACSIM+ to run the HGSHP system simulation.

10. Read the simulation result file.

11. Estimate the HGSHP system operating cost by the buffer program. The system operation cost is calculated with the electricity price of $0.08/kW-hr. Then the system operation cost is written to a file, which will be read by GenOpt.

12. GenOpt reads in the objective function (the system operating cost) to judge whether the convergence (the smallest system operating cost) is reached or not. If the convergence is not reached, GenOpt will generate the new parameter (the setpoint value). And then go to Step 8 to rerun the simulation. If the convergence is reached, go to the next step.

13. If all the cases are optimized, go to the next step. If not, go to Step 2 to run the other cases.

14. After all the cases are optimized, the buffer program will read the results of all case and write a summary report file.

In order to run the optimization for a specified building type, location and control strategy, the buffer program needs six files.

1. “Building loads.lod” file, which contains the annual hourly heating and cooling loads of the specified building type and location.

2. “Weather.dat” file, which contains the selected local weather data.

3. “HGSHP basic size.dat” file, which contains the design results of a new HGSHP system and a GSHP system for the specified building type and location. Details about the design procedure are available in Chapter 6.

4. “PipeAndPumping.txt” file, which contains information of the specified HGSHP system layout, pipe and system flow for the specified building type.

5. “TowerAndPHE.txt” file, which is a database of cooling tower and plate frame heat exchanger. The database is calculated from the cooling tower and plate frame heat exchanger manufacturer’s catalog data.

6. “SystemData.dat” file, which contains the file name needed to run the buffer program. Also the file has the information about the variable names that are required for estimating the system operation cost.

In this section, the buffer program, which couples GenOpt and HVACSIM+, has been developed to optimize three control strategies for the HGSHP system designs, building types and locations. Using the buffer program, the best setpoint value of each

control strategy for each specified HGSHP system, building types and location are obtained automatically without manually setting up and running the simulations.

7.3 Investigation of Previously Developed Control Strategies

Using the buffer program, the best setpoint value of preciously developed (Yavuzturk and Spitler 2000) control strategy for each specified HGSHP system, building types and location are obtained. Based on the investigation, the author will try to find whether there is a common setpoint value which is generally applicable for all HGSHP systems. If so, generally applicable control strategies would be developed for all HGSHP systems.

Two building types and six cities have been used for the investigation of the three control strategies. For each building types and location, four different HGSHP systems with combination of different size of the GLHE and the cooling tower were designed. The study cases are listed in Table 7.3.

The three controls to be investigated are: heat pumps EFT, heat pumps ExFT, and the temperature difference between ExFT and the ambient wet-bulb temperature. A dead band of 1ºC was used for these three controls. E.g. if the objective (temperature or temperature difference) exceeds the setpoint value, the cooling tower turns on; if the objective (temperature or temperature difference) is lower than the setpoint value minus the dead band, the cooling tower turns off. Also for each HGSHP system, a heat pump EFT of 32.2ºC (90ºF) is used to control the cooling tower, which is referred as the base

case. The annual system operation cost with optimized control strategy is then compared to the base case.

Table 7.3 HGSHP systems with different sizes of GLHE and cooling tower

Building Type and Location	System Design Case	Office Building		Motel Building	
		GLHE size (m)	Cooling tower Size (Model)	GLHE size (m)	Cooling tower Size (Model)
Tulsa	A	8,606	ACT-50	9,716	ACT-10
	B	8,606	ACT-100	9,716	ACT-14
	C	11,408	ACT-30	14,712	ACT-8
	D	11,408	ACT-50	14,712	ACT-10
Albuquerque	A	8,092	ACT-9	6,174	ACT-11
	B	8,092	ACT-14	6,174	ACT-16
	C	11,302	ACT-7	13,124	ACT-9
	D	11,302	ACT-10	13,124	ACT-13
El Paso	A	4,744	ACT-14	3,000	ACT-15
	B	4,744	ACT-19	3,000	ACT-20
	C	13,616	ACT-10	15,892	ACT-12
	D	13,616	ACT-15	15,892	ACT-15
Memphis	A	7,974	ACT-12	8,432	ACT-11
	B	7,974	ACT-15	8,432	ACT-14
	C	12,586	ACT-9	14,748	ACT-9
	D	12,586	ACT-11	14,748	ACT-10
Baltimore	A	8,774	ACT-7	9,820	ACT-8
	B	8,774	ACT-11	9,820	ACT-12
	C	10,568	ACT-5	12,756	ACT-6
	D	10,568	ACT-8	12,756	ACT-9
Houston	A	5,232	ACT-14	4,048	ACT-15
	B	5,232	ACT-20	4,048	ACT-19
	C	15,927	ACT-10	20,976	ACT-12
	D	15,927	ACT-15	20,976	ACT-15

Run the buffer program, the setpoint of the applied control strategy for each HGSHP system was optimized and a minimum system operation cost was obtained. The annual operation costs of all cases are shown below. Figure 7.6, Figure 7.7 and Figure 7.8

shows system annual operation costs for the office building in Tulsa, Albuquerque, El Paso, Memphis, Baltimore and Houston.

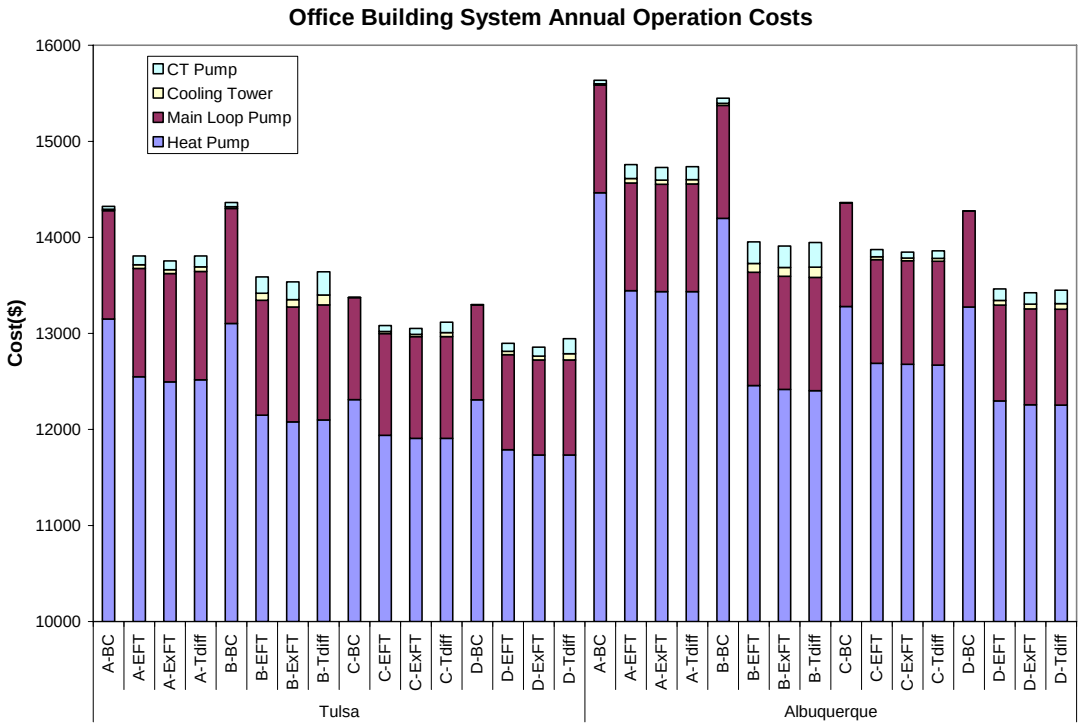

Figure 7.6 Office building system annual operation cost in Tulsa and Albuquerque.

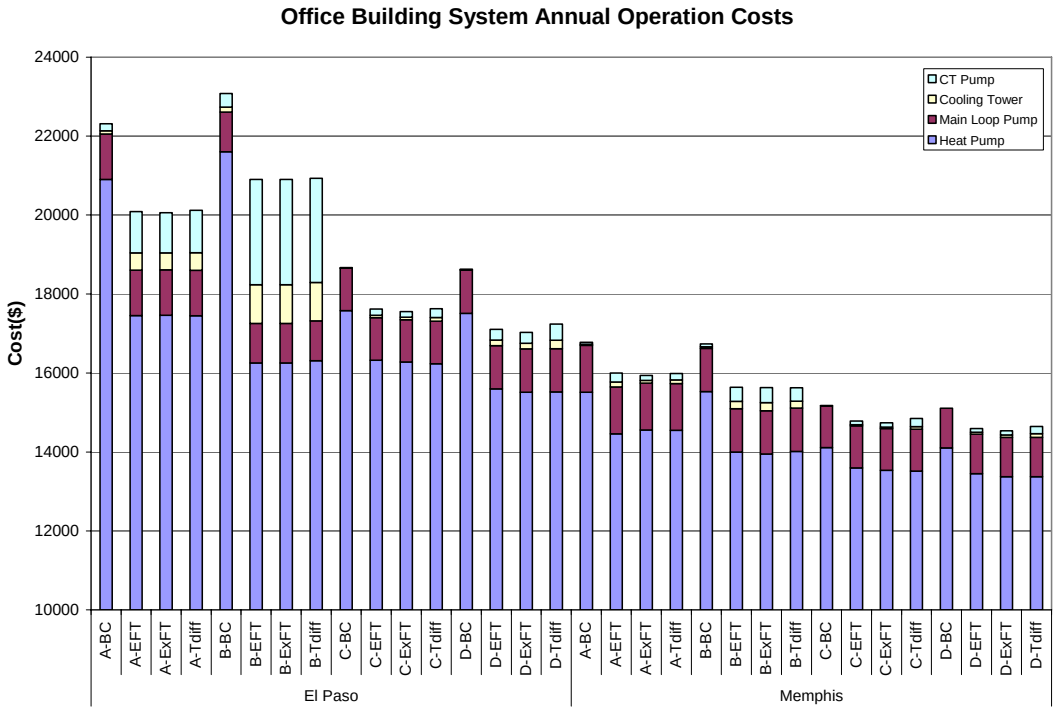

Figure 7.7 Office building system annual operation cost in El Paso and Memphis.

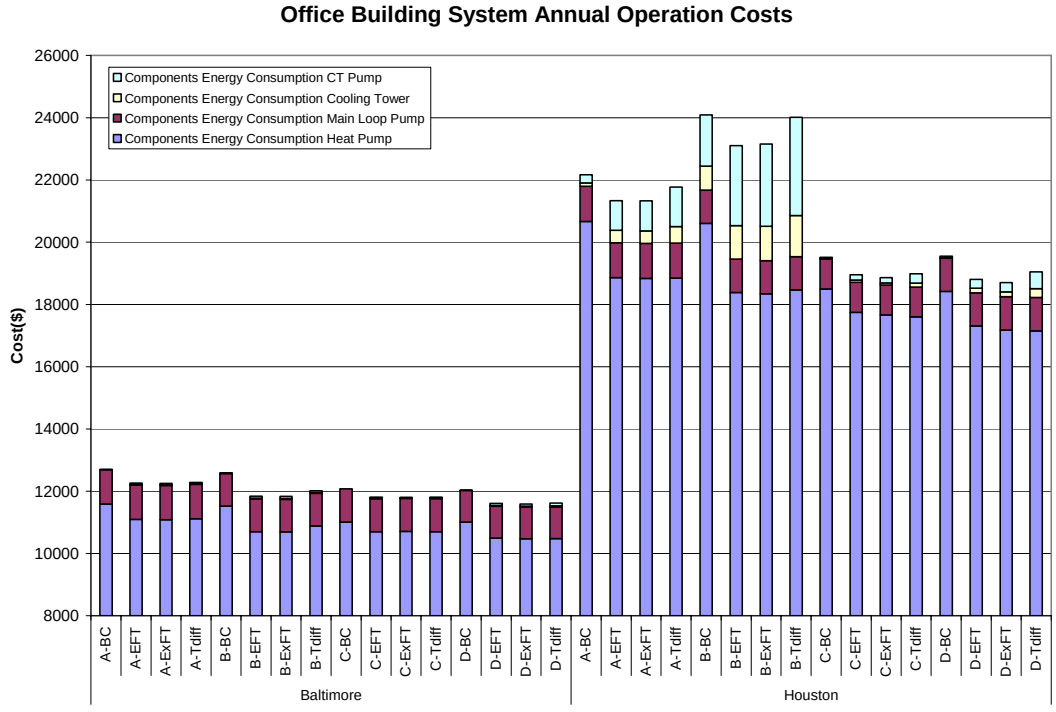

Figure 7.8 Office building system annual operation cost in El Paso and Memphis.

The annual system operation cost savings are shown in Figure 7.9 showing the annual system operation cost savings compared to the base case results. These results will be discussed after the motel results are presented.

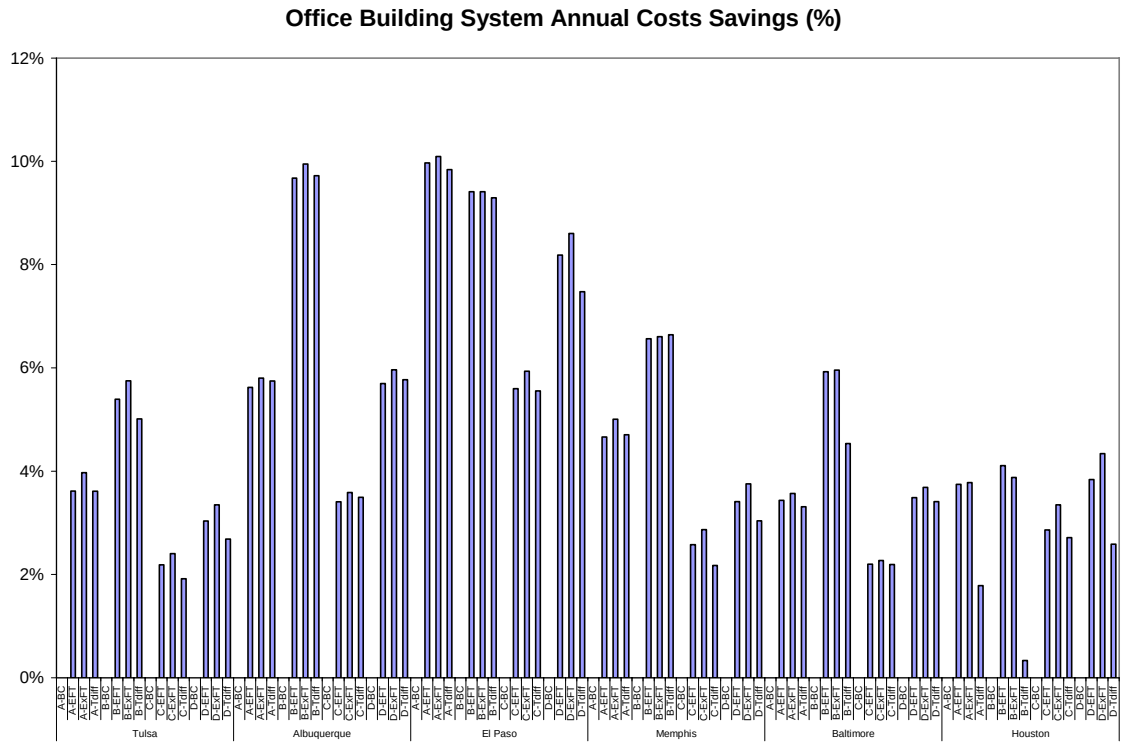

Figure 7.9 Annual operation cost saving for the office building (old controls).

Figure 7.10, Figure 7.11 and Figure 7.12 shows system annual operation costs for the motel building in Tulsa, Albuquerque, El Paso, Memphis, Baltimore and Houston.

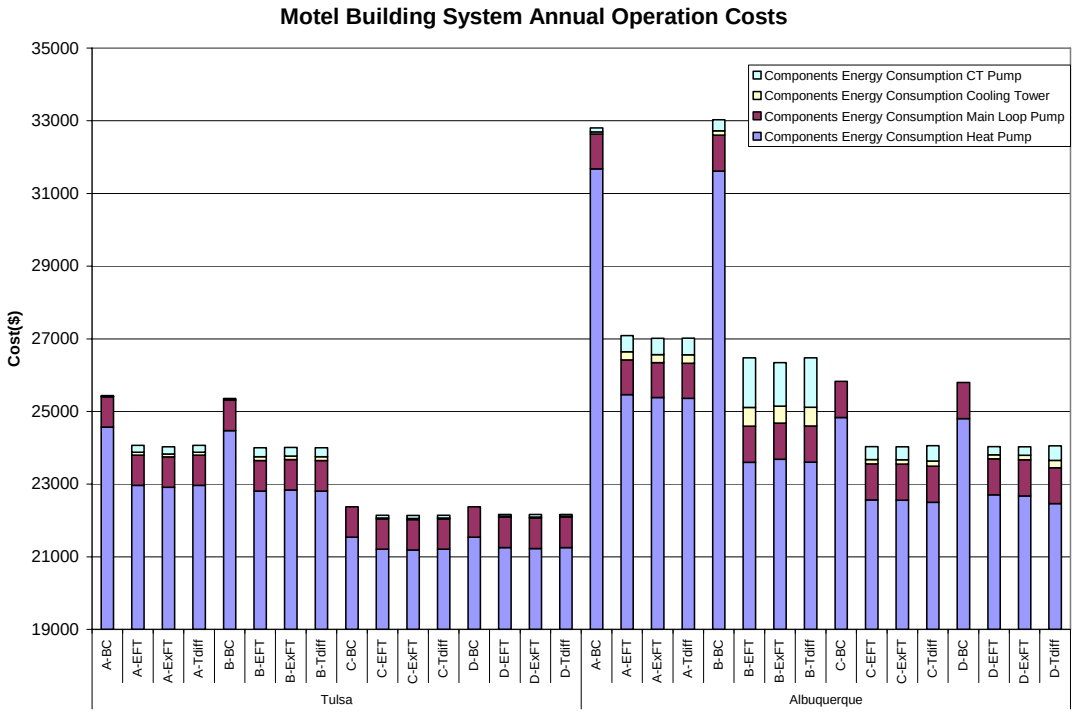

Figure 7.10 Motel building system annual operation cost in Tulsa and Albuquerque.

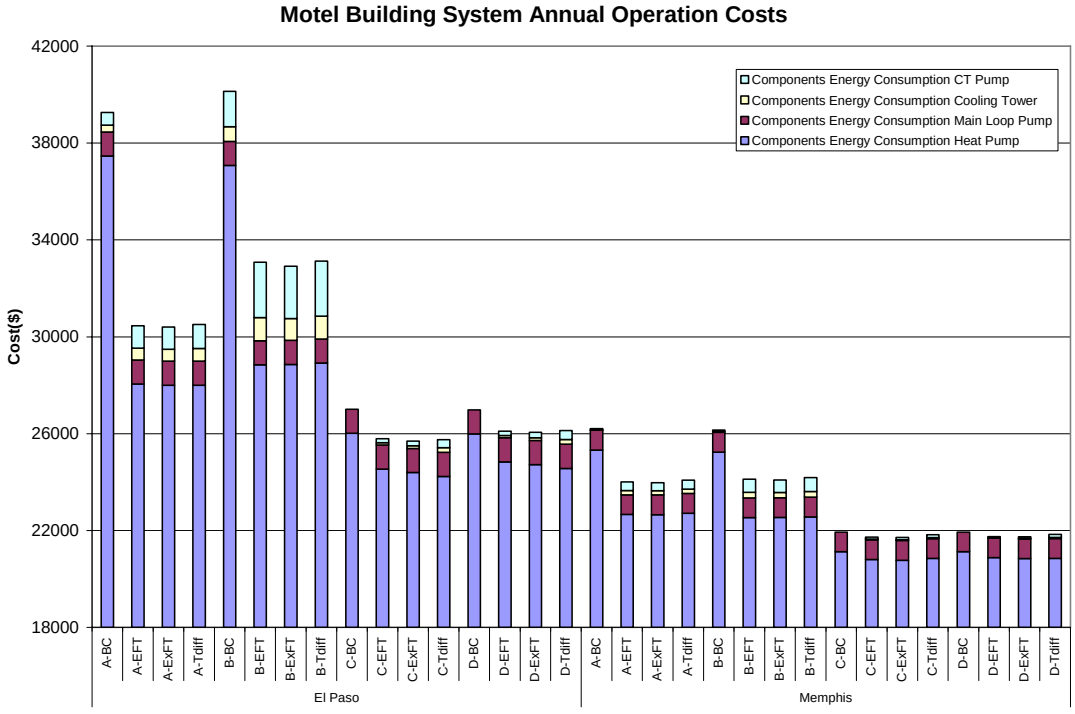

Figure 7.11 Motel building system annual operation cost in El Paso and Memphis.

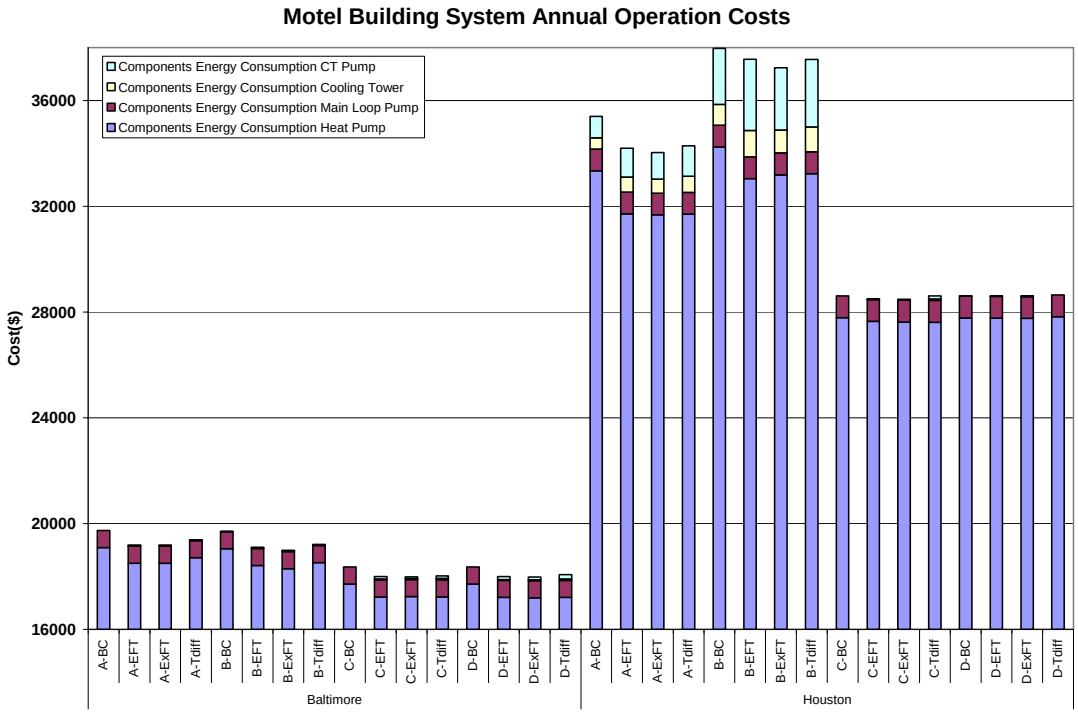

Figure 7.12 Motel building system annual operation cost in Baltimore and Houston.

The annual system operation cost savings are shown in Figure 7.13 showing the annual system operation cost savings compared to the base case results.

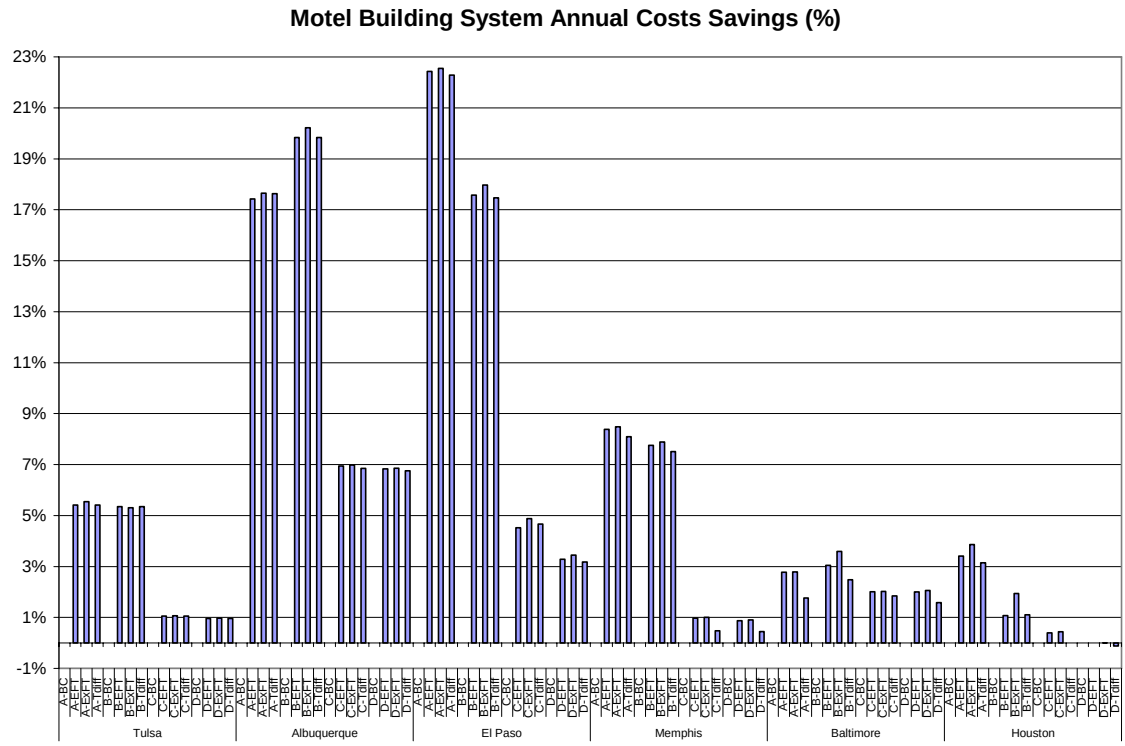

Figure 7.13 Annual operation cost saving for the motel building (old controls).

As can be seen in Figure 7.6-7.8 and Figure 7.10-7.12, for the cases with the same system design, the HGSHP systems with three optimized control strategies have almost the same operating cost. The set T_{diff} control strategy did not show any significant saving compared to the set EFT and ExFT control strategies when they were optimized. Some cases with the set T_{diff} control strategy even had a higher operation cost than the base case. However, the set T_{diff} control strategy depends on an accurate measurement of the wetbulb temperature, which is problematic. Therefore, the set T_{diff} control strategy would be not recommended if the optimized setpoint values for the other control strategies are available.

In Figures 7.6-7.8 and Figures 7.10-7.12, for the cases with the different system designs, the HGSHP systems with a relatively larger GLHE size and a relatively larger cooling tower size would have a relatively lower operation cost. However, these HGSHP systems have a relatively higher first cost.

In Figure 7.9 and Figure 7.13, compared to the base case with a control strategy of setting heat pump EFT as 32.2ºC (90ºF), the three control strategies with optimized setpoint values show high variance for the system operation cost savings. For the office building, the operation cost savings for the different cases ranges from about 2% to 11%. For the motel building, the operation cost savings for the different cases ranges from about 0% to 23%. For some cases, the operation cost savings were negative because the base case control strategy (EFT setpoint) offered a minimum operating cost.

The optimized setpoint of the three controls strategies can be seen in Figure 7.14 both for the office building and motel building. For each specific building type and location, the optimized setpoint values of the specific control strategy are different for different HGSHP system designs. In this figure, the maximum, the minimum and the mean optimized setpoint values caused by different HGSHP system designs are plotted. For a specific building type and location, the different HGSHP system designs would bring a quite difference of the best setpoint values. Also the best setpoint values of each control strategy for different building types and locations are scatter over a wide range. Taking the Tulsa office and motel building as examples, Figure 7.15 shows the annual energy costs for the four different HGSHP system designs vs. the different setpoints of the setting EFT control strategy. The setpoint value of the setting EFT control strategy

varies from 10ºC to 32.5ºC. As can be seen in Figure 7.15, with the variation of the setpoint value, the system operation cost varies moderately and the difference between the maximum operation cost and the minimum operation cost is about 6%. Although Figure 7.15 does not show the exact best setpoint value for each system design, the figure shows the best setpoint values for different building types and system designs as ranging from 22ºC to 25ºC. The results are consistent with those in Figure 7.14. Therefore, for these three control strategies, there is no generally-applicable setpoint for different combinations of HGSHP system design, building type and location. In general, the setpoint of the setting EFT control strategy ranges between 10ºC (50ºF) and 25ºC (77ºF); the setpoint of setting ExFT control strategy ranges between 15ºC (59ºF) and 30ºC (86ºF); and the set temperature difference of setting T_{diff} control strategy ranges between 2ºC (3.6ºF) and 15ºC (27ºF).

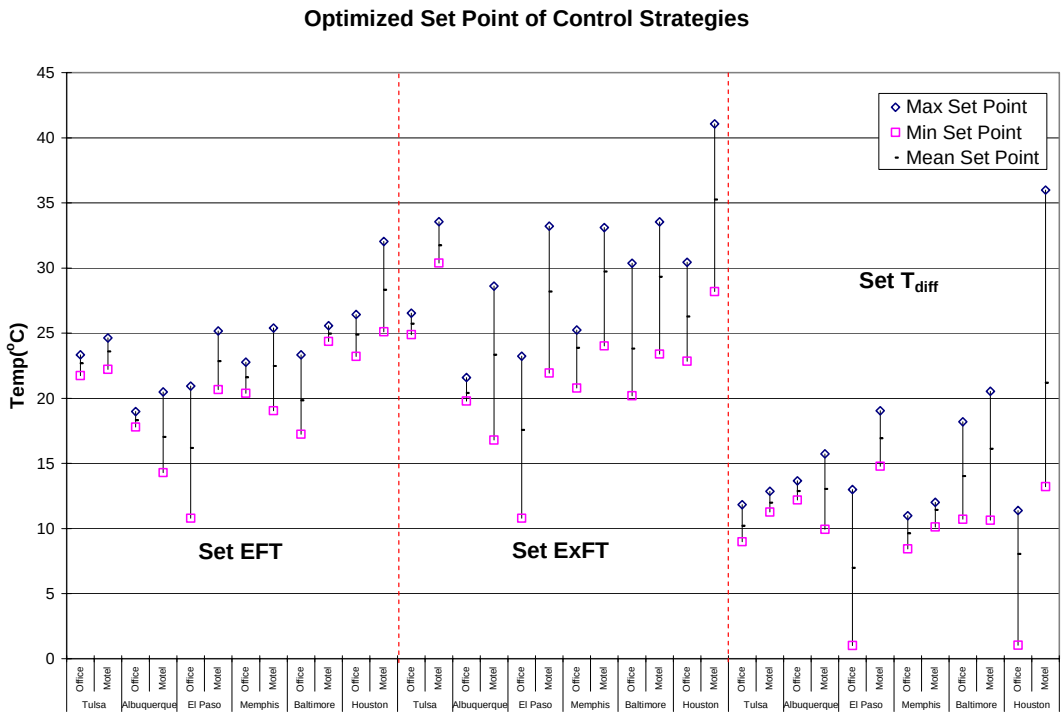

Figure 7.14 Optimized setpoint of three control strategies for office and motel building.

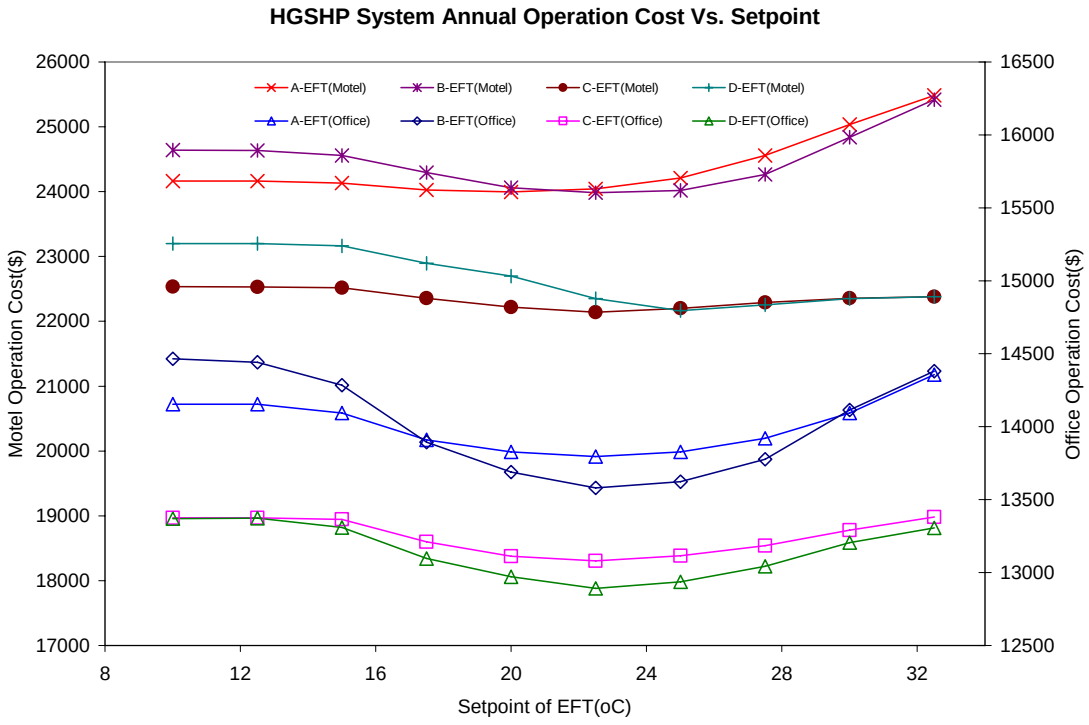

Figure 7.15 The sensitivity of the HGSHP system operation costs to the setpoint of the setting EFT control in Tulsa, office building.

7.4 Development of New Control Strategies

The investigation of the previously developed control strategies (Yavuzturk and Spitler 2000) showed for these control strategies there are no generally-applicable setpoints that can be used widely. To get a minimum operation cost of each specified HGSHP system, a buffer program is required to get the best setpoint, which is usually not feasible for the designer and engineer. Therefore, in this section, new control strategies will be developed, which aim to be generally-applicable for all HGSHP systems.

7.4.1 Control Strategy Based on System Loads

The primary idea of this control strategy is that when there are higher cooling loads, it might be good to run the cooling tower more to reject more heat from the loop. Therefore, the loads on the heat pumps might be used to control the cooling tower.

In practice, the ΔT across the heat pumps might be a sufficient indicator of the system loads. A detailed study of the system loads was carried out for the HGSHP systems with the optimized control strategies in last section. The system loads and the heat pump power consumptions for the office and the motel building in Tulsa, OK are shown in Figure 7.16. In this figure, the system loads and the heat pump power consumption are plotted against the ΔT across the heat pumps. As shown in Figure 7.16, most of the system cooling loads occur when the heat pump ΔT is less than -6 ºC (-10.8 ºF). 87.3% of the office building cooling loads and 94.4% of the motel building cooling loads occurred when the heat pump ΔT is less than -6 ºC. As a result, 81.3% of the heat pump power for the office building and 86.2% of the heat pump power for the motel

building consumed when the heat pump ΔT is less than -6 ºC. In the HGSHP system, the system flow rate was about 2.3gpm/ton for the office building and about 2.1gpm/ton for the motel building.

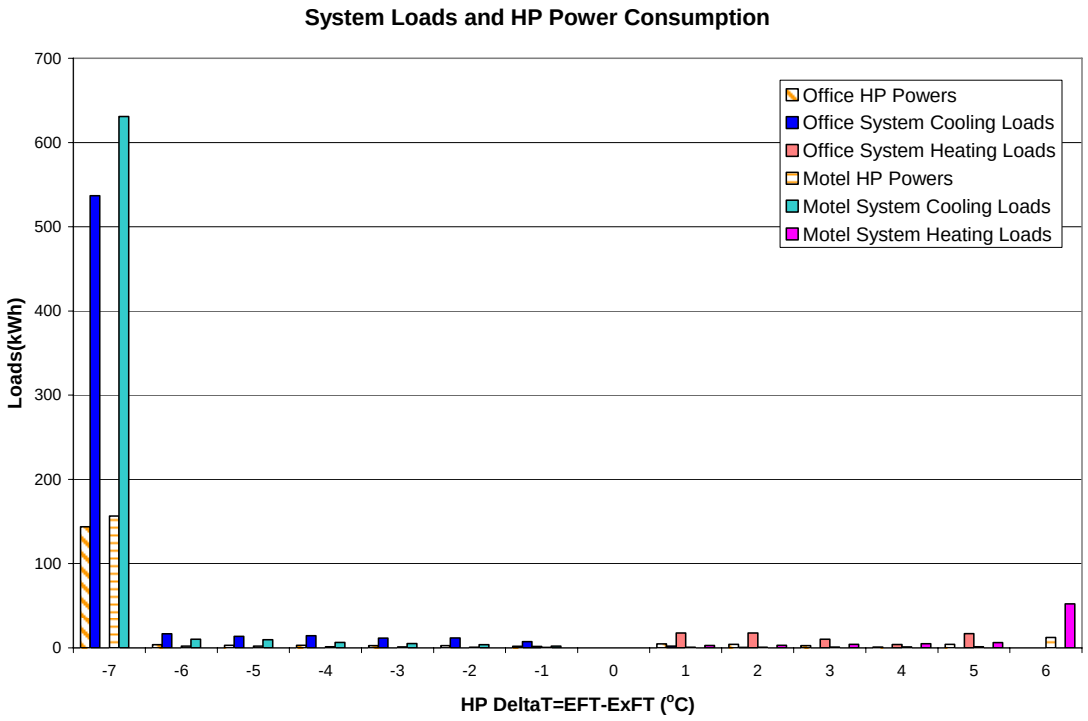

Figure 7.16 System loads and heat pump power consumptions of office and motel building in Tulsa, OK.

A new control strategy is then developed for the HGSHP system. The temperature difference across the heat pumps is used to control the cooling tower.

- When ΔT ≤ -6 ºC (-10.8 ºF), cooling tower is always on.
- When -6 ºC (-10.8 ºF) < ΔT < 0 ºC (0ºF), one of three alternatives:

- When EFT >22 ºC (71.6 ºF), cooling tower is on; when EFT ≤ 21 ºC (69.8 ºF), cooling tower is off. This control strategy is labeled as "Load + EFT".

- When ExFT > 24 ºC (75.2 ºF), cooling tower is on; when ExFT ≤ 23ºC (73.4 ºF), cooling tower is off. This control strategy is labeled as "Load + EFT".

- When T_{diff} > 10 ºC (18 ºF), cooling tower is on; when T_{diff} ≤ 9 ºC (16.2 ºF), cooling tower is off. The T_{diff} is the temperature difference between the heat pump ExFT and outdoor air wetbulb temperature. This control strategy is labeled as "Load + T_{diff}".

  The setpoint value of each control strategy is selected from the Figure 7.14 based on the optimization work of these three control strategies.

- When ΔT > 0 ºC (0 ºF), cooling tower is off.

The results for the new control strategies are shown below in Figures 7.17, 7.18 and 7.19 for the office building and Figures 7.20, 7.21 and 7.22 for the motel building. The figures show percent savings of the system annual operation costs for the three optimized control strategies discussed above in Section 7.3 and the three control strategies based on the system loads developed in this section.

As can be seen in the figures, for the office and motel building, most of the new control strategy cases, which do not have the benefit of individually optimized setpoints,

have similar or better savings than the individually optimized control strategy cases in the last section. In some motel cases, the new control strategy gave negative energy savings. The reason is that in these cases, the GLHE length is sized large enough to remove most of the cooling loads and the cooling tower run only a few hours (cooling tower energy consumption from the Figure 7.11 to 7.13). Using the new control strategy, the cooling tower ran more hours but did not yield too much energy savings for the heat pumps. And the total energy consumption of the system got higher because of the energy consumed by the cooling tower and the secondary loop circulation pump.

The new control strategies are generally-applicable for the different combinations of HGSHP system design, building type and location, without individually optimizing setpoint for a specific building and location combination. The new control strategies of "Load + EFT" and "Load + ExFT" use easy-to-measure quantities — loop temperatures to control the cooling tower and are physically feasible.

One issue of system loads control strategies needed to be considered is how to determine the setpoint of the heat pump ΔT. The system load control strategies relies on the heat pump ΔT as a subobject measure of load. In practice, the heat pump ΔT value varies with the different system flow rates. To apply this system load control strategy in practice, the system design flow rate and the system design heat rejection rate are required to determine the temperature difference setpoint. In a variable flow rate system, the heat pump ΔT value typically varies from 4.5 ºC (8.0 ºF) to 6.7 ºC (12.0 ºF) under design condition. The actual design heat pump ΔT would be used in practice as the setpoint.

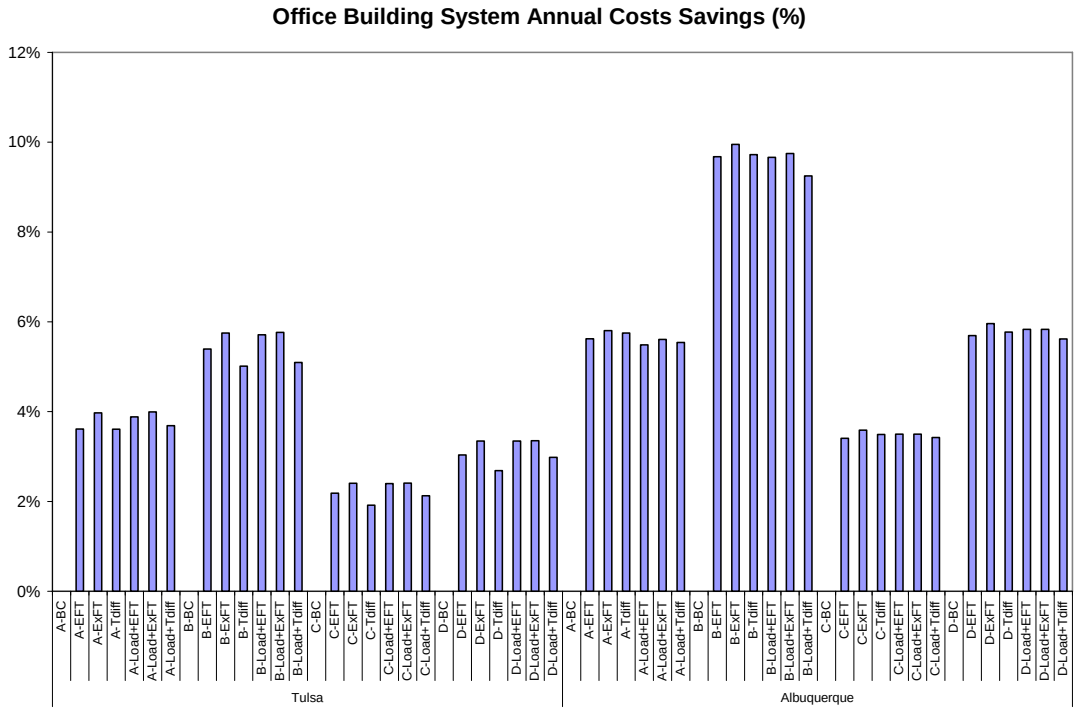

Figure 7.17 Annual operation cost saving for the office building in Tulsa and Albuquerque (system loads controls).

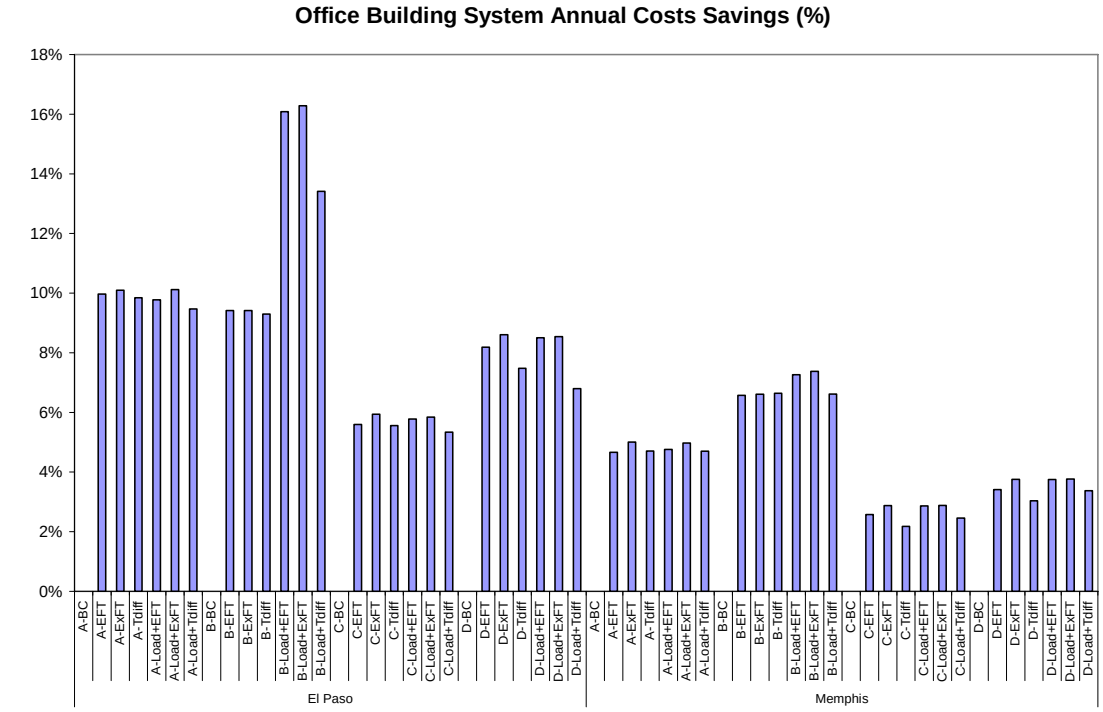

Figure 7.18 Annual operation cost saving for the office building in El Paso and Memphis (system loads controls).

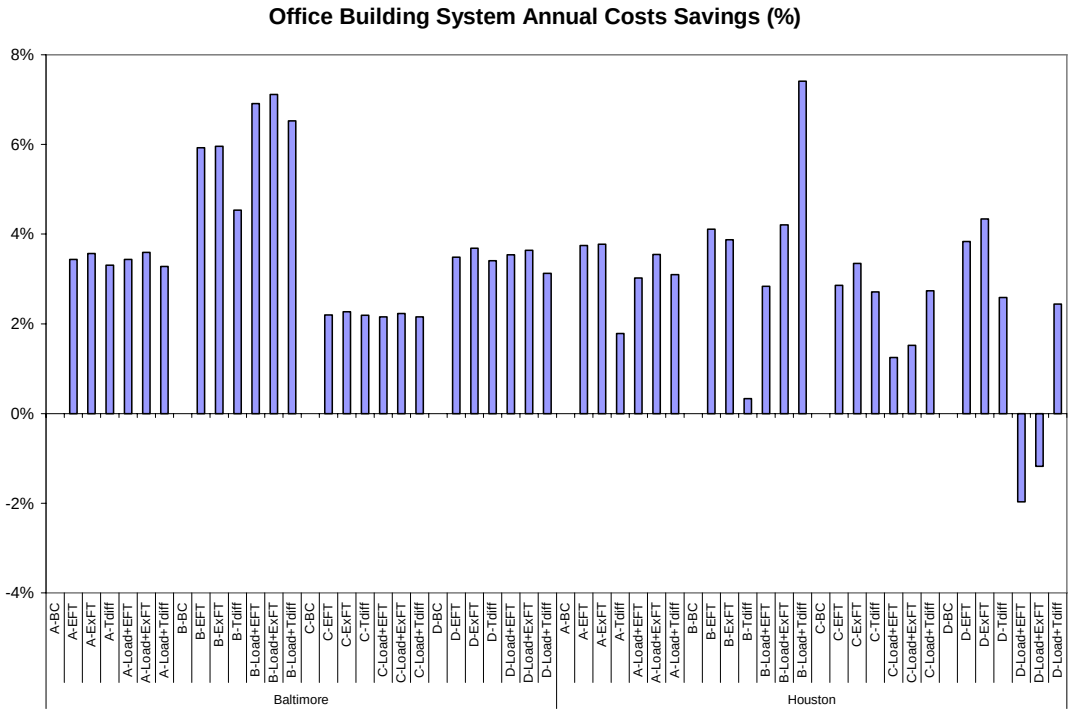

Figure 7.19 Annual operation cost saving for the office building in Baltimore and Houston (system loads controls).

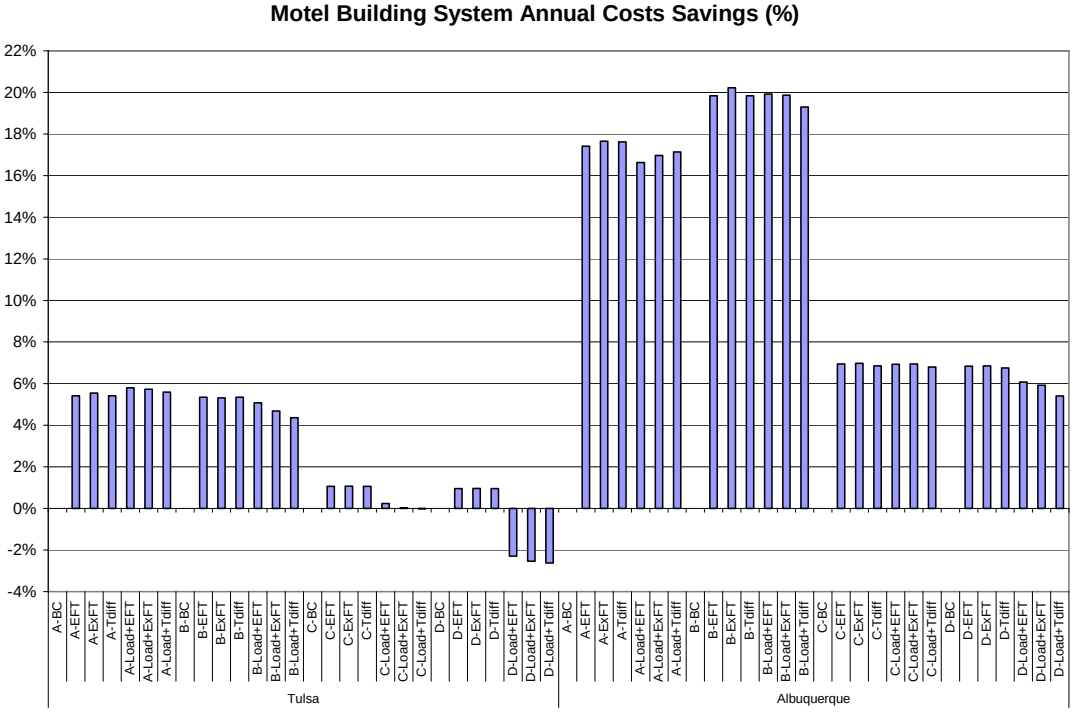

Figure 7.20 Annual operation cost saving for the motel building in Tulsa and Albuquerque (system loads controls).

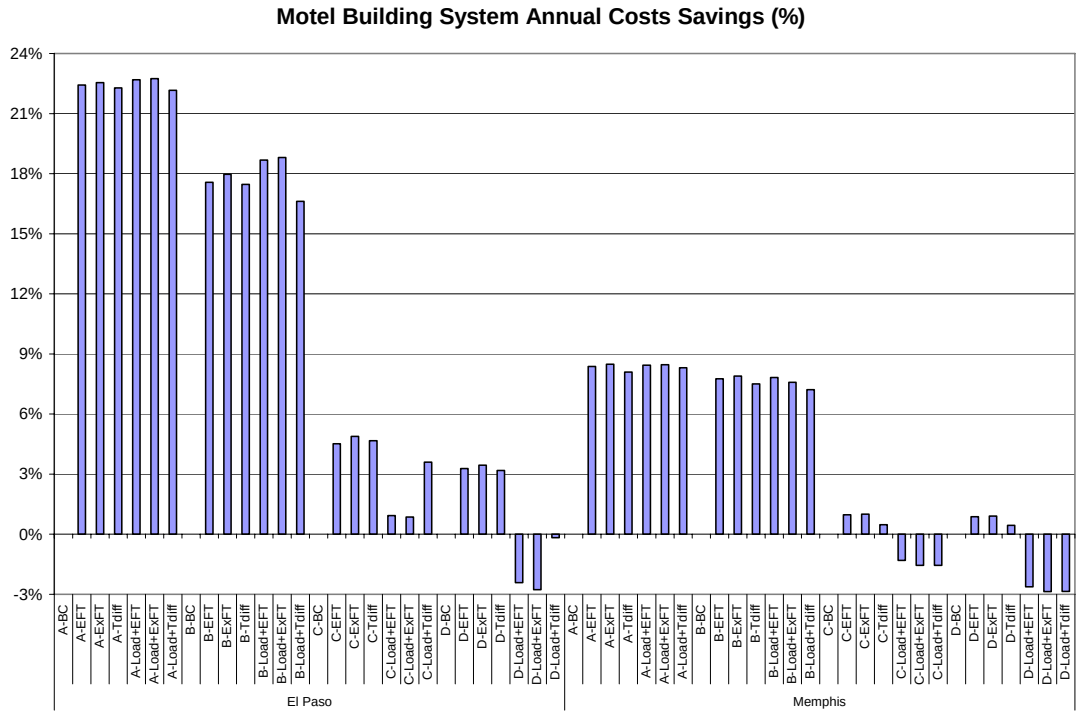

Figure 7.21 Annual operation cost saving for the motel building in Tulsa and Albuquerque (system loads controls).

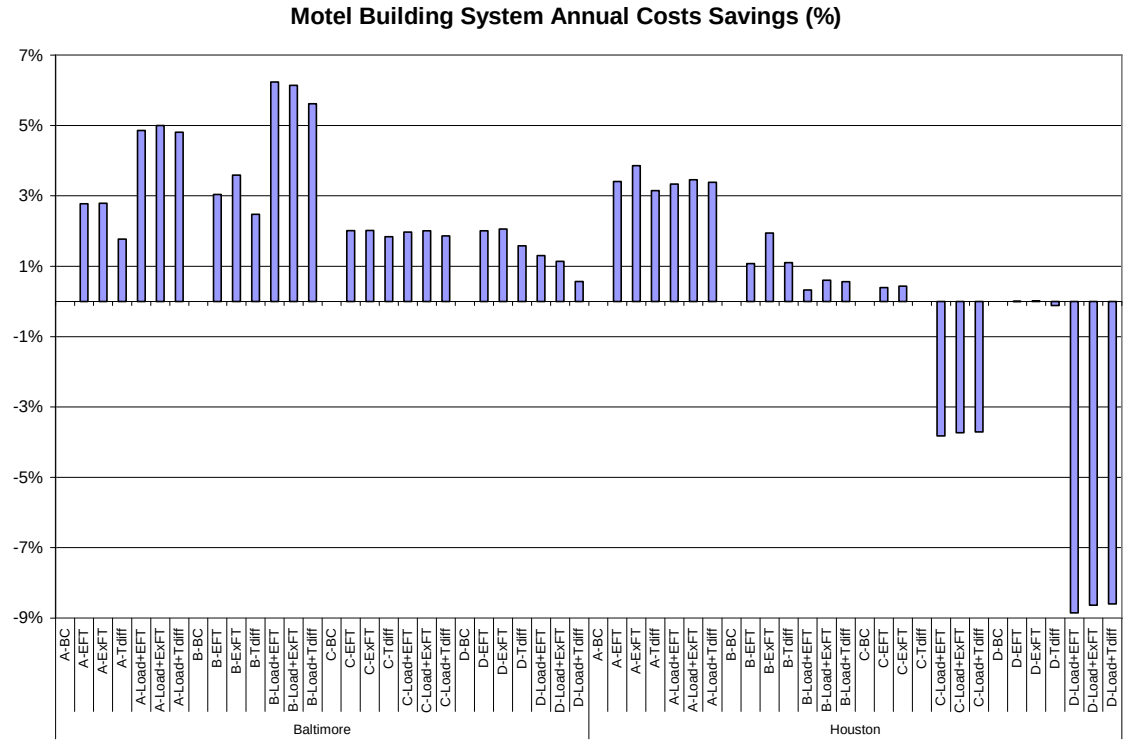

Figure 7.22 Annual operation cost saving for the motel building in Tulsa and Albuquerque (system loads controls).

7.4.2 Forecast Control

The general idea of the forecast control strategy depends on the ability to predict the future loads of heat pumps. Based on the forecast heat pump loads (for the next 12 hours, 24 hours or other periods), a new control strategy would estimate the energy consumption of running the cooling tower and the possible energy savings of heat pumps from running the cooling tower in the coming time. Then the control strategy will decide whether to run the cooling tower or not. One of the advantages of the forecast control strategy is that it is adaptive. However, this control strategy depends on the ability to estimate the possible energy savings of heat pumps in future from running cooling tower at the current time. It also depends on the availability of a forecast loads.

The proposed procedure of the forecast control strategy is summarized as follows:

1. Obtain the heat pump loads for the next 24 hours (or other periods).

   There are several ways to get the heat pump loads. One is forecasting the heat pump loads for the next 24 hours. Another way is using the historical loads as the forecast loads. Considering that much of time the building loads will be similar to the previous week, the historical heat pump loads a week ago might be used for the control strategy instead of the forecasted heat pump loads.

2. Obtain the outdoor wetbulb temperature at the current time.

3. Estimate the cooling tower heat rejection rate if the cooling tower is on at the current time.

Without running the system simulation, it is difficult to get the cooling tower heat rejection rate when the cooling tower is on. An algorithm is developed to estimate the cooling tower heat rejection rate without running the system simulation.

In an HGSHP system, the cooling tower heat rejection rates and the temperature difference between the heat pump ExFT and the outdoor air wetbulb temperature, $\Delta T_{ExFT_{HP}} - T_{wb}$, are shown below in Figure 7.23. Therefore, a linear correlation between the cooling tower heat rejection rate and the temperature difference $\Delta T_{ExFT_{HP}} - T_{wb}$ is developed to estimate the cooling tower heat rejection rate. In practice, this correlation could be revised continuously based on recent measured data.

Applying this linear correlation, the heat pump ExFT and the outdoor air wetbulb temperature at the current time are available and then the cooling tower heat rejection rate, $\dot{q}_{CT}$, is calculated.

$$\dot{q}_{CT} = f(ExFT_{HP} - T_{wb}) \tag{7-2}$$

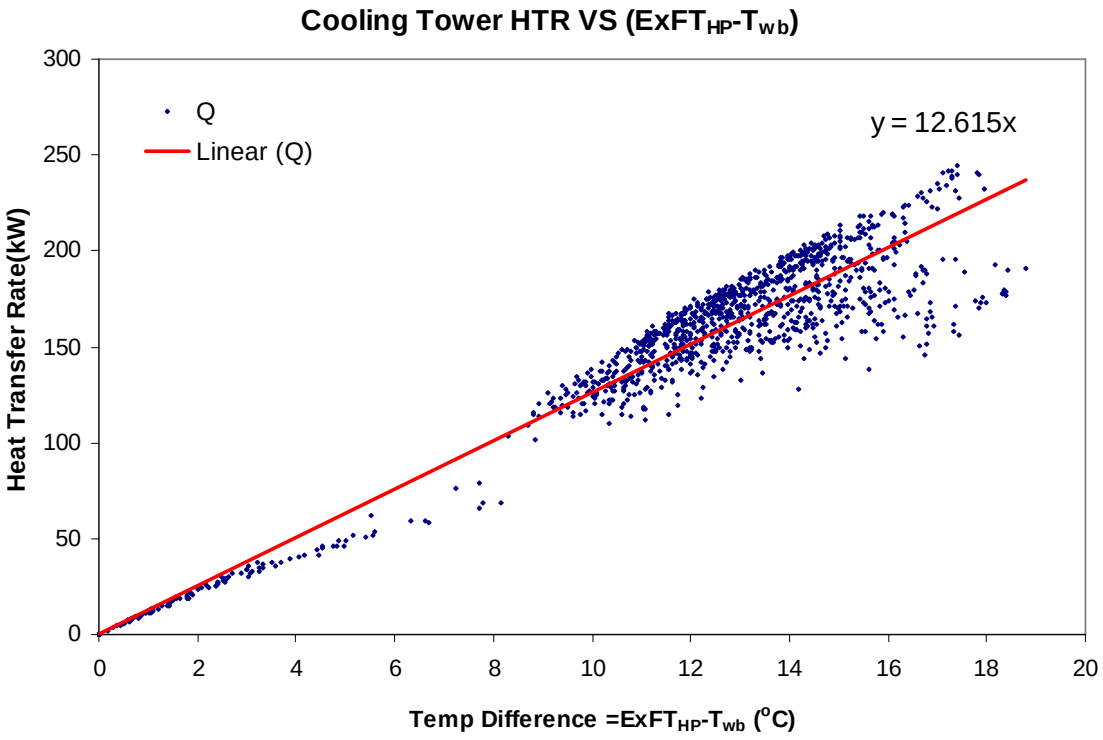

Figure 7.23 The correlation between the cooling tower HTR and the temperature difference $\Delta T_{ExFT_{HP}-T_{wb}}$

4. Calculate the heat pump entering fluid temperature differences in the next 24 hours if the cooling tower is on in the coming hour.

   In the HGSHP system, when the cooling tower is on and has a heat rejection rate of $\dot{q}_{CT}$, the heat rejection rate of the GLHE decreases by $\dot{q}_{CT}$. As a result, the exiting fluid temperature of the GLHE (the heat pumps' EFT) will drop by ΔEFT_{HP}, which gives a reduction of heat pumps power consumption. Therefore, if the heat pump EFT difference ΔEFT_{HP} is available, there is possibility to obtain the heat pumps' power savings caused by running the cooling tower.

Using the g-function-based GLHE model developed in Section 4.1.8, the GLHE ExFT differences (heat pumps EFT difference, ΔEFT_{HP}) in the 24 hours caused by a heat pulse of $\dot{q}_{CT}$ are calculated using the following equation.

$$\Delta EFT_{HP,i} = (q_{CT,i} - q_{CT,i-1})R_{BH} + \sum_{i=1}^{24} \frac{(q_{CT,i} - q_{CT,i-1})}{2\pi k_{ground}} g\left(\frac{t_n - t_{n-1}}{t_s}, \frac{r_b}{H}\right) \quad (7\text{-}3)$$

Where:

t = Time, (s)

t_s = Time scale, defined as $t_s = H^2 / 9\alpha$, (-)

$\Delta EFT_{HP,i}$ = The heat pump EFT difference at i^{th} time step, (ºC)

$q_{CT,i}$ = Heat rejection pulse of the cooling tower at i^{th} time step, (W/m)

H = Borehole depth, (m)

k_{ground} = Ground thermal conductivity, (W/m-K)

r_b = Borehole radius, (m)

R_{BH} = Borehole thermal resistance, (m-K/W)

i = The index to denote the end of a time step.

The exiting fluid temperature difference of a GLHE caused by a single hourly heat pulse is shown in Figure 7.24. As seen in the figure, the temperature difference reaches a peak when the heat pulse is applied. After the heat pulse is back to zero, the temperature difference drops quickly. After 24 hours, the temperature difference almost equals zero.

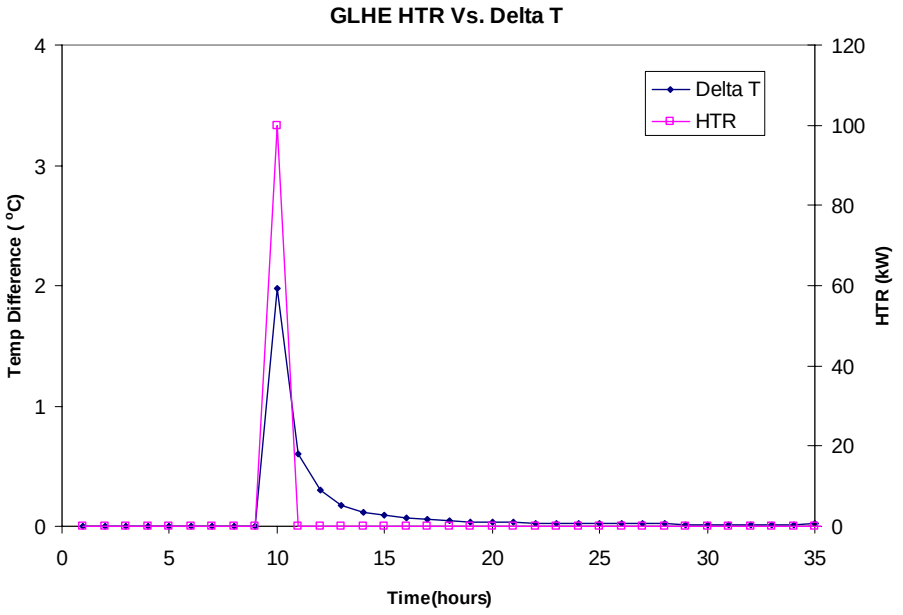

Figure 7.24 GLHE temperature differences in 24 hours caused by a single heat pulse.

5. Estimate heat pumps' COP and ΔCOP for the next 24 hours.

Figure 7.25 shows the COP of a selected heat pump against the heat pump EFT. A linear correlation is developed to approximately estimate the heat pump COP from the heat pump EFT. The heat pump EFT at the current time is used to calculate the heat pump COP and this COP value is applied for the next 24 hours.

Knowing the heat pump EFT difference, ΔEFT_{HP}, this linear correlation also is used to calculate the heat pump ΔCOP.

$$\Delta COP_i = f(\Delta EFT_{HP,i}) \qquad (7\text{-}4)$$

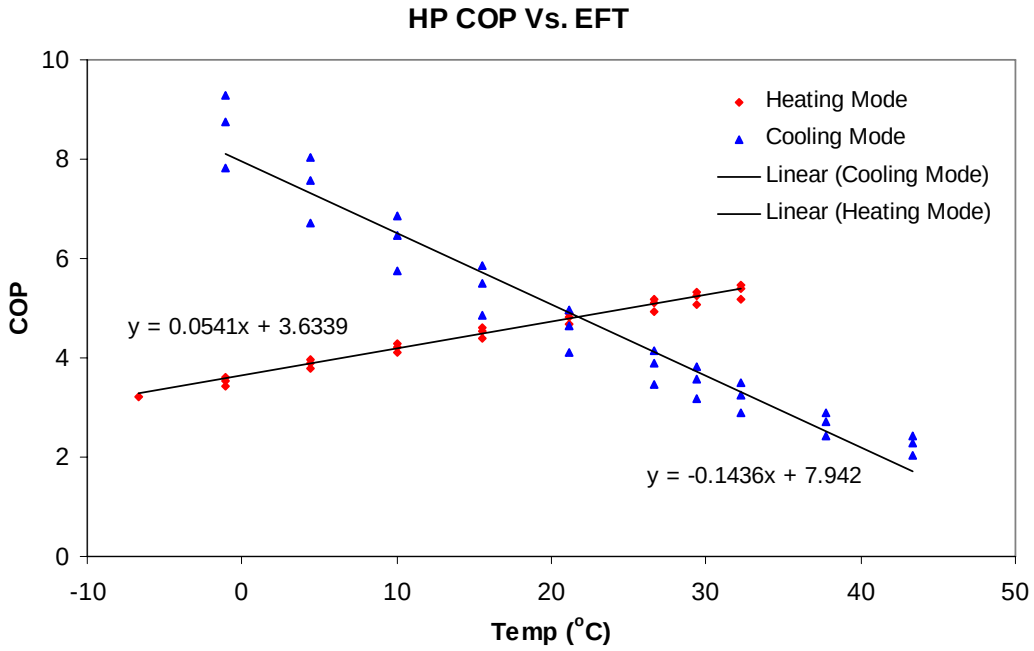

Figure 7.25 COP of a heat pump (ClimateMaster GS060) against the heat pump EFT.

6. Calculate the heat pumps power savings.

   Knowing the heat pump ΔCOP and the heat pump loads in the next 24 hours, the total heat pump power savings in the next 24 hours are then calculated.

$$\Delta Power_{HP} = \sum_{i=1}^{24} \left(\frac{CoolingLoad_i}{COP_i} - \frac{CoolingLoad_i}{COP_i + \Delta COP_i} \right) \qquad (7\text{-}5)$$

7. Determine to run the cooling tower or not.

   The power required to run the cooling tower and secondary loop circulation pump, $Power_{CT}$, is known. This power consumption is then compared to the heat pump power saving, $\Delta Power_{HP}$. IF the $Power_{CT} < \Delta Power_{HP}$, cooling tower is on; if the $Power_{CT} \geq \Delta Power_{HP}$, cooling tower is off.

In this research, two methods were used to get the heat pump loads in the next 24 hours. The first one is to use heat pump loads calculated from EnergyPlus, which are the exact loads for the next 24 hours. This method is labeled as "Forecast" in the result figures and represents a perfect forecast. Another method is to use the heat pumps' loads one week ago to represent the loads for the next 24 hours. This method is labeled as "Historical" in the result figures. These two methods bracket what could be done with this strategy.

The results for the "Forecast" and "Historical" control strategies are shown below in Figures 7.26, 7.27 and 7.28 for the office building and are shown in Figures 7.29, 7.30 and 7.31 for the motel building. The figures show percent savings of the system annual operation costs for the three optimized control strategies discussed above in Section 7.3, the control strategies based on the system loads developed in Senction 7.4.1, and the forecast/historical control strategies developed in this section.

As can be seen in the figures, for the office building, most of the forecast control strategy cases had the highest percent savings compared to the previous control strategies. Without the perfect prediction of the loads, the historical control strategy cases applied the loads week ago but still have good percent savings. For the motel building, most of the cases with the forecast/historical control strategy have good percent savings compared to the other controls. But maximum savings are not guaranteed. In some motel cases, the forecast/historical control strategies gave negative energy savings as well the heat pump ΔT control. Again, the cooling tower ran more hours than the base case but did not yield energy savings for the heat pumps.

The new control strategies are capable of being applied for the different combinations of HGSHP system design, building type and location. At every time step, the control strategy estimates the possible energy savings of heat pumps in future from running cooling tower at the current time and then determines to run the cooling tower or not. Therefore, the forecast control strategy is a real-time control strategy and is adaptive.

This forecast control strategy depends on the availability of a forecast loads. As an alternative, the historical loads are used. In the process of the forecast control strategy, approximate correlations are used to calculate the cooling tower heat rejection rate and the heat pump COP. Also a wetbulb temperature is required for this control strategy. These issues bring some uncertainties in the actual performance of the forecast control strategy.

In am attempt to further improve the historical control strategy, a new approach is investigated to provide more accurate prediction loads instead of using the loads that occurred one week ago. The new "Historical" load prediction scheme is: for working days from Monday to Friday, use the loads happened in the last working day; for the weekend, use the loads happened in the last weekend day. The office building results are shown in Figure 7.32 and the motel building results are shown in Figure 7.33. The investigation results of the new "Historical" control strategy showed that the percent savings of the system annual operation costs is decreased (1% to 4%) for the office building and the percent savings is increased (1%) for the motel building. The reason is that for the motel building, the system operation schedule is continuous during the weekday and weekend. Therefore the new load prediction scheme is able to get more

accurate load prediction than the old scheme for the motel building. For the office building, the system operation schedule is discontinuous between the weekday and weekend. The system loads on Monday and Friday would have quite significant difference for the office building. Therefore, the new load prediction scheme is not able to bring a more accurate load prediction than the old scheme and it has a lower energy saving.

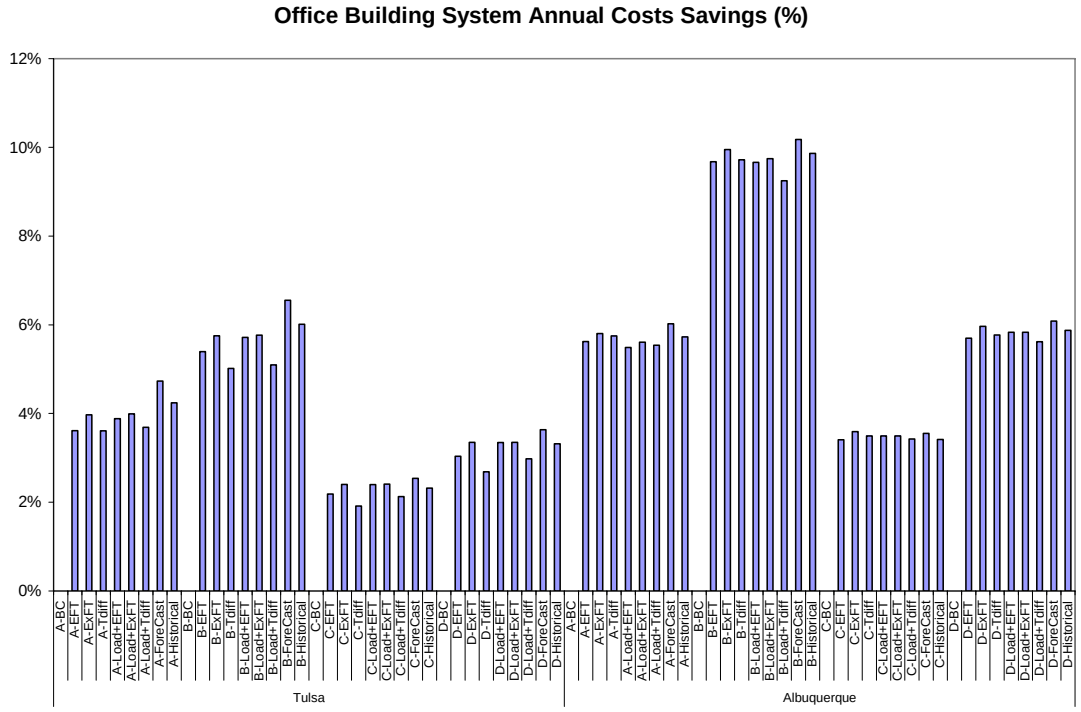

Figure 7.26 Annual operation cost saving for the office building in El Paso and Memphis (Forecast/Historical controls).

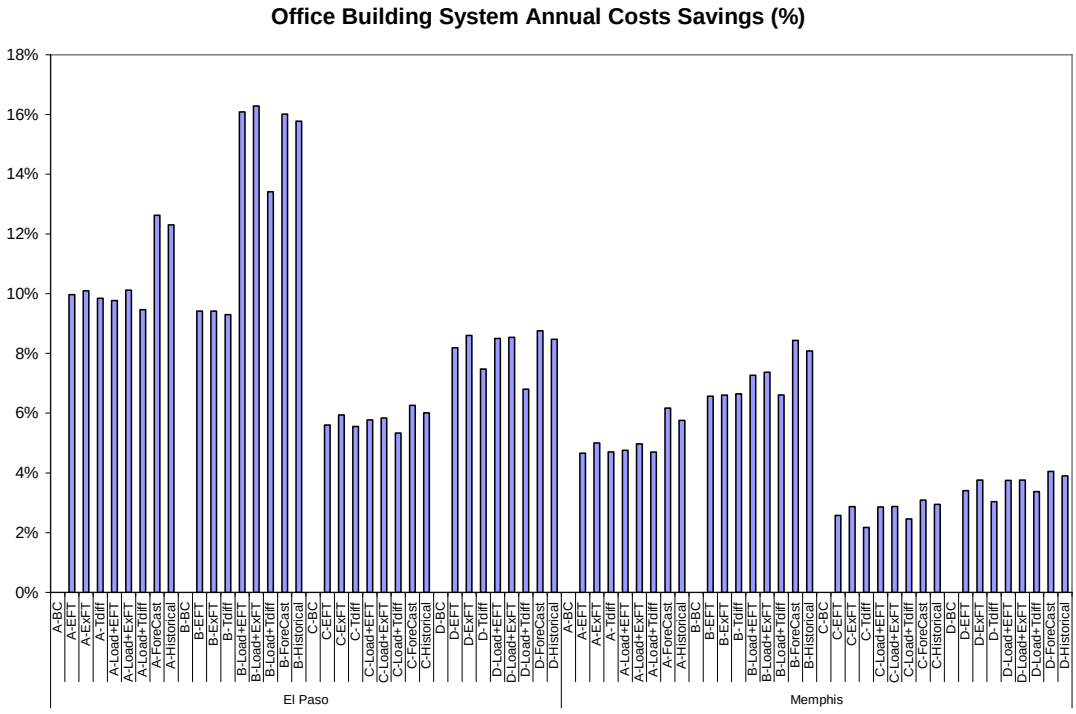

Figure 7.27 Annual operation cost saving for the office building in El Paso and Memphis (Forecast/Historical controls).

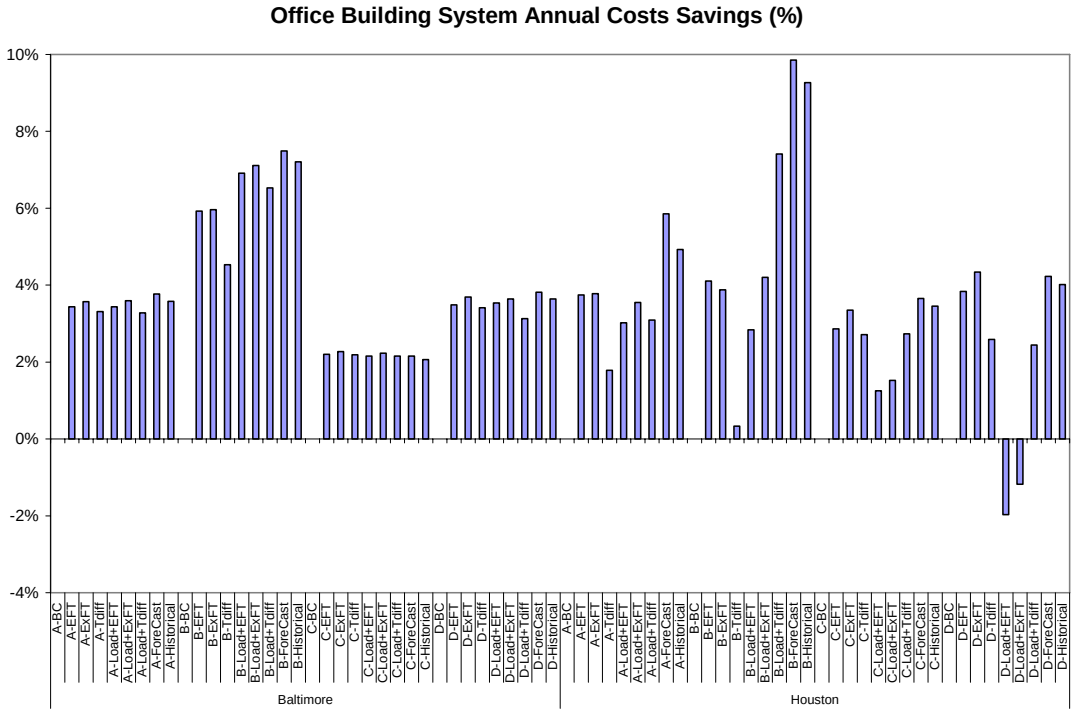

Figure 7.28 Annual operation cost saving for the office building in Baltimore and Houston (Forecast/Historical controls).

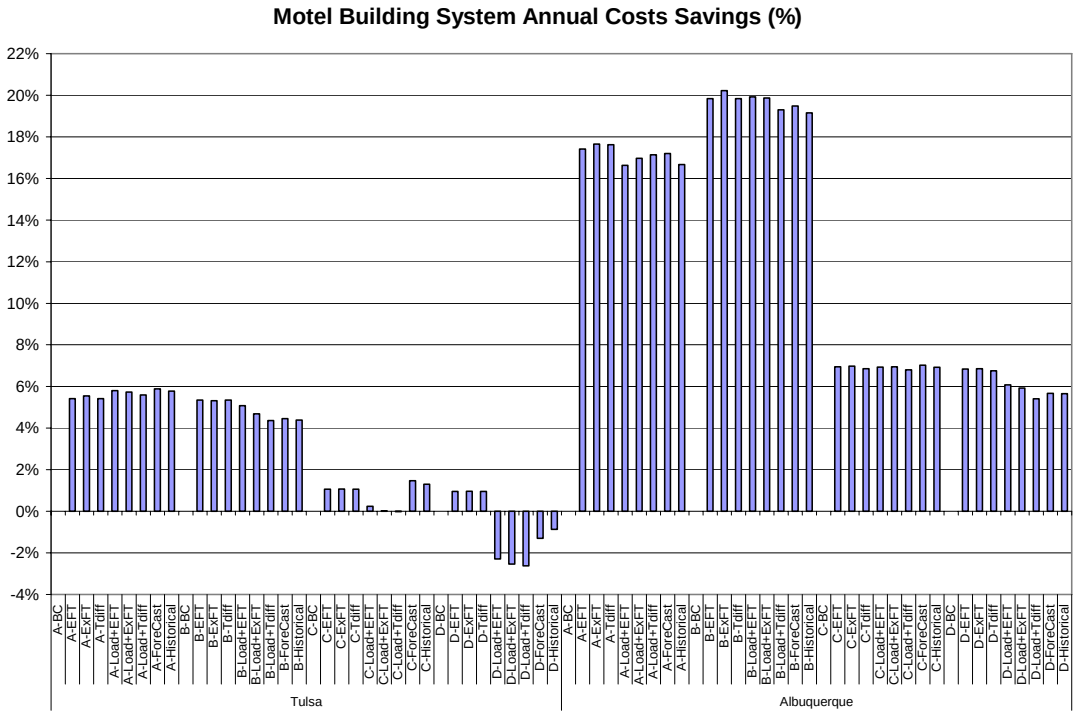

Figure 7.29 Annual operation cost saving for the motel building in Tulsa and Albuquerque (Forecast/Historical controls).

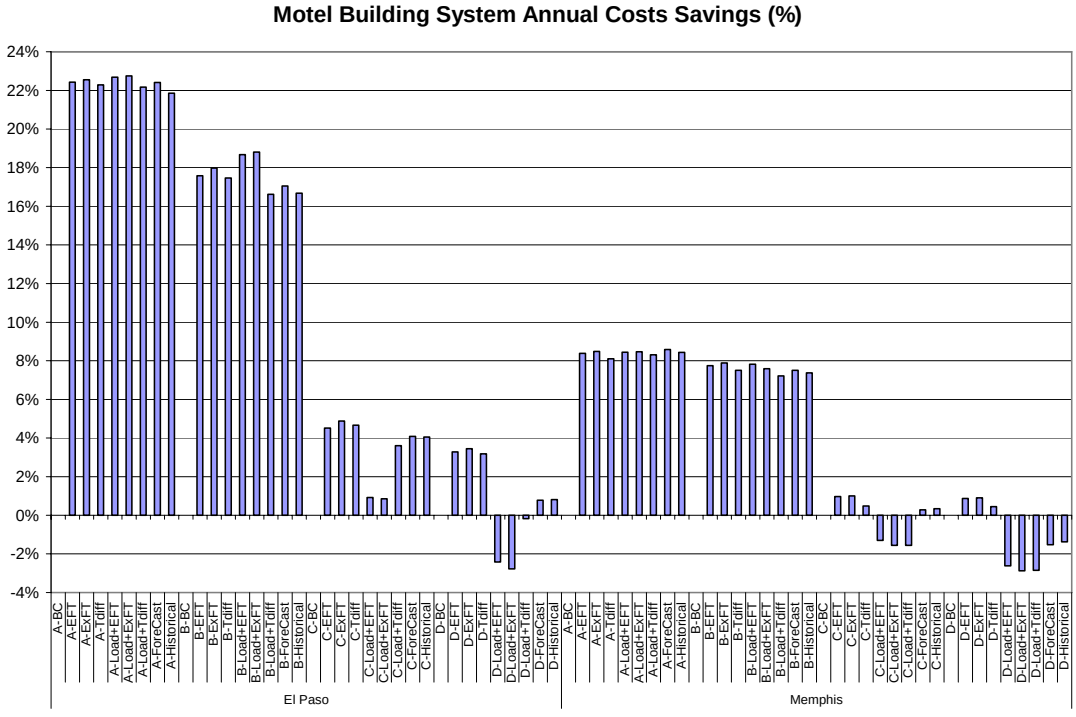

Figure 7.30 Annual operation cost saving for the motel building in El Paso and Memphis (Forecast/Historical controls).

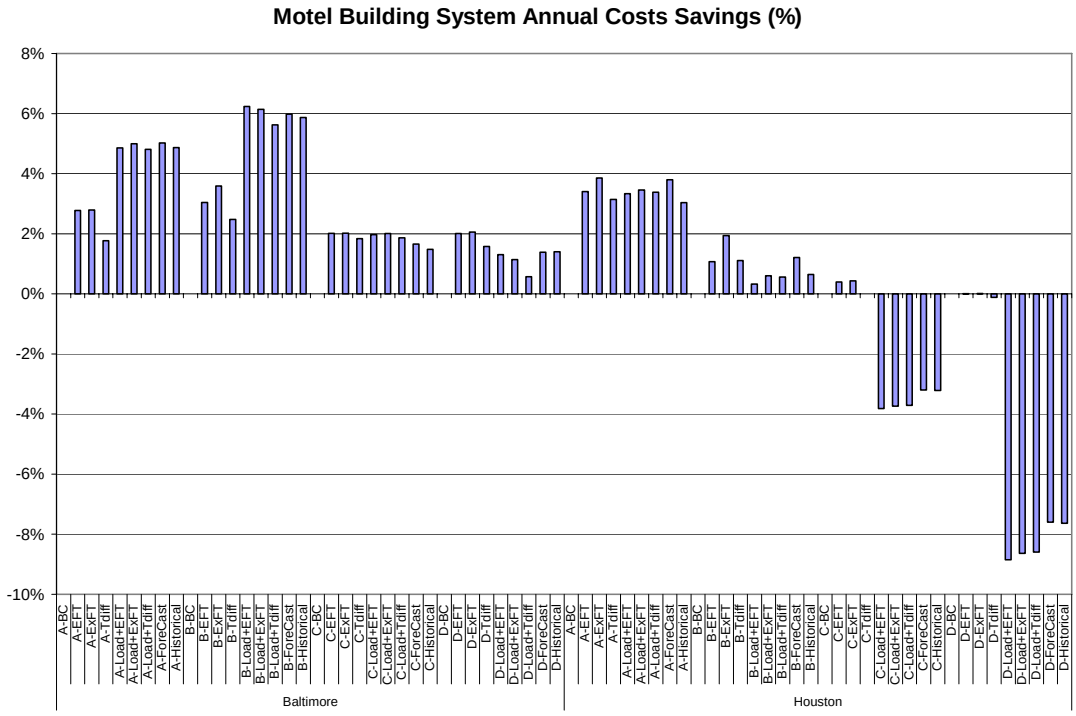

Figure 7.31 Annual operation cost saving for the motel building in Baltimore and Houston (Forecast/Historical controls).

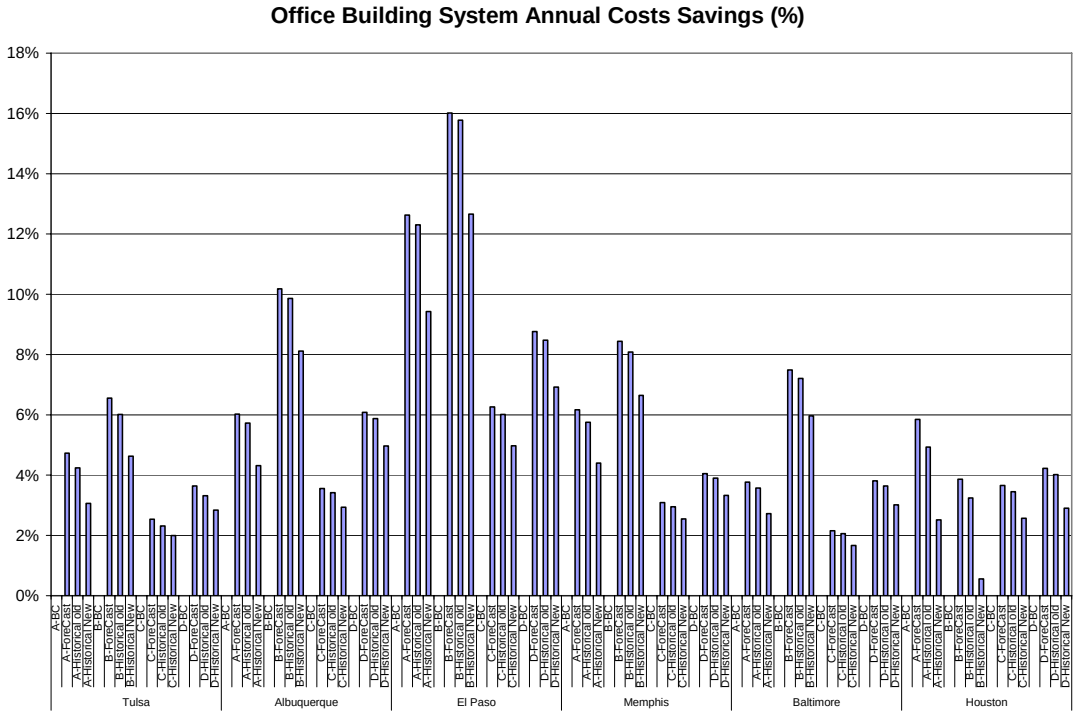

Figure 7.32 Annual operation cost saving for the office building in six climate zones (Forecast, Old/New Historical controls).

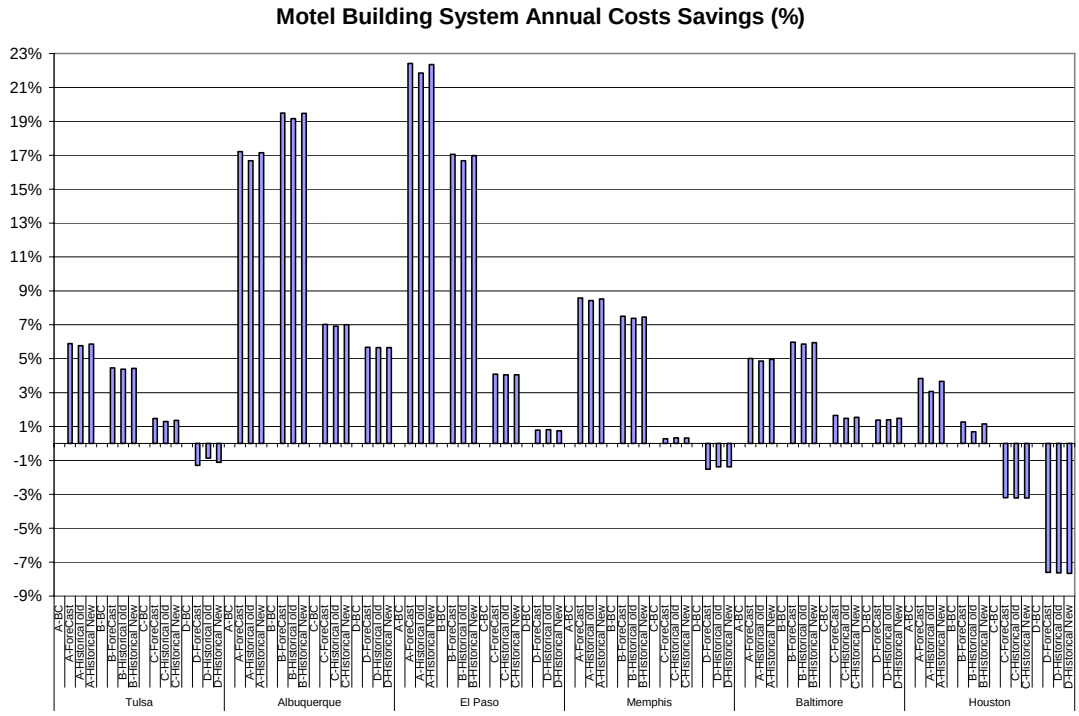

Figure 7.33 Annual operation cost saving for the motel building in six climate zones (Forecast, Old/New Historical controls).

7.4.3 Varied EFT/ExFT Control

A new control strategy based on the long term variations of loop temperature is developed for the HGSHP systems in this section. The original idea of this control strategy depends on the variation of loop temperature. When there are higher cooling loads, the loop temperature would rise; it might be good to run the cooling tower more to reject more heat from the loop. When there are lower cooling loads, the loop temperature would drop; it might be good to decrease the run time of cooling tower. Therefore, the variation of loop temperature might be used to control the cooling tower. In practice, the procedure is described as follows:

1. Measure the loop temperature variation in the past time (48 hours, one week or other period).

2. If the loop temperature rises, which indicates there are more cooling loads in the system, then lower the setpoint value of EFT/ExFT to run the cooling tower more. If the loop temperature drops, which indicates there are less cooling loads in the system, raise the setpoint value of EFT/ExFT to run the cooling tower less.

The relationship between the setpoint of EFT/ExFT and the variations of the loop temperature can be represented by the equations below:

$$EFT_{\text{setpoint}} = C_1 \times (EFT_{avg} - T_{ground}) + C_2 \quad (7\text{-}6)$$

$$ExFT_{\text{setpoint}} = C_1 \times (ExFT_{avg} - T_{ground}) + C_2 \quad (7\text{-}7)$$

Where:

EFT_{setpoint} , $ExFT_{\text{setpoint}}$ = The setpoint value of EFT/ExFT for the control, (ºC);

EFT_{avg} , $ExFT_{avg}$ = Average entering/exiting fluid temperature to the heat pump over the last N hours, (ºC);

N = Number of hours in averaging period;

T_{ground} = The undisturbed ground temperature, (ºC);

C_1 , C_2 = Coefficients to be determined.

An investigation of the optimization setpoint of EFT and ExFT as a function of the temperature difference between the EFT_{avg} and T_{ground} is showed as Figure 7.34. For

different combinations of HGSHP system design, building type and location, there are quite constant linear relationships between the setpoint of EFT/ExFT and the ΔT. Also the N value is almost a constant value for the different combinations of HGSHP system design, building type and location: N =210 hours for the setting EFT case and N =215 hours for the setting ExFT case. Therefore, these two linear equations in Figure 7.34 are applied for the new control strategies. In addition, the supplemental cooling tower is on when the entering fluid temperature to the heat pump exceeds 29.4ºC (85ºF) or when the exiting fluid temperature of the heat pump exceeds 37.8ºC (100ºF). The setting varied EFT/ExFT setpoint is shown in Figure 7.35. When the averaged EFT/ExFT is lower than the undisturbed ground temperature, the cooling tower is off.

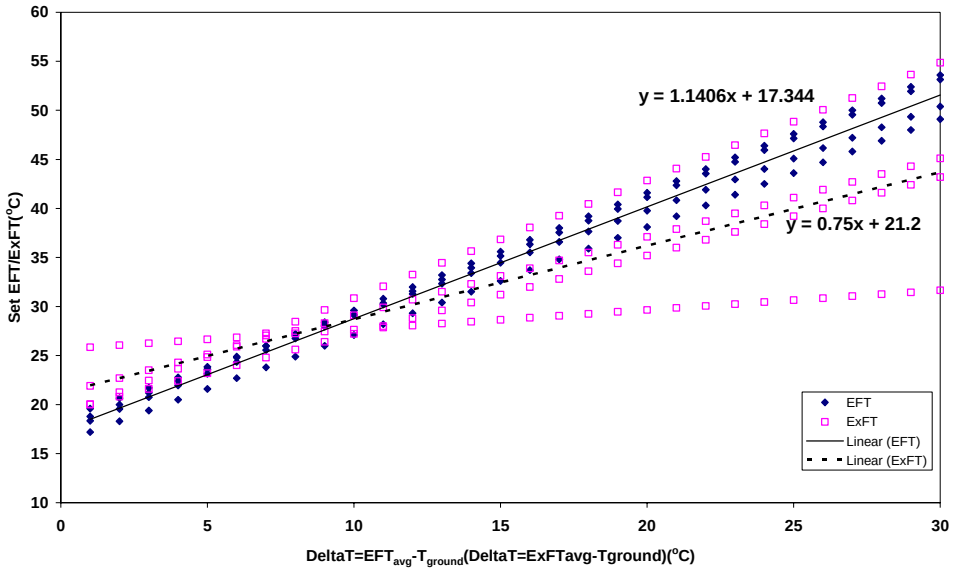

Figure 7.34 The linear relationship between the EFT_{set}/$ExFT_{set}$ and the deltaT.

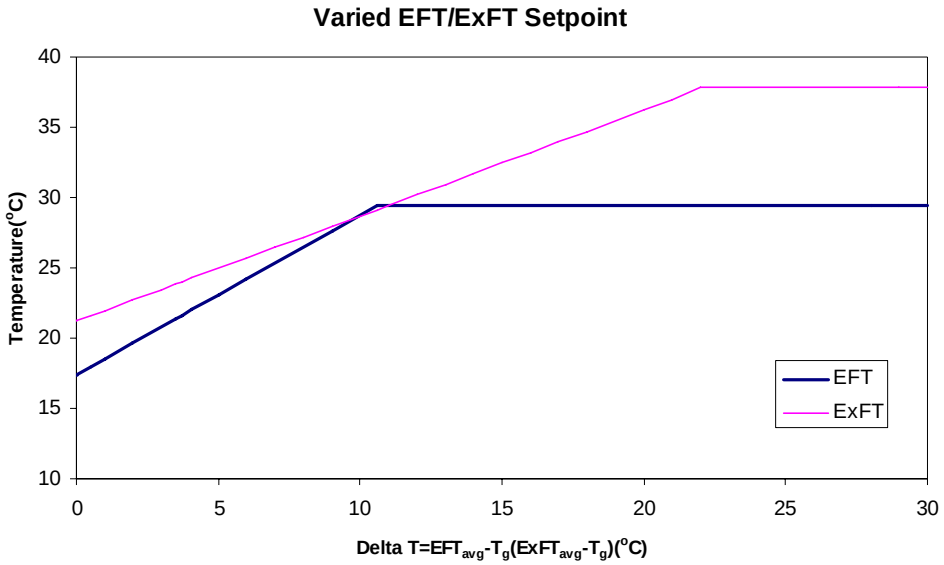

Figure 7.35 The setting varied EFT/ExFT setpoints for the varied EFT/ExFT control strategies.

The results for the varied EFT/ExFT control strategies are shown below in Figures 7.36 and 7.37 for the office building and are shown in Figures 7.38 and 7.39 for the motel building. The two new control strategies are labeled as "Varied EFT" and "Varied ExFT". As can be seen in the figures, for the office and motel building, most of cases with the new varied EFT/ExFT control strategy have similar or better savings than the individual optimized control strategy cases described in Section 7.3. For the motel building, some of the cases with the new varied EFT control strategy had a smaller energy saving than the varied ExFT control strategy cases. The investigation of the detailed results showed the system energy was related to the constant setting heat pump EFT of 29.4ºC (85ºF) or ExFT 37.8ºC (100ºF). In some cases (Tulsa motel system A) these two setting temperatures were too high and the heat pumps could have more energy savings by running the cooling tower more hours. In some cases (Houston motel system

D) the setpoint temperature was too lowe and the cooling tower ran more hours but did not yield much energy savings for the heat pumps. Therefore, to apply this varied EFT/ExFT control strategy in practice, it is recommended that the engineer adjusts the constant heat pump EFT/ExFT based on the system measured operation data. If the heat pump EFT/ExFT always meets the setpoint temperature, it is recommended to lower the setting EFT/ExFT to run the cooling tower more. If the heat pump EFT/ExFT seldom meets the setpoint temperature, it is recommended to raise the setpoint EFT/ExFT to run cooling tower less.

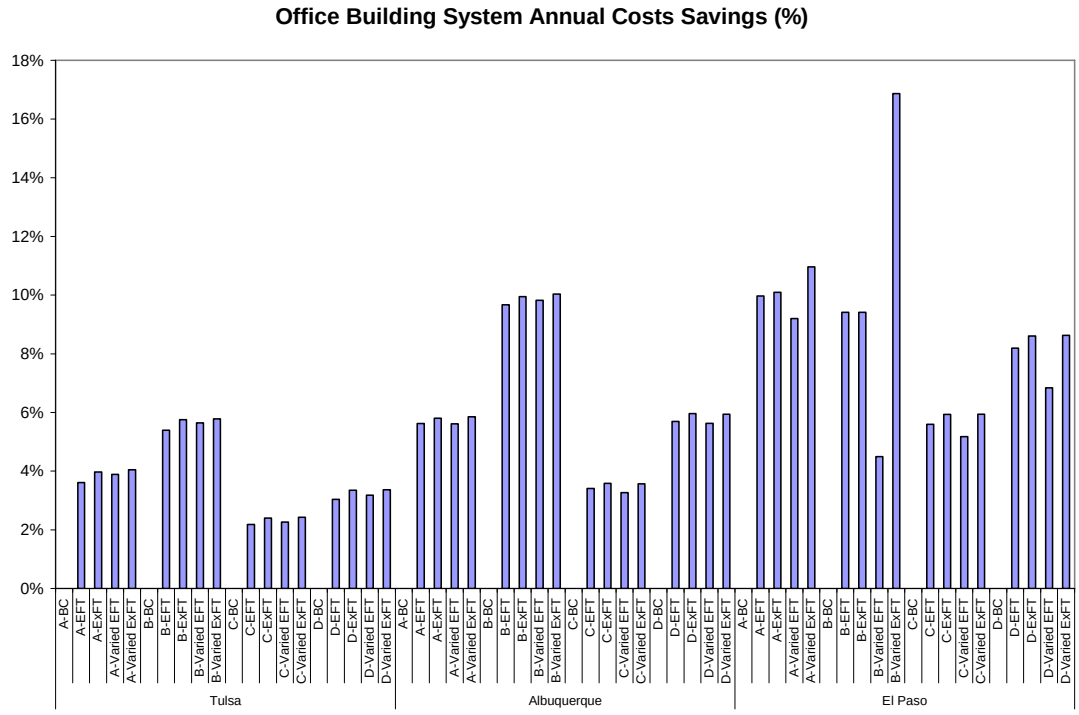

Figure 7.36 Annual operation cost saving for the office building in Tulsa, Albuquerque and El Paso (Varied EFT/ExFT controls).

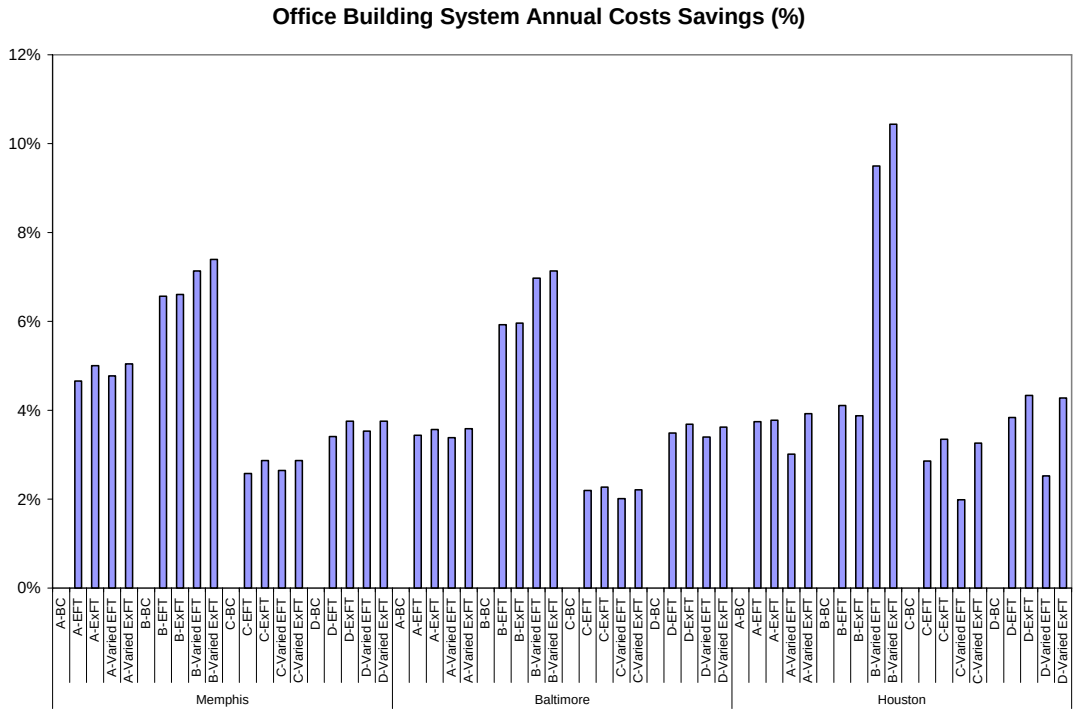

Figure 7.37 Annual operation cost saving for the office building in Memphis, Baltimore and Houston (Varied EFT/ExFT controls).

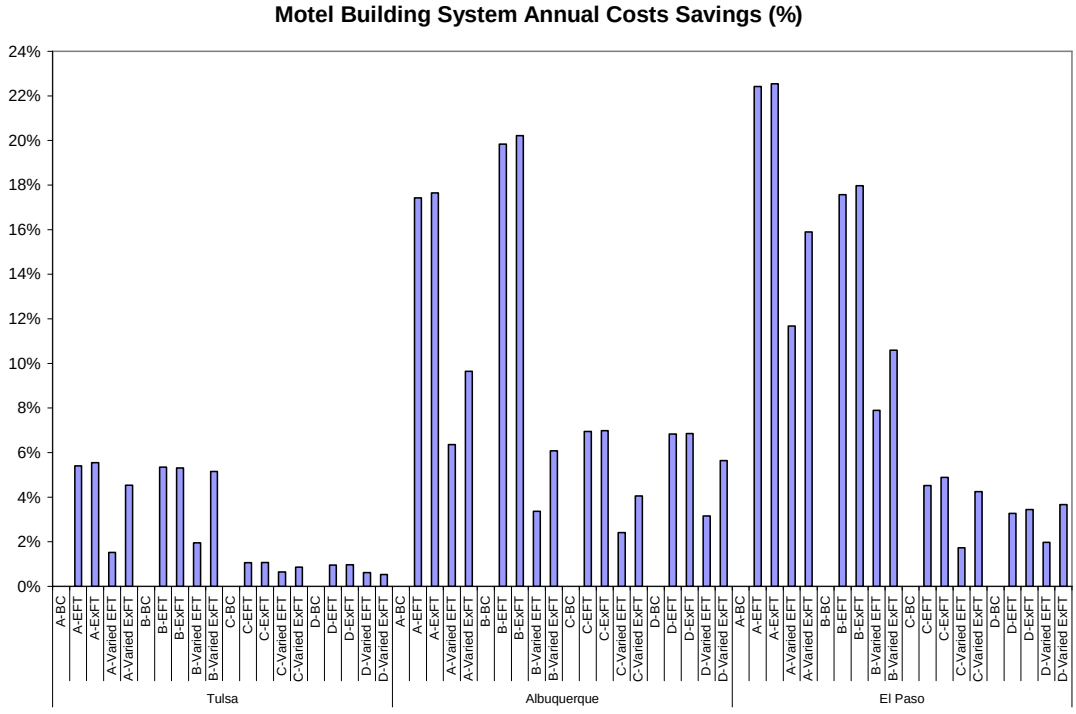

Figure 7.38 Annual operation cost saving for the motel building in Tulsa, Albuquerque and El Paso (Varied EFT/ExFT controls).

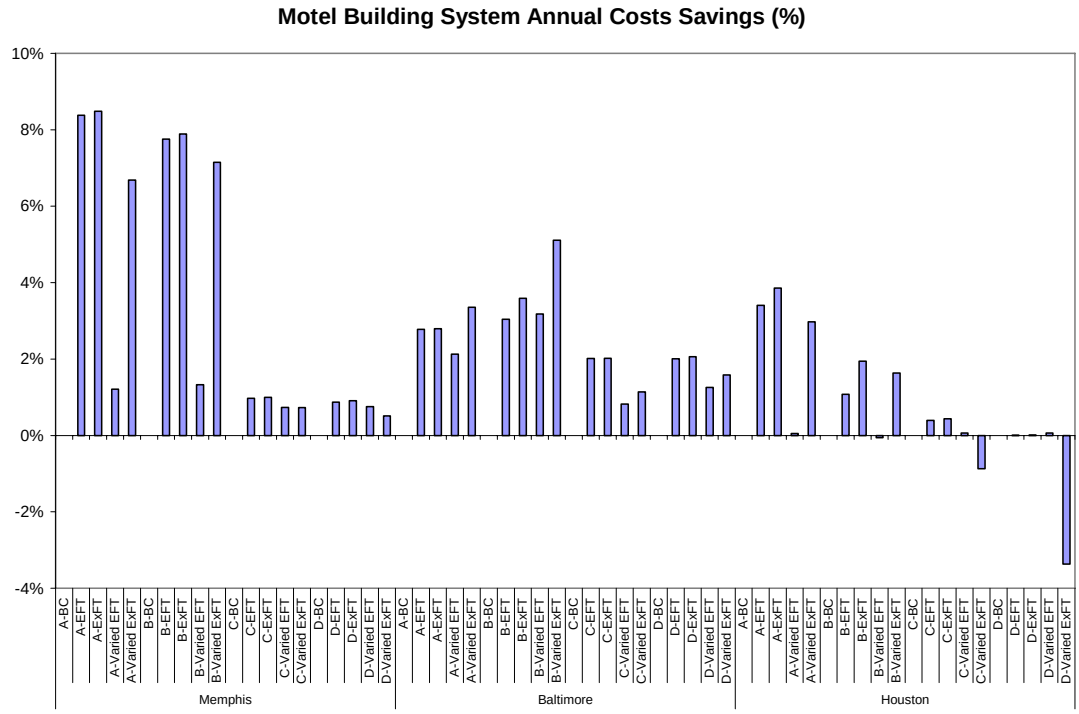

Figure 7.39Annual operation cost saving for the motel building in Memphis, Baltimore and Houston (Varied EFT/ExFT controls).

7.5 Results Verification

The results presented in the above sections only show annual performance. The system performance over a few days is highly desired so that the various control schemes can be compared in some detail. The office building in Tulsa is chosen for additional review.

- The HGSHP system design (A) for the office building in Tulsa is reviewed.
- Totally five control strategies for this HGSHP system are reviewed:
    - base case with set EFT 32.2 ºC (90 ºF).

- set EFT of 23.3 ºC (73.9 ºF), this control setpoint gives 3.6% savings in annual operation cost over the base case.
- Load ($\Delta T \leq$ -6 ºC (-10.8 ºF)) + EFT (22 ºC (71.6 ºF)), and this control gives 3.9% savings in annual operation cost over the base case.
- Forecast control with perfect loads prediction, and this control gives 4.7% savings in annual operation cost over the base case.
- Varied EFT with additional setting EFT of 22 ºC (71.6 ºF), this control setpoint gives 3.5% savings in annual operation cost over the base case.

- A shoulder season day, February 28th, and a summer day, July 1st, were chosen for an in-depth review.

Figure 7.40 shows the heat pump entering fluid temperature and cooling tower state (0: Off/1: On) for the control 1 to control 3 in February 28th. Also the system heating and cooling loads are plotted in this figure. As can be seen, the morning starts off with a short period of heating followed by a period of cooling. In the base case, the setpoint of EFT is 32.2 ºC (90 ºF) and the heat pump EFT never goes higher than this set point. Therefore, the cooling tower never turns on. However, the heat pump entering fluid temperature is above 23.3 ºC (73.9 ºF) for several hours, which is the setpoint of the EFT control, therefore the cooling tower has three hours on. In Figure 7.40, the temperature difference of heat pumps, ΔT_{HP} , is also plotted (positive for cooling mode). In the morning, the system has some cooling loads but not enough to make ΔT_{HP} exceed 6 ºC

(10.8 ºF) or make the heat pump EFT to be higher than 22 ºC (71.6 ºF). Therefore, the cooling tower remains off. At 12:00, the system has a higher cooling load and the heat pump ΔT_{HP} is greater than 6 ºC (10.8 ºF). Therefore, the cooling tower turns on until 18:00.

Figure 7.41 shows the heat pump entering fluid temperature and cooling tower state (0: Off/1: On) for the control 1, control 2 and control 4 in February 28th. As can be seen, at 11:00, the forecast control with perfect load prediction shows there are significant cooling loads in the coming hours. The control strategy then determines whether to run the cooling tower or not by estimating the possible energy savings of heat pumps in the next 24 hours from running cooling tower at the current time. The state of the cooling tower is on from 11:00, which means the heat pump energy savings in the next 24 hours exceeds the energy input for the cooling tower and the circulation pump during that time. Using the forecast control, the cooling tower is on from 11:00, even through at this hour, the system does not have too much cooling demand, but the system will benefit from running the cooling tower during that time.

Figure 7.42 shows the heat pump entering fluid temperature and cooling tower state (0: Off/1: On) for the control 2 and control 5 in February 28th. Also the varied setpoint value of control 5 is plotted in Figure 7.42. As can be seen in the figure, at 12:00 PM, the entering fluid temperature of heat pump is 17.8 ºC (64 ºF) and greater than the varied EFT setpoint of 17.7 ºC (63.9 ºF). Therefore, the cooling tower turns on until 19:00.

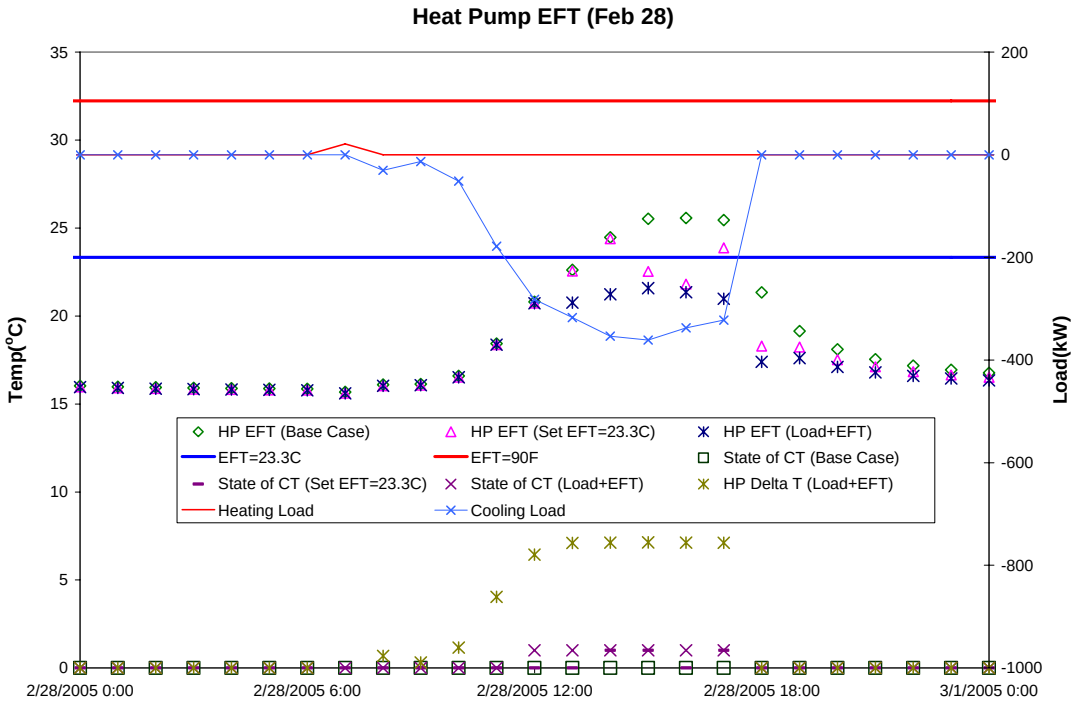

Figure 7.40 Heat pump EFT and cooling tower state of Load + EFT control strategy (Feb 28th)

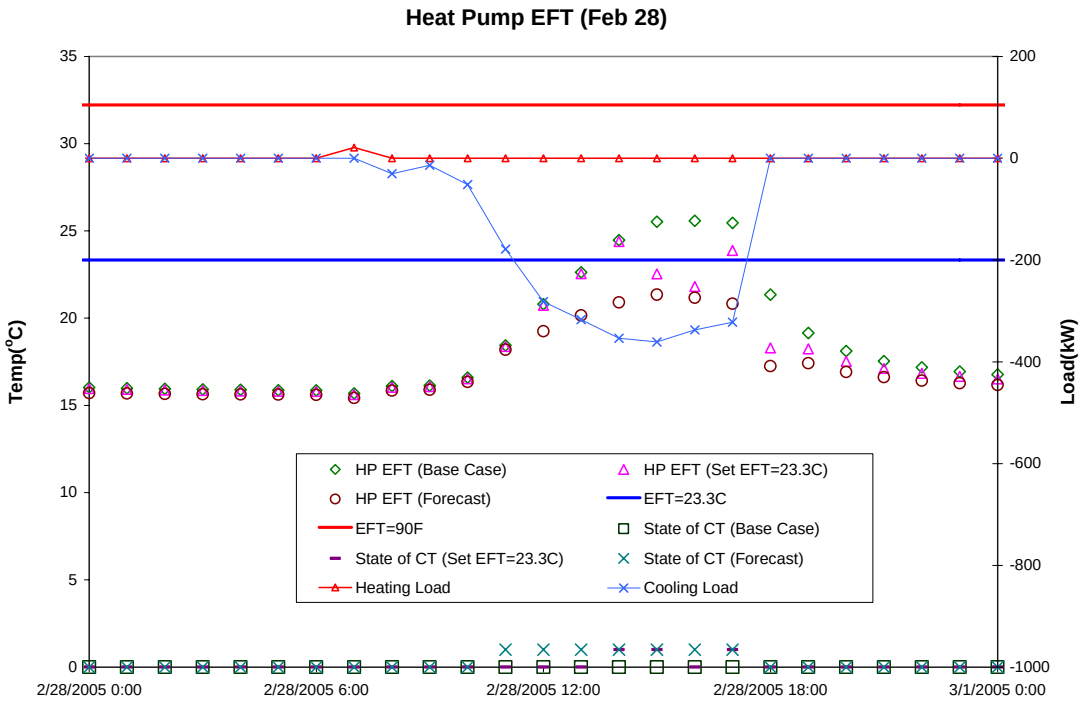

Figure 7.41 Heat pump EFT and cooling tower state of forecast control strategy (Feb 28th)

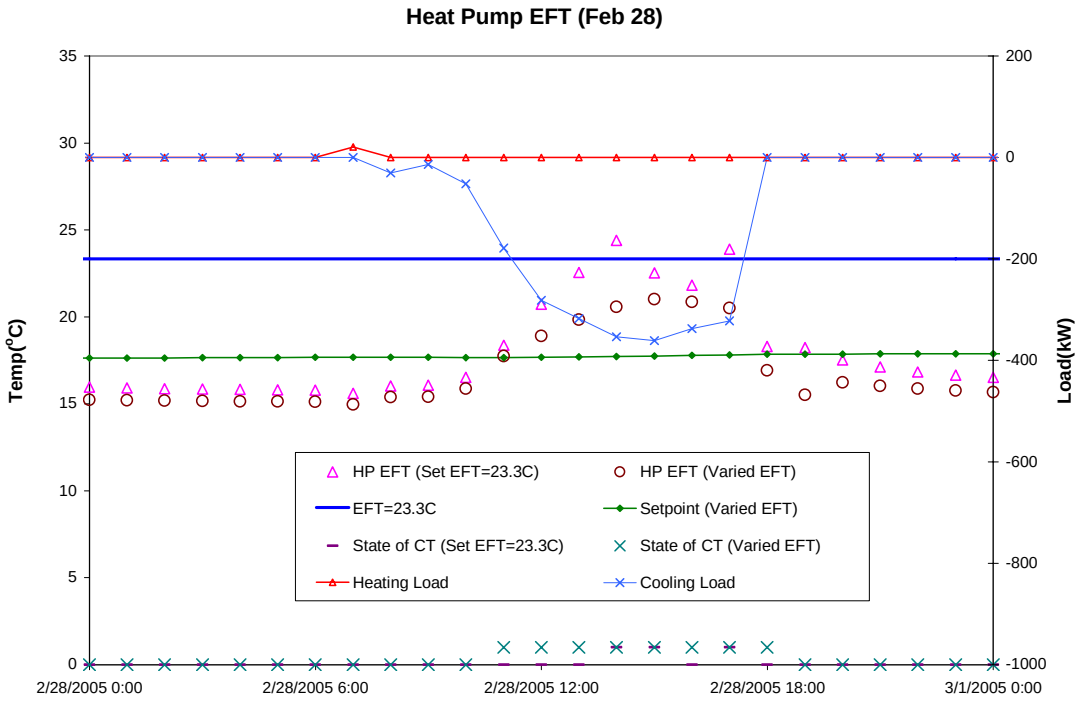

Figure 7.42 Heat pump EFT and cooling tower state of varied EFT control strategy (Feb 28th)

Figure 7.43 shows the heat pump cooling COP for all the controls in February 28th. Figure 7.44 shows the heat pump power consumption for all the controls. As can be seen, the base case has the lowest COPs because it has the highest heat pump EFT. The varied EFT control has the highest COPs because it runs the cooling tower longer than the other controls. As a result, the base case has the highest heat pump power consumption and the varied control has the lowest heat pump power consumption.

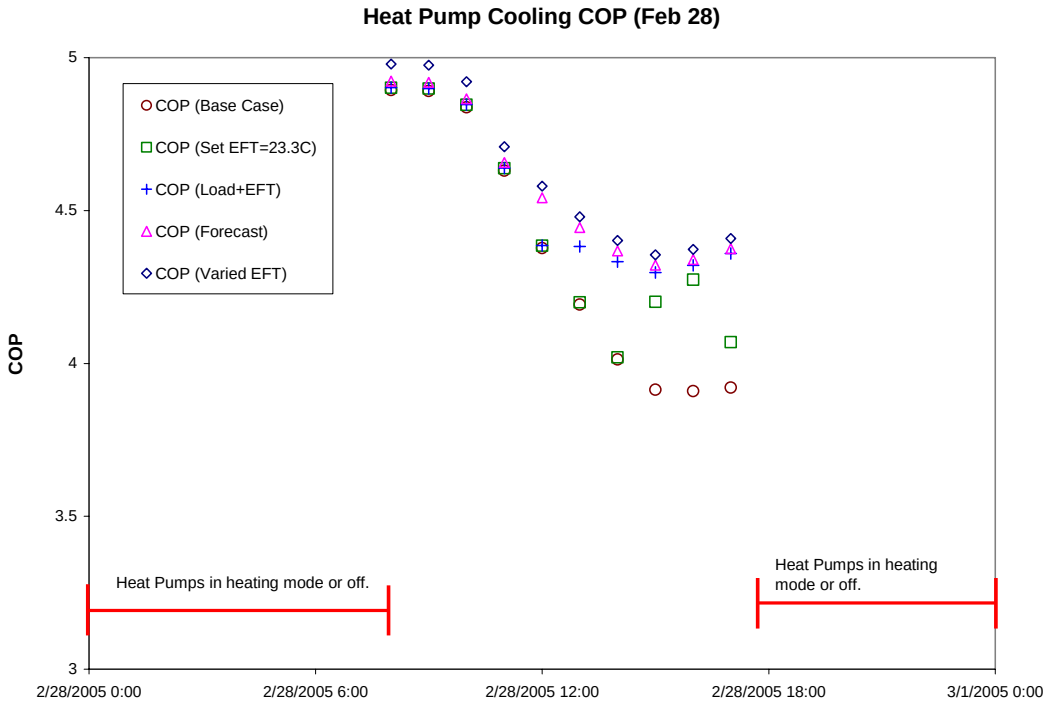

Figure 7.43 Heat pump cooling COP of all control strategies (Feb 28th)

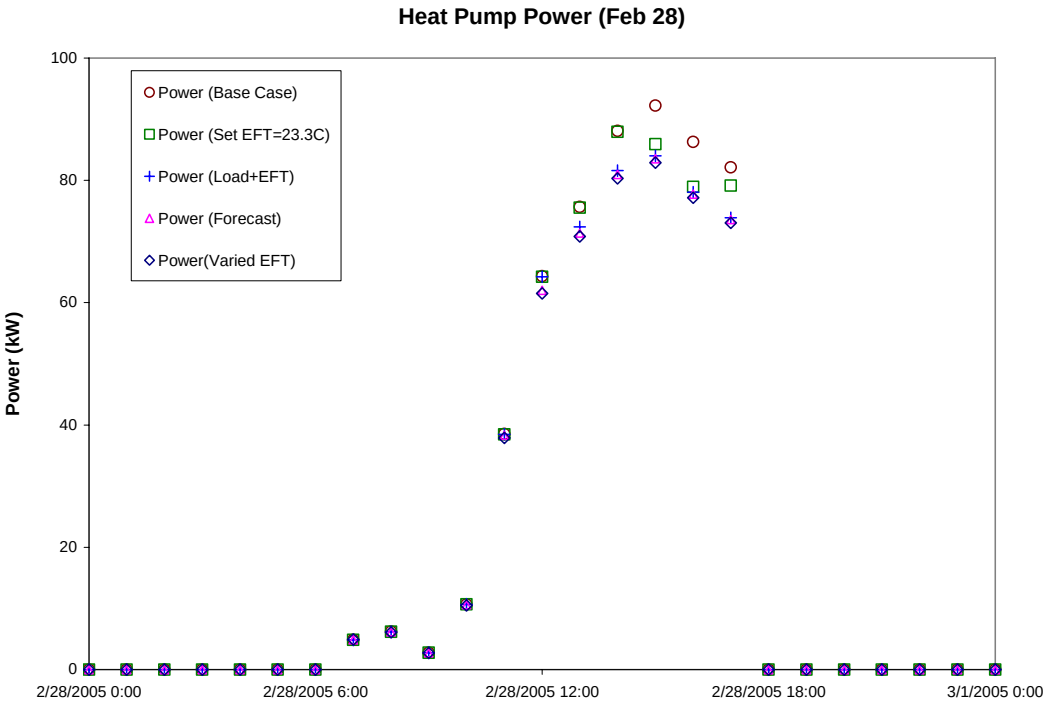

Figure 7.44 Heat pump power of all control strategies (Feb 28th)

Table 7.4 lists the system energy for consumption by component and the total system energy consumption for the day February 28th. As in shown, the forecast control has the biggest percent saving for this day.

Table 7.4 System energy consumption (Feb 28th)

Energy Consumption	Base Case	Set EFT	Load + EFT	Forecast	Varied EFT
Heat Pump (kWh)	551.8	534.7	517.1	511.9	507.9
Main Circ Pump (kWh)	40.1	40.1	40.1	40.1	40.1
Cooling Tower run time (hours)	0	3	6	7	8
Cooling Tower Fan (kWh)	0.0	3.4	6.7	7.8	9.0
Cooling Tower Circ Pump (kWh)	0.0	1.4	2.8	3.3	3.8
Total (kWh)	591.9	582.6	572.8	570.2	568.7
Saving (%)	--	1.6%	3.2%	3.7%	3.9%

Figure 7.45 shows the heat pump entering fluid temperature and cooling tower state (0: Off/1: On) for the control 1 to control 3 in July 1st. Also the system heating and cooling loads are plotted in this figure. In this summer day, the system has no heating load and has cooling loads for 10 hours. In the base case, the heat pump EFT goes above the set point of 32.2 ºC (90 ºF) and the cooling tower turns on for 10 hours. In the set EFT case, there are more hours that heat pump EFT goes above the set point of 23.3 ºC (73.9 ºF) and the cooling tower runs 12 hours. In the daytime, the system has significant cooling demand and the temperature difference of heat pumps, ΔT_{HP} (positive for cooling mode) is higher than 6 ºC (10.8 ºF). Therefore, the cooling tower is turned on for 10 hours.

Figure 7.46 shows the heat pump entering fluid temperature and cooling tower state (0: Off/1: On) for the control 1, control 2 and control 4 in July 1st. As can be seen, at

5:00 in the morning, the system has no cooling demand. However, the forecast control predicts there will be more cooling loads in the coming hours. If the cooling tower turns on at the current time, the system would have more energy savings from the heat pumps in the next 24 hours than the power consumed by the cooling tower and the circulation pump. Therefore the cooling tower turns on at 5:00 and 6:00 although there is no cooling demand at these tow hours. As a result, at the first few hours in the work time, the forecast control has the lower heat pump EFTs than the other controls.

Figure 7.47 shows the heat pump entering fluid temperature and cooling tower state (0: Off/1: On) for the control 2 and control 5 in July 1st. Also the varied setpoint value of control 5 is plotted in Figure 7.47. As can be seen in the figure, at 8:00 AM, the entering fluid temperature of heat pump is 37.5 ºC (99.5 ºF) and greater than the varied EFT setpoint of 22 ºC (71.6 ºF). Therefore, the cooling tower turns on until 21:00.

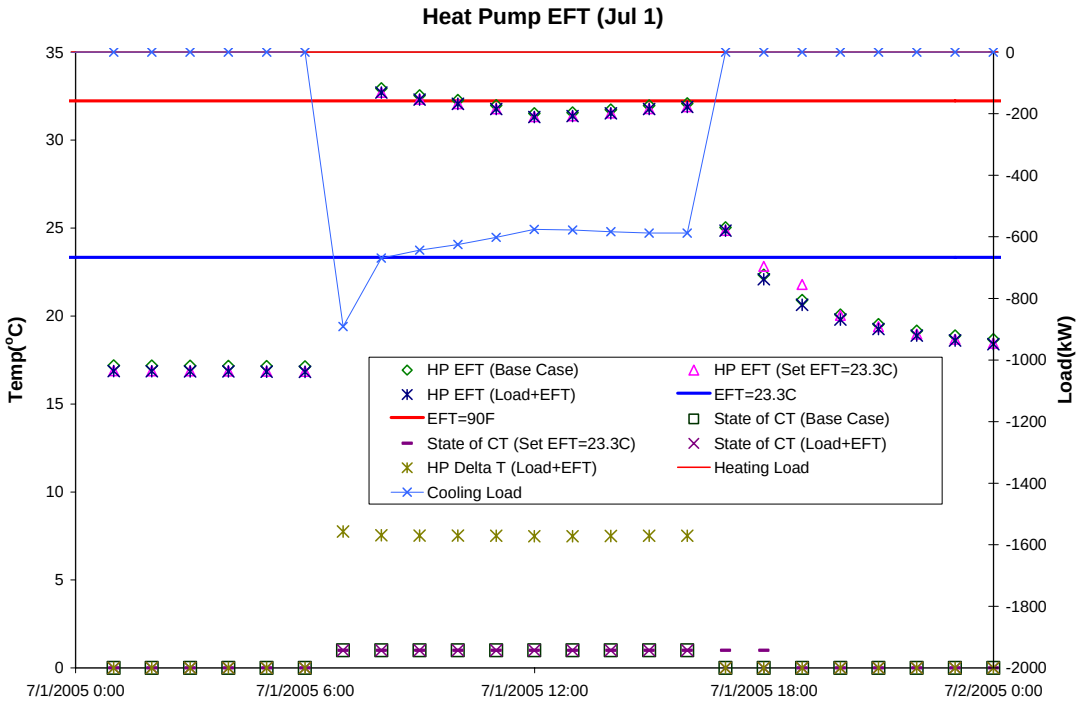

Figure 7.45 Heat pump EFT and cooling tower state of Load + EFT control strategy (July 1st)

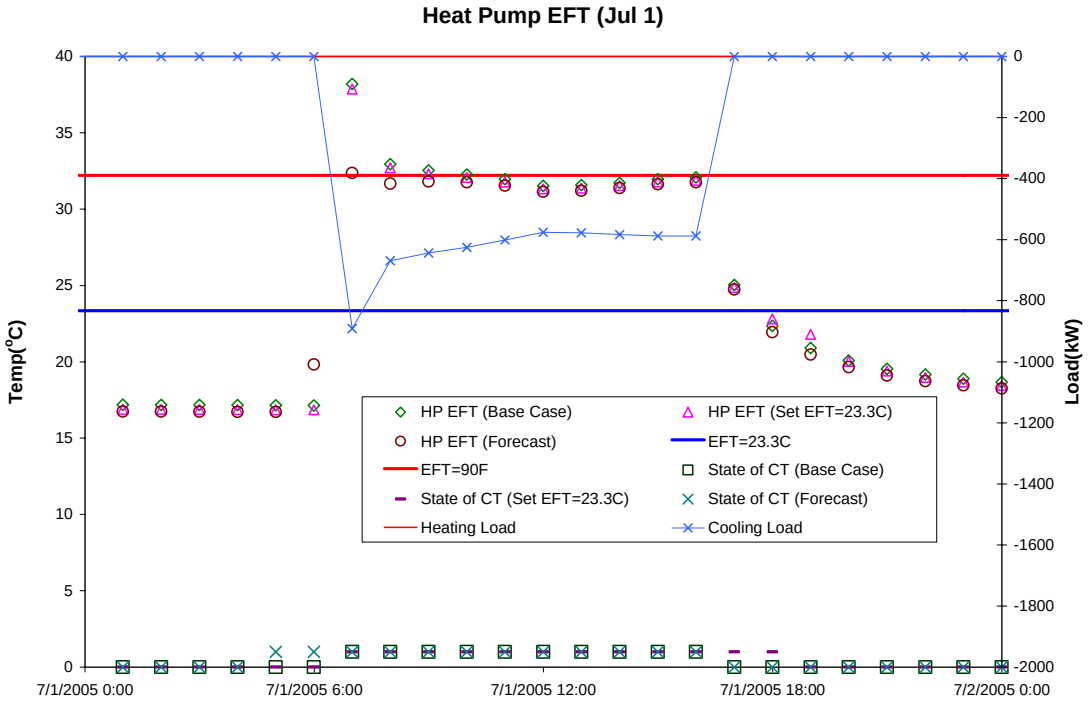

Figure 7.46 Heat pump EFT and cooling tower state of forecast control strategy (July 1st)

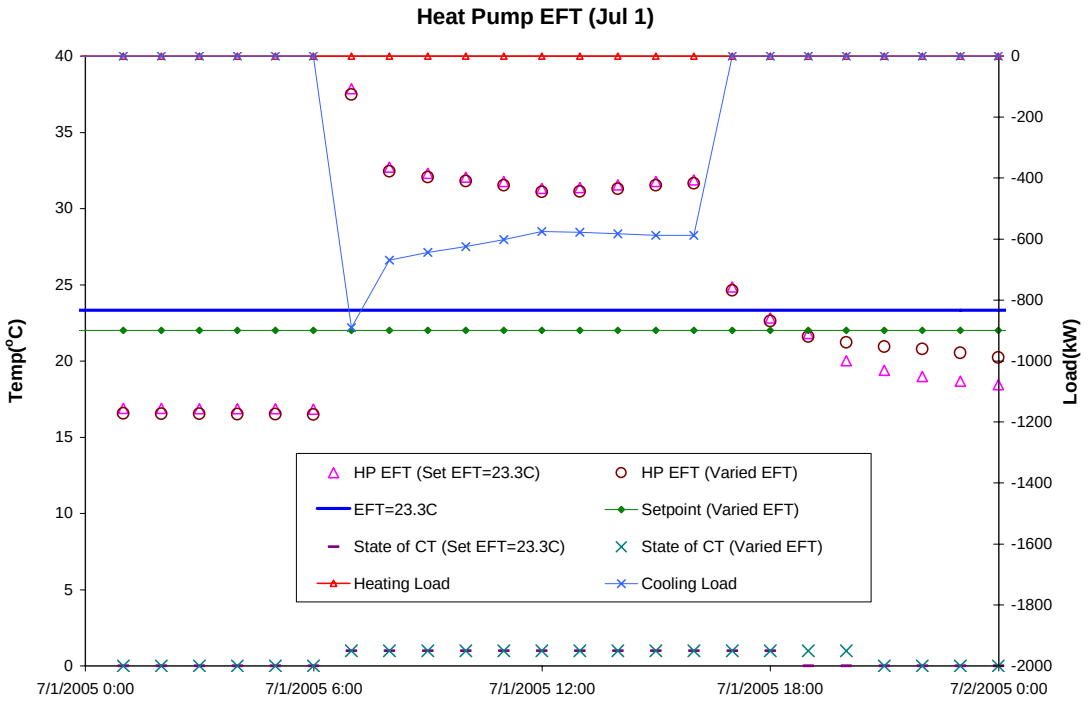

Figure 7.47 Heat pump EFT and cooling tower state of varied EFT control strategy (July 1st)

Figure 7.48 shows the heat pump cooling COP for all the controls in July 1st. Figure 7.49 shows the heat pump power consumption for all the controls. As can be seen, in the first few hours of the day time, the forecast control has the highest COPs because it pre-runs the cooling tower in the morning before the working hours to cool down the ground. As a result, in the first few hours of the work time, the heat pumps have a higher COP caused by the lower heat pump EFT.

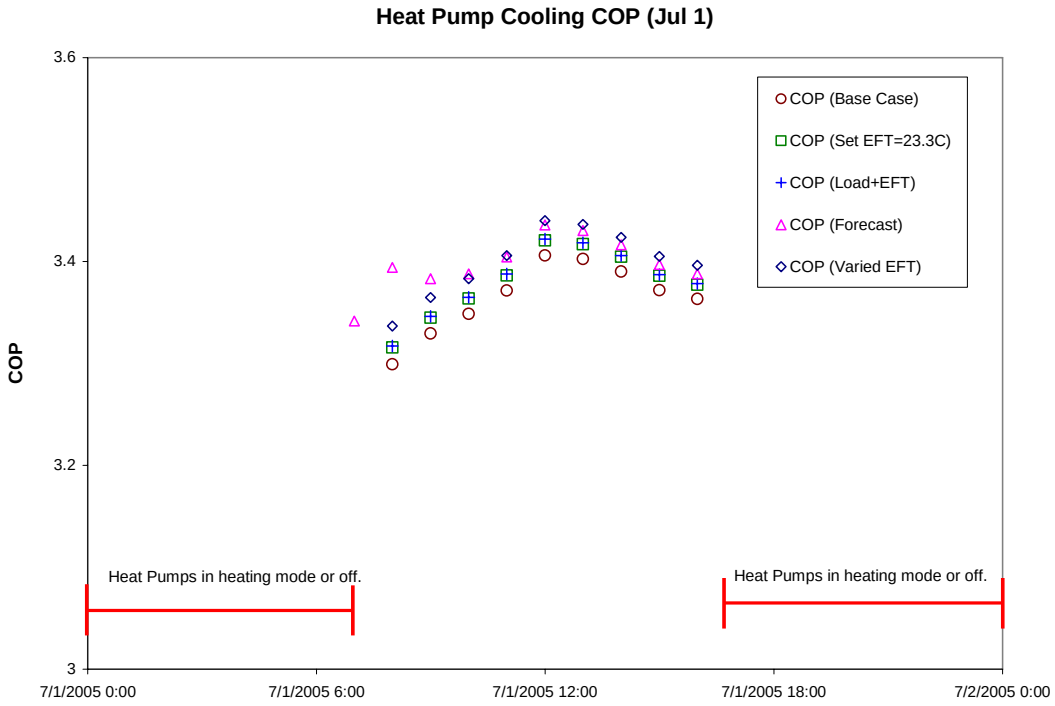

Figure 7.48 Heat pump cooling COP of all control strategies (July 1st)

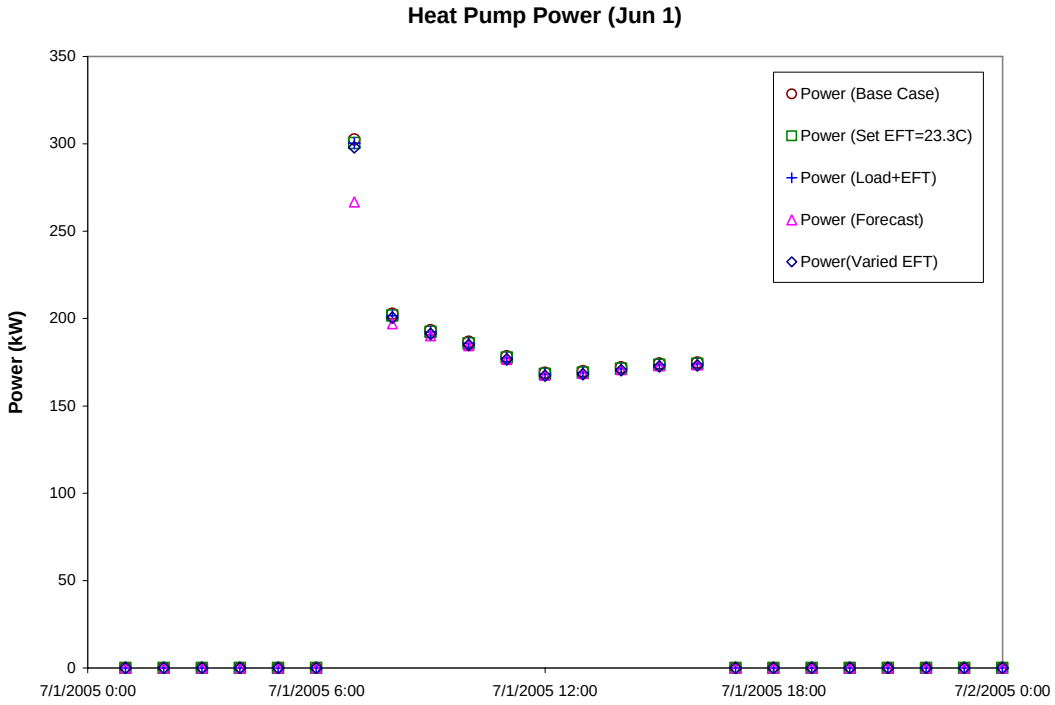

Figure 7.49 Heat pump cooling power of all control strategies (July 1st)

Table 7.5 lists the system energy for consumption by component and the total system energy consumption for the summer day July 1st. As in shown, the forecast control has the biggest percent savings for this day. In this day, the set EFT and forecast control both run the cooling tower for 12 hours. But the system energy consumptions show about 2% energy difference. In this case, the forecast control runs the cooling tower more efficaciously by running at more advantageous times than the set EFT control.

Table 7.5 System energy consumption (July 1st)

Energy Consumption	Base Case	Set EFT	Load + EFT	Forecast	Varied EFT
Heat Pump (kWh)	1923.4	1914.3	1913.5	1868.3	1902.5
Main Circ Pump (kWh)	81.5	81.5	81.5	81.5	81.5
Cooling Tower run time (hours)	10	12	10	12	14
Cooling Tower Fan (kWh)	11.2	13.4	11.2	13.4	15.7
Cooling Tower Circ Pump (kWh)	4.7	5.7	4.7	5.7	6.6
Total (kWh)	2030.8	2026.8	2020.9	1980.8	2020.2
Saving (%)		0.2%	0.5%	2.5%	0.5%

7.6 Conclusions

This chapter aims to develop generally applicable optimal control strategies. Two building types and six U.S. cities are chosen to provide different building loads profile for the study of HGSHP system controls. A buffer program has been developed to optimize the setpoint of the different control strategies for different combinations of HGSHP system design, building type and location.

Several control strategies have been developed and investigated:

- Previously developed (Yavuzturk and Spitler 2000) control strategies

Three control strategies had been developed by Yavuzturk and Spitler (2000) : 1) set heat pump EFT; 2) set heat pump ExFT; and 3) set temperature difference between the heat pump ExFT and outdoor air wetbulb temperature. Using the buffer program, these three control strategies were optimized.

The optimization results showed that the HGSHP systems with three optimized control strategies had almost the same operating cost. The set T_{diff} control strategy did not show any significant saving compared to the set EFT and ExFT control strategies when they were all optimized. However, the set T_{diff} control strategy depends on an accurate measurement of the wetbulb temperature, which is problematic. Therefore, the set T_{diff} control strategy would be not recommended if the optimized setpoint for the other control strategies is available.

The optimization results also showed that the optimized setpoint of the three control strategies for different building types and locations are scattered over a wide range. Therefore, for these three control strategies, there is no generally-applicable setpoint being applicable for different combinations of HGSHP system design, building type and location.

- Control strategy base on the system loads

A new control strategy based on the system loads has been developed. An investigation of the optimization results of three old control strategies showed, for the HGSHP systems with variable speed pumping design, more than 80% of the system cooling loads and heat pump energy consumptions occurred at the heat

pump ΔT being less than -6 ºC (-10.8 ºF). Therefore, the temperature difference across the heat pumps is used to control the cooling tower. Three control strategies, which combine the heat pump ΔT and set EFT/ExFT/T_{diff}, have been developed for the HGSHP systems.

The new control strategies are generically applicable for the different combinations of HGSHP system design, building type and location. Without requiring to run the optimization program, the systems still have a good operation cost saving. The new control strategies of "Load + EFT" and "Load + ExFT" use the easy-to-measure quantities — loop temperatures to control the cooling tower and are physically feasible.

- Forecast/historical control

A forecast/historical control strategy has been developed. Using the forecast/historical system loads, the control strategy estimates the possible energy savings of heat pumps in future from running cooling tower at the current time and then determines to run the cooling tower or not. A procedure has been developed to realize this forecast/historical control strategy. Two different approaches were used to get the predicted system loads: 1) perfect forecast system loads from EnergyPlus+; 2) historical system loads happened one week ago.

The results showed that most of the forecast control strategy cases had the highest percent savings compared to the previous control strategies. Without the perfect prediction of the loads, the historical control strategy cases still have good

savings. A new historical load prediction scheme was developed to aim to provided a more accurate load prediction for the control. However, the performance of this new historical load prediction scheme depends on the building operating schedule.

The forecast/historical control strategies are generically capable for the different combinations of HGSHP system design, building type and location. At every time step, the control strategy estimates the possible energy savings of heat pumps in future from running cooling tower at the current time and then determines to run the cooling tower or not. Therefore, the forecast control strategy is a real-time control strategy and is adaptive.

- Varied EFT/ExFT control strategy

A new varied EFT/ExFT control strategy based on long term variation of the loop temperature has been developed. An investigation of the optimization showed there are quite constant linear relationships between the setpoint of EFT/ExFT and the averaged loop temperature variation over the last N hours. The number of hours in the averaging period can be set as a constant. Therefore, the linear function is used to calculate the setpoint of EFT/ExFT based on the variation of the EFT/ExFT over the last N hours. Coupled with a constant setting EFT/ExFT, the varied EFT/ExFT control strategies have been developed for the HGSHP systems.

The results showed the cases with the varied EFT/ExFT case have similar system energy savings compared to the individual optimized control strategy case. However, the system energy saving is related to the constant EFT/ExFT setting temperatures. Adjusting the constant EFT/ExFT setpoint temperature based on the real system operation data is highly recommended when applying this varied EFT/ExFT control strategy.

8 CONCLUSIONS AND FUTURE WORK

8.1 Summary of Work

This research aims at developing optimal control strategies and set points for HGSHP systems to improve the system performance. The research has successfully meet the four sub-objectives as follows:

- Developing HGSHP system simulation and requisite component models

In Chapter 4, all requisite component models for the HGSHP system simulation have been developed or presented, including: two GLHE models, two heat pump models, two open-circuit cooling tower models, one closed-circuit cooling tower model, two variable speed pump models, two plate frame heat exchanger models. All have been cast as HVACSIM+ component models. The HGSHP system simulation has been implemented in HVACSIM+.

A new scheme has been developed for accelerating the multiyear simulation of HGSHP system. The accelerated algorithm has two parts: a variable time step aspect and a simplified life cycle cost calculation procedure. The comparison between the detailed simulation scheme and the accelerated algorithm showed the difference of optimized setpoint values is less than 0.8ºC and the relative error of the system operation cost is less than 1%.

- Validating HGSHP system simulation

In Chapter 5, the HGSHP system simulation was validated against the experimental data collected from the OSU HGSHP research facility (Hern 2004). The validation covered a 12 month period, including a continuous 7-month cooling season and portions of two heating seasons.

In this HGSHP system validation, two approaches were used for the simulation. First, the HGSHP system was simulated with the cooling tower on/off operation set as a boundary condition taken from the experiment, in which the behavior of each component model was the first concern. After the calibration of each component model, the HGSHP system was simulated with a temperature difference control strategy. The simulation gave total energy consumption about 0.2% higher than the experiment.

- Developing new design procedures of HGSHP system

In Chapter 6, HGSHP system configurations (parallel-connected and serial connected) were investigated first. A parallel-connected HGSHP system was chosen for further investigation. Then for the parallel-connect HGSHP system, a strategy for controlling the flow distribution between GLHE and PHE/cooling tower was developed. Applying this flow distribution control strategy, flow is able to pass through each component without requiring excessive pumping power.

In Chapter 6, a new design procedure, implemented in GLHEPRO, was developed for sizing the HGSHP system components. The new design procedure is capable

of being used for both a new HGSHP and a "retrofit" HGSHP system. Also in Chapter 6, a new algorithm was developed to size the cooling tower based on the local peak wetbulb temperature and the peak ExFT of heat pump. This procedure gives a much smaller cooling tower size than that given by the Kavanaugh (1998) design procedure.

Chapter 6 presents a comparison study of three HGSHP system design method for commercial applicationd: Kavanaugh and Rafferty method; GLHEPro method and GenOpt method. An office building and a motel building in six U.S. cities were used as the test building. In general, the HGSHP designed from the new GLHRPRO design procedure would have a smaller GLHE and cooling tower size and a smaller system life cycle cost than the system designed from the Kavanaugh and Rafferty procedure.

- Investigation and Optimization of HGSHP system control

In Chapter 7, two building types and six U.S. cities are chosen for the study of HGSHP system controls. A buffer program has been developed to optimize the setpoint of the candidate control strategies for different combinations of HGSHP system design, building type and location. Also the buffer program can be modified to run the simulation for the generic control strategy and to optimize the HGSHP system design.

In Chapter 7, three previously developed control strategies (Yavuzturk and Spitler 2000) were investigated. Using the buffer program, the three control strategies

have been optimized to try to find a best setpoint being generically applicable for all HGSHP systems. With individual optimized control, the office building system operation cost savings range between 2% and 11% of the base case. For the motel building, the system operation cost savings range from 1% to 23% compared to the base case. In general, the setpoint of setting EFT control strategy ranges between 10ºC (50ºF) and 25ºC (77ºF); the setpoint of the setting ExFT control strategy ranges between 15ºC (59ºF) and 30ºC (86ºF); and the set temperature difference of setting T_{diff} control strategy ranges between 2ºC (3.6ºF) and 15ºC (27ºF). However, the study results showed there is no point that is optimal for all building/climate combinations.

In Chapter 7, three new control strategies were developed: the system load control strategy, the forecast/historical control strategy and the varied EFT/ExFT control strategy.

Most of the system load control strategy cases, which do not have the benefit of individually optimized setpoints, have similar or better savings than the individually optimized control strategy cases described above (Office: savings from 2% to 16%; Motel: savings from 0% to 23%). The system load control strategies relies on the heat pump ΔT as a subobject measure of load. In practice, the heat pump ΔT value varies with the different system flow rates. To apply this system load control strategy in practice, the system design flow rate and the system design heat rejection rate are required to determine the temperature difference setpoint. In a variable flow rate system, the heat pump ΔT value

typically varies from 4.5 ºC (8.0 ºF) to 6.7 ºC (12.0 ºF) under design condition. The actual design heat pump ΔT would be used in practice as the setpoint.

The forecast control strategy cases have typically higher percent savings compared to the system load control strategies (Office: savings from 2% to 16%; Motel: savings from 0% to 23%). Realistically the perfect prediction of the loads is not possible, an alternative strategy is to use historical loads from 1 weeks earlier as a subrogate. The historical control strategy cases have good savings, typically not more 1% lower than the savings from the forecast control strategy. The forecast/historical control strategy depends on the ability to estimate the possible energy savings of heat pumps using the GLHE g-functions. In the forecast control strategy, approximate correlations are used to calculate the cooling tower heat rejection rate and the heat pump COP. These issues would bring challenges when integrating the forecast/historical control strategy into an actual HGSHP control system. But the forecast/historical control strategy is a real-time control strategy and is adaptive. If the g-functions of the GLHE are available, the forecast/historical control strategy will bring more energy savings than the other control strategy.

A new varied EFT/ExFT control strategy based on long term variation of the loop temperature has been developed. A linear relationship between the setpoint of EFT/ExFT and the averaged loop temperature variation was developed. Coupled with a constant setting EFT/ExFT, the varied EFT/ExFT control strategies have been developed for the HGSHP systems.

The systems with the varied EFT/ExFT control strategy have similar system energy savings compared to the individual optimized control strategy case. However, the system energy saving is related to the constant EFT/ExFT setting temperatures. Adjusting the constant EFT/ExFT setting temperature based on the real system operation data is highly recommended when applying this varied EFT/ExFT control strategy.

These three new control strategies do not require running optimization but the systems still have a good percent energy savings. They approach being generically applicable for the different combinations of HGSHP system design, building type and location.

8.2 Recommendations for Future Research

Recommendations for future research including the following:

- The validation of variable convective resistance aspect of the GLHE model

A validation of variable convective resistance aspect of the GLHE model is highly desirable. A varied flow rate experiment can be designed so as to transition between laminar flow and turbulent flow in the borehole tube. The measured experimental flow rates, the inlet and outlet fluid temperature of the borehole can be used for validation of the variable convective thermal resistance case.

- 3-d or 2-d radial-axial GLHE model

During the simulation process of the GLHE model, it was found the GLHE model caused some errors when the time step was too small or the GLHE length was too large. In the GLHE model, there was an assumption that the fluid temperature changed linearly along the length of the borehole. However, in the real heat transfer process of the borehole, the fluid temperature changes more like an exponential decay (representing long term temperature rise or fall). When the time step is big enough and the loop length is not too long, the linear assumption does not cause too much errors of the calculated outlet fluid temperature. However, when the time step is small and inlet fluid temperature changes suddenly, using the linear assumption, the simulated fluid outlet temperature could be out of the range. To solve this problem, a 3-d model or a 2-d radial-axial model which addresses the fluid temperature gradient along the borehole is required. Also in the GLHE experiments, a phenomena of heat transport delay was observed. For the borehole of 75 m (258ft) deep, it took about 7 minutes for the fluid to pass through. The current GLHE model is not able to address the fluid transport delay issue. Again a 3-d model or 2-d radial-axial model will help to address the fluid transport delay issue, which happens in the real borehole heat transfer process.

- The buried pipe model and the exposed pipe model

In the HGSHP system, there is buried piping that connects the GLHE to the plant building, buried piping that connects the cooling tower to the plant building, and exposed piping that connects the components inside the building. For lack of a method to predict the heat transfer of these pipes, a heuristic pipe model was

taken by using the measured heat gain or loss as an input. As horizontally-buried piping is a common feature of GSHP systems, it would be useful to have a horizontally-buried piping component model. Also an exposed pipe model is desired.

- Comparison of HGSHP design procedure to two current projects.

The HGSHP design procedure developed in this research has been compared against the Kavanaugh and Rafferty (1997) procedure and the GenOpt design procedure. Two projects are currently in progress related to the design of HGSHP systems. One is the ASHRAE Research Project 1384 being performed at the Solar Energy Laboratory, University of Wisconsin. Another project is being carried out by Andrew Chiasson at the University of Wyoming. Both of these projects are aimed at developing design procedures for HGSHP systems. When some results of these two projects are available, a comparison of design results for HGSHP system of different design procedures is highly desired.

- Testing of the system loads control strategy and varied EFT/ExFT control strategies.

The system loads control strategy and varied EFT/ExFT control strategies have been developed and it is desired to test the new control strategies in the actual HGSHP system.

- Improvement of the forecast/historical control strategy

The forecast/historical control strategies depend on an accurate measurement of the wetbulb temperature, which is problematic. Therefore, the outdoor drybulb temperature at current time might be used for predict the heat rejection rate of the cooling tower, which is measured more accurately and easily than the wetbulb temperature. However, the correlation between the cooling tower heat rejection rate and outdoor drybulb temperature is unknown. Therefore, further investigation is required.

- Self-training feature of the control strategies

For the new control strategies, a possible way to improve the performance of the controls is to add self-training feature into the controls. For example, in the forecast/historical control strategy, approximate correlations are used to calculate the cooling tower heat rejection rate and the heat pump COP. These correlations might not predict the cooling tower heat rejection rate and the heat pump COP perfectly in a real HGSHP system. Then a self-training feature can be added into the control strategy. For example, using the historical data of the cooling tower rejection rate, the temperature difference between the heat pump ExFT and the outdoor wetbulb temperature are collected into a database. Using some algorithms, the correlation between the cooling tower heat transfer rate and the temperature difference will be updated using the new collected historical experimental data. By this self-training feature, even if the initial correlation has a poor prediction of the cooling tower heat rejection rate, after collecting a mount of experimental data, the correlation will be updated based on the experimental data.

As a result, the control strategies will have a more accurate prediction of the cooling tower heat rejection rate. Similar approaches will be applied to the calculation of heat pump COP.

9 REFERENCES

Al-Khoury, R., P. G. Bonnier, et al. 2005. Efficient finite element formulation for geothermal heating systems. Part I: Steady state. International Journal for Numerical Method in Engineering. 63: 988-1013.

ASHRAE. 1995. Commercial/institutional ground-source heat pumps engineering manual. Atlanta: American Society of Heating, Refrigerating, and Air-Conditioning Engineers, Inc.

ASHRAE. 2000. ASHRAE Handbook. Atlanta: American Society of Heating, Refrigerating and Air-Conditioning Engineering, Inc.

ASHRAE. 2005. ASHRAE Handbook. Atlanta: American Society of Heating, Refrigerating and Air-Conditioning Engineering, Inc.

Austin, W., C. Yavuzturk, et al. 2000. Development of an in-situ system for measuring ground thermal properties. ASHRAE Transactions. 106(1): 365-379.

Ayub, Z. H. 2003. Plate heat exchanger literature survey and new heat transfer and pressure drop correlations for refrigerant evaporators. Heat Transfer Engineering. 24(5): 3-16.

Al-Khoury, R., P. G. Bonnier and R. B. J. Brinkgreve. 2005. Efficient finite element formulation for geothermal heating systems. Part I: Steady state. International Journal for Numerical Method in Engineering. 63: 988-1013.

ASHRAE. 1995. Commercial/institutional ground-source heat pumps engineering manual. Atlanta: American Society of Heating, Refrigerating, and Air-Conditioning Engineers, Inc.

ASHRAE. 2000. ASHRAE Handbook. Atlanta: American Society of Heating, Refrigerating and Air-Conditioning Engineering, Inc.

ASHRAE. 2005. ASHRAE Handbook-fundamentals. Atlanta: American Society of Heating, Refrigerating and Air-Conditioning Engineering, Inc.

Austin, W., C. Yavuzturk and J. D. Spitler. 2000. Development of an in-situ system for measuring ground thermal properties. ASHRAE Transactions. 106(1): 365-379.

Ayub, Z. H. 2003. Plate heat exchanger literature survey and new heat transfer and pressure drop correlations for refrigerant evaporators. Heat Transfer Engineering. 24(5): 3-16.

Barrow, H. and K. Sherwin. 1994. Theoretical investigation of the effect of the fouling on the performance of a tube and plate heat exchanger. Heat Recovery System & CHP. 14(1): 1-5.

Bennet, J., J. Claesson and G. Hellstrom. 1987. Multipole method to compute the conductive heat flow to and between pipes in a composite cylinder. Report.

University of Lund, Department of Building and Mathematical Physics. Lund, Sweden.

Benton, D. J., C. F. Bowman, M. Hydeman and P. Miller. 2002. An improved cooling tower algorithm for the CoolToolsTM simulation model. ASHRAE Transactions. 108(1): 760-768.

Bernier, M. A. 1994. Cooling tower performance: theory and experiments. ASHRAE Transactions. 100(2): 114-121.

Bernier, M. A. 2001. Ground-coupled heat pump system simulation. ASHRAE Transactions. 107(1): 605-616.

Bernier, M. A., P. Pinel, R. Labib and R. Paillot. 2004. A multiple load aggregation algorithm for annual hourly simulations of GCHP systems. HVAC&R Research. 10(4): 471-487.

Bi, Y., L. Chen and C. Wu. 2002. Ground heat exchanger temperature distribution analysis and experimental verification. Applied Thermal Engineering. 22(2): 183-189.

BLAST. 1986. BLAST(Building Loads and System Thermodynamics). Report. University of Illinois, Urbana-Champaign.

Bose, J. E. 1984. Closed loop ground coupled heat pump design manual. Report. Engineering Technology Extension Oklahoma State University.

Briggs, R. S., R. G. Lucas and Z. T. Taylor. 2002. Climate Classification for Building Energy Codes and Standards. Report. Pacific NW National laboratory. http://www.energycodes.gov/implement/pdfs/climate_paper_review_draft_rev.pdf.

Carslaw, H. S. and J. C. Jaeger. 1947. Conduction of Heat in Solids. Oxford, U.K.: Claremore Press.

Carslaw, H. S. and J. C. Jaeger. 1959. Conduction of heat in solids. Oxford, U.K.: Claremore Press.

Cecchini, C. and D. Marchal. 1991. A simulation model of refrigerant and air-conditioning equipment based on experimental data. ASHRAE Transactions. 97(2): 388-393.

Chen, X. 1996. Addition of annual building energy analysis capability to a design load calculation program. Master Thesis. Oklahoma State University. Stillwater, Oklahoma.

Chiasson, A. D., J. D. Spitler, S. J. Rees and M. D. Smith. 2000. A model for simulating the performance of a pavement heating system as a supplemental heat rejecter with closed-loop ground-source heat pump systems. ASME Journal of Solar Energy Engineering. 122: 183-191.

Chiasson, A. D. and C. Yavuzturk. 2003. Assessment of the viability of hybrid geothermal heat pump systems with solar thermal collectors. ASHRAE Transactions. 109(2): 487-500.

Chiasson, A. D., C. Yavuzturk and W. J. Talbert. 2004. Design of school building HVAC retrofit with hybrid geothermal heat-pump system. Journal of architectural engineering. 10(3): 103-111.

Clark, D. R. 1985. HVACSIM+ Building Systems and Equipment Simulation Program Reference Manual. NBSIR 84-2996. National Bureau of Standards.

CRI. 2006. GS2000TM. Caneta Research Inc. http://www.canetaenergy.com/GS2000.html

Deerman, J. D. and S. P. Kavanaugh. 1991. Simulation of vertical U-tube ground-couple heat pump systems using the cylindrical heat source solution. ASHRAE Transactions. 97: 287-295.

Deng, Z. 2004. Modeling of standing column wells in ground source heat pump systems. Ph.D. Thesis. Oklahoma State University. Stillwater, OK.

Deng, Z., S. J. Rees and J. D. Spitler. 2005. A model for annual simulation of standing column well ground heat exchangers. HVAC&R Research. 11(4): 637-655.

DesignBuilder. 2006. DesignBuilder software. http://www.designbuilder.co.uk

Diao, N. R., H. Y. Zeng and Z. H. Fang. 2004. Improvement in modeling of heat transfer in vertical ground heat exchangers. HVAC&R Research. 10(4): 459-470.

Didion, D. A. and W. J. Mulroy. 1983. A laboratory investigation of refrigerant migration in a split-unit air conditioner. BNDIR 83-2756. Report. Washington, D.C: National Bureau of Standards.

Dobson, M. K., D. L. O'Neal and W. Aldred. 1995. Modified analytical method for simulating cyclic operation of vertical U-tube ground-coupled heat pumps. Proceedings of the 1995 ASME/JSME/JSES International Solar Energy Conference. pp: 69-76. Maui, HI, USA. Mar 19-24 1995.

DOE. 2006. Federal Energy Management Program Assessment of Hybrid Geothermal Heat Pump Systems. http://www.pnl.gov/techreview/hybrid-new/hybrid-ghp.html

DOE. 2007. EnergyPlus energy simulation software. http://www.eere.energy.gov/buildings/energyplus/

EPRI. 1993. Water-loop heat pump systems controls guide. Report. Electric Power Research Institute.

Eskilson, P. 1987. Thermal analysis of heat extraction boreholes. Doctoral Thesis. University of Lund, Department of Mathematical Physics. Lund, Sweden.

Eskilson, P. and J. Claesson. 1988. Simulation model for thermally interacting heat extraction boreholes. Numerical Heat Transfer. 13(2): 149-165.

Feng, X. 1999. Energy analysis of BOK building. Master thesis. Oklahoma State University. Stillwater, Oklahoma.

Fujii, H., R. Itoi and T. Ishikami. 2004. Improvements on analytical modeling for vertical U-tube ground heat exchangers. Transactions - Geothermal Resources Council. 28: 73-77.

GaiaGeothermal. 2006. Ground Loop Design 3.0. Gaia Geothermal. http://www.gaiageo.com/software/software.html

GBTI. 2006. Ground Loop Design (GLD). Geothermal Bore Technologies Inc. http://www.groundloopdesign.com/gld.html

Gehlin, S. and B. Nordell. 2003. Determining undisturbed ground temperatures for thermal response test. ASHRAE Transactions. 109(1): 151-156.

Gentry, J. E. 2007. Simulation and validation of hybrid ground source and water-loop heat pump systems. Master Thesis. Oklahoma State University. Stillwater, Oklahoma.

Gentry, J. E., J. D. Spitler, D. E. Fisher and X. Xu. 2006. Simulation of a hybrid ground source heat pump system and validation of the system model. Proceedings of the 7th International Conference on System Simulation in Buildings. Liège, Belgium. December 11-13, 2006.

GeoKISS. 2006. GCHPCalc 4.1.2. Ground Source Heat Pump Design Keep It Simple & Solid. http://www.geokiss.com/software/Ver40_Instructions.PDF

Gilbreath, C. S. 1996. Hybrid ground source heat pump systems for commercial applications. Master. The University of Alabama, Department of Mechanical Engineering. Tuscaloosa, Alabama.

Gu, Y. and D. L. O'Neal. 1998. Development of an equivalent diameter expression for vertical U-tubes used in ground-coupled heat pumps. ASHRAE Transactions. 104(2): 347-355.

Gu, Y. and D. L. O'Neal. 1998. Modeling the effect of backfills on U-tube ground coil performance. ASHRAE Transactions. 104(2): 356-365.

Hasan, A. and K. Siren. 2002. Theoretical and computational analysis of closed wet cooling towers and its applications in cooling of buildings. Energy and Buildings. 34(5): 477-486.

Hellstrom, G. 1991. Ground heat storage. Thermal analyses of duct storage systems I: Theory. Lund, Sweden.: University of Lund, Department of Mathematical Physics.

Hellstrom, G., L. Mazzarella and D. Pahud. 1996. Duct ground storage model TRNSYS version. Report. Department of Mathematical Physics, University of Lund, Sweden.

Hern, S. 2004. Design of an experimental facility for hybrid ground source heat pump systems. Master Thesis. Oklahoma State University. Stillwater, Oklahoma.

Hopkins, P. L. 1983. Performance of a vertical heat pump ground-coupling device. Unpublished Master Thesis. Oklahoma State University. Stillwater, Oklahoma.

IGSHPA. 1997. Closed-loop/Ground-source heat pump systems. Installation guide. Stillwater, Oklahoma: International Ground Source Heat Pump Association.

Incropera, F. P. and D. P. DeWitt. 2002. Fundamentals of Heat and Mass Transfer. 5th Edition. Hoboken, NJ: John Wiley & Sons.

Ingersoll, L. R. and H. J. Plass. 1948. Theory of the ground pipe heat source for the heat pump. Heating, Piping & Air Conditioning. July: 119-122.

Ingersoll, L. R., O. J. Zobel and A. C. Ingersoll. 1954. Heat conduction with engineering, geological, and other applications. New York: McGraw-Hill.

Iu, I., P. K. Bansal, S. Rees, D. Fisher and J. Spitler. 2003. Energy efficiency analysis of a unitary heat pump system. Proc. International Conference on Building Systems and Facilities Management - Integrating Innovations and Technologies For a Built Environment. pp: 334-341. Singapore. October 8-10, 2003.

Jin, H. and J. D. Spitler. 2002. A parameter estimation based model of water-to-water heat pumps for use in energy calculation programs. ASHRAE Transactions. 108(1): 3-17.

Jin, H. and J. D. Spitler. 2003. Parameter estimation based model of water-to-water heat pumps with scroll compressors and water/glycol solutions. Building Services Engineering Research and Technology. 24(3): 203-219.

Kavanaugh, S. 1995. A design method for commercial ground-coupled heat pumps. ASHRAE Transactions. 101(2): 1088-1094.

Kavanaugh, S. P. 1985. Simulation and experimental verification of vertical ground-coupled heat pump systems. Ph.D. Oklahoma State University. Stillwater, Oklahoma.

Kavanaugh, S. P. 1998. A design method for hybrid ground-source heat pump. ASHRAE Transactions. 104(2):

Kavanaugh, S. P. and K. Rafferty. 1997. Ground-source heat pumps: Design of geothermal systems for commercial and institutional buildings. Atlanta: American Society of Heating, Refrigerating and Air-Conditioning Engineers, Inc.

Khan, J.-U.-R., B. A. Qureshi and S. M. Zubair. 2004. A comprehensive design and performance evaluation study of counter flow wet cooling towers. International Journal of Refrigeration. 27(8): 914-923.

Khan, M. H. 2004. Modeling, simulation and optimization of ground source heat pump systems. Master thesis. Oklahoma State University. Stillwater, OK.

Khan, M. H., A. Varanasi, J. D. Spitler, D. E. Fisher and R. D. Delahoussaye. 2003. Hybrid ground source heat pump system simulation using visual modeling tool for HVACSIM+. Proceedings of Building Simulation 2003. pp: 641-648. Eindhoven, Netherlands. August 11-14, 2003.

Klein, S. A. 1996. TRANSYS manual, a transient simulation program. Madison:Solar Energy Laboratory, University of Wisconsin.

Kloppers, J. C. and D. G. Kroger. 2005. Cooling tower performance evaluation: Merkel, Poppe, and e-NTU methods of analysis. Journal of Engineering for Gas Turbines and Power. 127(1): 1-7.

Kohl, T., R. Brenni and W. Eugester. 2002. System performance of a deep borehole heat exchanger. Geothermics. 31: 687-708.

Kohl, T. and R. J. Hopkirk. 1995. "FRACTure" A simulation code for forced fluid flow and transport in fractured, porrous rock. Geothermics. 24(3):

Lash, T. 1992. Simulation and analysis of a water loop heat pump system. Master Thesis. University of Illinois at Urbana-Champaign, Department of Mechanical Engineering.

Lebrun, J. and C. A. Silva. 2002. Cooling tower - Model and experimental validation. ASHRAE Transactions. 108(1): 751-759.

Lebrun, J., C. A. Silva, F. Trebilcock and E. Winandy. 2004. Simplified models for direct and indirect contact cooling towers and evaporative condensers. Building Services Engineering Research and Technology. 25(1): 25-31.

Lei, T. K. 1993. Development of a computational model for a ground-coupled heat exchanger. ASHRAE Transactions. 99(1): 149-159.

Liu, X. and J. D. Spitler. 2004. Simulation based investigation on the design of hydronic snow melting system. Proceedings of the Transportation Research Board 83rd Annual Meeting. Washington, D.C. January 11-15, 2004.

Means. 2006. RSMeans mechanical cost data 2006. Kingston: R.S. Means Co.

Mei, V. C. and V. D. Baxter. 1986. Performance of a ground-coupled heat pump with multiple dissimilar U-tube coils in series. ASHRAE Transactions. 92(2): 30-42.

Merkel, F. 1925. Verduftungskuhlung. Forschungarbeiten. No. 275.

Muraya, N. K. 1994. Numerical modeling of the transient thermal interference of vertical U-tube heat exchangers. Ph.D. Dissertation. Texas A&M University.

Muraya, N. K., D. L. O'Neal and W. M. Heffington. 1996. Thermal interference of adjacent legs in a vertical U-tube heat exchanger for a ground-coupled heat pump. ASHRAE Transactions. V102(2): 12-21.

Nelder, J. A. and R. Mead. 1965. A simplex method for function minimization. Computer Journal. 7: 308-313

O'Neill, Z. D., J. D. Spitler and S. J. Rees. 2006. Modeling of standing column wells in ground source heat pump systems. Proceedings of the 10th International Conference on Thermal Energy Storage. Pomona, NJ.

Parise, J. A. R. 1986. Simulation of vapor-compression heat pumps. Simulation. 46(2): 71-76.

Patankar, S. V. 1991. Computation of conduction and duct flow heat transfer. Maple Grove, Minnesota: Innovative Research, Inc.

Phetteplace, G. and W. Sullivan. 1998. Performance of a hybrid ground-coupled heat pump system. ASHRAE Transactions. 104(1): 663-670.

Rabehl, R. J., J. W. Mitchell and W. A. Beckman. 1999. Parameter estimation and the use of catalog data in modeling heat exchangers and coils. HVAC&R Research. 5(1): 3-17.

Ramamoorthy, M., H. Jin, A. Chiasson and J. D. Spitler. 2001. Optimal sizing of hybrid ground-source heat pump systems that use a cooling pond as a supplemental heat rejecter- A system simulation approach. ASHRAE Transactions. 107(1): 26-38.

Rees, S. J. 2000. An introduction to the finite volume method: Tutorial series. Report. Oklahoma State University. Stillwater, OK.

Remund, C. P. 1999. Borehole thermal resistance: Laboratory and fields studies. ASHRAE Transactions. 105(1): 439-445.

Rottmayer, S. P., W. A. Beckman and J. W. Mitchell. 1997. Simulation of a single vertical U-tube ground heat exchanger in an infinite medium. ASHRAE Transactions. 103(2): 651-659.

Shonder, J. A., V. Baxter, J. Thornton and P. Hughes. 1999. A new comparison of vertical ground heat exchanger design methods for residential applications. ASHRAE Transactions. 105(2): 1179-1188.

Shonder, J. A., V. D. Baxter, P. J. Hughes and J. W. Thornton. 2000. A comparison of vertical ground heat exchanger design software for commercial applications. ASHRAE Transactions. 106(1): 831-842.

Shonder, J. A. and J. Beck. 2000. Field test of a new method for determining soil formation thermal conductivity and borehole resistance. ASHRAE Transactions. 106(1): 843-850.

Shonder, J. A. and j. V. Beck. 1999. Determining effective soil formation thermal properties from field data using a parameter estimation technique. ASHRAE Transactions. 105(2): 458-466.

Signorelli, S., T. Kohl and L. Rybach. 2005. Sustainability of production from borehole heat exchanger fields. Proceedings World Geothermal Congress 2005. Antalya, Turkey. April, 2005.

Singh, J. B. and G. Foster. 1998. Advantages of using the hybrid geothermal option. The Second Stockholm International Geothermal Conference. The Richard Stockton College of New Jersey. http://intraweb.stockton.edu/eyos/energy_studies/content/docs/proceedings/SINGH.PDF.

Soylemez, M. S. 1999. Theoretical and experimental analyses of cooling towers. ASHRAE Transactions. 105(1): 330-337.

Spitler, J. D. 2000. GLHEPRO -- A design tool for commercial building ground loop heat exchangers. Proceedings of Fourth International Heat Pumps in Cold Climates Conference. Aylmer, Qubec. August 17-18, 2000.

Spitler, J. D. 2003. MAE5633: Advanced thermal systems course notes. Oklahoma State University. Stillwater, Oklahoma.

Spitler, J. D. 2006. GLHEPRO 3. International Ground Source Heat Pump Association. http://www.hvac.okstate.edu/glhepro/index.html

Stabat, P. and D. Marchio. 2004. Simplified model for indirect-contact evaporative cooling-tower behaviour. Applied Energy. 78(4): 433-451.

Stefanuk, N. B. M., J. D. Aplevich and M. Renksizbulut. 1992. Modeling and simulation of a superheat-controlled water-to-water heat pump. ASHRAE Transactions. 98(2): 172-184.

Sutton, M. G., R. J. Couvillion, D. W. Nutter and R. K. Davis. 2002. An algorithm for approximating the performance of vertical bore heat exchangers installed in a stratified geological regime. ASHRAE Transactions. 108(2): 177-184.

Tang, C. C. 2005. Modeling packaged heat pumps in a quasi-steady state energy simulation program. Master Thesis. Oklahoma State University. Stillwater, Oklahoma.

Webb, R. L. 1984. A unified theoretical treatment for thermal analysis of cooling towers, evaportive condensers and fluid coolers. ASHRAE Transactions. 90(2): 398-415.

Webb, R. L. and A. Villacres. 1984. Algorithms for performance simulation of cooler colers, evaporative condensers and fluid coolers. ASHRAE Transactions. 90(2): 416-458.

Wetter, M. 2000. GenOpt Generic Optimization Program. Lawrence Berkeley National Laboratory.

Xu, X. and J. D. Spitler. 2006. Modeling of vertical ground loop heat exchangers with variable convective resistance and thermal mass of the fluid. Proceedings of the 10th International Conference on Thermal Energy Storage. Pomona, NJ.

Yavuzturk, C. 1999. Modeling of vertical ground loop heat exchangers for ground source heat pump systems. Ph. D. thesis. Oklahoma State University. Stillwater, Oklahoma.

Yavuzturk, C. and J. D. Spitler. 1999. A short time step response factor model for vertical ground Loop heat exchangers. ASHRAE Transactions. 105(2): 475-485.

Yavuzturk, C. and J. D. Spitler. 2000. Comparative study to investigate operating and control strategies for hybrid ground source heat pump systems using a short time-step simulation model. ASHRAE Transactions. 106(2): 192-209.

Yavuzturk, C. and J. D. Spitler. 2001. Field validation of a short time-step model for vertical ground loop heat exchangers. ASHRAE Transactions. 107(1): 617-625.

Yavuzturk, C., J. D. Spitler and S. J. Rees. 1999. A transient two-dimensional finite volume model for the simulation of vertical U-tube ground heat exchangers. ASHRAE Transactions. 105(2): 465-474.

Young, R. 2004. Development, verification, and design analysis of the borehole fluid thermal mass model for approximating short term borehole thermal Response. Master Thesis. Oklahoma State University. Stillwater, OK.

Zalewski, W. and P. A. Gryglaszewski. 1997. Mathematical model of heat and mass transfer processes in evaporative fluid coolers. Chemical Engineering and Processing. 36(4): 271-280.

Zeng, H., N. Diao and Z. Fang. 2002. A finite line-source model for boreholes in geothermal heat exchangers. Heat Transfer- Asian Research. 31(7): 558-567.

Zeng, H., N. Diao and Z. Fang. 2003. Heat transfer analysis of boreholes in vertical ground heat exchangers. International Journal of Heat and Mass Transfer. 46(23): 4467-4481.

APPENDIX A One-Dimensional Numerical Model Validation

The one-dimensional numerical model developed in Section 4.1.2 was validated using GEMS2D (Rees 2000). Totally six group of test cases were carried out for the validation of the one-dimensional numerical model. The varied parameters of borehole include: borehole diameters, shank spacing, grout conductivities, soil conductivities, grout heat capacities and fluid factors. The selected values included the common values used in the vertical ground loop heat exchangers and were listed in Table 4.1. The remaining parameters common to all test cases were given in Table 4.2.

In Section 4.1.2, only detailed comparison result of case 1A was provided. In this appendix, comparison results of all test cases were listed in six groups with respect to the varied parameters. The case number in the following figures can be checked out in Table 4.1.

Group 1: Borehole Diameter Validation

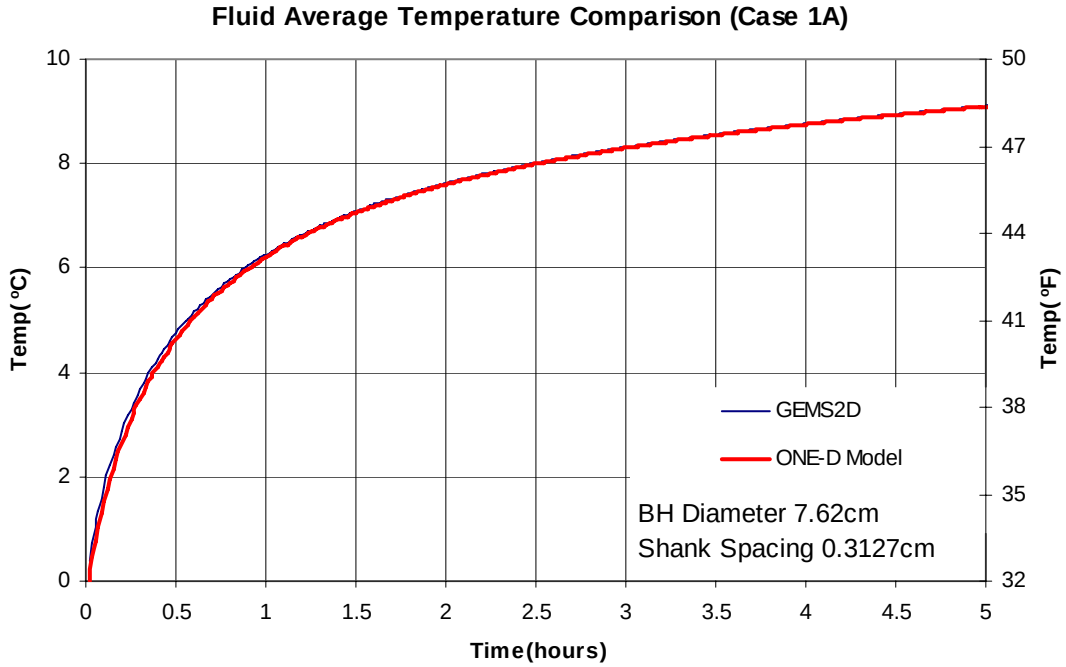

Figure A.1 Comparison of the one-dimensional model and GEMS2D model temperature predictions for Test Case 1A.

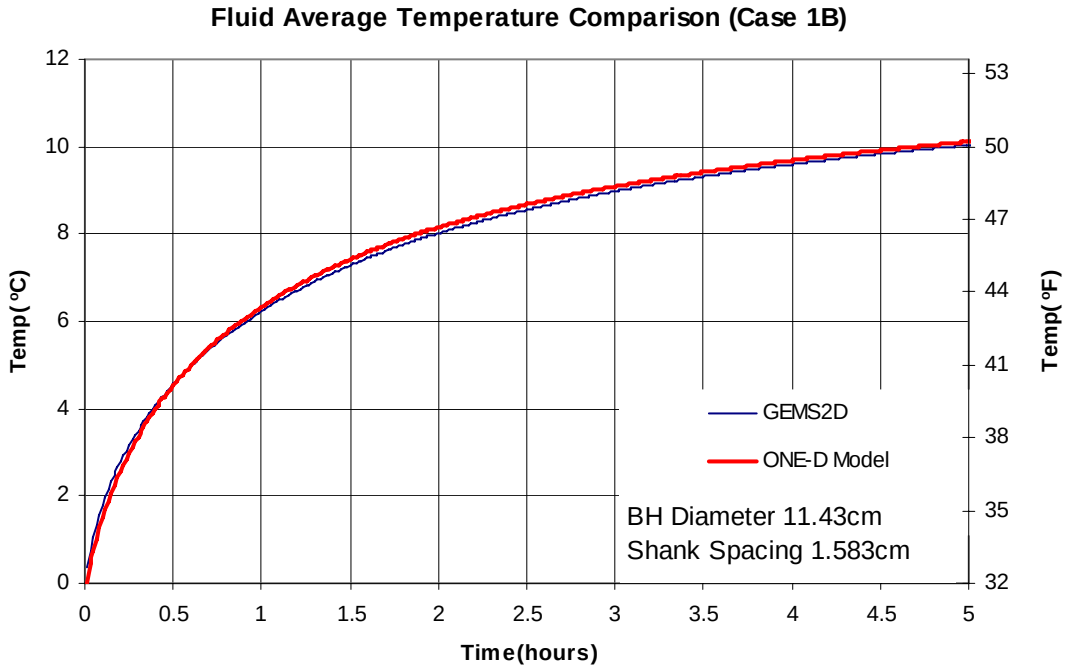

Figure A.2 Comparison of the one-dimensional model and GEMS2D model temperature predictions for Test Case 1B.

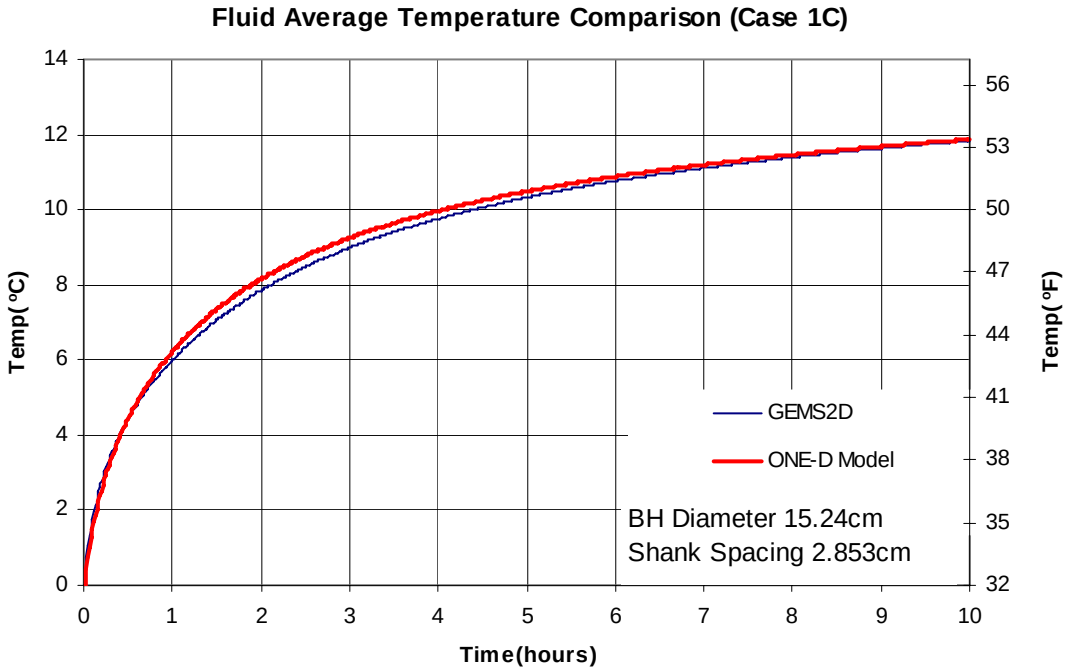

Figure A.3 Comparison of the one-dimensional model and GEMS2D model temperature predictions for Test Case 1C.

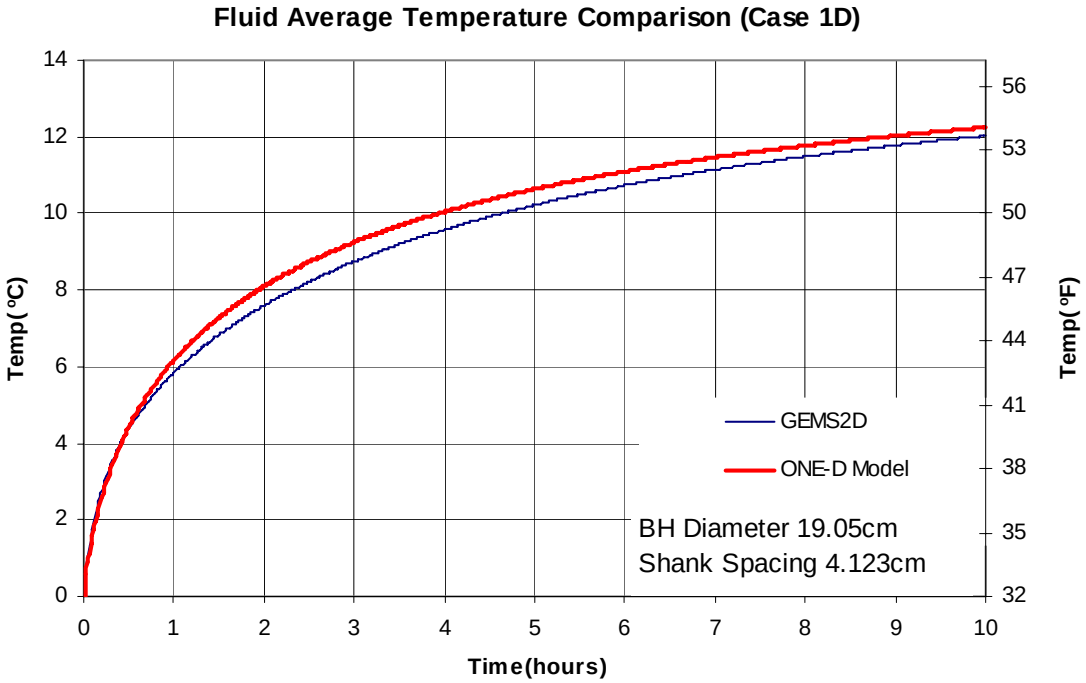

Figure A.4 Comparison of the one-dimensional model and GEMS2D model temperature predictions for Test Case 1D.

Group 3: Shank Spacing Validation

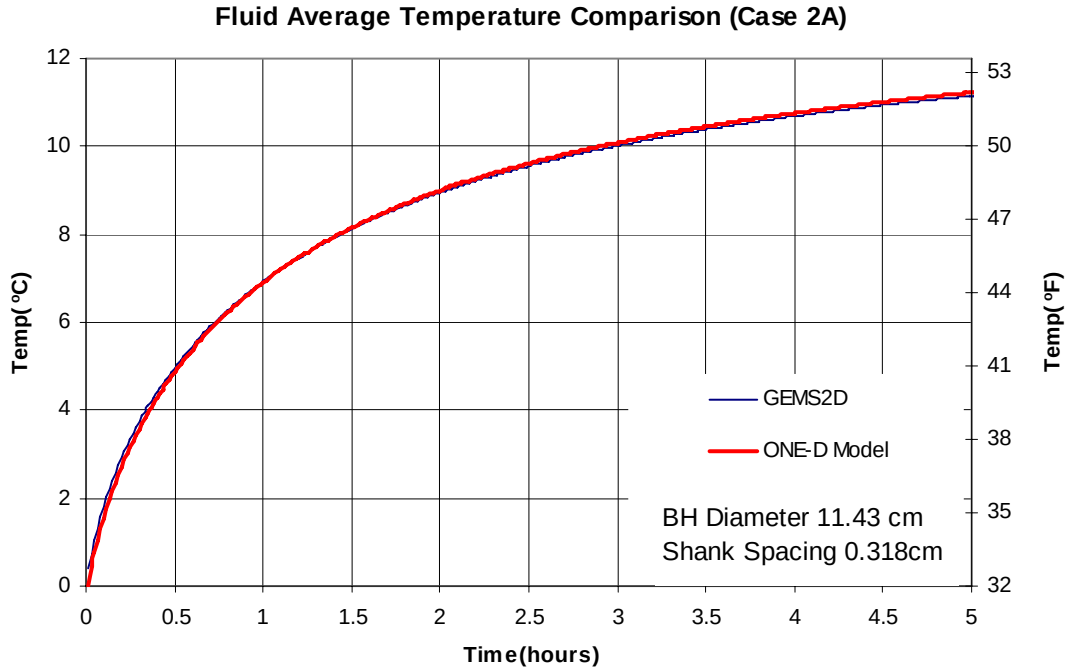

Figure A.5 Comparison of the one-dimensional model and GEMS2D model temperature predictions for Test Case 2A.

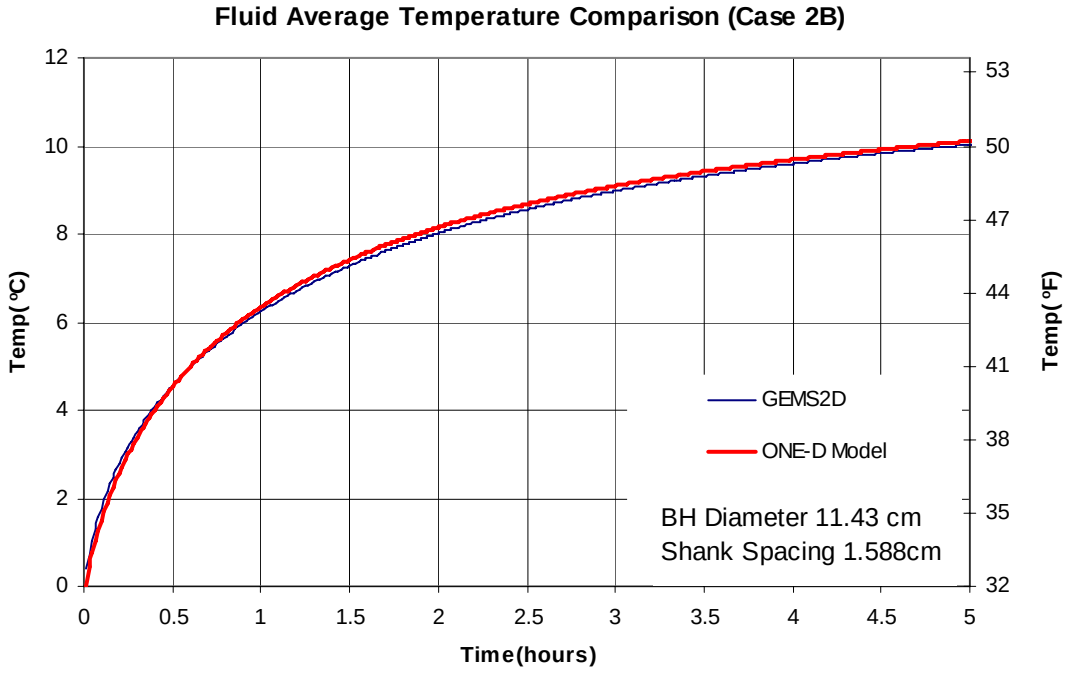

Figure A.6 Comparison of the one-dimensional model and GEMS2D model temperature predictions for Test Case 2B.

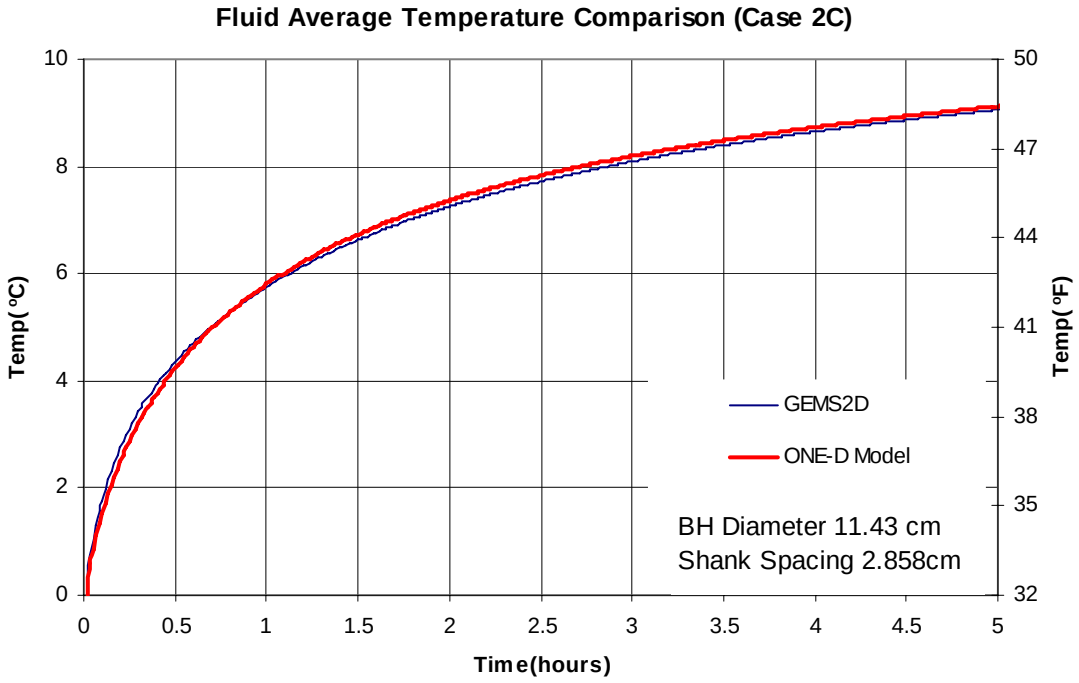

Figure A.7 Comparison of the one-dimensional model and GEMS2D model temperature predictions for Test Case 2C.

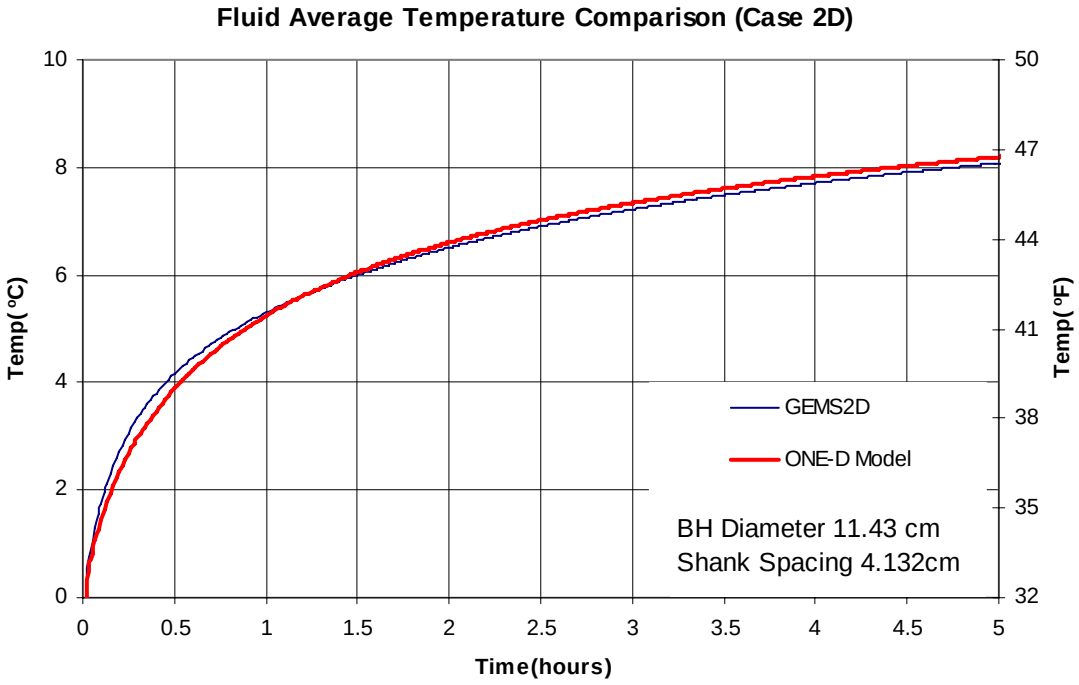

Figure A.8 Comparison of the one-dimensional model and GEMS2D model temperature predictions for Test Case 2D.

Group 3: Grout Conductivity Validation

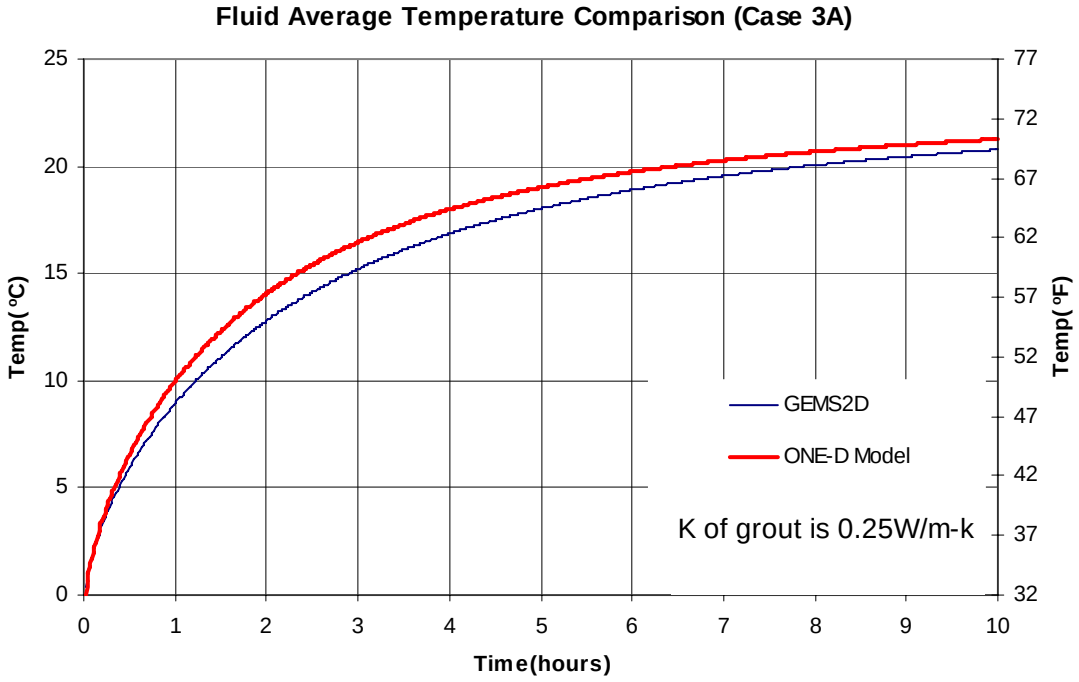

Figure A.9 Comparison of the one-dimensional model and GEMS2D model temperature predictions for Test Case 3A.

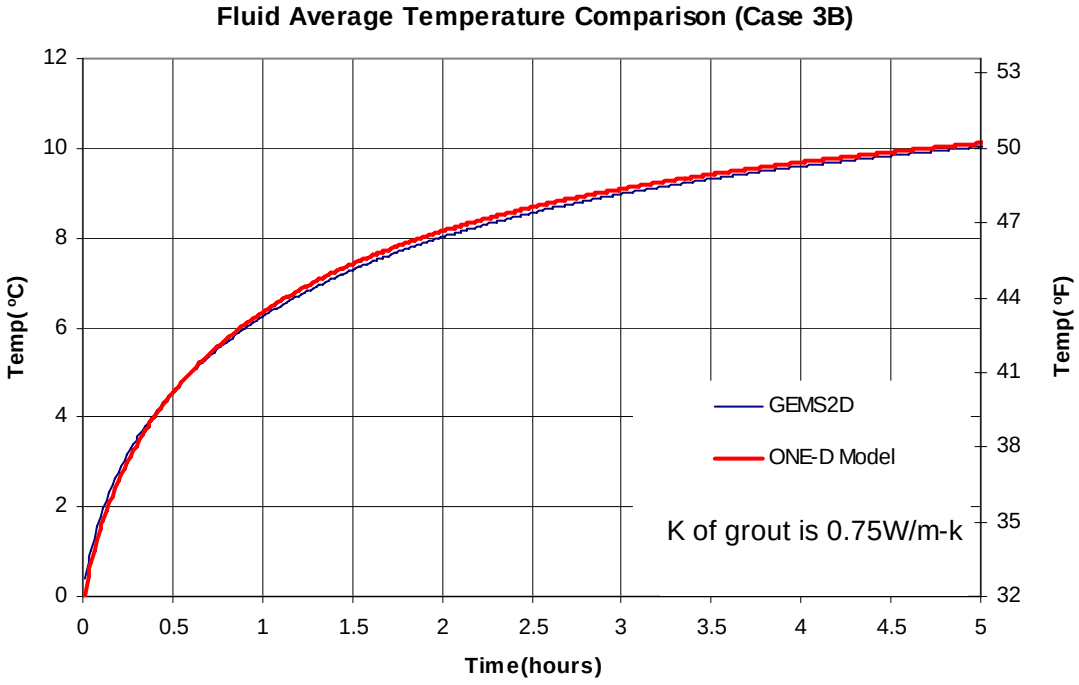

Figure A.10 Comparison of the one-dimensional model and GEMS2D model temperature predictions for Test Case 3B.

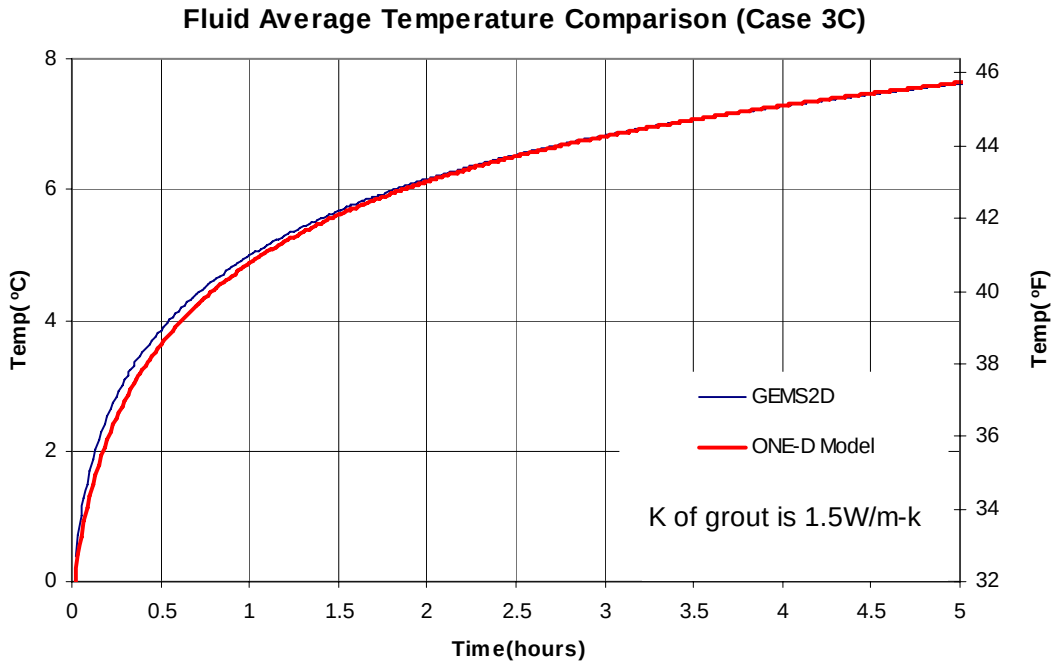

Figure A.11 Comparison of the one-dimensional model and GEMS2D model temperature predictions for Test Case 3C.

Group 4: Ground Conductivity Validation

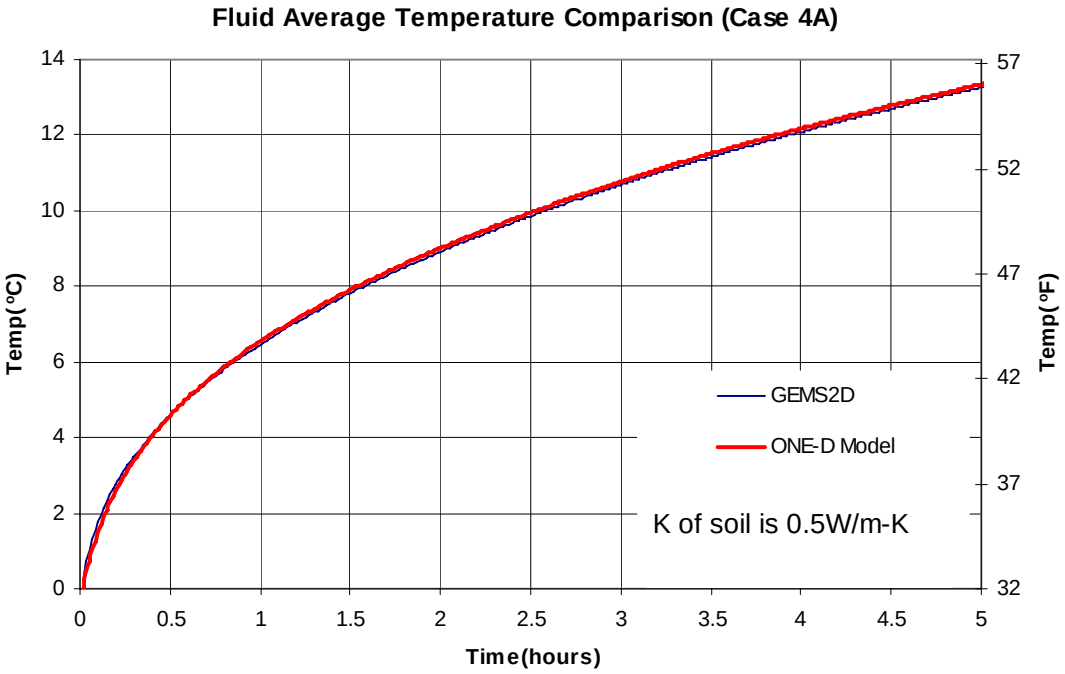

Figure A.12 Comparison of the one-dimensional model and GEMS2D model temperature predictions for Test Case 4A.

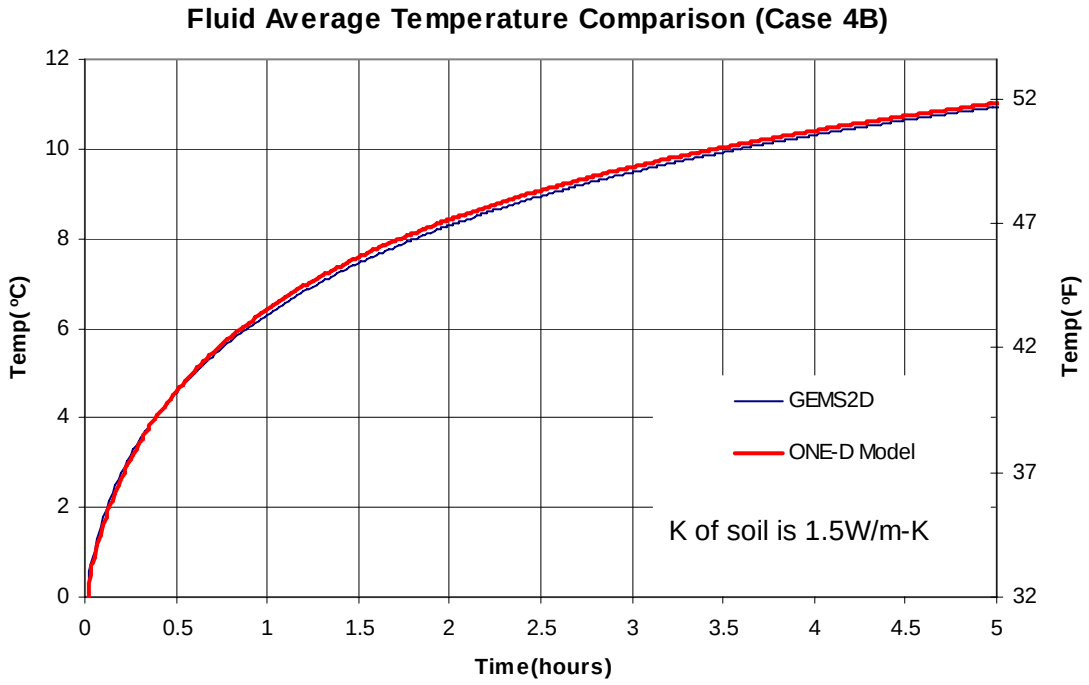

Figure A.13 Comparison of the one-dimensional model and GEMS2D model temperature predictions for Test Case 4B.

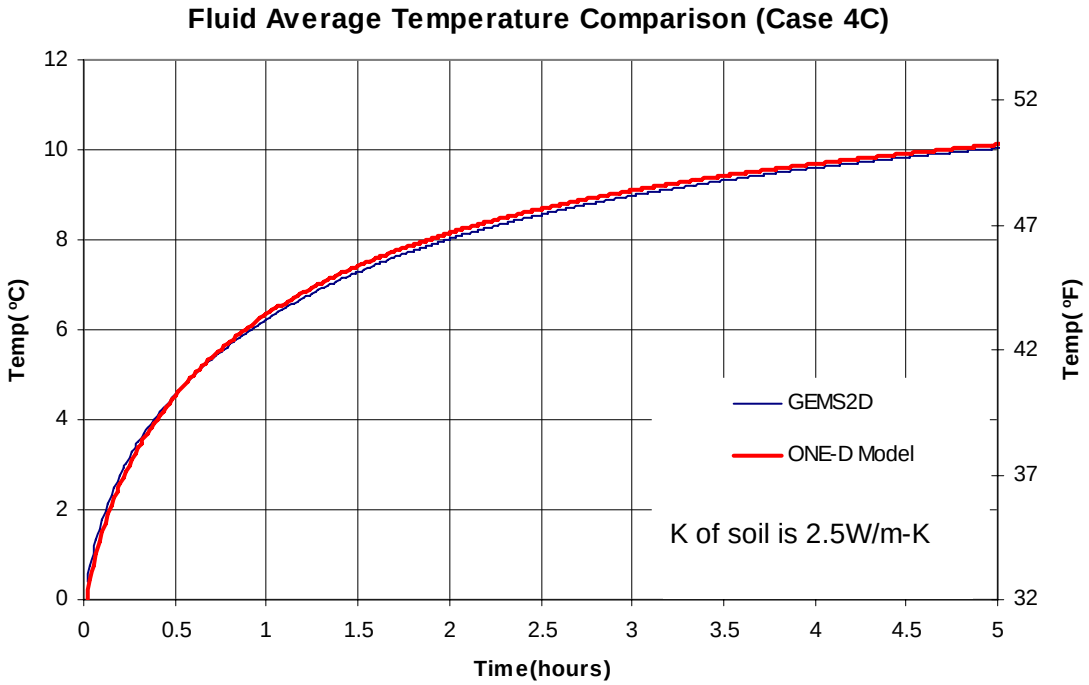

Figure A.14 Comparison of the one-dimensional model and GEMS2D model temperature predictions for Test Case 4C.

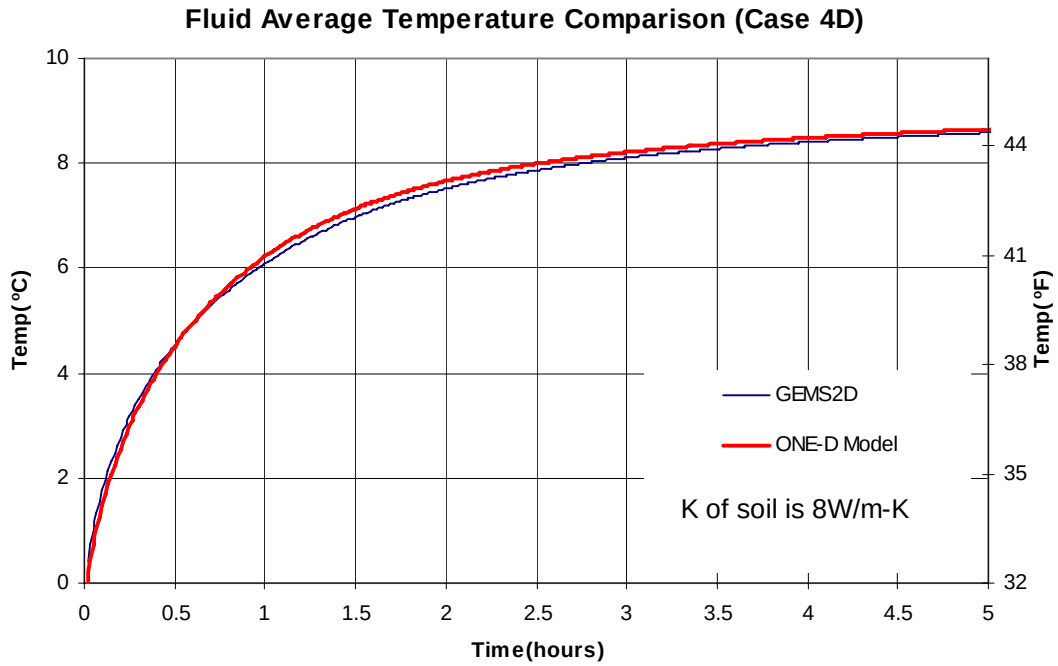

Figure A.15 Comparison of the one-dimensional model and GEMS2D model temperature predictions for Test Case 4D.

Group 5 Grout Heat Capacity Validation

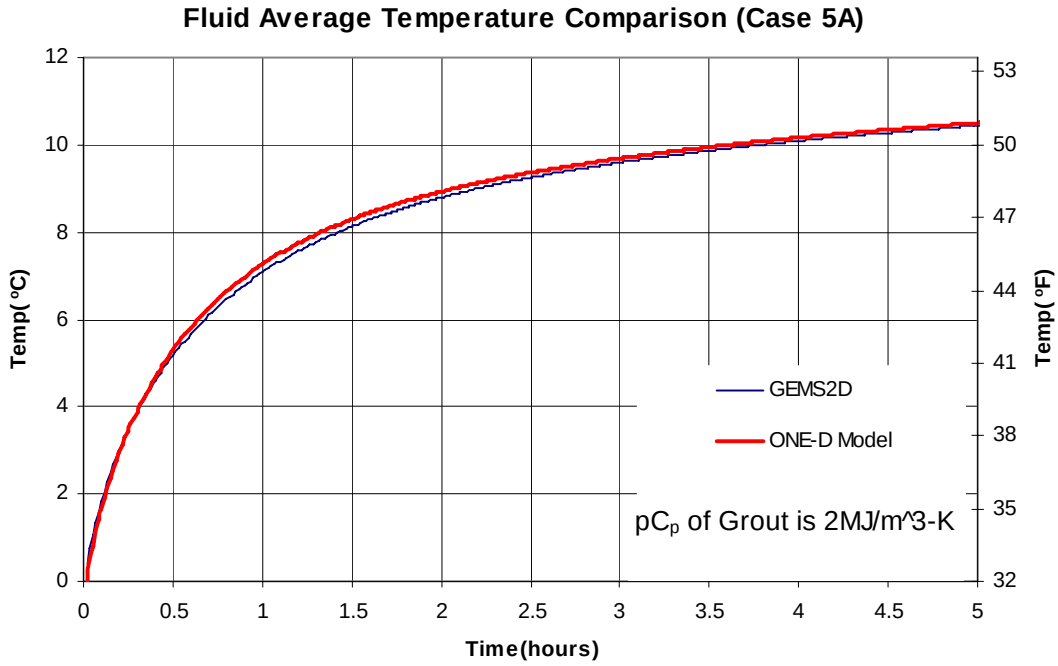

Figure A.16 Comparison of the one-dimensional model and GEMS2D model temperature predictions for Test Case 5A.

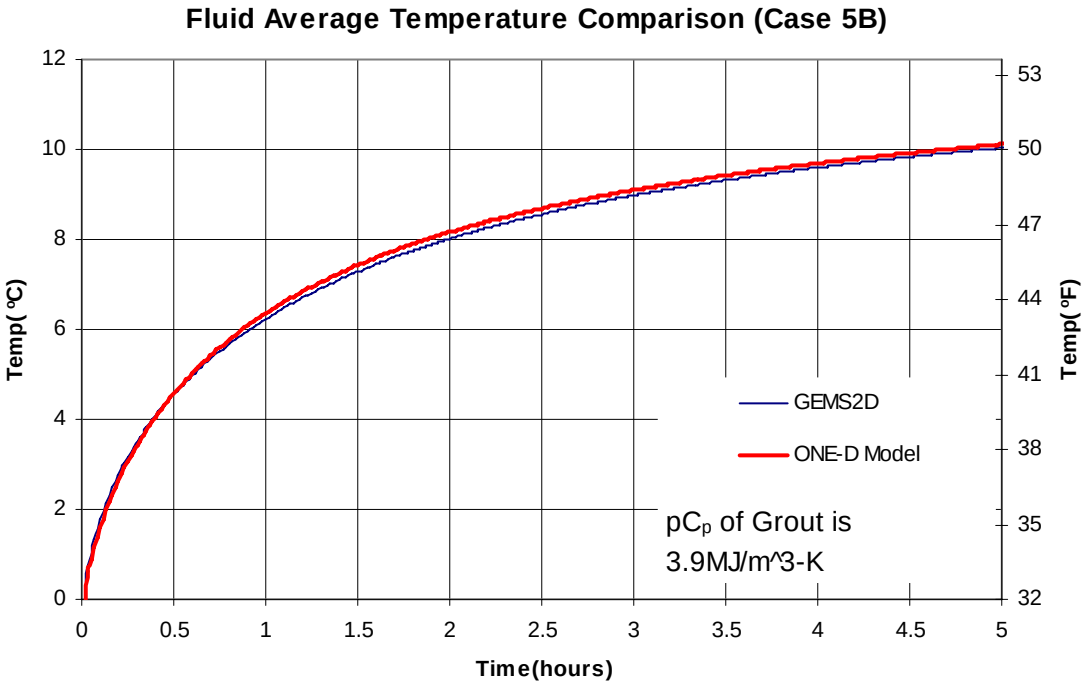

Figure A.17 Comparison of the one-dimensional model and GEMS2D model temperature predictions for Test Case 5B.

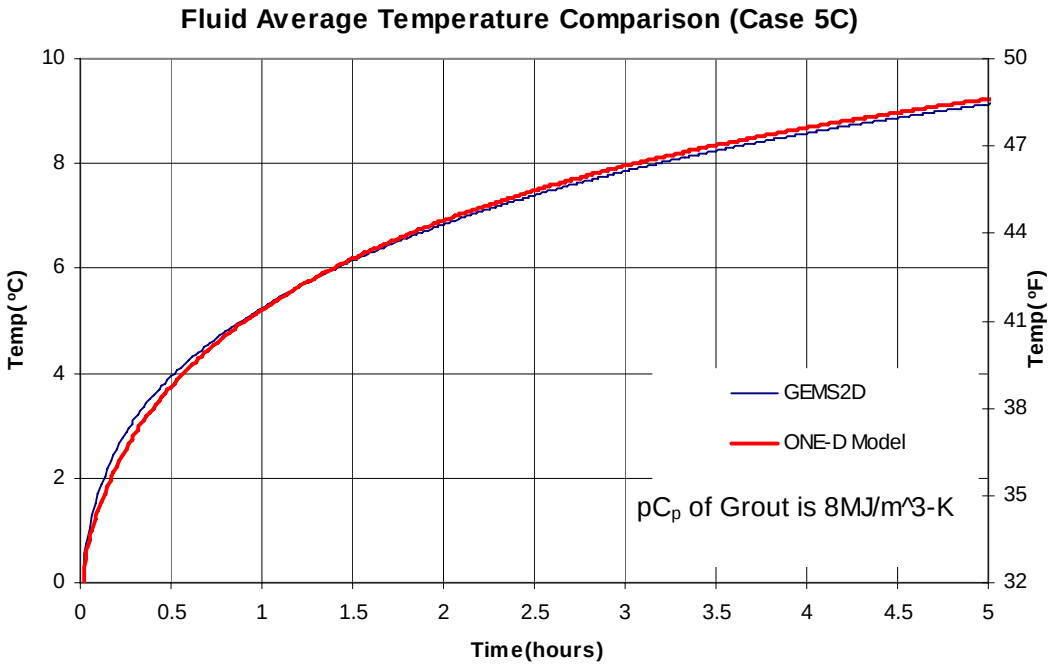

Figure A.18 Comparison of the one-dimensional model and GEMS2D model temperature predictions for Test Case 5C.

Group 6 Fluid Factor Validation

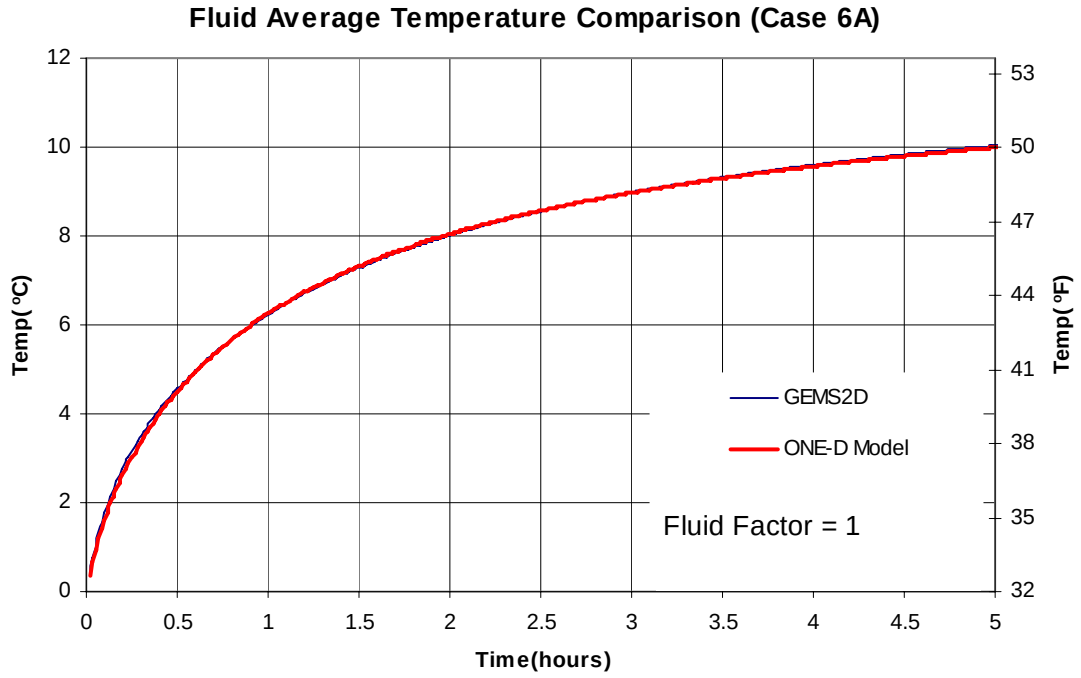

Figure A.19 Comparison of the one-dimensional model and GEMS2D model temperature predictions for Test Case 6A.

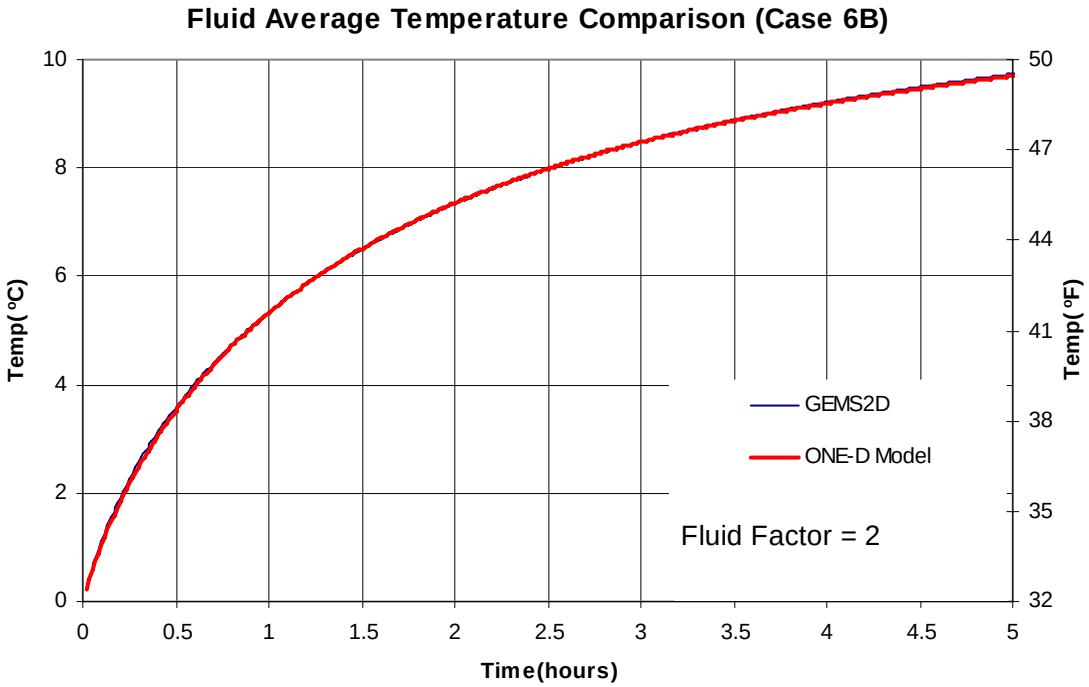

Figure A.20 Comparison of the one-dimensional model and GEMS2D model temperature predictions for Test Case 6B.

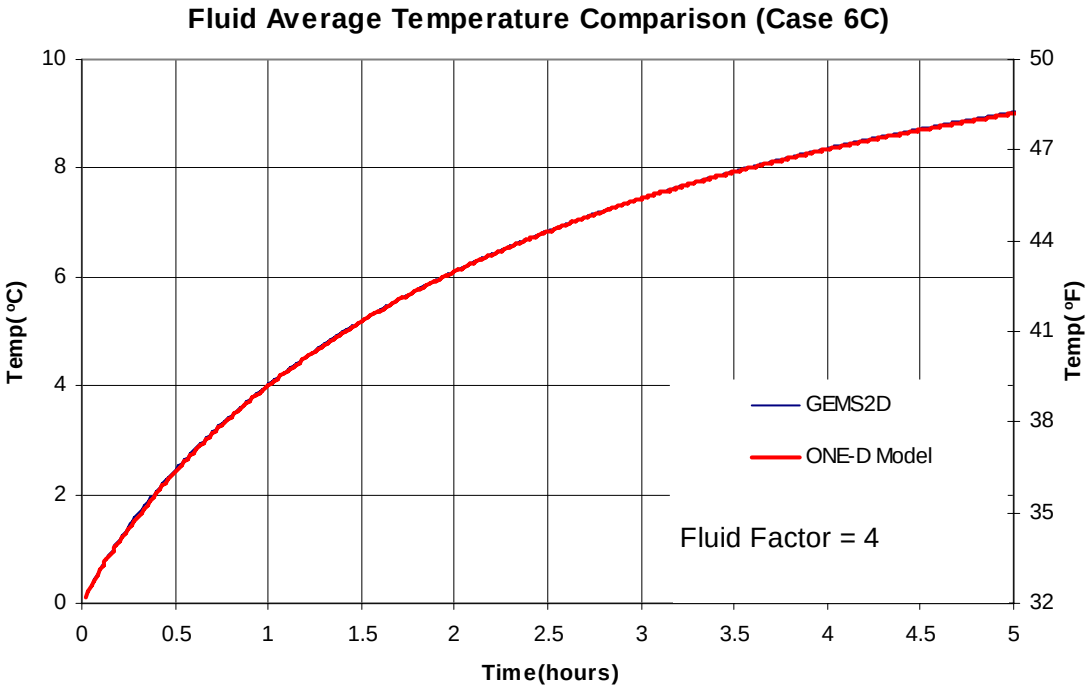

Figure A.16 Comparison of the one-dimensional model and GEMS2D model temperature predictions for Test Case 6C.

APPENDIX B Building Loads in Different Climates

Currently, only the office building and motel building have used for the control strategies investigation. Also only four cities in Table 7.1 have been chosen for the investigation. In Section 7.1, only the office building loads in El Paso, NM and the motel building loads in Tulsa, OK were presented. In this appendix, all the building loads for these four cities are presented. The buildings were modeled and simulated using EnergyPlus.

Office Building

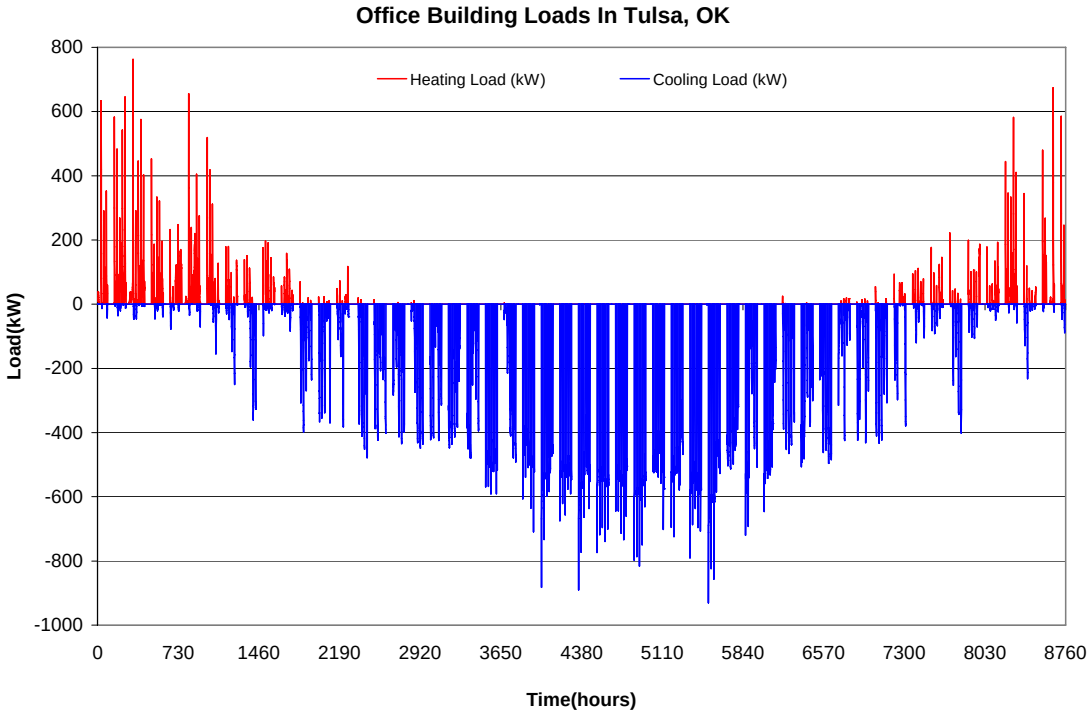

Figure B.1 Office building loads in Tulsa, OK.

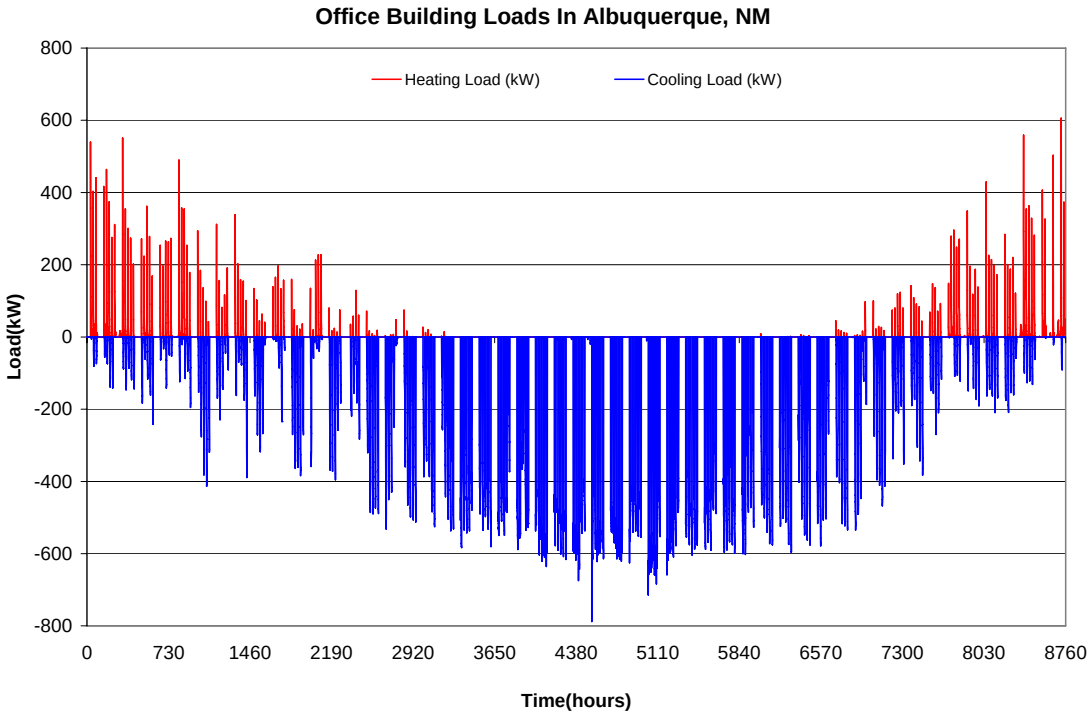

Figure B.2 Office building loads in Albuquerque, NM.

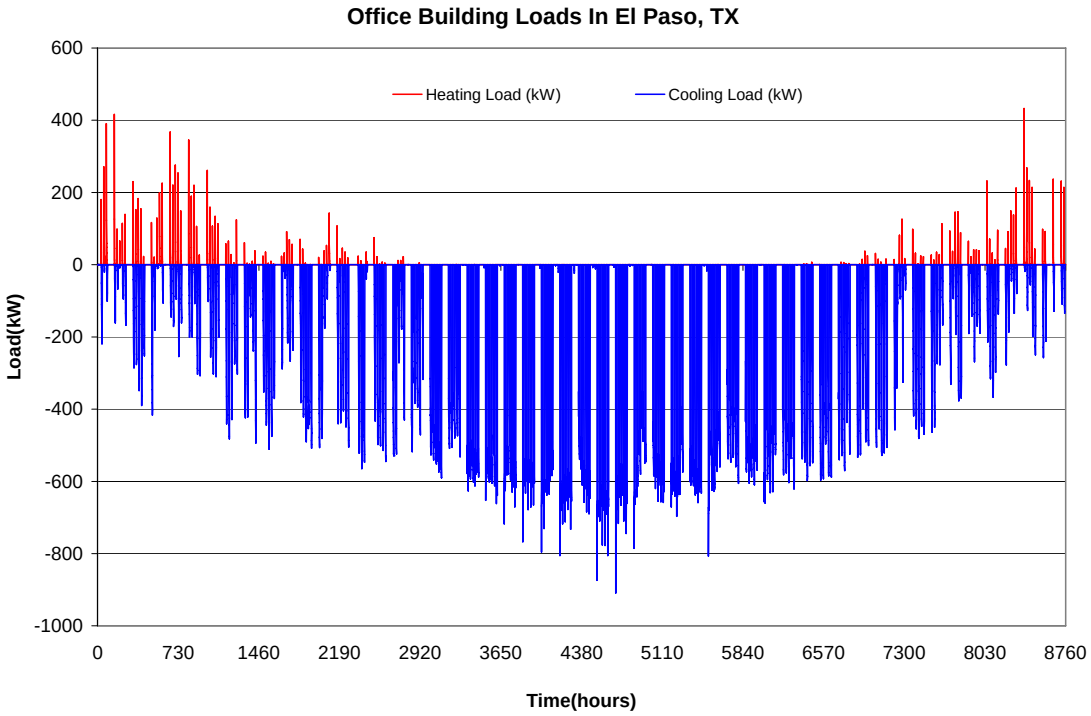

Figure B.3 Office building loads in El Paso, TX.

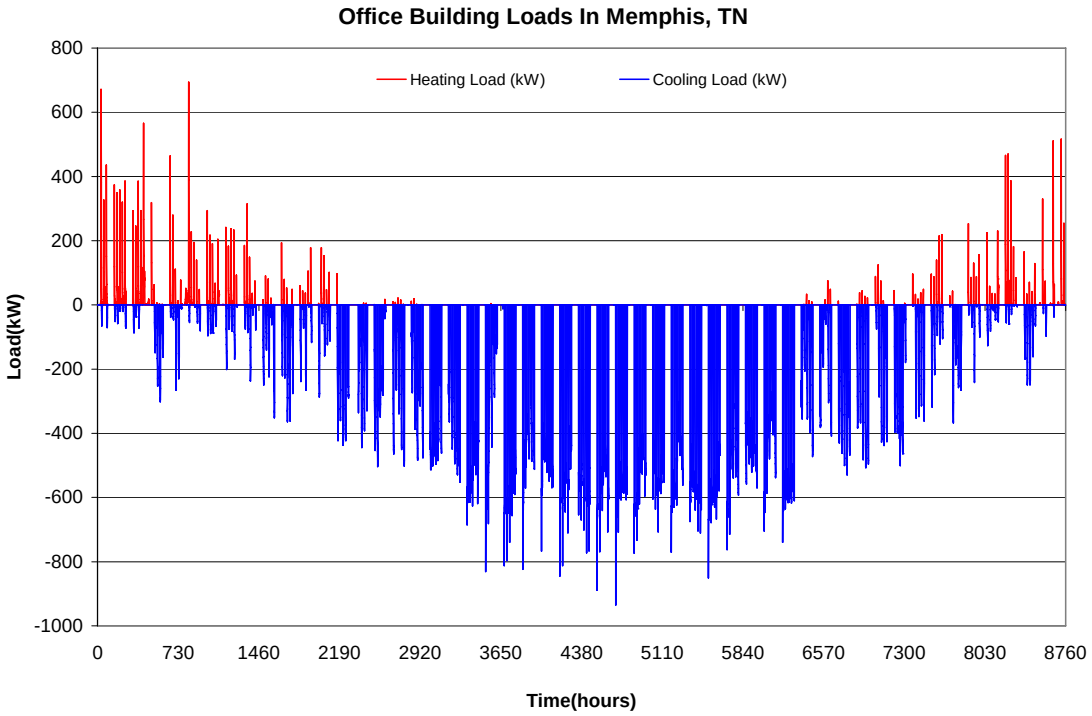

Figure B.4 Office building loads in Memphis, TN.

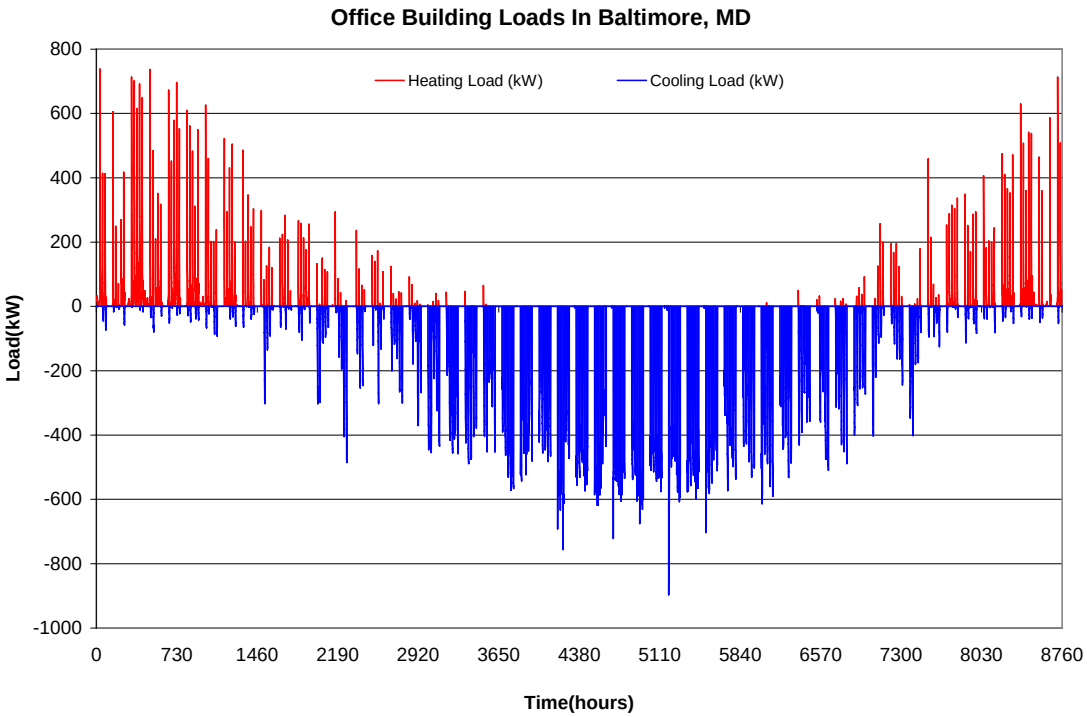

Figure B.5 Office building loads in Baltimore, MD.

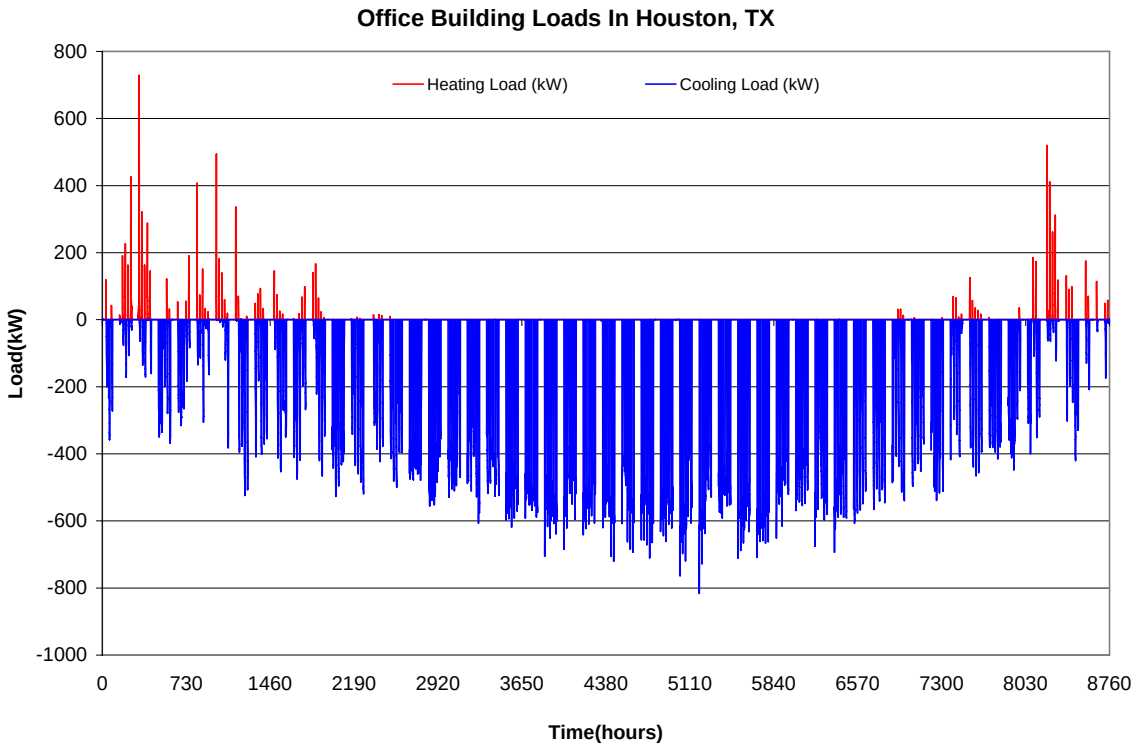

Figure B.6 Office building loads in Houston, MD.

Motel Building

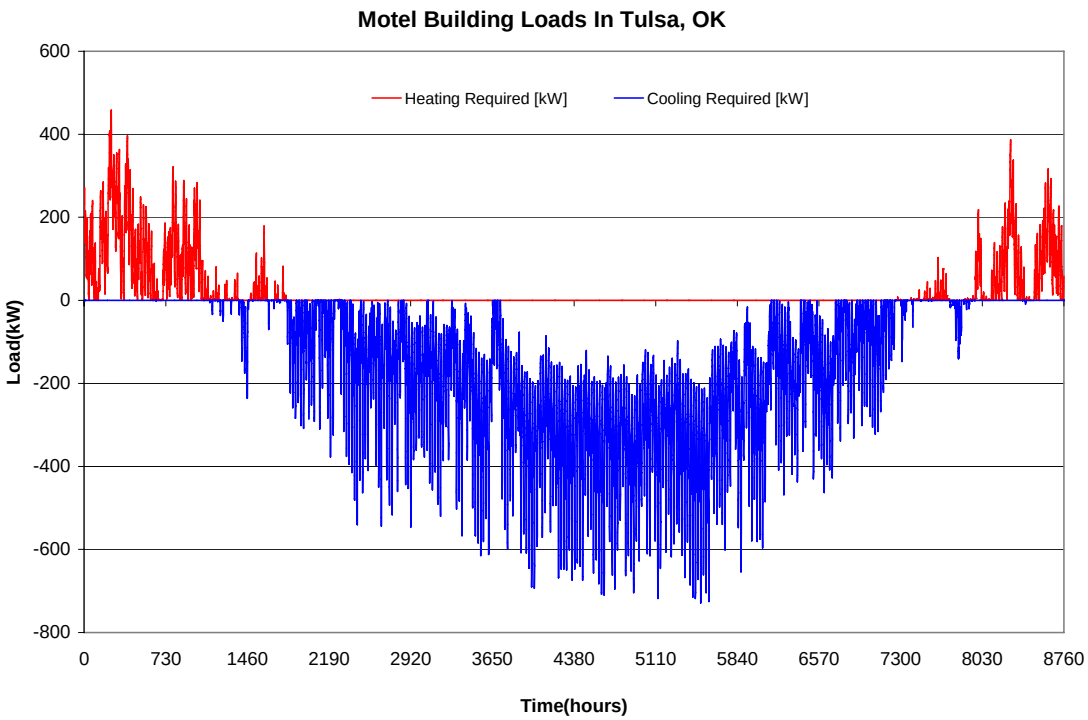

Figure B.7 Motel building loads in Tulsa, OK.

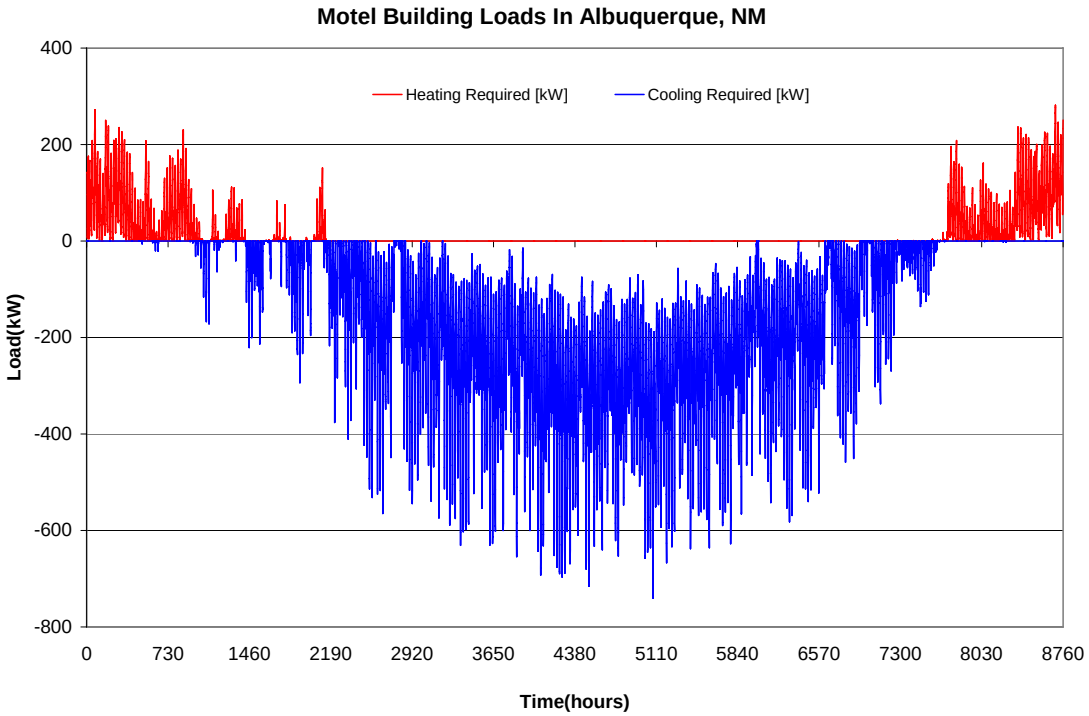

Figure B.8 Motel building loads in Albuquerque, NM.

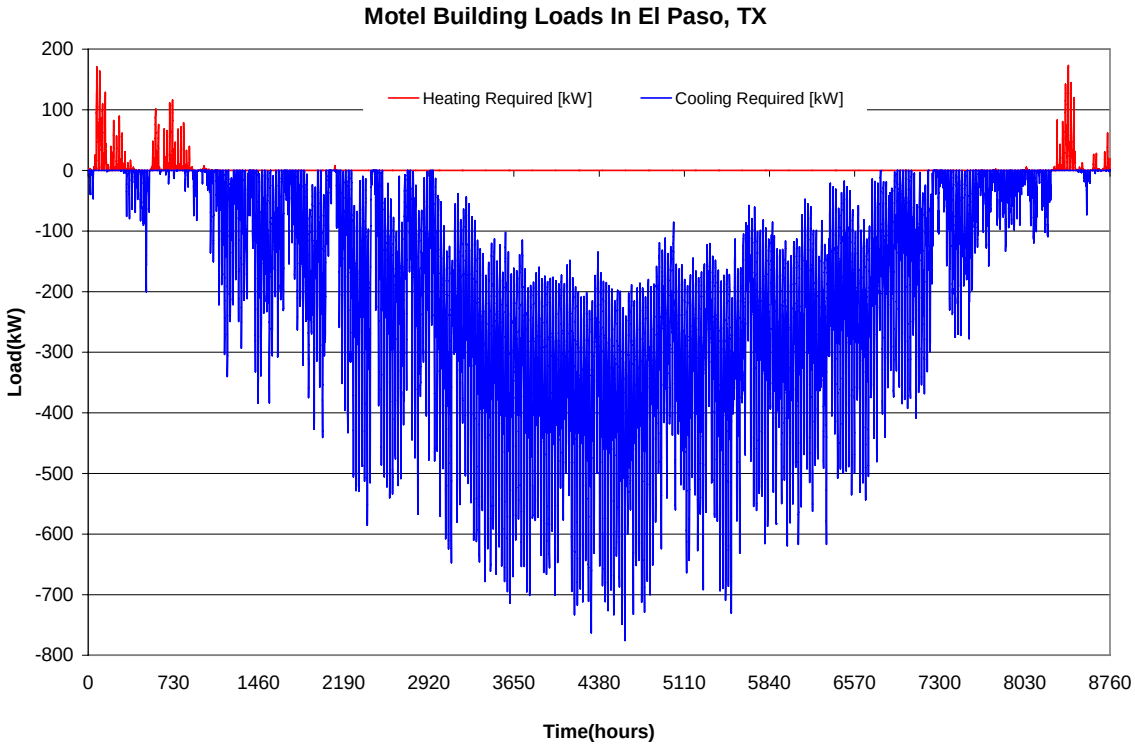

Figure B.9 Motel building loads in El Paso, TX.

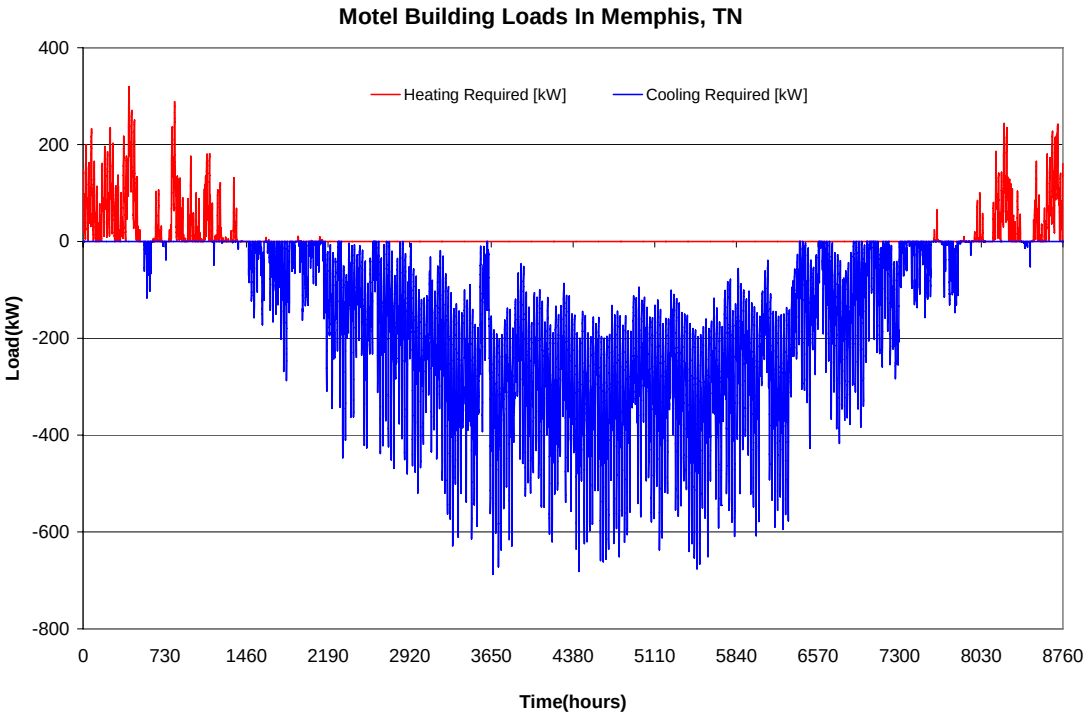

Figure B.10 Motel building loads in Memphis, TN.

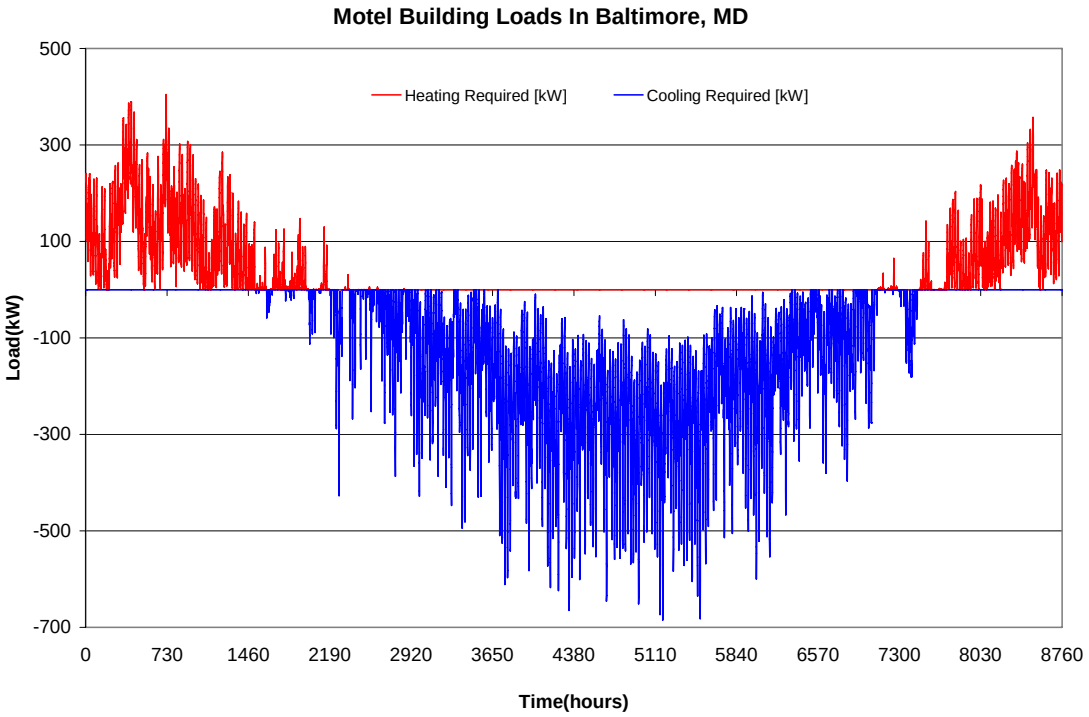

Figure B.11 Motel building loads in Baltimore, MD.

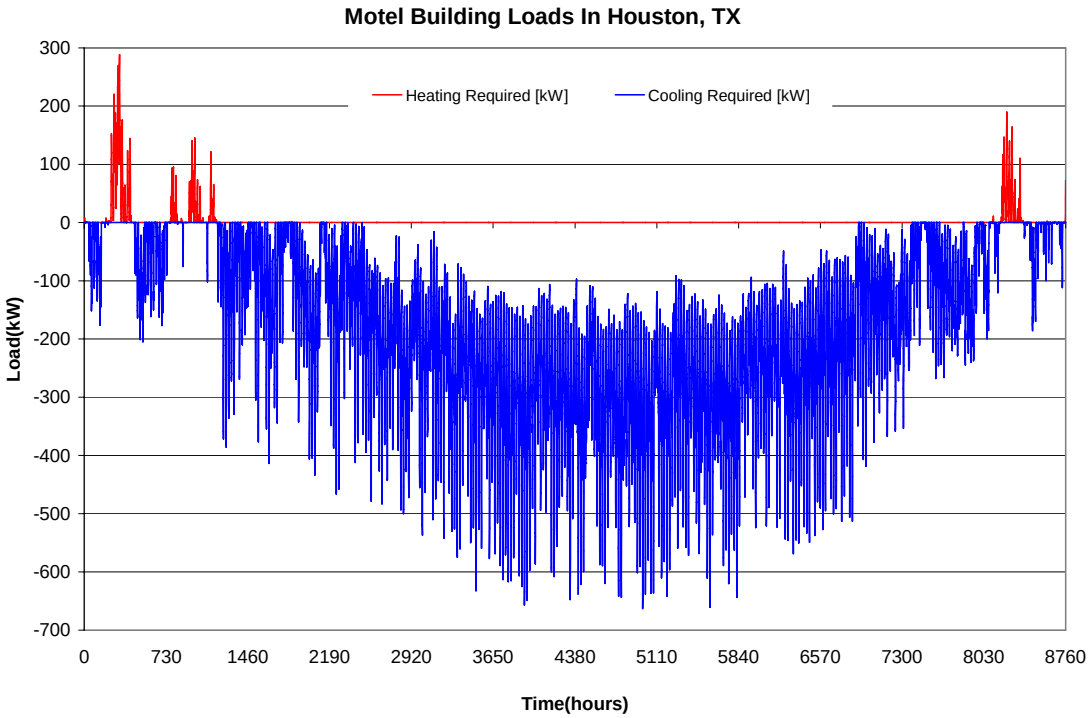

Figure B.12 Motel building loads in Houston, MD.

VITA

Xiaowei Xu

Candidate for the Degree of

Doctor of Philosophy

Thesis: SIMULATION AND OPTIMAL CONTROL OF HYBRID GROUND SOURCE HEAT PUMP SYSTEMS

Major Field: Mechanical Engineering

Biographical:

Personal Data: Born in Jiangyin, Jiangsu Province, China on March 3rd, 1977.

Education: Received Bachelor of Science degree in Thermal Engineering from Tsinghua University, Beijing, China in June 2000. Received Master of Science degree in Mechanical Engineering from Tsinghua University from Tsinghua University, Beijing, China in June 2003. Completed the requirements for the Doctor of Philosophy degree with a major in Mechanical Engineering at Oklahoma State University, Stillwater, Oklahoma in December 2007.

Experience: Worked at Tsinghua University as a research assistant from summer 2000 to spring 2003. Worked at Oklahoma State University as a research assistant from summer 2003 to 2007.

Professional Memberships: American Society of Heating, Refrigerating and Air-Conditioning Engineers, The International Ground Source Heat Pump Association, International Building Performance Simulation Association.

Name: XIAOWEI XU Date of Degree: December, 2007
Institution: Oklahoma State University Location: OKC or Stillwater, Oklahoma

Title of Study: SIMULATION AND OPTIMAL CONTROL OF HYBRID GROUND SOURCE HEAT PUMP SYSTEMS

Pages in Study: 395 Candidate for the Degree of Doctor of Philosophy

Major Field: Mechanical Engineering

Scope and Method of Study: The objective of the study was development of optimal control strategies for hybrid ground-source heat pump (HGSHP) systems in order to improve the performance of HGSHP systems. The investigations of the four sub-objectives were carried out, including: development of HGSHP system simulation and requisite component models, validation of HGSHP system and component simulation, development of an HGSHP system design procedure, investigation and development of generally applicable optimal control strategies.

Findings and Conclusions: All requisite component models for the HGSHP system simulation have been developed. The HGSHP system simulation has been implemented in HVACSIM+. The HGSHP system simulation was validated against the experimental data collected from the OSU HGSHP research facility. After the calibration of each component model, the simulation gave total energy consumption about 0.2% higher than the experiment.

A parallel-connected HGSHP system was chosen for the study and a strategy for controlling the flow distribution between GLHE and PHE/cooling tower was developed. A temperature limit-optimized simulation-based method was developed for sizing the HGSHP system components and was implemented in GLHEPRO. A comparative study of three hybrid ground source heat pump system design procedures was carried out. In general, the HGSHP designed from the new design procedure would have a smaller GLHE and cooling tower size and a smaller system life cycle cost than the system designed from the Kavanaugh and Rafferty procedure (1997).

Two building types and six U.S. cities were chosen to provide different building load profile for the study of HGSHP system controls. Three control strategies developed by Yavuzturk and Spitler (2000) were investigated first. The investigation results showed, for the three control strategies, there is no generally-applicable setpoint for different combinations of HGSHP system design, building type and location. Three new control strategies have been developed in this research: a system load control strategy, a forecast/historical control strategy and a varied EFT/ExFT control strategy. Using these new control strategies, without individually optimizing setpoint for a specific building and location combination, the systems will have savings from 1% to 26% compared to the base cases.

ADVISER'S APPROVAL: Jeffrey D. Spitler